Abstract

Subsidences in ground surface are caused by collapses of underground cavities by internal erosion with ground water percolation around and through the cavity. During the last few decades, there is an increased record of road cave-in accidents. Specially, many road cave-ins were caused by underground cavities developed through defects in buried sewer and drain pipes. Researchers have found that, there is a tendency of forming cave-ins when the age of buried pipe exceeds 25 years. Hence, vulnerability of road cave-in accidents is increasing all over the world, with most of the buried sewer and drain lines reaching their lifespan.

Although modern techniques like Ground Penetrating Radar (GPR) and Geoelectric Tomography are available to detect the subsurface cavities, those technologies can only identify air filled voids separately from soil and having many other limitations. Maximum depth which can accurately detect is limited to few meters; in clayey and high moist soils this will be further limited to 1-1.5m maximum. Therefore, it is very difficult to detect cavities in deeper ground and it can ultimately cause ground subsidence by expansion towards the surface. Cavities are generally associated with process of loosening around it. Therefore, it will be better in detecting the loosened soil conjunction with air-filled cavity, rather than targeting air-filled cavity only. Thereby, even cavities in deeper ground can be detected by signs of capturing the loosened region in the subsurface. This will lead to improve the accuracy and efficiency of current methods in inexpensive manner. At present, cavity formation, extents of loosening and mechanical properties of loosened soil around cavity are not well addressed.

There are several objectives of this study. First is to understand the extents of loosening with respect to the potential cavity size and to identify the parameters which affect the scale and rate of loosening. An attempt was made to create loosened soil in laboratory by dissolving water soluble material of pre-selected size and shape in Toyoura sand. The above mentioned objectives were achieved by conducting series of two-dimensional model tests by introducing a potential cavity and forming loosening by expanding the cavity by water infiltration and drainage. Effect of cavity size, density, ground compaction and rate of drainage on loosening and cavity expansion was studied through the two dimensional tests.

As the second part of the study, quantitative study on mechanical properties of loosened soil was evaluated by triaxial tests after forming ground loosening inside the specimen. Simultaneously, influence of density, cavity size and location on scale of loosening was studied by changing conditions of the experiment. In each test, variation of axial strain, radial strain and volumetric strain during process of loosening was obtained and Poisson's ratio and shear modulus of loosened sand was evaluated. Furthermore, extent of loosening in triaxial specimen was studied by X-ray CT scan, in order to compare the different behaviour in two dimensional and three dimensional responses.

Results obtained for Toyoura sand from two dimensional model tests show that, height of the loosened region is extending up to five times of cavity height and radial expansion is limited compared to vertical expansion. Furthermore, It was found that ground collapse around the potential cavity was higher when the cavity was located above the ground water table rather than beneath the water table. Cavity formed in compacted or dense soil was more stable compared to loose soil and extents of loosening were proportional to cavity size. Further observed that, suction supports the stability of cavity and abrupt failure of cavity ceiling was caused by rapid drainage.

Extent of loosening was nearly limited to two times of the initial cavity height in triaxial tests. Density has affected the axial and radial deformations caused by loosening and lower density (Dr=37%) samples were observed with four times larger strains than medium dense samples (Dr=63%). Similarly, lower confining pressure (50kPa) shows nearly three times larger deformations than high confining pressure (100kPa). Loose sand and coarse sand (Silica) was subjected to further propagation of loosening under repetitive infiltration on already loosened soil. Evaluated Poisson's ratio of loosened sand shows complex variation throughout the entire test and difficult to understand the relationship with scale of loosening. This might be due to non-uniform distribution of soil and voids. Parametric study showed that Young's modulus of loosened region was 50-60% of the non-loosened region. Overall stiffness of ground with loosening was 70-85% of stiffness of controlled specimen.

As a conclusion the cavities in subsurface are more vulnerable for cave-in and loosening expands at least twice of the cavity height. Overall stiffness of the ground is decreasing significantly even by having a smaller void.

Acknowledgement

Reading for a master degree at University of Tokyo, Japan would be a remarkable lifetime opportunity that anyone can ever be dreamed off. There were many helping hands behind this achievement. In that context, I make this opportunity to convey my sincere thanks to all who contributed in various ways to complete my master degree.

First, I would like to express my heartfelt gratitude to my supervisor, Associate professor Reiko Kuwano and the Japanese government for accepting a student like me from a developing country and offering a chance to develop their human resources in this manner. Furthermore, my deepest gratitude goes to my supervisor's excellent guidance, kindness, encouragement, commitment and patience extended throughout this research.

I convey my deepest gratitude to my co advisor, Associate Professor Taro Uchimura for his valuable suggestions, comments, criticisms and commitment given upon this research.

I would also like to acknowledge Prof. Junichi Koseki, for his valuable comments, suggestions, clarifications, appreciations and criticisms given in lab seminars. Not only that, but also I had a vast knowledge about Japanese society, by having valuable and interesting discussions with him during the laboratory life.

My special heartfelt gratitude goes to Mr. Takeshi Sato, the technician of Koseki lab for his enormous assistance. It was a great honor in my life to work with such a genius and humble person. He assisted me with his technical knowledge as well as by making me laugh whenever I was down and tired with my testing apparatus. He was not only the technician, but was the best friend in the experimental room.

I am grateful to Mrs.Yukika Miyashita, the lab technician of Koseki laboratory for her assistance extended to me whenever I was facing technical problems with my apparatus and computers.

My appreciation and gratitude go to Mrs. Kichibayashi and Ms. Michie Torimitsu, the secretaries of Kuwano lab and Koseki Lab for their kind support in handling the administrative aspects during these two years.

I appreciate the assistance and guidance given by Dr. Taka-aki Mizutani and Mr. So Hirai, staff of Port and AirPort Research Institute, Kurihama, Japan. Unless their guidance, it would be difficult to complete X-ray CT test with my tight experimental schedules. Similarly, I would like to thank Ms. Mari Sato, Doctoral student of Kuwano lab for her assistance given to successfully complete the X-ray CT test and throughout these two years whenever I requested her assistance.

Many thanks go to Ms. Sho Oh, my tutor who supported her best to make my life easier in Japan. Then specially thank Mr. Laxmi Suwal, my senior student who taught me about testing apparatus. I really appreciate his patience and kindness during answering for all my unwise questions in the initial period of my research. Furthermore, I wish to express my

gratitude to all my colleagues in Kuwano and Koseki lab for their assistance and for making these two years joyful.

I would like to thank my friend Aruna Bandara, master student of Department of Urban Engineering, University of Tokyo for his technical assistance given me during analysis of X-ray CT images. Then my heartfelt thanks to my beloved husband, Indunil Galhena for his comments and suggestions given for my research as well as understanding and encouraging me for 2 years of life in Japan.

I owe to my loving parent, sister and brother who live in Sri Lanka for their dedication and commitment given to make my education effective and fruitful.

My sincere gratitude goes to Ministry of Science, Culture and Education, Japan for offering me financial assistance for my study in Japan.

At last but not least, I am grateful to all the people who met me so far in my life and helped me even by a single word for the betterment of my life.

Table of Content

Chapter 06- Results and discussion – Triaxial tests

Chapter 07- Results and discussion – Visualization of loosening by X-ray CT

Chapter 08- Conclusions and future recommendations

Appendices (I,II,III)

References

List of Figures

Chapter 02- Literature Review

Chapter 03- Testing apparatuses and methodology

Chapter 04- Theories and data analysis

Chapter 05- Results and discussion – Model tests

Chapter 06- Results and discussion – Triaxial tests

Chapter 07- Results and discussion – Visualization of loosening by X-ray CT

List of Tables

CHAPTER 1
INTRODUCTION

1.1. Background

The Earth's subsurface can be disturbed by various underground constructions which will cause sinkholes or cave-ins when these are abandoned. Ground cave-ins usually formed by the propagation of cavities under the ground surface due to subsurface erosion. Underground cavities exist in different scales which can damage the structural integrity of soils differently. The reported disasters related to ground cave-ins have been increased during the last few decades. Among them, the number of road subsidence in urban areas, caused by internal erosion, which occurs due to leakages in buried sewer pipes and drain pipes has become significant.

The number of defects in buried pipes is increased with the age of pipe, and frequent defects were observed after 30-40 years of service period (Kuwano et al, 2006). The threat of ground cave-in formations has greatly increased due to the pipes which are exceeding 50 years of service life is rapidly increasing in all over the world can cause for enormous problems in near future.

However this theme of study is still at preliminary stage, in the geotechnical research field. The main reason is, when road cave-ins were formed, it is difficult to conduct detailed geotechnical investigations in that location, because the fast road restoration is required to avoid the difficulties related to public transportation. Furthermore, it is not easy to identify the locations of existing cavities prior to the failure, except by technologies such as Ground Penetrating Radar (GPR) or by Geo-electric-resistivity tomography. These technologies are based on a physical contact between the cavity and the surrounding soil and use the electrical resistance differences of the void and the surrounding soil.

1.2. Significance of study

Urbanization makes underground lifeline structures more congested and complicated. Many large scale cave-ins were caused at highway intersections, where the buried service lines are crossing each other. Careless and unacceptable pipe laying constructions at these

intersections are very common in all over the world. However, at the time of laying these pipe lines, many related local authorities may not be aware the risk of cave-ins.

Most of already conducted researches related to this subject are focusing on cave-in formation by dissolving of lime layers. Cave-ins occur in normal soil is still not addressed properly in quantitative manner.

Most of the people are not aware of the severity of such cave-ins because these accidents are much localized. But, it is a threat for human lives as well as for the economy of that country. Whenever road cave-ins happened, all utilities such as sanitary and storm water sewers, water, cable, gas, electricity and phone can be affected by these sinkholes. Specially, when this happens in main highways, situation becomes very difficult to control. In such cases, most of other utilities except sewer system can be disconnected by turning off a valve or the flipping of a switch. However, it is not that easy with the sewer systems, where sewer systems are mostly operated by gravity without any external forces. Therefore, huge masses of sewerage can be streamed in to the fallen sink halls which will create all sorts of social inconveniences. As a reason, the restoration work will take long time and even natural water sources can be contaminated and sewer overflow can be expected even from nearby residences in the upstream. As an example, sewer collapse with sinkholes in Tucson, Arizona caused expense of $7.7 million for emergency response and repair works ("Sewer Collapse Causes Sinkholes in Tucson", 2004).

A survey conducted in Japan (Kuwano et al, 2006) stated that the vulnerability of forming cave-ins is increased when the sewer pipe exceeds the age of 25 years. However, the same authors (Kuwano et al, 2006) have expressed that there are many other reasons although the defects of sewer pipes are thought be the most significant factor for the cave-ins. Size and material of the pipe, improper construction techniques, lack of compaction in backfill, destruction by other pipes lines due to lack of integrated service maps are also playing a vital role.

Currently available underground cavity detection technologies have many limitations and specially, they are successfully working only in shallower depth. That means, when the location of the cavity is deep in the ground, the detection of the cavity is not easy. Hence, it is possible that the hidden cavity expands for a long time to eventually cause sudden failure in ground surface. However, the form of existing underground cavities may not exist as a clear void. Therefore the probability of accurately of detecting the cavity is still low.

Sinkholes are mostly associated with loosened soil around the initial cavity. Soil sited on ceiling of initially formed cavity can be eroded in to the void with the circulation of ground water. Fine soil particles can be easily washed in to void with the water infiltration in rainy season causing the loosening in surrounded area. Loosening pattern is related with grain size distribution. In uniform sand, initial cavity shrinks and surrounding soil subjected to volume expansion, which causes soil loosening around cavity. In case of sand with fines, fines from soil located around cavity easily wash away and loosening forms

without significant expansion of initial cavity. In this study, loosening formed by volume expansion of near cavity ground with shrinkage of cavity was simulated in uniform grains. Since loosening spreads significantly in vertical direction, it will be more reliable to target on the loosened soil combined with the void, rather than only focusing on detection of void, in developing a detection mechanism.

If the variation of mechanical properties of such loosened soil is known, it will be able to confirm the availability of existing cavities with higher accuracy after conjunction with current technologies. And this will facilitate to detect the cavities even at deep ground, since the loosened part is gradually propagating towards the ground surface before the subsidence occurs.

Detail investigation on exact location of the accidents is almost impossible due to need of fast restoration of roads. Therefore, main objective of this research is to analyze the variation of mechanical properties of loosened sand which is associated with underground cavities by laboratory experiments. These experiments will reveal important properties in loosened soil which may be important to upgrade the current subsurface void detection technologies to improve the accuracy by detecting the loosened soil separately from normal ground. Furthermore, significant parameters (density, depth, cavity size, etc.) which are affecting the degree of ground deformation around cavity will be discovered.

1.3. Objectives

This study was carried out with following objectives.

1. To identify the parameters which are affecting the underground cavity expansion and propagation towards the surface through;

   Series of small scale two dimensional model tests (dimensions 300 x240x50) and triaxial compression tests (ϕ=75mm, h=150mm) were carried to observe the effect of the density, cavity size, cavity location, confining pressure and particle grain size on ground deformation cause by cavities.

2. To analyze the mechanical properties such as radial strain, axial strain, volumetric strain, small strain modulus, Poisson's ratio and shear strength of loosened soil associated with underground cavities through;

   Series of small triaxial compression tests (ϕ=75mm, h=150mm) were conducted by forming artificial loosening by dissolving a water soluble material inside a Triaxial apparatus. Related stresses and strains were measured and above mentioned parameters were computed before and after formation of loosening.

3. To observe the soil deformation causes by repetitive water infiltration on already loosened soil which is accompanied a void through;

Initial cavity was simulated by a water soluble material inside a triaxial apparatus. Water soluble material was dissolved and small voids and associated ground loosening was formed. Water infiltration was done in this stage and soil deformation causes on already loosened soil and the effect on existing void were observed.

4. To visualize the extent and the shape of ground loosening causes by cavity failure.

This was observed by series of model tests simultaneously with achieving objective 1. Furthermore, one triaxial test specimen with similar properties as explained in objective 3, was scanned by X-ray Computed Tomography to visualize the exact phenomena during testing.

1.4. Scope of study

1. This study is mainly focused on Toyoura sand which is a well sorted sand having specific gravity, G_s = 2.656; mean diameter, D_{50} = 0.19mm; fines content, F_c =0.1%. Furthermore Silica sand was used for two tests to compare the effect of particle size on above mentioned objectives.

2. Quantitative analysis on stress, strain characteristics on loosened sand was computed based on small triaxial compression apparatus. Confining pressure of 50kPa was used to represent the shallow ground conditions. However two more tests with 100kPa of cell pressure were conducted to observe the effect of confining pressure on above desired parameters.

3. Exact density reduction in the loosened ground was not focused through and methodology was not designed to obtain that property.

1.5. Research outline

Ultimate objective of this study is to analyze the mechanical properties of loosened sand associated with underground cavities by laboratory experiments. At very first stage, decision was made to use the triaxial apparatus with forming artificial loosening inside the specimen. Since it is difficult to allow sand particles to wash out from the specimen through bottom drainage valve, it was decided to place a water soluble material of known shape and size in predefined location in the specimen and form artificial loosening by dissolving it.

In order to confirm the previous mechanism and for further investigation on effect of some parameters on degree of loosening, series of two dimensional model tests were carried out. In this case, Toyoura sand was used in an acrylic model after placing a glucose block at the

bottom central area. With water infiltration and drainage, soil sited above the glucose was settled down and cavity was moving up. Finally, it was possible to observe some deformed area where soil was loosened. The effective maximum height and width of that deformed region was evaluated and presented as a ratio of initial width and height of glucose block. Important facts about effect of soil density, compaction effort, drainage rate on scale of loosening was found.

Once, the mechanism of artificial loosening formation was successfully confirmed, the same was implemented in to Triaxial test. Since it was observed by model tests that, there was a maximum extent for loosening; two regions were defined in the triaxial specimen as normal and loosened regions. Assumption was made as fixing of two separate sets of deformation transducers in those two regions will facilitate to compare the strains at loosened and normal regions in the same specimen. Therefore three clip gauges were used in three different locations, at closer to bottom porous stone, center and closer to upper porous stone. Similarly one set of LDTs were fixed to measure the strain at lower half of the specimen and the other at upper half. By using those results, it was possible to interpret the axial strain, radial strain, volumetric strain, Young's modulus and Poisson's ratio for lower and upper halves separately. The effect of density, cavity size, location, confining pressure and particle size on above parameters were checked by series of tests.

Although, the extent of loosening was observed in the two-dimensional model ground, there was no way to accept that the same behaviour will take place in three dimensional cases in triaxial specimen. Therefore, with available time, it was decided to conduct an X-ray Computed Tomography scan on one representative case in triaxial test to observe the ground loosening phenomena and extent of loosening to confirm our imaginations. As a result of that, scaled down, triaxial test was conducted under accelerated test conditions with controlling important conditions as close as possible to other triaxial tests. This was performed outside the University of Tokyo, at Port and Airport Research Institute (PARI), Kurihama, Tokyo, Japan. This was done with the assistance from Sato. M, doctoral student in the same lab, University of Tokyo. It was confirmed that the mechanism which was expected and imagined was correct and extents of ground loosening was almost compatible with previously obtained results.

This study is mainly based on tree types of tests. Those are the two dimensional model tests, triaxial compression test with quantitative measurements and X-ray Computed tomography on triaxial test with qualitative measurements.

1.6. Structure of the dissertation

This thesis has been structured into eight chapters. Description on content of each chapter is briefly explained below.

Chapter 1- Introduction

Background of road cave-ins, problems related with these accidents, significance of the study, objectives and scope of this research was discussed.

Chapter 2- Literature Review

Introduction to cave-ins, role of buried pipes on cave-ins, some case studies of severe cave-ins, currently available technologies on identification of underground voids and limitations of those methods were discussed.

Chapter 3- Methodology

Development of methodology, material properties, specimen preparation and testing procedure of model test, triaxial test and X-ray CT scan was discussed.

Chapter 4- Theory and data analysis

General theories of soil mechanics, data analysis procedure of model tests and triaxial tests were discussed in detail.

Chapter 5- Results and discussion - Model tests

Results obtained from two-dimensional model test were discussed in detail

Chapter 6- Results and discussion - Triaxial tests

Quantitative results obtained from two-dimensional model test were discussed in detail.

Chapter 7- Results and discussion – X-ray CT images on Triaxial test

Visualization of loosening formation in triaxial test was illustrated by X-ray CT scan images

Chapter 8- Conclusions and recommendations

Conclusions made by all three types of tests, limitations of this research and recommendations for future works will be explained.

CHAPTER -02

LITERATURE REVIEW

2.1. Sinkholes in general

Sinkhole can be generally defined as any sudden subsidence of the earth. Normally this is caused by internal erosion taken place in supportive soil medium or dissolving of underlying rock or limestone layers. Before causing a sinkhole, probably there will be an underground cavity either a naturally formed or manmade. Soil above the initiated cavity will be progressively eroded in to cavity, with circulation of ground water table. This will cause progressive expansion of affected area; once cavity ceiling is unable to bear the overburden stress there will be a subsidence. Sinkholes range in size from several meters to hundreds of meters according to the real cause and underlying soil and geology condition. Similarly, cave-ins may be quite shallow or may extend hundreds of feet deep.

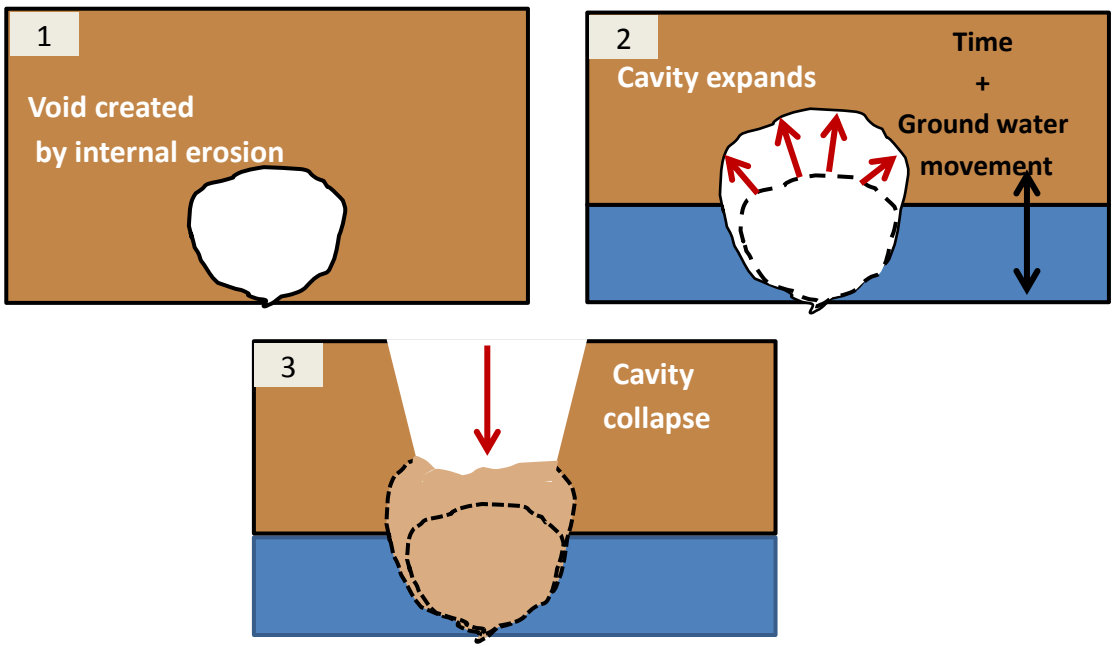

Figure 2. 1: Sinkhole formation – general mechanism

Cavity formation can be either due to natural processes or by manmade issues. Naturally formed sinkholes are mostly caused by dissolving of limestone with millions of years. As

an example, Florida is always facing sinkhole accidents due to its geology which has thousands of feet thick limestone underlies the entire city. Limestone is deposited as layers and chemical composition, hardness of each layer can be slightly different. Therefore, with time, limestone can be fractured and become weak with dissolution. During the natural process of precipitation, carbon dioxide (CO2) in the atmosphere can dissolved to the falling rain and makes the water slightly acidic in nature. When this water percolates through the alkaline limestone layers through the formed fractures and week layers, a chemical erosion process can occur in limestone. This whole process can happen over and over for thousands of years forming cavities underneath the overlying sediment layers, ultimately collapsing or subsiding forming natural sinkholes. Furthermore, decreasing of ground water table in drought seasons will reduce the buoyant support of cavity ceiling which can increase the vulnerability of cavity collapse. When such droughts and lower ground water levels are followed by heavy rainfall the condition becomes more dangerous. Figure 2.2 illustrates the process (Southwest Florida Water Management District 2008).

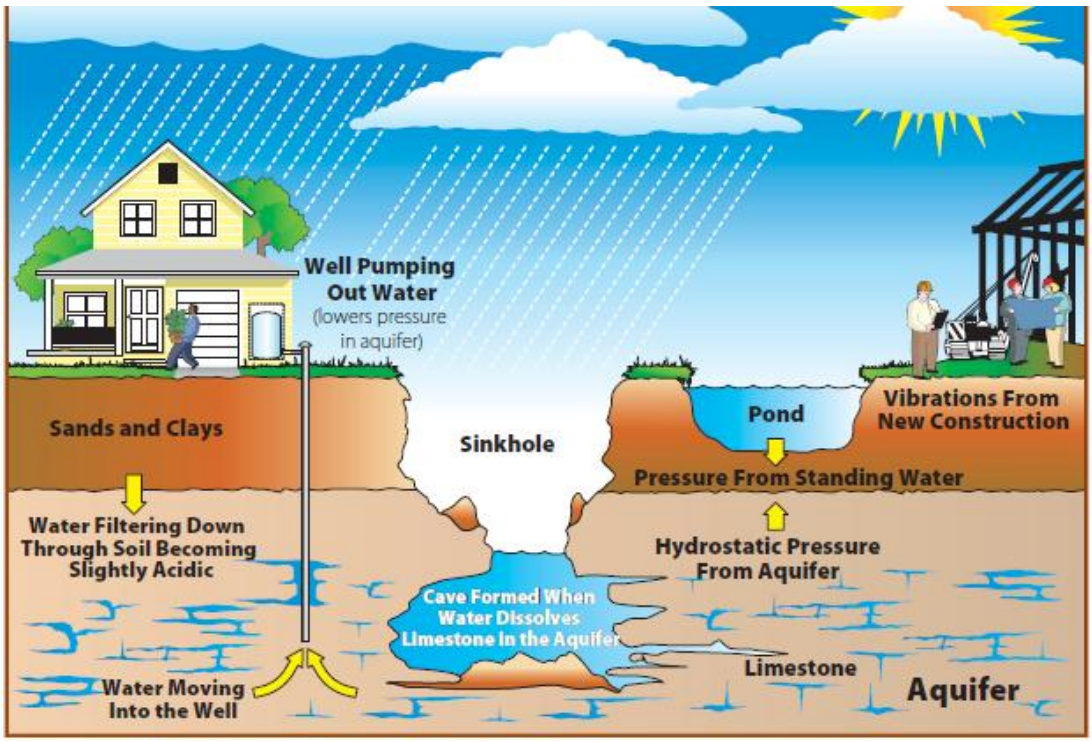

Figure 2. 2: Formation of sinkhole by dissolving of limestone
(Southwest Florida Water Management District 2008)

(a) Winter Park, Florida, USA opened up in 1981 (b) Mulberry, Florida, USA in 1994

Figure 2. 3: Sinkholes caused by dissolving of underlying limestone ('Pictures of Sinkholes' 2009)

Number of cave-ins caused by human activities has rapidly increased in last few decades with urbanization. Possible causes are mentioned below and few examples for cave-in accidents recorded due to different human activities are shown in Figure 2.4.

- Small cracks, openings or leakages available in old sewer pipes and abundant drain pipes (Careless connections, deterioration and fatigue by repetitive loading on pipes)
- Abundant tunnels, trenches and mines
- Cracks in sea walls which allow lateral passing water and fine soils through the wall.

(a)Picher, Oklahoma, USA in 2008
Cause: Mining for zinc and lead

(b) Guatemala in June 2010
Cause: Heavy rain and damage of sewer line

(c) Lisbon, Portugal in 2003
Cause: Damage of a sewer pipe

Figure 2. 4: Sinkholes caused by human activities (Pictures of Sinkholes'2009)

2.2. Influence of buried pipes against cave-ins

2.2.1. General phenomenon of cavity formation by buried pipes

Failure of buried pipes has become a major cause for occurrence of road cave-ins. Urbanization has made ground underneath roads much more complicated and congested with buried service pipes. There are many service pipes are laid as water, gas, electric wire, telephone wire, sewer and drain pipes. Somehow it is possible to identify the cracks or leakages whenever caused in gas or water pipes. Since, gas leakages or high pressure water leakages can be easily noticed. However, it is mostly impossible to notice whenever drain pipe or sewer pipe was damaged. There are many cracks; damages can be existed due to pipe deterioration, gaps between pipes or due to poor construction practice. Even abundant drainage pipes, which are not closed, can support this phenomenon. Whenever such opening is created in a buried pipe, soil sited over it can be flow in pipe with groundwater percolation in rainy season. This process will lead to create a small void over pipe opening (Figure 2.5). This void can expand with time causing surrounding area to be loosened by washing fine particles with infiltration. This void and loosened region will be expanded

and continued till cavity ceiling is capable to resist against the overburden stress. Once it is failed, ground surface will be sinking in casing road surface to be damaged.

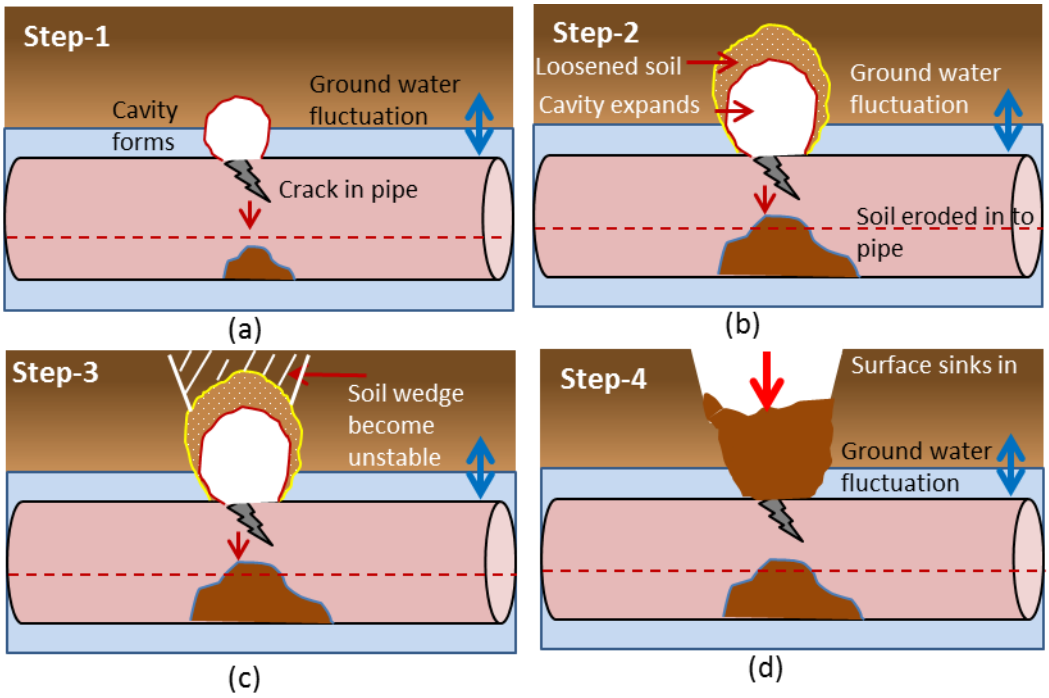

Figure 2. 5: Formation of sinkholes due to leakages of buried sewer/drain pipes

Whenever road cave-in accident is occurred, it is really difficult to find the exact reason for the scenario. One reason is the chance of conducting a detail investigation is mostly impossible due to fast road restoration is required to prevent social inconveniences. Furthermore, sinkhole will mostly destroy all the service lines passing through that point and ground will be congested and difficult to find the exact cause. There can be many reasons to such internal erosion to be taken place. Main reasons will be pipe deterioration with age and poor construction methods. The probability will again depend on size and material of pipe, ground condition and variation of ground water level.

2.2.2. Influence of age of pipe on probability of cave-ins

It is obvious that, there should be a close relation between cave-in probability and age of the pipe since it was buried. This relation was observed by a team of Japanese researches (Kuwano, R 2011) and survey has been conducted in 23 wards of Tokyo; they observed that vulnerability of cave-in is increased when the age exceeds 25-50 years (Figure 2.6). Next problem is most of such infrastructure development was started after the 2nd world war after 1945 in many countries and pipes which exceeding age of 50 years is increasing rapidly (Figure 2.7). Therefore cave-in accidents related with buried pipes are increasing all over the world in recent history.

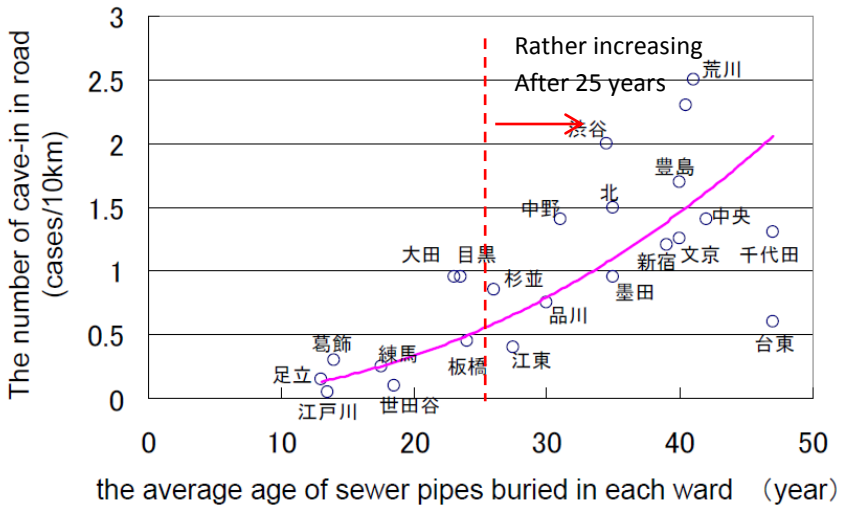

Figure 2. 6: Relationship between age of buried pipe and cave-in (Kuwano, R 2011)

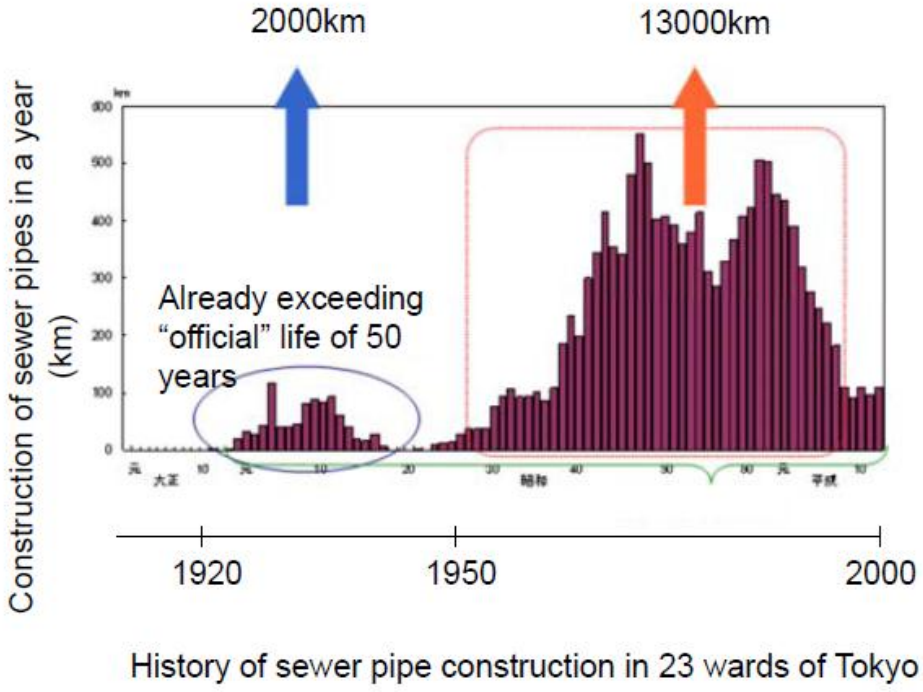

Figure 2. 7: History of sewer pipe construction in Tokyo (Kuwano, R 2011)

2.2.3. Possible motives for sewer pipe defects

Kuwano et al. 2006-A has revealed that there can be many other reasons for pipe defects though it was assumed as age of the pipe would be the main cause. Their survey reveals that (Figure 2.8) number of pipe defects caused by inadequate constructions (30%) is larger than defects caused by natural deterioration (19%). Similarly destruction of pipes when they are crossing each other is also higher due to lack of maps which illustrate the

arrangement of overall lifeline system. Types of pipe defects include similar percentage of pipe failure and gaps between joints due to poor construction (Figure 2.9). Deterioration of steel sewer pipes is always accelerated by chemical reaction with H_2S emitted by of sewer. Therefore, usage of steel pipes for sewerage has reduced in modern constructions.

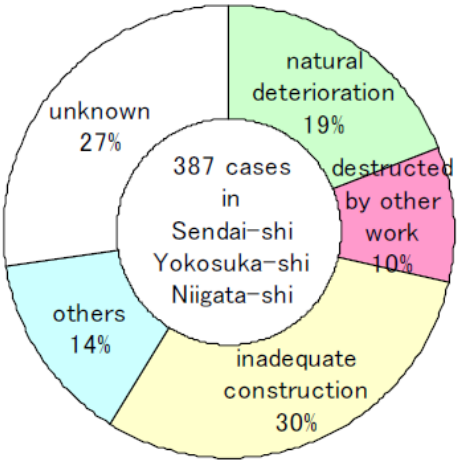

Figure 2. 8: Reasons for pipe defects (Kuwano et al. 2006-A)

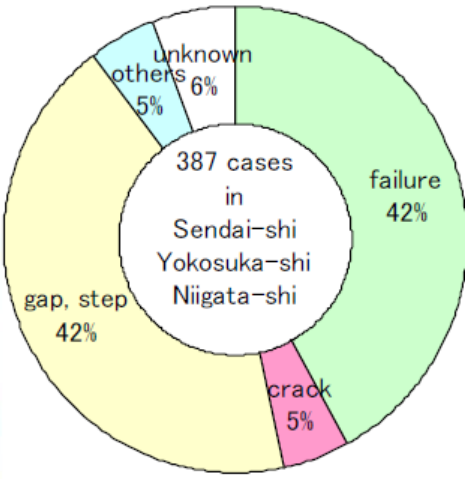

Figure 2. 9: Type of pipe defects

Figure 2.10: Cave-in caused by gap existed in a vinyl Chloride pipe (Kuwano, R 2011)

Figure 2.11: Cave-in caused by corrosion of steel pipe (Kuwano, R 2011)

Figure 2. 12: Sewer pipes have destructed by other pipe lines (Kuwano, R 2011)

Figure 2. 13: A sewer pipe destroyed by a pile constructed for a building (Kuwano, R 2011)

Figure 2. 14: Abundant pipe has not been properly closed or removed (Kuwano, R 2011)

2.2.4. Influence of rainfall on cave-ins

Location of the pipe crack related to the groundwater level is a very important regarding speed of cavity formation. When the pipe defect is above the normal ground water level, chance of water percolation through the defect point is increasing in rainy season. This can happen with rain water infiltration and also fluctuation f ground water level. This fact was further supported by the survey conducted by Kuwano et al. 2006-A. The number of cave-ins occurred in Nagoya-shi, Japan from 1998 to 2000 has been plotted with rainfall data in Figure 2.15. It can be clearly observed that, number of cave-ns has increased in rainy season and just after heavy rainfall.

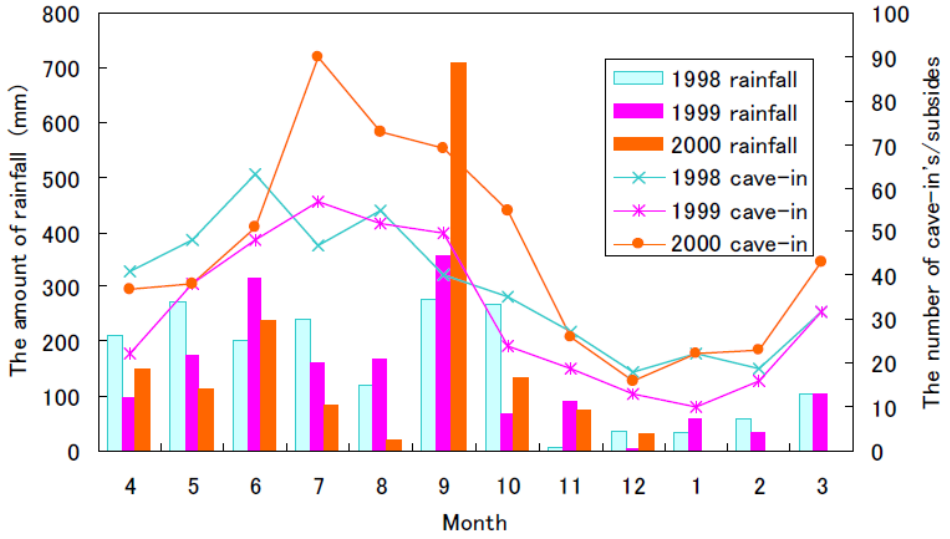

Figure 2. 15: Rainfall vs. number of cave-ins in Nagoya-shi, Japan (Kuwano et al. 2006-A)

2.3. Ground loosening associated with cavity formation

2.3.1. Loosening development for various soils

It was found in the cave-in's survey (Kuwano et al. 2006-B) that small gap/crack of pipes may cause cave-in's in the road and heavy rainfall was one of the most important factors. Following these facts, a series of model tests had been performed by Sato, M and Kuwano, R 2008, observing outflow of soil through 5mm opening in the bottom of a soil chamber. The model apparatus used for that study is shown in Figure 2.16 with dimensions. A cavity and associated loosening has been formed above the 5mm opening at the model base, by water flowing in and out repeatedly.

Two sandy materials which have different grain size distribution have been used. One is Toyoura sand, clean uniform fine sand, and the other is natural sand which contains fines of around 10%. Result shows, loosening speeded in different manner in two types of sand and uniform grain size sand shows rapid and expanded loosening behaviour than sand which has 10% of fines. But, the volume of cavity created is smaller in Toyoura than natural sand. Which means the density reduction or loosening is larger in natural sand which can be due to escaping or washing out of fines from loosened region. Same author has found that, when the fine content is over 20%, fines has resisted against sand washing away from ground.

When the sand and gravel is mixed loosening has spread much faster by erosion of sand while gravel stays stable with holding the whole soil skeleton (Kuwano, R 2011). Model tests conducted related to that study is shown in Figure 2.18. Furthermore speed of expansion of loosening is comparatively larger in gravel soil than natural sand with 10% of fines.

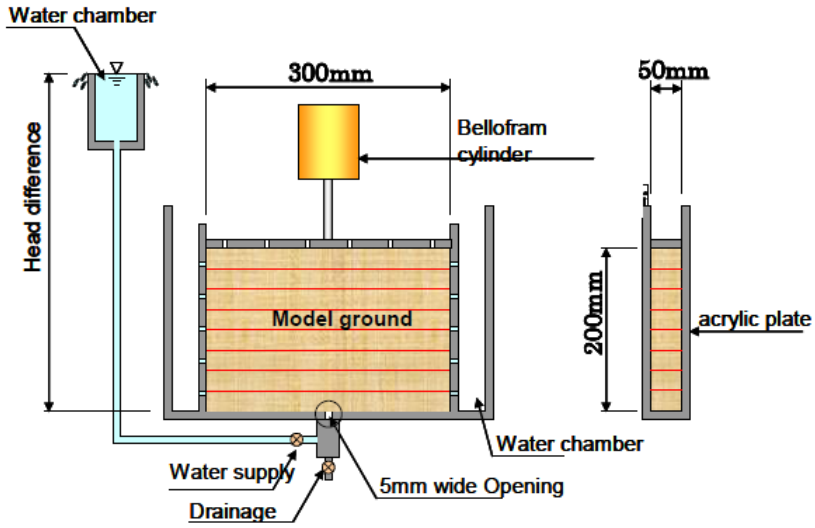

Figure 2: Model test apparatus for generating cavity/loosening in soil

Figure 2. 16: Model test apparatus for generating cavity and loosening (Sato, M and Kuwano, R 2008)

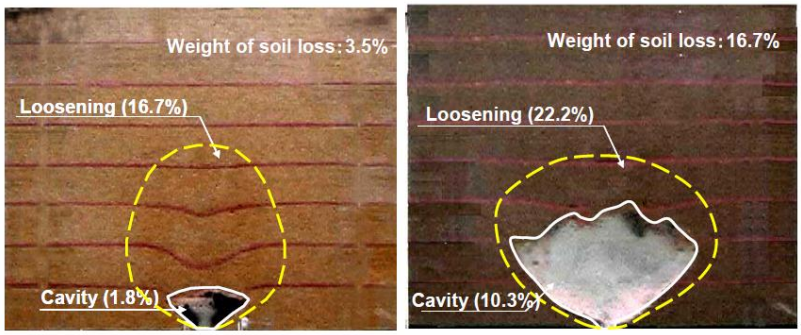

(a) Toyoura sand after 3 cycles (b) Natural sand after 13 cycles

Figure 2. 17: Cavity and loosening for different sands (Sato, M and Kuwano, R 2008)

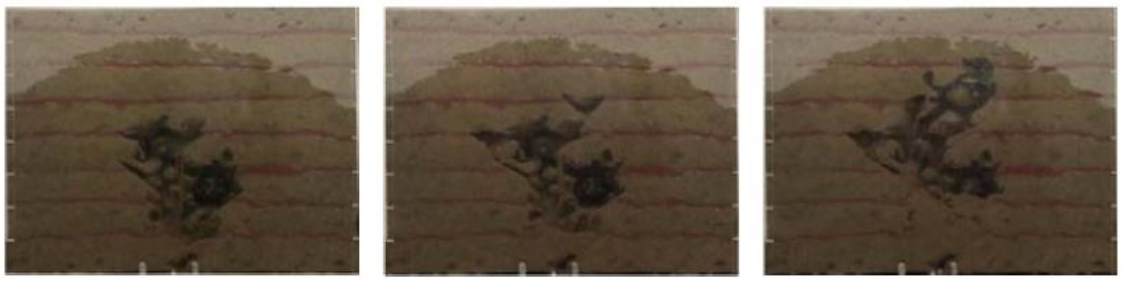

Figure 2. 18: ground loosening observed in sandy gravel (Kuwano, R 2011)

2.3.2. Observation of cavity and loosening by X-ray CT

Formation of cavity and propagation of loosening related to a pipe defect was discussed in two dimensional model tests. However, in reality condition and extend of loosening can be different from two dimensional manner. Therefore Kuwano, R 2011 has observed the 3-dimensional behaviour of cavity formation through X-ray CT images. Cylindrical soil chamber (130mm in diameter and 100mm in height) has been used with 5mm square opening at base. Water has been flown in and out to create loosening and after three cycles loosened region was observed as in Figure 2.19. It shows loosening is always propagated after each cycle of water as non-uniform manner. Even by a small opening of 5x5mm has caused a smaller cavity, but with highly expanded loosening (10-15 times cavity height) in uniform sand. Similar test has been conducted for natural sands (Figure 2.20) and loosening has not spread widely as Toyoura sand.

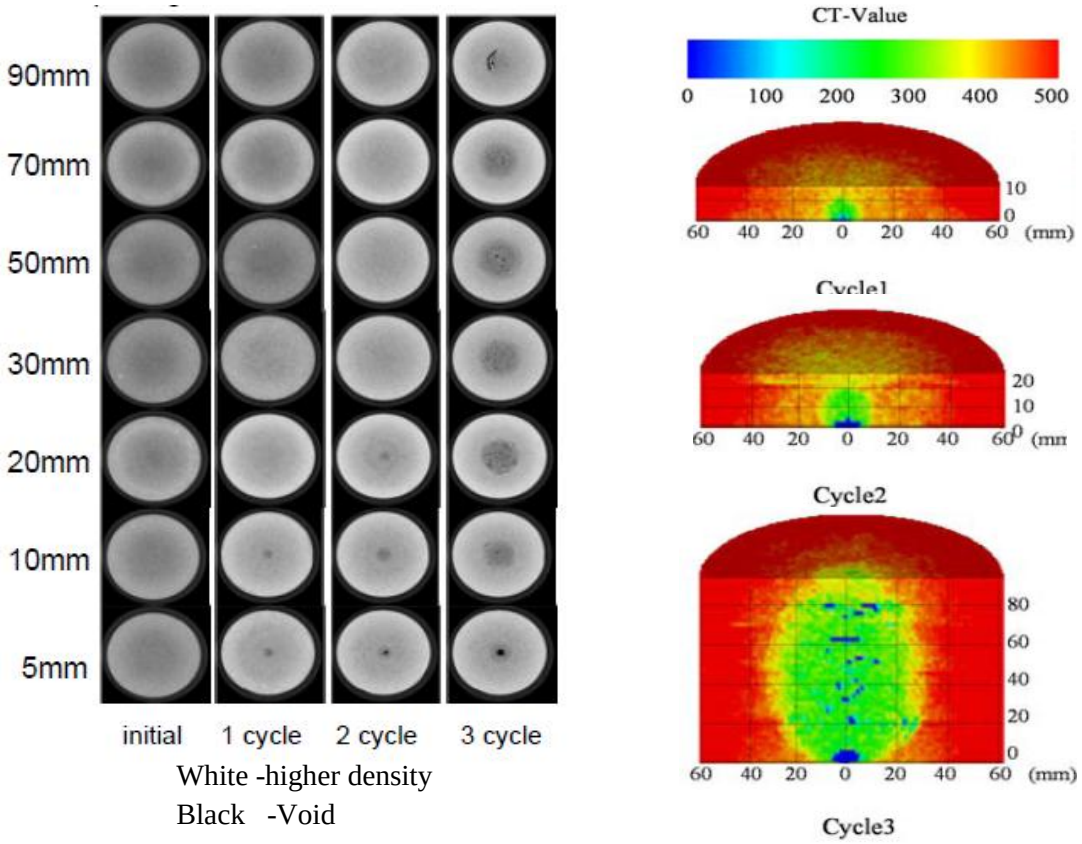

Figure 2. 19: Cavity and loosening development for Toyoura sand (Kuwano, R 2011)

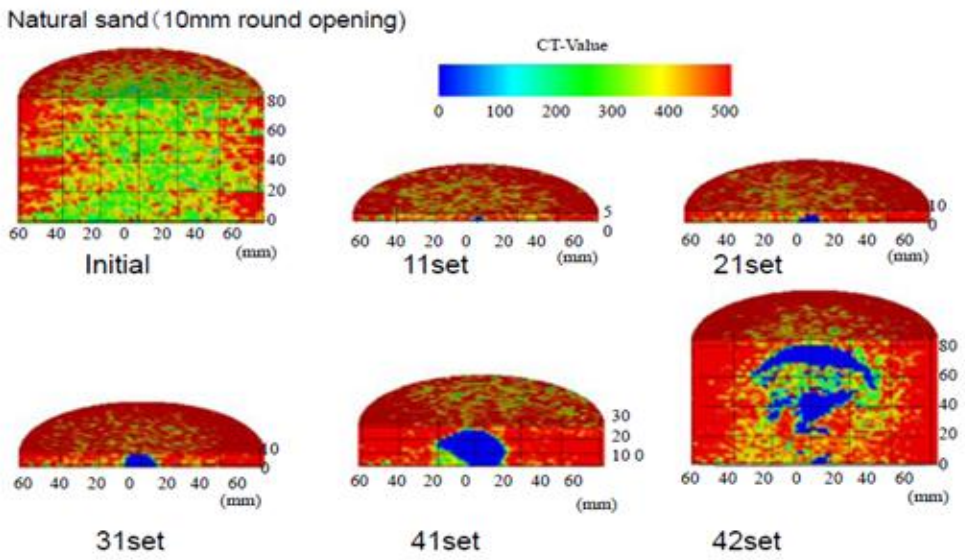

Figure 2. 20: Cavity and loosening development for natural sand (Kuwano, R 2011)

Furthermore, Cavity and loosening formation with respect to the shape of the defect has been observed by a simple model test with Toyoura sand as shown in Figure 2.21. Circumferential and longitudinal shape cracks has simulated by a 5mm wide opening created on pipes as shown in Figure 2.22 and Figure 2.23(Kuwano., 2006-c) . Three water cycles has flew in and drained out from the opening at the bottom. Each cycle carries 100ml. Then the soil behaviour was visualized and volume of the cavity is compared to the diameter of the pipe. Results show the mechanism of cavity generation was affected with the shape of defect but the degree of cavity generation was constant for both defects.

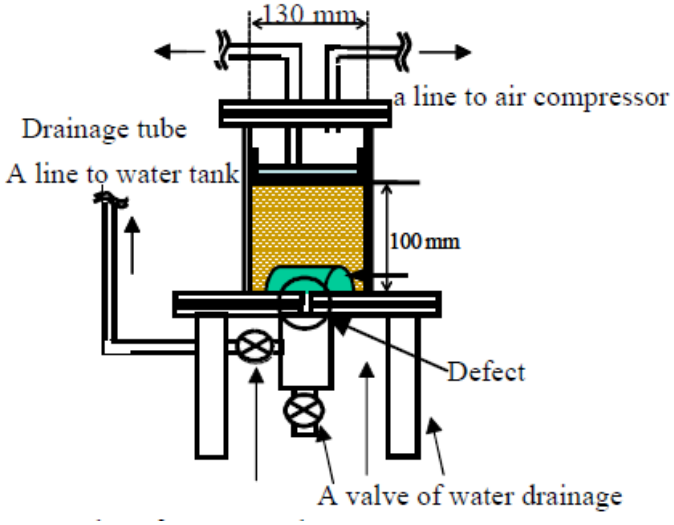

Figure 2. 21: Schematic diagramme of test apparatus (Kuwano, R 2011)

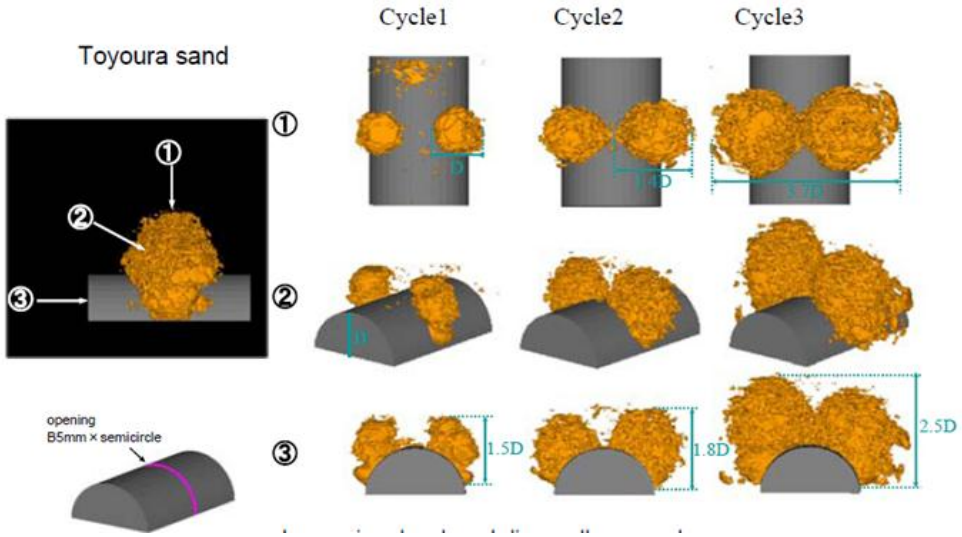

Figure 2. 22: Loosening developed by circumferential crack in a pipe (Kuwano, R 2011)

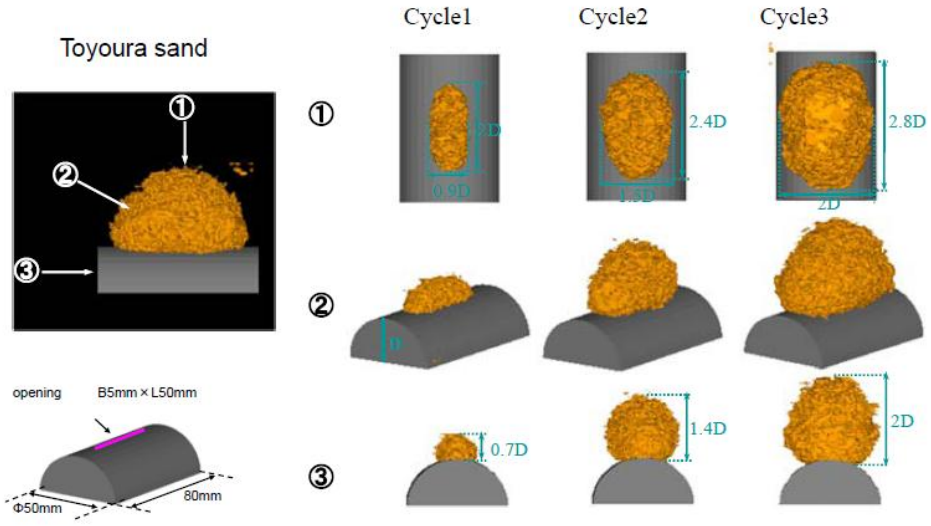

Figure 2. 23: Loosening developed by longitudinal crack in a pipe (Kuwano, R 2011)

2.3.3. Ground water seepage and expansion of cavity

Direction of underground water seepage can be different and it depends on many local factors. During rainy season, rain water infiltrates and flows down under gravity. Meanwhile groundwater table is also increasing and seepage can be even horizontal. Therefore, there can be a relationship between water seepage direction and cavity expiation. This was analyzed by (Sato, M 2011) using model tests with changing the seepage direction. It is clearly observed that expansion of cavity depends on the ground water level and the direction of seepage (Figure 2. 24).

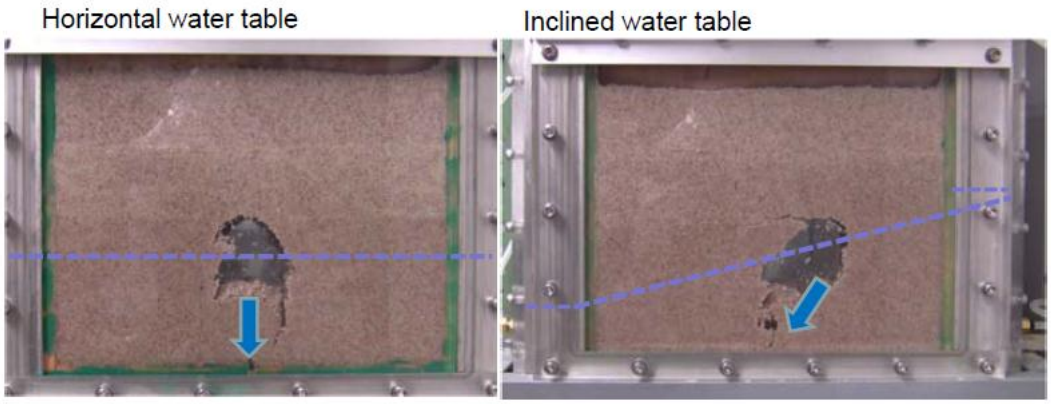

Figure 2. 24: Relationship with cavity expansion and direction of seepage

2.3.4. Influence from buried structures on cavity formation

There are many abundant and functioning underground structures such as tunnels, oil tanks, septic tanks, storages, etc. Soil structure interaction with such structure can support to originate some voids which can be a cave-in with time. This effect has been observed by Sato, M 2011 in her master studies by using 2-D model tests. Toyoura sand has used and buried structure has represented by a wooden block as shown in Figure 2.25. Internal erosion has been created by water flowing in and out by 5mm wide opening at base bottom.

Figure 2. 25: Cacity formation and buried structues

2.3.5. Cavity formation in granular backfill behind a seawall due to seawall defects

Other than the defects on buried pipes one direct cause of forming cave-ins in coastal region is defects develops in vertical sea walls. Obviously, top layer of backfill behind the sea wall is unsaturated and located above the ground water table, which has characteristic profiles of suction. Suction value depends on degree of saturation and intensity of capillary actions. Rebar corrosion, steel pile corrosion can develop small cracks and holes in sea walls which makes it permeable. In such cases ground water level fluctuation, infiltration, ground vibration can trigger fine particles of backfill behind the sea wall to be washed out and cause internal erosion. When this process continues for a long time, eventually it can

create cavities and finally ground subsidence. This phenomenon was studied by Sekiguchi et al. 2003. In order to observe the effects of suction on formation of cavities and their stability, model tests with simulating a vertical sea wall with a small aperture below the mean sea level has been observed as in Figure 2.26. Silica sand and water is placed in a glass flume and they are separated by a vertical partition of Perspex which has a small aperture. Once sand is placed, three tensiometers have set above the water table to measure the suction variation. Then the water is flown in to model such a way that water level reaches the specified level while the aperture is sealed. Once water reached above the aperture, seal has been removed and it has observed that, sand washed out through the aperture and created a cavity as shown in Figure 2.27. Variation of suction during cavity development is different in three tensiometers (Figure 2.28). Location C shows increment in suction till crack is developed in sand, with soil washing out through the aperture. When this crack was developed to bring enough seepage through the aperture, progressive cavity expansion has observed; which has caused to reduce the suction. This simple model tests explain the importance of studying the suction properties during cavity formation

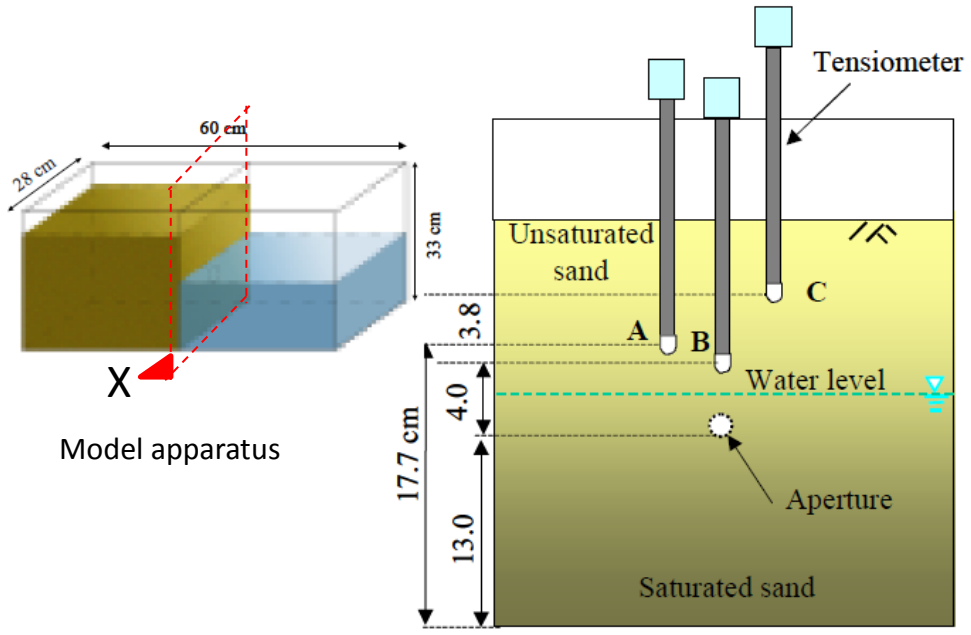

Figure 2. 26: Model apparatus simulating a vertical sea wall with a defect (Sekiguchi et al. 2003)

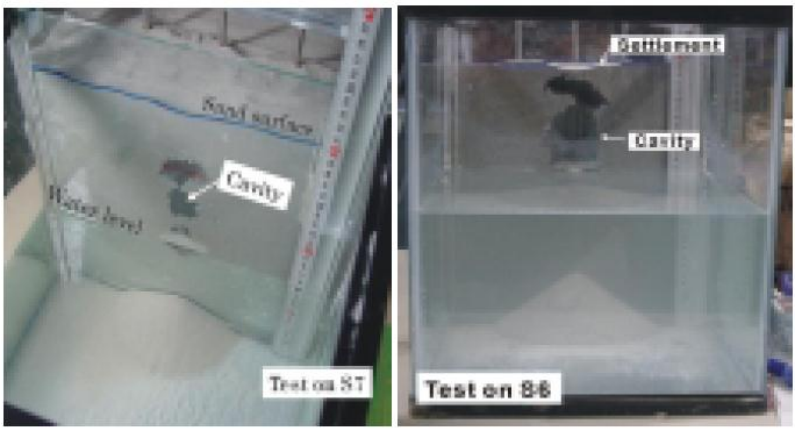

Figure 2. 27: Wall defect has caused cavity in granular backfill (Sekiguchi et al. 2003)

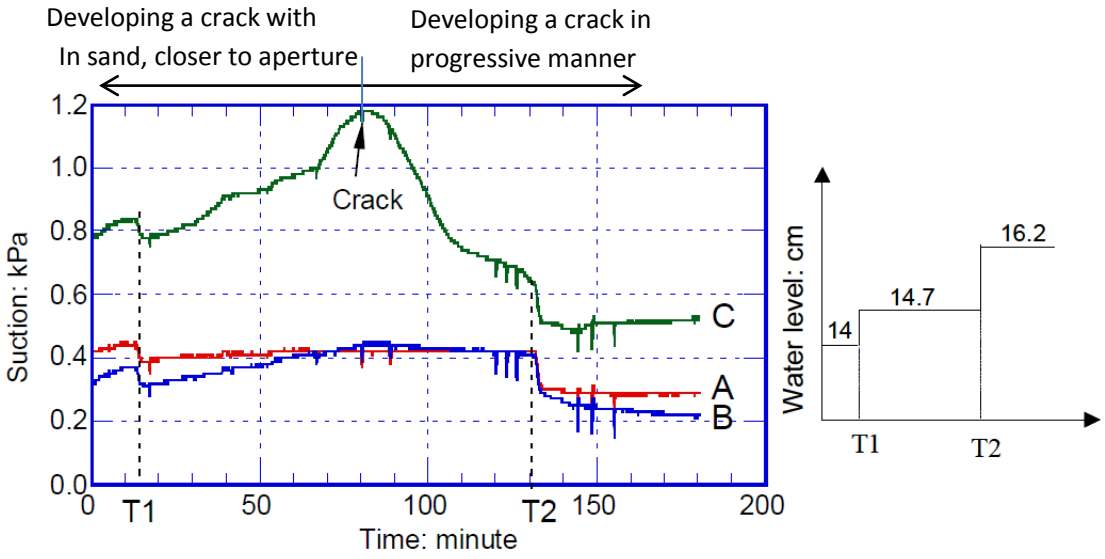

Figure 2. 28: Variation of suction during cavity formation (Sekiguchi et al. 2003)

2.3.6. Soil: structure interaction and collapse of cavities

Most cave-ins show various impacts on the existing structures standing on ground surface. Therefore it is important to study the impact of cavity collapse on buildings. This has been studied by Caudron et al. 2006 by conducting physical and numerical models. A model ground with rigid steel U shape frame has been used with a special device (Nakai et al. 1997) to create the cavity in a controlled manner in several steps (Figure 2.29). Arrangement for cavity creation has facilitated with ten small pieces (width of 25mm for each, together maximum width becomes 250mm, height can be 25, 50, 75 or 100mm) which can be moved down in order to open the cavity step by step, till the failure is achieved. Building model is designed to represent a simple structure with elastic behaviour as its stiffness and its dimensions follow the scale factors. Schematic figure of the building

model is shown in Figure 2.30. Building model is equipped with strain gauges and displacement sensors.

Analogical soil is used with metallic rods with 3 different sizes; 3, 4 and 5mm of diameter. Cohesive soil has been created above the cavity by soaking the connecting rods in an aqueous solution of glue followed by dehydration.

Two tests have performed as green field condition without building model and next are placing it on ground surface. First, stable cavity with 250mm in width and 50mm in height is created by moving the concerned pieces. Each moving piece is equipped with small force sensor in order to measure the variation of forces applied by soil. Soil mass movement is followed by Particle Imagery Velocimetry (PVI) supported by high definition images taken during the test. After soil deformation is observed with creating the cavity, water is infiltrated drop by drop on the center of cavity roof until sinkhole expands towards the top of surface with causing failure.

Result shows, test without building model has no significant ground movement before weakening the cavity top by adding moisture while different behaviour was observed in other test (Figure 2.31). In the test with building model, failure of cavity was more sudden and cohesive layer has break and fall into cavity. Comparison of subsidence in two tests is different to each other as shown in Figure 2.32.

Results show that, in both cases subsidence is significant and damageable to the building. However, it is clear that it would be cost effective to consider the soil-structure interactions when designing the buildings in sinkhole prone areas.

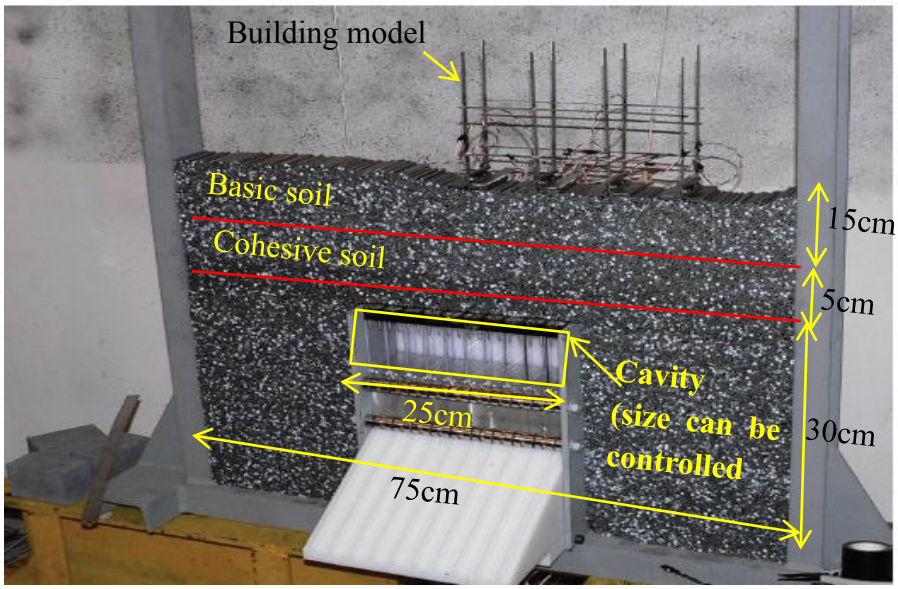

Figure 2. 29: model apparatus with arrangement of controllable cavity and scaled down building model (Caudron et al. 2006)

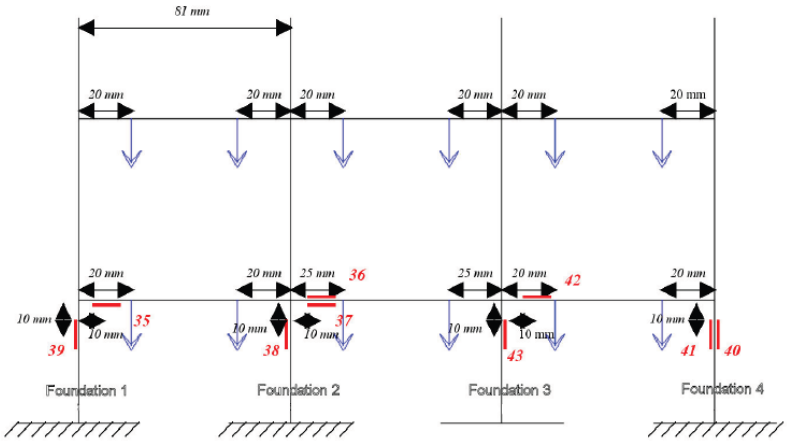

Figure 2. 30: Schematic of building model (Caudron et al. 2006)

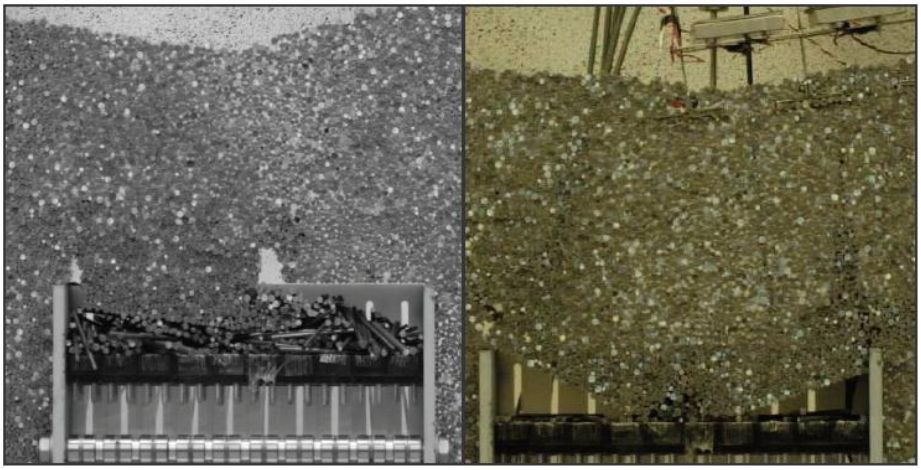

Figure 2. 31: Difference of failure type (left-no building model, right –with building model)

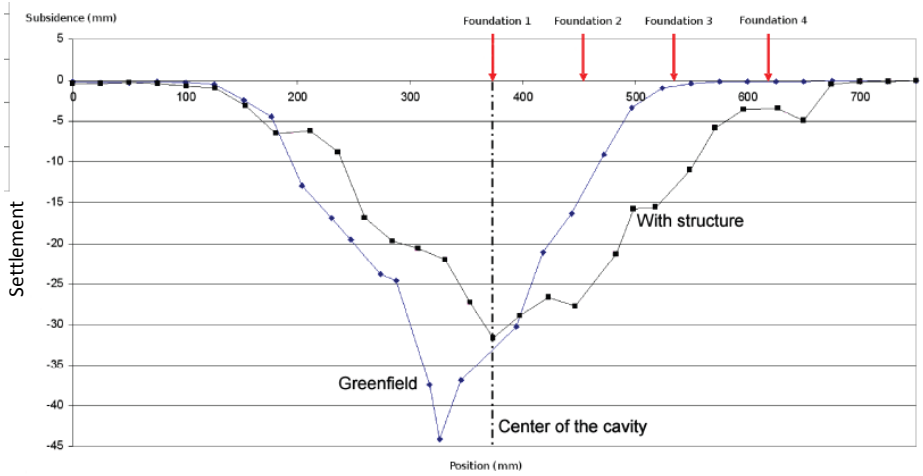

Figure 2. 32: Comparison of the subsidence between Greenfield and with the building model –Red arrows represents the location of four foundations (Caudron et al. 2006)

2.4. Modern techniques to detect underground cavities

2.4.1. General

Detection of exist underground cavities are essential to prevent cave-in accidents, as well as to make cost effective designs. Many construction projects had to modify after finding cavities after starting excavation works. In such a case, modification of foundation design is essential, though it cause delay in completion as well as increase the cost. Furthermore, very old sewer and drain pipe systems in urbanized areas are common in all over the world, which needs to be rectified. These kinds of works become much easier if they can confirm the existence of underground cavities.

Conducting bore hole survey was the cheapest option to check the existence of cavities before starting a project. This method is still using in Karst areas, since lime layers are expanding over long distance. However, this is not accurate enough or user-friendly to check the sewer systems or large area of land. Recently, imaging subsurface by geophysical surveys has become very famous to detect underground voids. All of those techniques are based on physical contrast between void and surrounding soil. Among these, geoelectric tomography and Ground Penetrating Radar (GPR) is widely used in modern industrial applications.

2.4.2. Geoelectric tomography

Geoelectric tomography is the imaging of distribution of electrical resistivity in a body by injecting currents across many different couples of electrodes. ("Geoelectric Tomography" 2006). This can be used to detect the voids by measuring lateral and vertical changes in electric resistivity of subsurface; because electric resistivity of void is higher than soil. This principle of air filled cavity detection by using the difference in electric resistance between a cavity and limestone was proposed by Palmer, 1959. Similar principle is currently applying to distinguish the air-filled voids from different soil. The electrical resistivity method employs a direct current (DC) applied to a pair of electrodes in contact with the ground; the voltage or electrical potential is measured between a second pair of electrodes. Data can be collected by use of automated resistivity measurements, which allow placement of multiple electrodes at equal spacing along a survey line. Each electrode is connected to a computer-controlled device that sequences electrical pulses between selected combinations of electrode configurations. The applied current, the resulting voltage potentials, and the electrode geometry are recorded by software. In general, the greater the distance between electrodes, the greater the depth of current penetration. Larger electrode spacing in an array gains more depth of penetration, and a smaller electrode spacing gains more resolution. Location of electrodes and obtained apparent resistivity is illustrated by a sample result in Figure 2.33. (Use of Electrical Resistivity to Detect Underground Mine Voids in Ohio, 2002). Furthermore, Figure 2.34 illustrates some results obtained room an investigation carried on suspected underground mine-void complex with electrical resistivity along State Route 32 in Jackson County, Ohio.

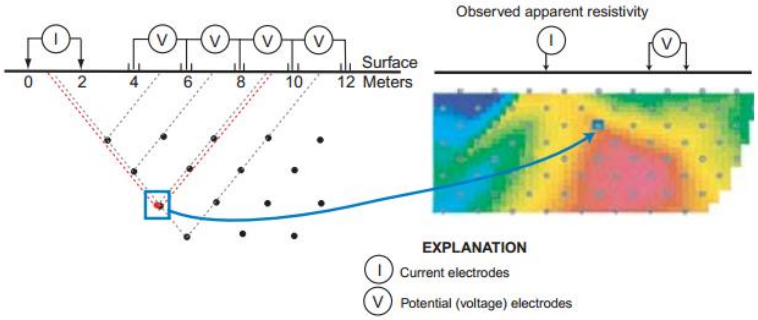

Figure 3. Pseudosection by use of axial dipole-dipole array configuration (Oldenburg and Jones, 1998). The resistivities in the pseudosection are contoured; in many cases, pseudosections are color contoured so that high resistivities are "hot" colors (red) and low resistivites are "cold" colors (blue).

Figure 2. 33: Pseudo section by use of axial dipole-dipole array configuration (Oldenburg and Jones, 1998)

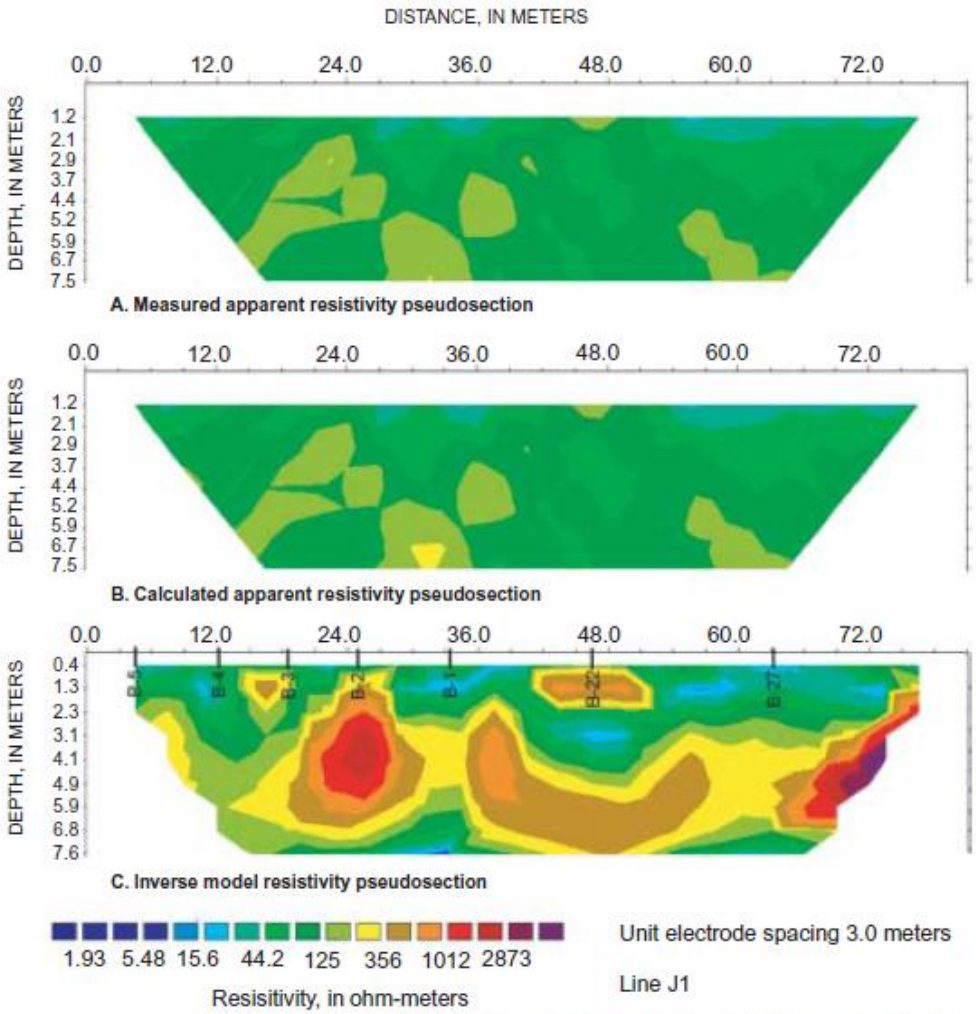

Figure 4. Dipole-dipole resistivity survey results along State Route 32 in Jackson County, Ohio. High- resistivity anomalies (>1,000 Ω•m (ohm-meters); for example, at approximately 26 meters horizontal and 3.5 meters vertical in the inverse section (C)) are interpreted to be air-filled mine voids. Locations of borings also are shown on the inverse model section.

Figure 2. 34: Sample geoelectric resistivity survey (Use of Electrical Resistivity to Detect Underground Mine Voids in Ohio, 2002)

2.4.3. Ground Penetration Radar (GPR)

GPR system is another well famous and useful technology use in modern industry to detect underground voids. It is based on detecting of reflected short pulse electromagnetic radar energy which is transmitted into the ground. Short pulse means high frequency (10-1000 MHz) and propagation of this radar signal depends on high frequency electric properties of the ground. In practice, waves are transmitted into the subsurface by portable emitting antenna. Once a wave strikes an object, part of the wave is reflected back to the receiving antenna. Measurements can be continuously recorded with a higher resolution. Conceptual illustration is given in Figure 2.35 (Gad et al. 2005).

Changes in the ground material at layer boundaries cause transmitted signal to be reflected in a different manner. Power of the reflected radar, radar signal velocity and the attenuation depend on the dielectric constant or relative permeability of the material. Table 2.1 lists some geological materials with their dielectric constant, velocity, conductivity and attenuation at radar frequencies.
Range of the GPR is highly limited since energy of the transmitted waves is absorbed by ground material. This absorption is smaller for material such as granite, dry sand, snow and water. Therefore GPR will penetrate much deeper (still few meters) than materials like some clay, which absorbs much electromagnetic energy (Davis J.L. and Annan A.P. 1985). Sample radar received by antenna above a cave exists in karst area is shown in Figure 2.36. Some, distortion of radar is recorded at the boundary of the cave and surrounding soil.

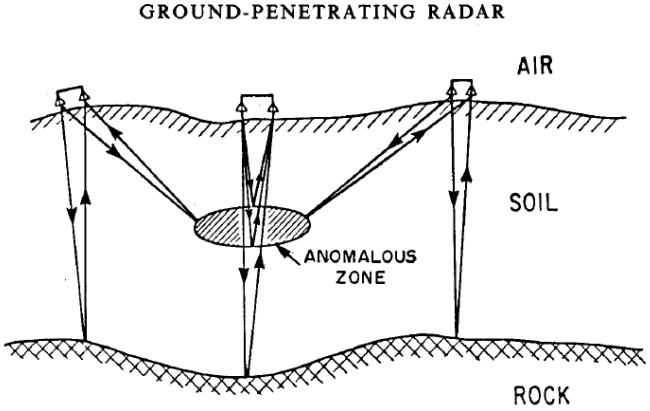

(a) Conceptual illustration of the radar being used in the reflection profiling mode over bedrock

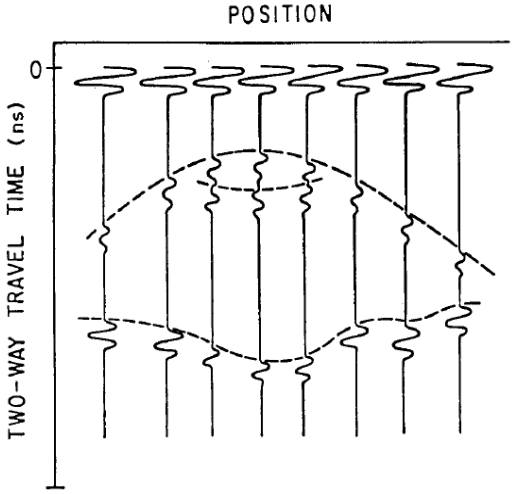

(b) Resulting radar record obtained over the idealized situation in (a)

Figure 2. 35: Conceptual illustration of GPR system (Davis J.L. and Annan A.P. 1985**)**

Table 2. 1: Typical dielectric constant, electrical conductivity, velocity and attenuation observed in common geo materials (Davis J.L. and Annan A.P. 1985)

Material	K	σ (mS/m)	V (m/ns)	α (dB/m)
Air	1	0	0.30	0
Distilled water	80	0.01	0.033	2×10^{-3}
Fresh water	80	0.5	0.033	0.1
Sea water	80	3×10^{4}	0.01	10^{3}
Dry sand	3–5	0.01	0.15	0.01
Saturated sand	20–30	0.1–1.0	0.06	0.03–0.3
Limestone	4–8	0.5–2	0.12	0.4–1
Shales	5–15	1–100	0.09	1–100
Silts	5–30	1–100	0.07	1–100
Clays	5–40	2–1000	0.06	1–300
Granite	4–6	0.01–1	0.13	0.01–1
Dry salt	5–6	0.01–1	0.13	0.01–1
Ice	3–4	0.01	0.16	0.01

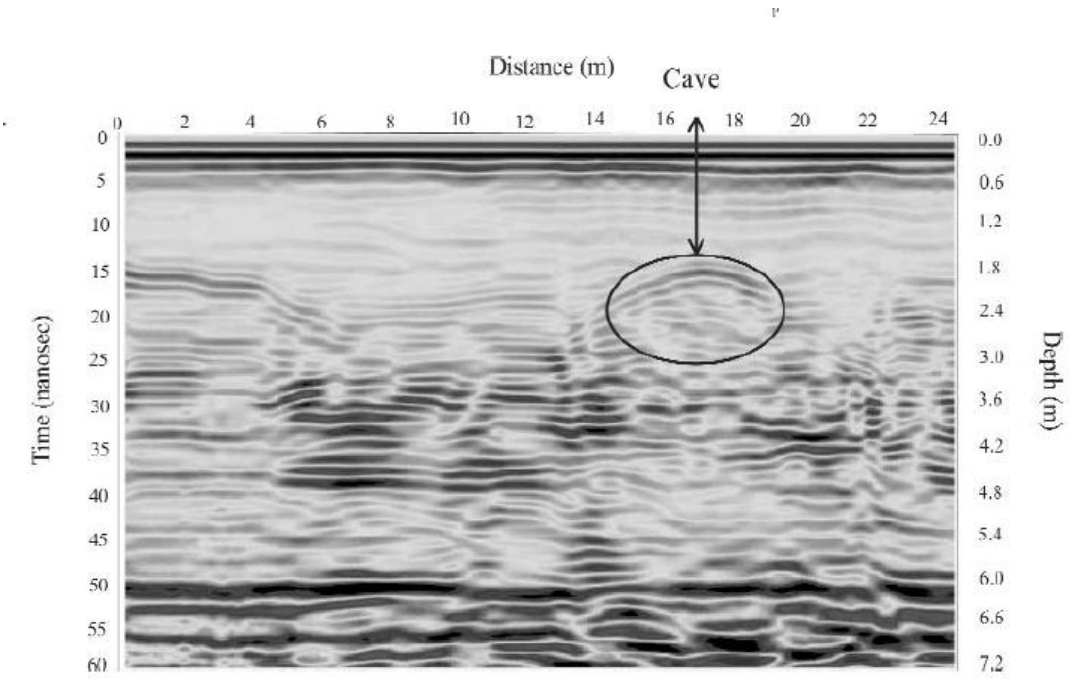

Figure 2.36: Sample radar recorded in ground with a cave (Gad et al. 2005)

Limitations of GPR technique

- Maximum applicable depth is only about 15 m in granular material and this depth highly depends on electric conductivity of soil. For high conductivity materials like clay having high moisture content this is limited to 1-1.5 meters.
- Normally these results are highly subjected to noise due to disturbances caused by buried objects such as boulders, animal skeletons and tree roots. An unnecessary reflection receives and scattering occurs due to such objects. Therefore it is very difficult to identify and confirm a cavity due to these reasons.
- GPR records can be further disturbed by other electromagnetic transmissions used by cellular telephones, radios, television, and microwave transmitters. Such unnecessary reflections can be limited by shielded antenna into some extent.
- Unprocessed raw data is noisy and mostly difficult to accurately confirm presence of a cavity. Sophisticated image processing is required which consumes time and rigid computer software.
- This method is expensive and still difficult to apply in developing countries.
- Since voids are not fully filled with air, it becomes complicated to identify such cavities with loosening.

CHAPTER -03

Testing Apparatuses and methodology

3.1. Introduction and research design

Ultimate objective of the research is to analyze the mechanical properties of loosened sand associated with underground cavities by laboratory experiments. The procedure of developing the research methodology is shown in Figure3.1.

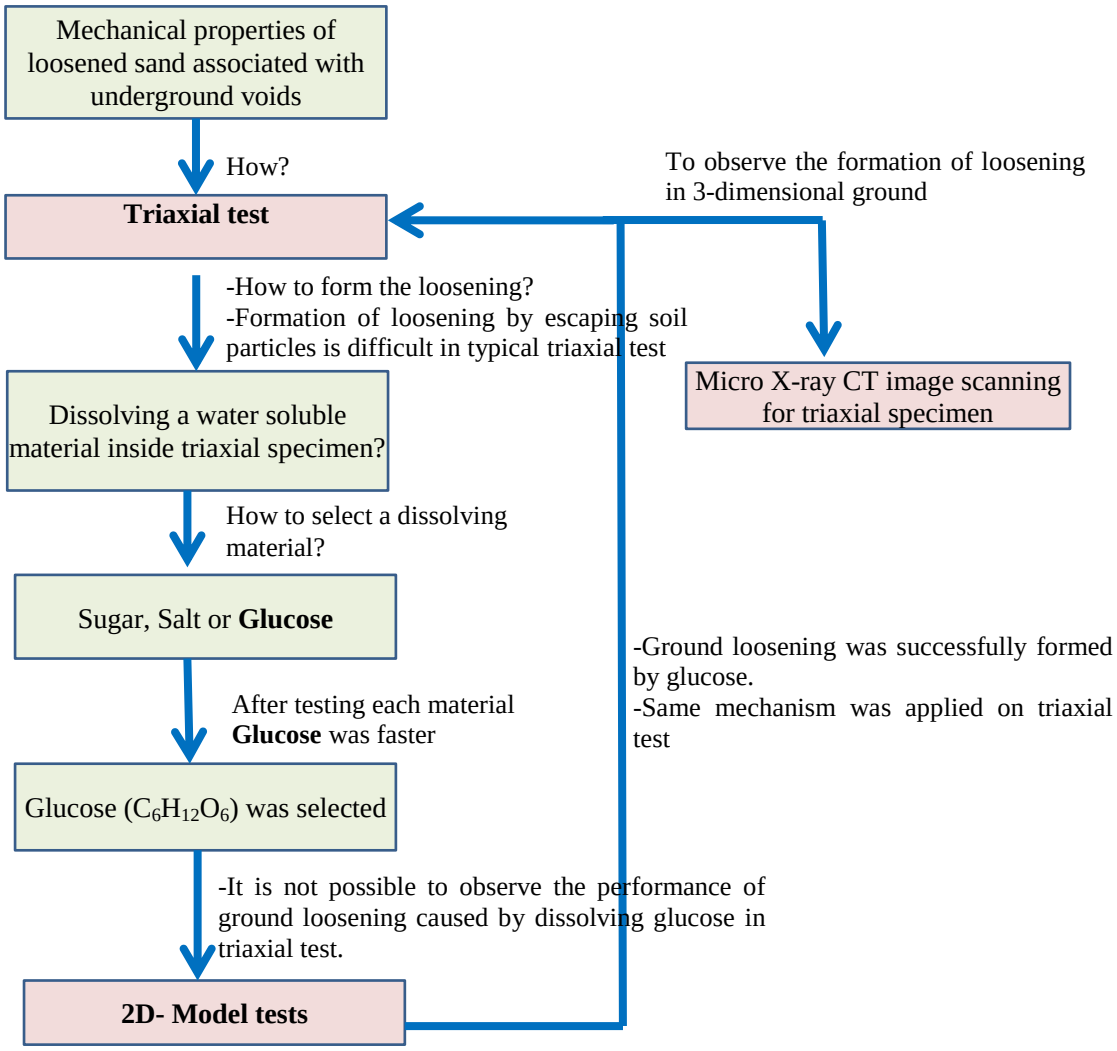

Figure 3.1: Design of experiments

The methodology was developed after solving important issues and making key decisions.

1. In order to find the properties of loosened sand, triaxial apparatus might be a good tool, since it has many advantages.
    a. The boundary conditions of stress in both horizontal and vertical directions are known. But in the general model tests, stress in horizontal direction is unknown. However, in both cases, the strains at both vertical and horizontal directions can be measured.
    b. Plane strain test can be used and the deformations can be analyzed by image analysis.
    c. Gravity model (1g) can be used for more accurate and reliable results. But, it is possible only to observe the behaviour of cavities at shallower depth. In the history, it has been experienced many cave-ins which are initiated at very deep locations. (>5-10meters) In order to represent such conditions in 1g model, the model will become very big and expensive. But in the triaxial test, effect of loosening and cavities at deeper locations can be analyzed easily by increasing the confining pressures.
    d. Centrifuge test is another good tool to observe the properties even at deep ground, and it will scale down the model ground in to smaller size. But, the particle size effect will highly affect the results.
2. There should be a mechanism to artificially form the ground loosening associated with cavities in triaxial test.
    a. One possible way is, to allow sand particles to escape from specimen during the drainage and form the loosening and internal erosion at bottom of the specimen. However, smooth escaping of sand through the drainage valves is not possible in typical triaxial apparatus.
    b. The other way is to use a water soluble material inside the specimen and dissolve it by inserting water. Then a cavity and loosening might be formed.
3. Therefore few water soluble materials (Sugar, Salt and Glucose) were tested by dissolving in Toyoura sand. Glucose showed better and faster results. So, it was decided to use glucose for this test series.
4. By directly testing or implementing this method in triaxial apparatus, doesn't allow observing the ground deformations caused by dissolving glucose. Therefore, it was decided to perform some two dimensional model tests with acrylic walls to confirm whether the mechanism is working or not.
5. Then series of model tests were done by dissolving glucose in Toyoura sand. It was found that the glucose was dissolved by causing ground deformation around the initial glucose block
6. Once the mechanism was confirmed by model test, it was decided to conduct the Triaxial test with forming loosened soil by the same mechanism and to find out the variation of strains, stress and stiffness of such soil.
   The imagined phenomenon of loosening in triaxial specimen during the test is shown in Figure 3.2.

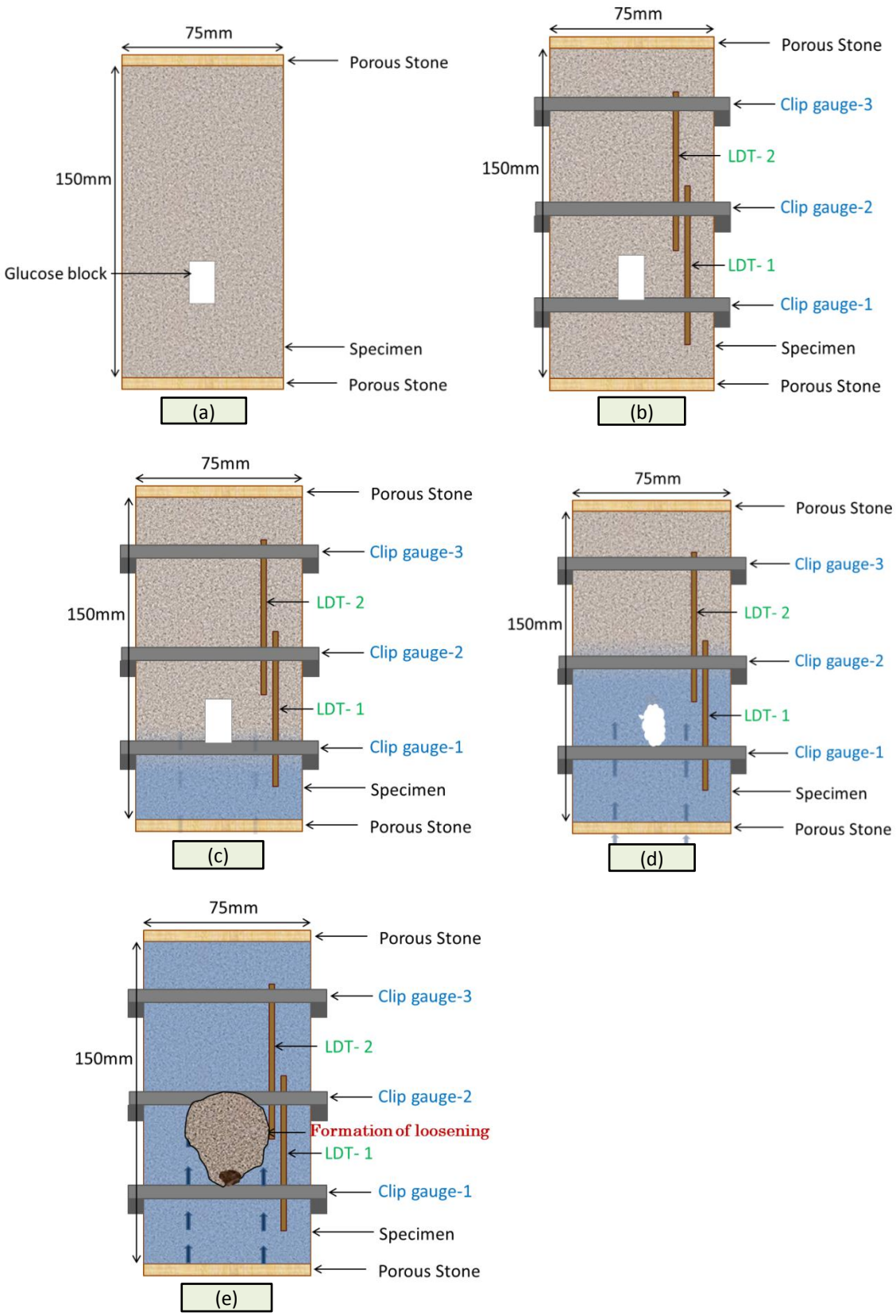

Figure 3.2: Imagination of forming ground loosening in triaxial apparatus (a) Erected specimen, (b) After fixing the LDTs and Clip Gauges, (c) Inserting of water, Dissolving of glucose, (e) After forming ground loosening around initial glucose block

7. Although, many triaxial tests were conducted, There was no exact and clear idea about extends of loosening. Because, the deformation or extends of loosening can be different in three dimensional case than what was observed by two dimensional model test. Hence, decision was finally made to observe the X-ray CT images for one entire triaxial test.

3.2. Material properties

3.2.1. Toyoura sand

Toyoura sand was used as the principle testing material in this research. Toyoura sand is a widely used testing material in Japan which is clean, fine-grained and uniformly graded sand with angular and sub-angular particle shapes. It was originated from Toyoura Beach area of Yamaguchi prefecture, Japan. It is standard sand used in geotechnical and concrete engineering laboratories in Japan and well accepted all over the world. It looks light yellowish- brown in color and well sorted. It is derived from the siliceous rocks and shale hence it contains well rounded quartz particles. Toyoura sand of batch "H" in IIS lab was used and a photograph of the Toyoura sand is shown in Figure 3.3 and its physical properties are shown in Table 3.1.

3.2.2. Silica sand

Silica sand is one of the popular varieties of sand in the world and also produced by degradation of quartz. The quartz crystals are broken down into small grains as Silica sand. The grain size of Silica sand varies from fine to coarse. In this study, Silica sand (No. 5) was used and a photograph of silica sand is shown in Figure 3.4 and physical properties are shown in Table 3.1 Furthermore, particle size distribution of both Toyoura and Silica sand is shown in Figure 3.5.

Table 3. 1: Properties of Toyoura sand and Silica sand

Property	Toyoura sand	Silica sand
Specific gravity – *(Gs)*	2.621	2.640
Mean particle Diameter- (D_{50}) *(mm)*	0.196	0.450
Maximum void ratio (e_{max})	0.946	0.787
Minimum void ratio (e_{min})	0.637	0.538
Coefficient of uniformity (*Uc*)	0.146	-
Fines content (%)	0.100	-

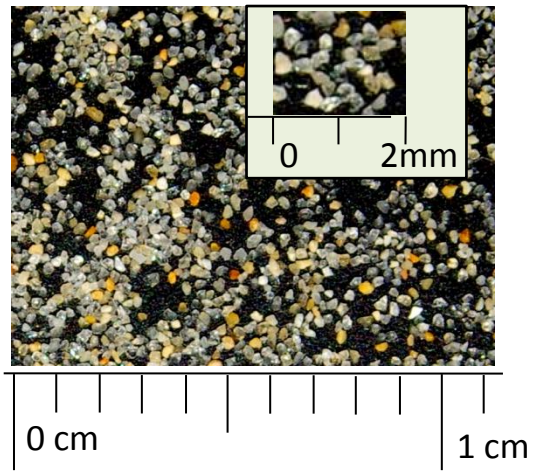

Figure 3. 3: Toyoura Sand

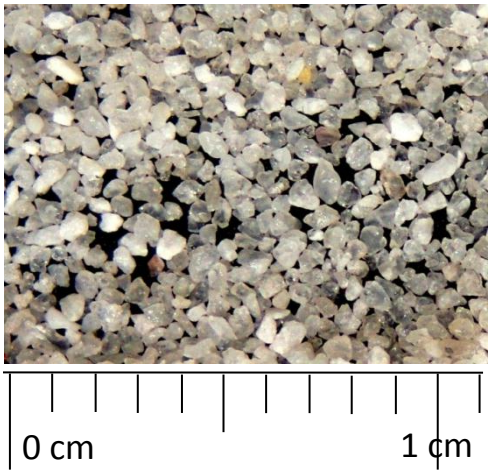

Figure 3. 4: Silica Sand

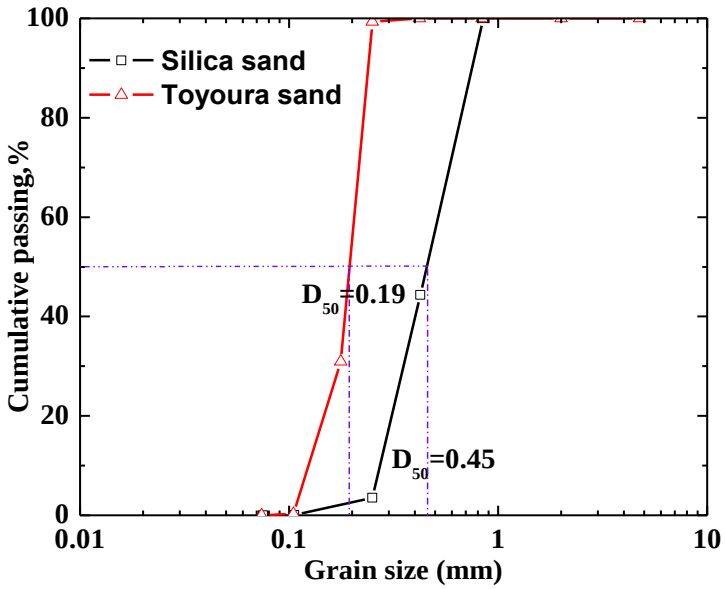

Figure 3. 5: Grain size distribution of Toyoura and Silica sand

3.2.3. Glucose ($C_6H_{12}O_6$)

The concept of forming a ground loosening by water soluble material was examined with different materials such as sugar, salt and glucose (Renuka & Kuwano, 2011). Glucose ($C_6H_{12}O_6$) was found to be the fastest dissolving material and selected as the best available material to create an artificial ground loosening. The cavity was represented by a cylindrical glucose block which was casted by compacting Glucose paste produced by mixing glucose powder with nearly 5% of water, in a hollow steel pipe. By changing the diameter of the mould, it was able to produce such blocks in different sizes (Figure 3. 6). Basically two sizes of glucose blocks were used for this study. Smaller one was with

1.2mm in diameter and 15 mm in height which has 0.25% of specimen volume. The larger one is 30mm in diameter and 15mm in height having 1.5% of the specimen volume.

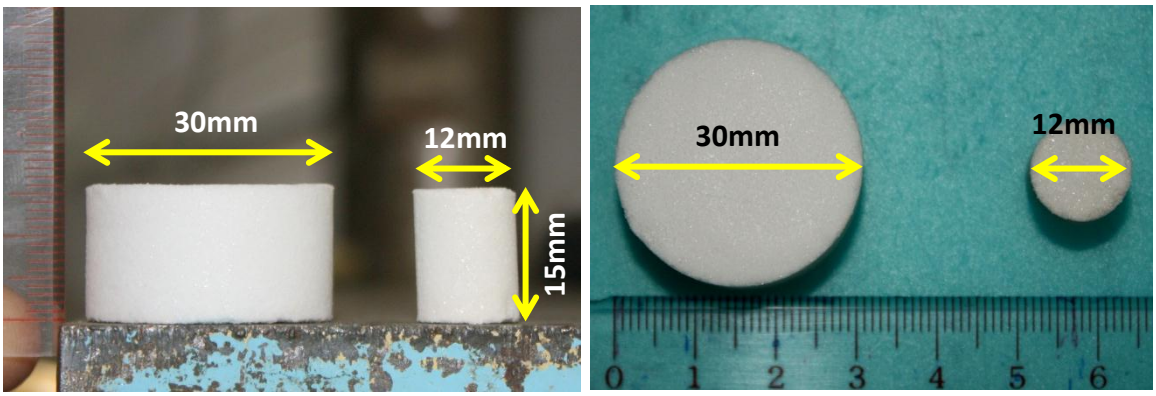

Figure 3. 6: Glucose blocks

3.3. Apparatus and testing procedure- Model Test

The purpose of this model test is to find a way of forming artificial ground loosening associated with underground cavities. The mechanism used here is to form the loosening by dissolving a water soluble material inside the model.

3.3.1. Apparatus and preparation of model ground

A test apparatus used in this study is shown in Figure 3.7. Model ground of 200m wide, 50mm long and 160mm high was made in a small chamber having an opening in the base plate with width of 5mm and length of 50mm through which water was supplied and drained.

Dry Toyoura sand was layered by air pluviation method and very thin coloured sand layers were used to separate each 2cm Toyoura sand layer, for observation purposes. The uniform density of the specimen was achieved by maintaining constant height of pouring. A geotextile layer was kept at bottom and top of the model to prevent washing out of sand during the drainage and punching of external loading system into soil, respectively. Brass weights were kept over sand to apply a vertical pressure similar to 10kN/m^2 of surcharge.

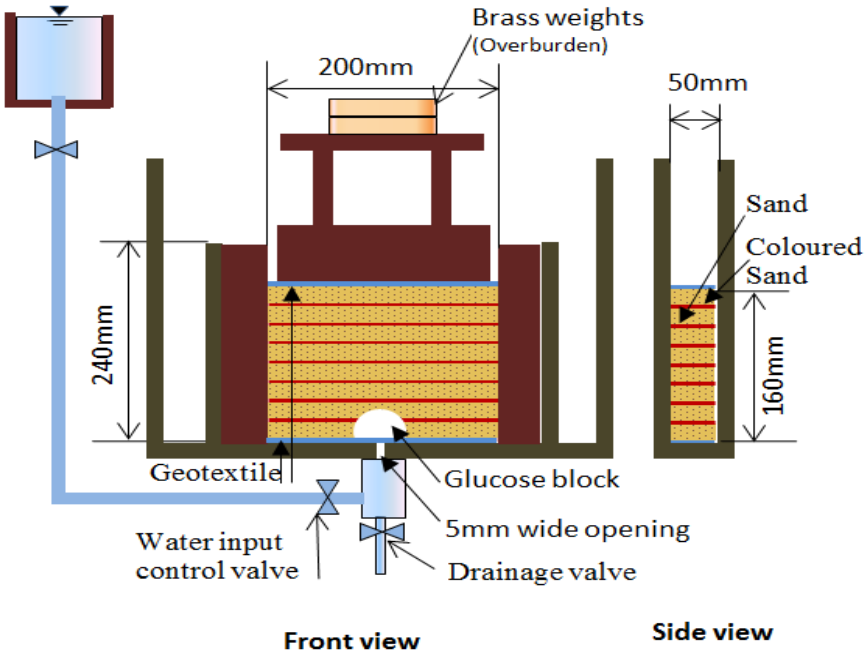

Figure 3.7: Schematic diagram of model ground.

3.3.2. Testing procedure

After setting the model ground as in Figure 3.8(a), coloured water was inserted to the model by 5mm wide, 50mm long opening which was located at bottom of the apparatus. Water was sent till the water level reached 24cm level in the model and at this moment model ground is submerged with 8cm water head. After water level reach the 24cm level, the inlet valve was closed for 5-10 minutes and allowed water level to be stay higher than the soil surface. At the end of the soaking time, water was allowed to drain out gradually which simulates the drop of ground water level. Water inflow rate was controlled at 16-20ml/minute for 4 test cases and other tests were conducted at 40ml/minute to observe the effect of water inflow rate.

Then the deformed soil model was tested for penetration resistance through different vertical profiles representing the center, left and right side of the cavity in order to observe the strength variation along the horizontal and vertical profiles.

The penetrometer (Figure 3.8(b)) was having a diameter of 3mm and apex angle of 60 degrees. The penetration is with a speed of 22mm/min which was driven by a motor and External Displacement Transducer (EDT) was fixed to measure the penetration depth. Penetrometer itself was connected to a small load cell having a capacity of 10kg which facilitated to find the resistance in "N". Load and related penetration depth were automatically recorded by connecting the load cell and EDT to the computer.

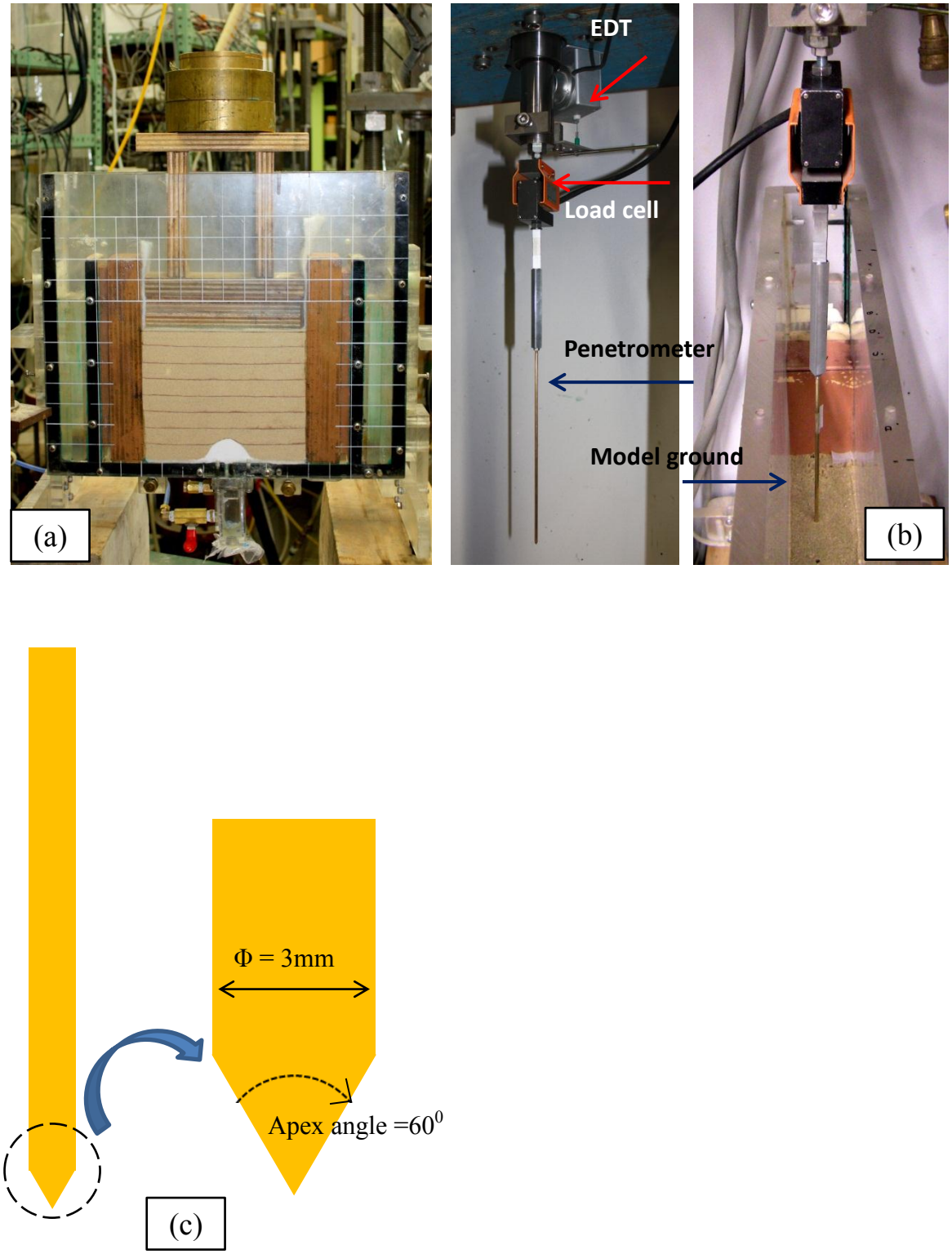

Figure 3.8: Devices of model test (a) Model ground (b) Load cell and EDT

(c) Penetrometer

3.4. Apparatus and testing procedure - Triaxial Test

3.4.1. Triaxial Apparatuses

3.4.1.1. Overall arrangement

The testing apparatus which used in this research is shown in Figure 3.9. Small size, gear driven, strain controlled Triaxial apparatus was used. The axial loading system consists of an AC servomotor and a reduction gear system, electromagnetic clutches and brakes. Schematic diagram of the triaxial apparatus and loading system is in shown in Figure 3.10 and Figure 3.11, respectively.

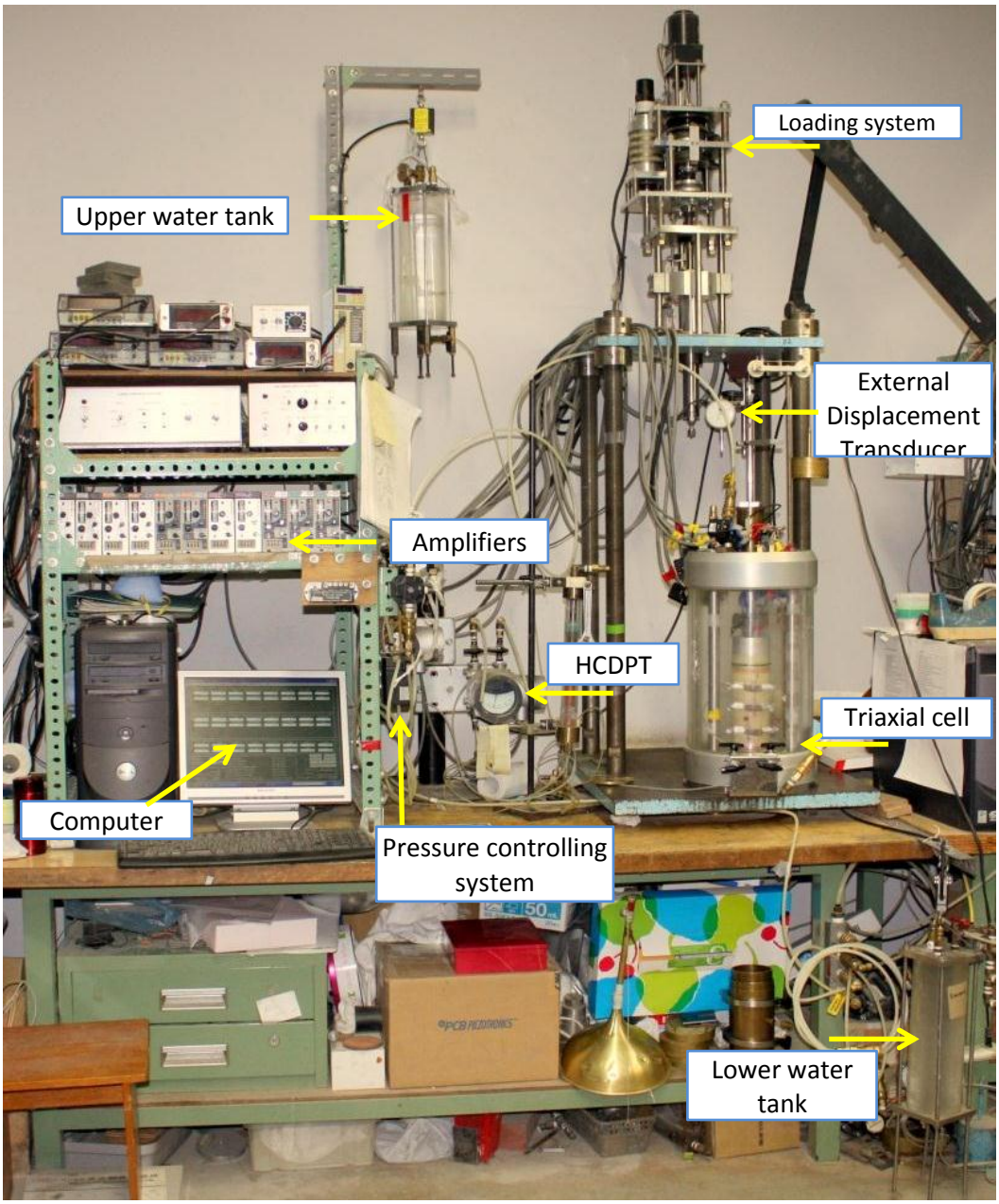

Figure 3.9: Testing (Triaxial) apparatus

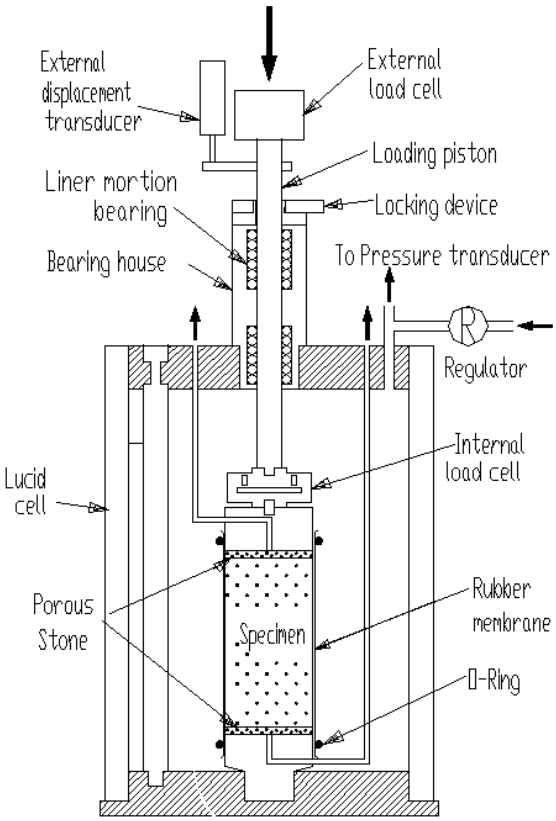

Figure 3.10: Schematic diagram of triaxial apparatus

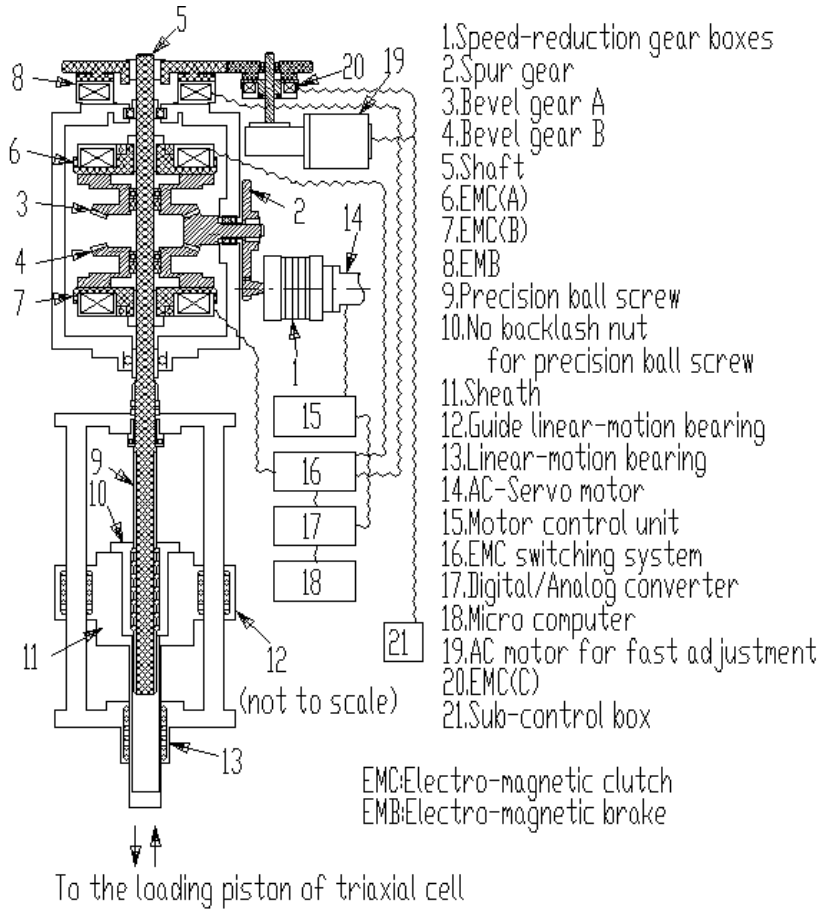

Figure 3.11: Schematic diagram-Loading system of triaxial apparatus

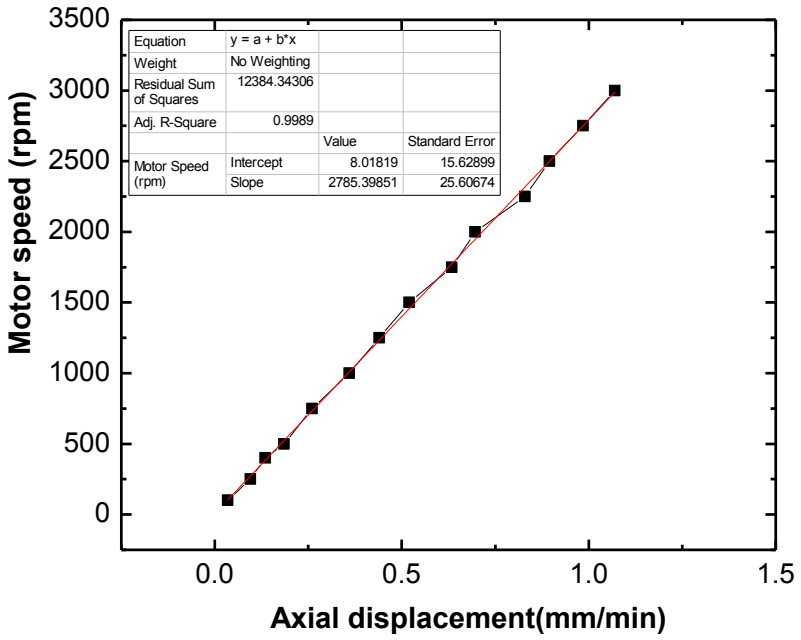

Figure 3.12: Calibration curve for motor speed

The special features that were available in the used triaxial apparatus are as follows.

1. The cell pressure is applied by means of air and adjusted by means of accurate regulators.
2. The readings of internally measured axial load, axial displacement and other parameters were converted to the voltage signals and then to digital signals with an analogue-to-digital (A/D) converter in order to measure and control automatically by the computer.
3. All the tubes which are connected to the sample are stiff nylon to avoid the volume change due to pressure changes.
4. Axial load is measured with an internal load cell which is placed inside the triaxial cell to eliminate the effect of piston friction.
5. High Capacity Differential Pressure Transducer (HCDPT) was used to accurately measure the effective confining pressure.

3.4.1.2. Strain control system

The apparatus is strain controlled and computerized the motor by software called Visual Show Basic. Both stress and strain are controlled automatically by computer, whenever the input values are given through the software. First, required strain rate is given as an input to the software interface and this digital signal will be converted in to analog signal by DA (Digital to Analog) board which is fixed to the computer. This signal will reach the Control box and servo motor with controlling the strain rate. Schematic diagram of the system is shown in Figure 3.13.

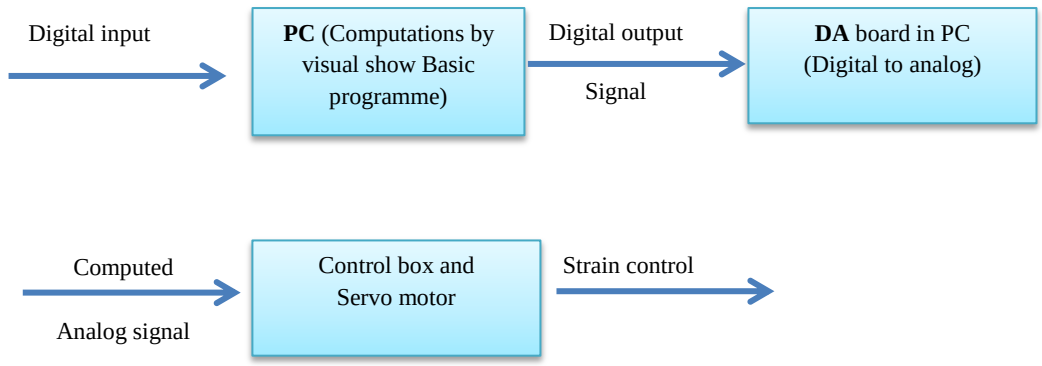

Figure 3.13: Strain control system

3.4.1.3. Cell pressure control system

Cell pressure was controlled by compressing the air inside cell by applying a regulated, controlled pressure from main power source. First, high pressure channel was regulated and the pressure at this stage is about 700 kPa. Regulated pressure is send to the volume

booster which is connected to an E/P (Electro Pneumatic) system. E/P is receiving the analog signal corresponds to the required cell pressure which is converted from D/A board.

Volume booster is a device which can reproduce pneumatic signals in 1:1 ratio whenever input isolation or increased flow capacity is required. During normal steady state process conditions, the signal input flow to the booster will pass through the bypass valve and into the actuator. Both booster ports remain tightly shut with preventing unnecessary air consumption. When large or faster variations in signal flow is required, bypass valve setting causes them to be registered sooner on the booster inlet than on its outlet which is connected to the actuator. When the differential pressure obtained exceeds the dead band value of the booster, set by the adjustable equalizing/bypass valve, the diaphragm assembly will move as to open one or other booster port and allow rapid change of pressure within the actuator. When the pressure balance is restored, the booster closes and allows the system to resume normal operation with the actuator being fed via the equalizing/bypass valve flow ('Volume booster', n.d.)

E/P is used for transfer energy from one point to other using actuators which are driven by fluids under pressure. When the pneumatic components are controlled by electric impulses, it is called as electro pneumatics. In this case, pumping air into a pneumatic cylinder was controlled by sending an electrical signal.

The schematic diagram of the system is shown in Figure 3.14.

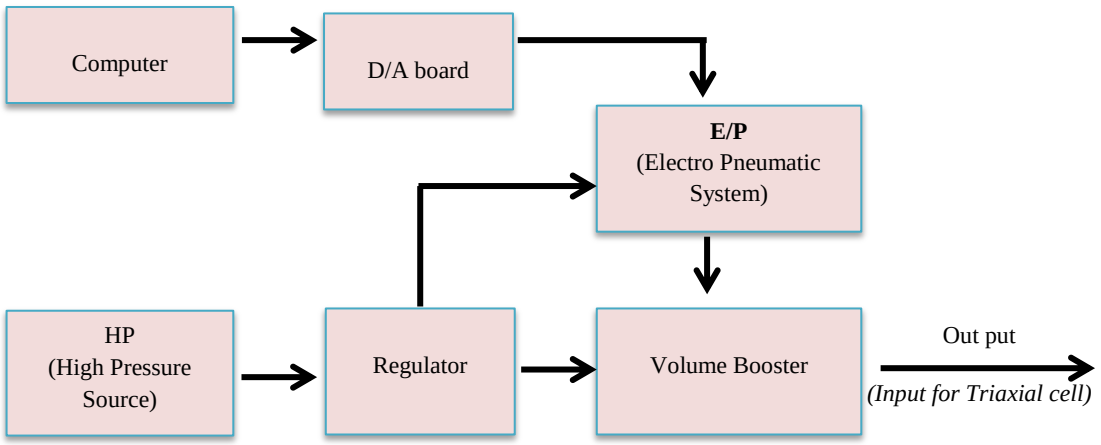

Figure 3.14: Cell pressure control system

3.4.1.4. Data acquisition system

This apparatus is a complex combination of many devices, and all the data is recorded to the computer automatically. All the transducers are connected to the computer through software called, "Digit Show Basic" which is written for Windows Operating System by C++ language. Actuated transducers will generate small voltage and then the voltage will be amplified by an amplifier. Amplified analog electric signal will be passed through a low pass filter with providing easy passage for low frequency signals and difficult

passage for high frequency signals. Then the filtered analog signal will be converted in to a digital electronic signal by using two 16-bit Contec AD converter board. Then two output files will be saved separately as one is for voltage and other with physical parameter which is automatically converted by using calibration factors, fed in to software prior to starting the test.

Physical stress value from the load cell is used to control the axial stress while strains evaluated by external displacement transducers are used to strain control. Schematic diagram of the data acquisition system is shown in Figure 3.15.

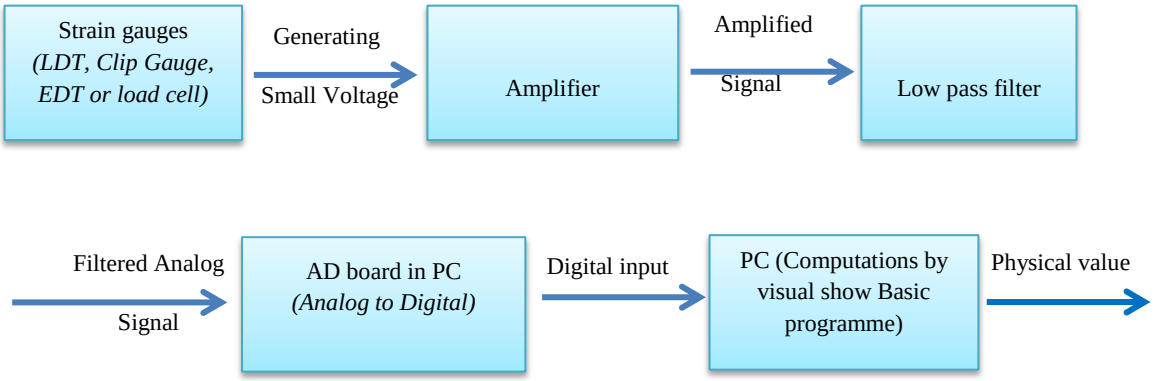

Figure 3.15: Data acquisition system

3.4.2. Devices for measuring of stresses

3.4.2.1. Load cell for axial stress

Axial stress is a very important parameter to be measured in triaxial apparatus. In conventional type of apparatuses, load cell was fixed outside the triaxial cell and then the output was affected by piston friction. Therefore in order to eliminate that limitation, the load cell has been fixed inside the triaxial cell in this modern apparatus (Suwal, L.P (unpub.) 2010).

A load cell having a capacity of 200kg (approximately 2kN) was used in this apparatus and it has been fixed to the loading piston and top cap as shown in Figure 3.16. It was manually calibrated (Figure 3.167) by using known weights and further it was facilitate 100kg to vary within 5V of digital output. The principle behind this load cell is; four electronic resistant strain gauges are set as two at compression side and two at tension side as forming a Whitestone Bridge. Therefore voltage difference can be detected whenever any axial load was changed in the loading piston.

Figure 3.16: Load cell

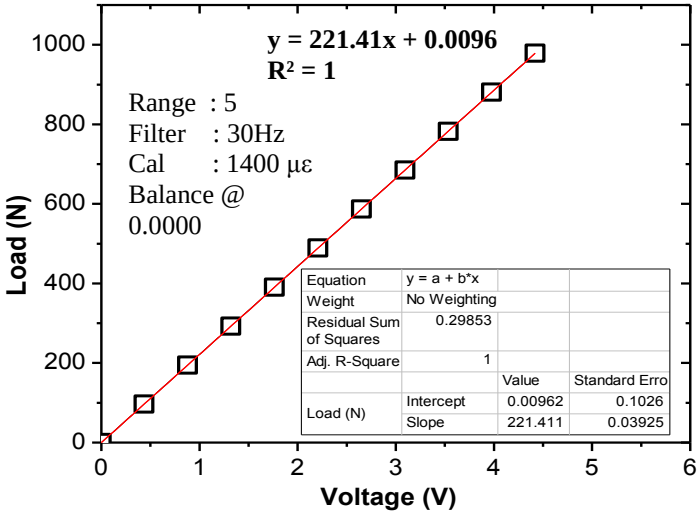

Figure 3.17: Calibration curve for load cell

3.4.2.2. HCDPT for effective cell pressure

High Capacity Differential Pressure Transducer (HCDPT) is a device which facilitates to directly measure the effective minor principal stress. HCDPT is having a chamber which is divided by a thin membrane into two chambers defining positive and negative pressure separately. Once a pressure difference is made in between those two chambers, the central membrane will be bended and it will be detected as a voltage difference. Generally, the positive side of HCDPT will be connected to inside the specimen and negative side will be connected to the triaxial cell. Then the effective minor principal stress of specimen can be measured directly. However in this study, the positive side of HCDPT was open to atmosphere and sand was tested under drained condition. Then the pore pressure inside the specimen was neglected. The cell pressure input was controlled by the electro-pneumatic (E/P) transducer. Figure of HCDPT and calibration curve is given in Figure 3. 18 and 3.19.

Figure 3. 18: HCDPT

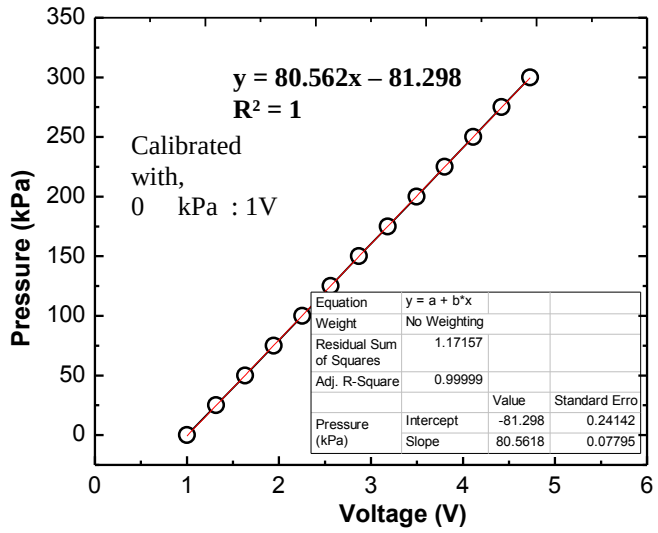

Figure 3. 19: Calibration curve for HCDPT

3.4.3. Devices for measuring of strains

3.4.3.1. External Displacement Transducer (EDT)

The External Displacement Transducer (EDT) is a device which is externally fixed as it touching a rigid horizontal plate connected to the loading piston and the vertical displacement of loading piston (equal to the deformation of specimen) can be measured referred to the initial condition. This is conventional type of transducer having a capacity of 20mm displacement, worked in linear proportionally between displacement and voltage. In this study, EDT was used to measure the axial strain during shearing the specimen. The EDT was calibrated by measuring the output voltage by virtue of adding and removing blocks with known standard heights. The picture of used EDT and its calibration chart were shown in Figure 3.20 and 3.21 respectively.

Figure 3.20: EDT

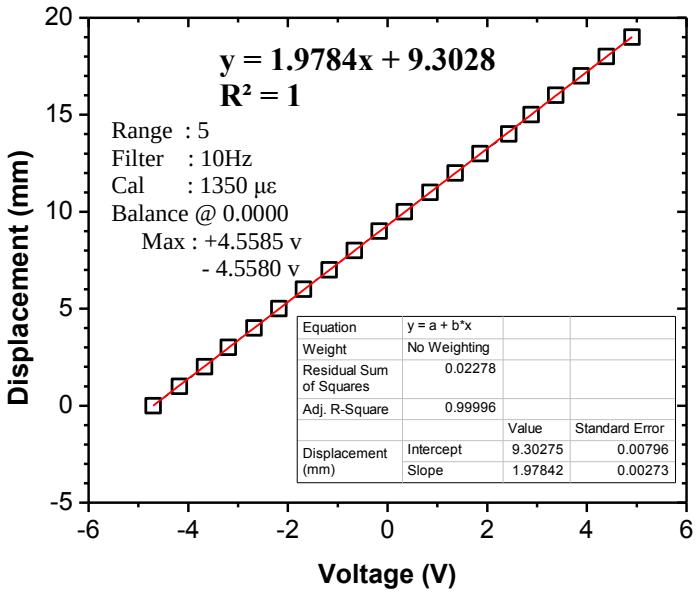

Figure 3.21: Calibration curve for EDT

3.4.3.2. Local Deformation Transducer (LDT)

Small strain behaviour of soil is very important in various geotechnical practices. In conventional system, the deformation was measured by the external measurement transducer and it involves bedding error at both longitudinal ends of the specimen and difficult to measures the strains less than 0.1%. This gives the overestimation of strain, in other words, underestimation of stiffness.

Various attempts to obtain more precise measurement on small strains have been made by many researches in the past. Different types of local strain measuring devices have been introduced in the recent past, such as electro level gauge by Burland and Symes (1982) and Jardine et al. (1984), Hall effect transducer by Clayton et al. (1989), non-contact type proximeter by E1-Horsi et al. (1981) and finally Local deformation transducer (LDT) by

Goto et al. (1991). LDT is very famous at the moment and it provides simple, cheap and precise measurements even between small strains of 10^{-6} and 10^{-2}.

This device is made of a thin and flexible narrow strip of phosphor bronze which consists of a pair of strain gauges. It was developed based on Wheatstone bridge by strain gauges as shown in Figure 3.22. When the LDT is subjected to any bending deformation caused by axial compression between both ends, a change in the voltage by strain gauges is occurred proportionally with change in deformation. This voltage and deformation relationship will be identified by calibrating the LDT by applying known small displacements through a micrometer.

The dimensions of the LDT's used in this study are approximately 70mm in length, 3mm in width and 0.2mm in thickness. Generally the recommended size of LDT for specimen size of Φ75 x 150mm is 120 x 3.5 x 3mm. In this study two sets of LDTs were used separately to measure the strains at upper and lower half of the specimen. Therefor the size of the LDT was scale down as mentioned earlier. These LDTs were made in Institute of Industrial science at the University of Tokyo. They were fixed vertically opposite sides of the specimen as explained later. Each LDT was attached on specimen by the help of the hinges glued to the membrane as shown in Figure 2.23 and two LDTs were always fixed vertically opposite sides of the specimen and the average was taken. Therefore in this study four LDTs were used and calibration curves are shown in Figure 3.24 to Figure 3.25.

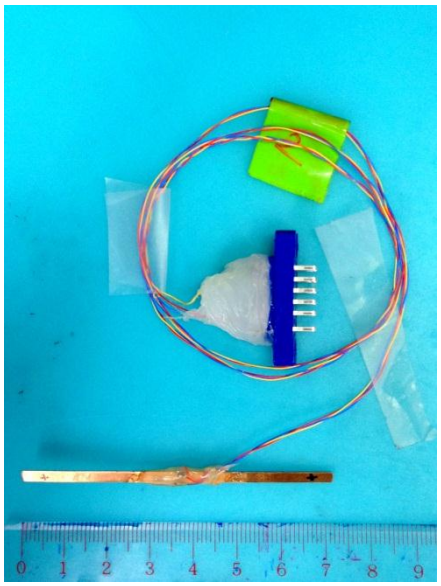

Figure 3.22: LDT

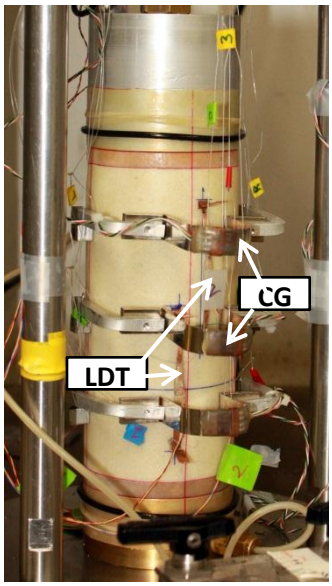

Figure 3.23: Fixing of LDT and CG

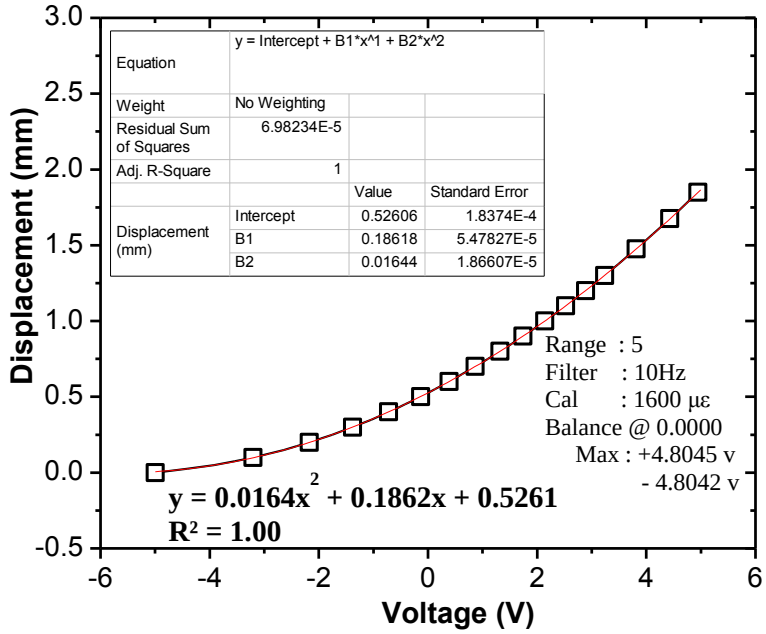

Figure 3. 24: Calibration curve for LDT1

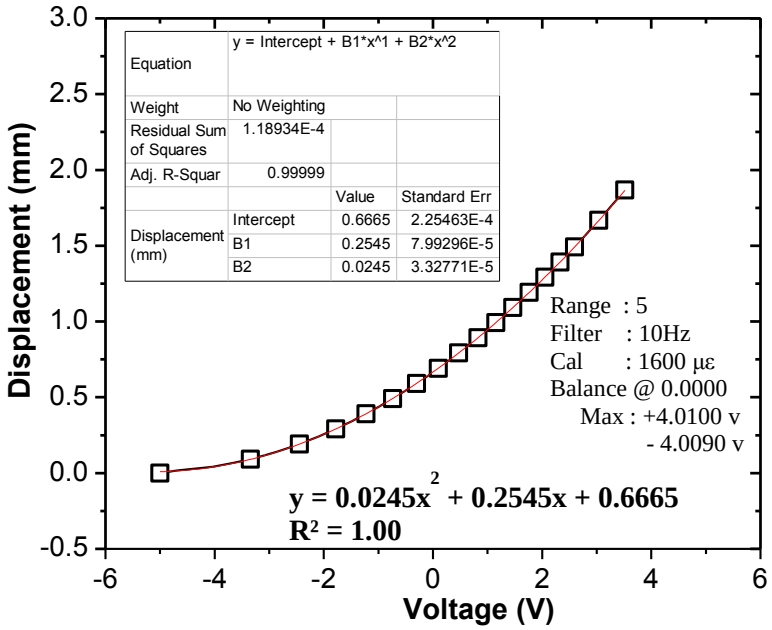

Figure 3.25: Calibration curve for LDT2

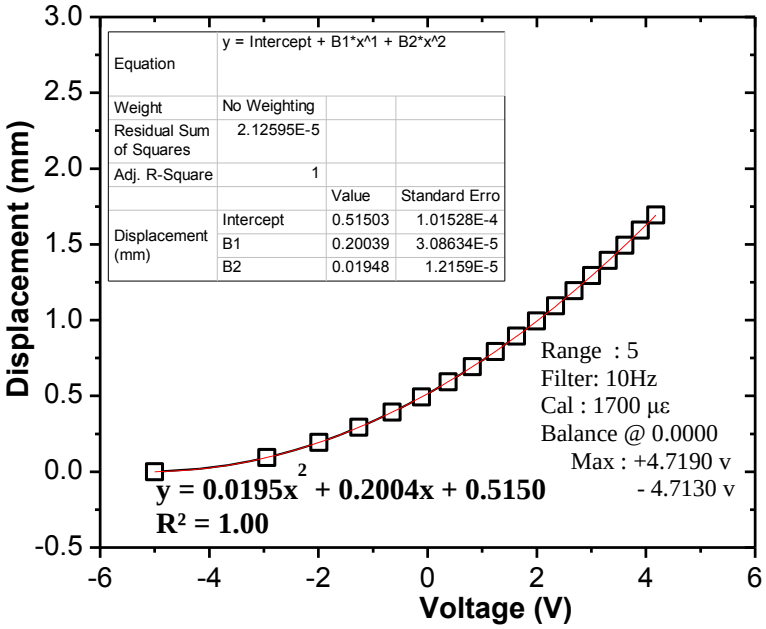

Figure 3.26: Calibration curve for LDT3

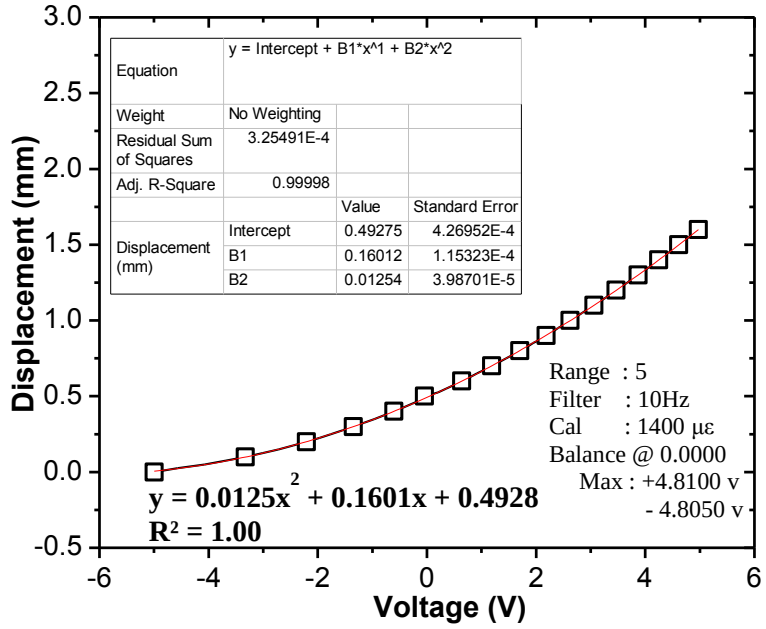

Figure 3.27: Calibration curve for LDT1

3.3.3.3. Clip gauges (CG)

Clip gauge is a device which can measure the small deformations of the specimen in radial direction (Figure 3.28). It consists of a U-shape metal frame with glued strain gauges at the curvature of U part. When the specimen is compressed or expanded, this changes caused in diameter is captured by the strain gauge and converted in to a small voltage difference. This deformation-voltage relationship can be found by calibrating the clip gauge by applying known small deformations through a micrometer.

In this study three clip gauges were used and it was fixed to specimen by using a small metal block. These metal blocks (10 x10 x 10mm) are having a tiny hole on top surface and a vertical side of block was glued to the membrane with facilitating to hold the sharp pin at the end of each CG arm. Calibration curves of three clip gauges are shown in Figure 3.29 to 3.31.

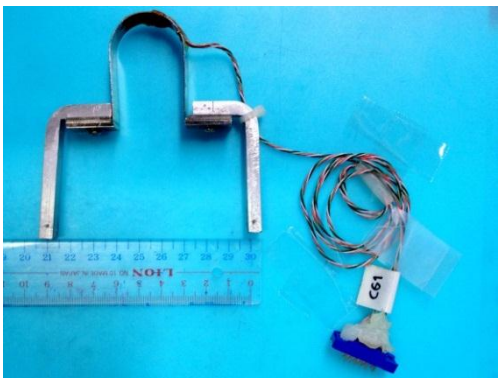

Figure 3.28: Clip Gauge

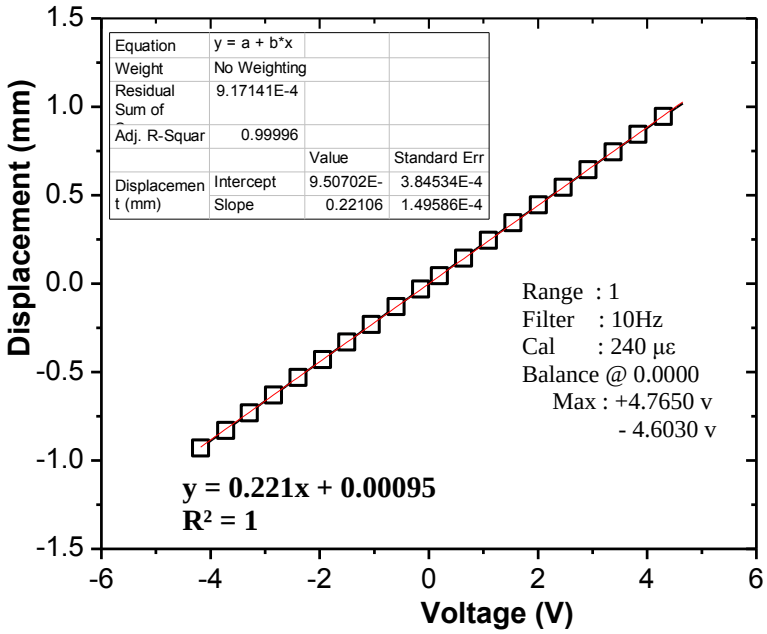

Figure 3.29: Calibration Curve for Clip Gauge 1

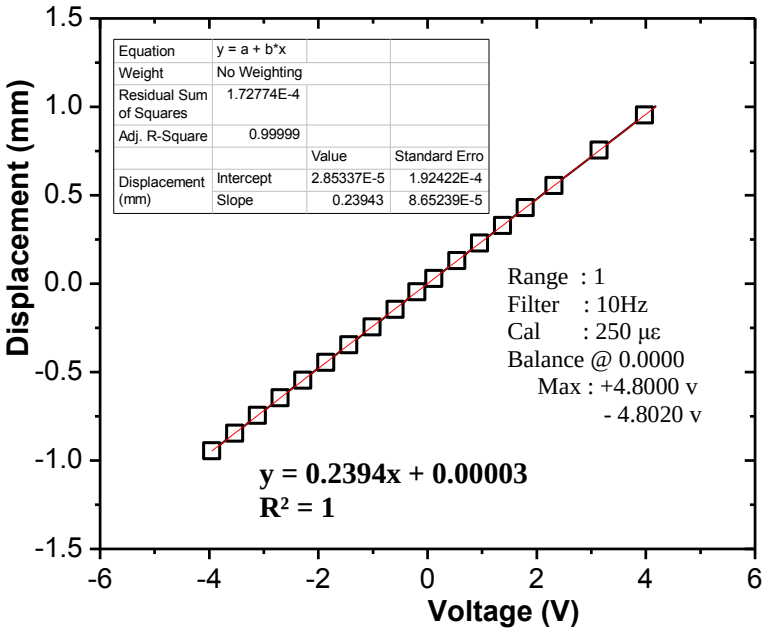

Figure 3.30: Calibration Curve for Clip Gauge 2

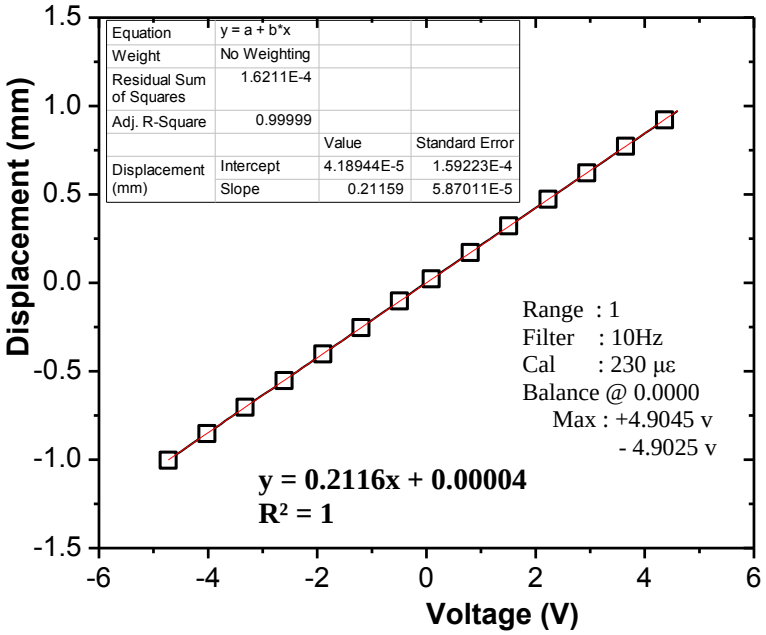

Figure 3.31: Calibration Curve for Clip Gauge 3

3.3.4. Measurement on water inflow and outflow

In order to form the artificial ground loosening by dissolving water soluble material inside the triaxial specimen, it is necessary to control the water inflow and outflow in a measurable way. Therefore, two water tanks hang by load cells were used as one at higher elevation and the other at lower elevation referred to triaxial specimen. Then the water was

sent to the specimen under gravity. The maximum capacity of load cells were 10kg and it was calibrated by applying known loads. Therefore the amount of water infiltrated in and drained out from the specimen was directly measured and saved in to the computer. Calibration curves are shown in Figure 3.32 and Figure 3.33.

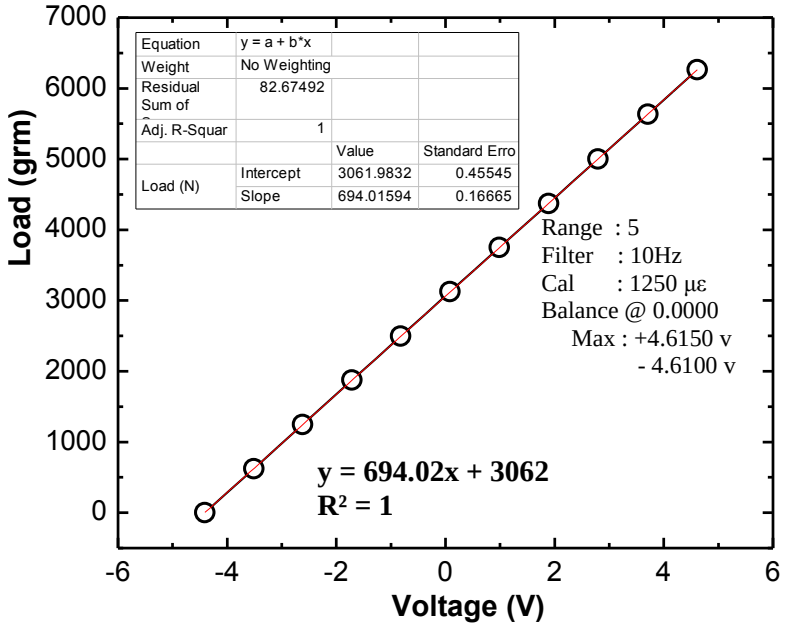

Figure 3.32: Calibration curve for load cell-upper water tank

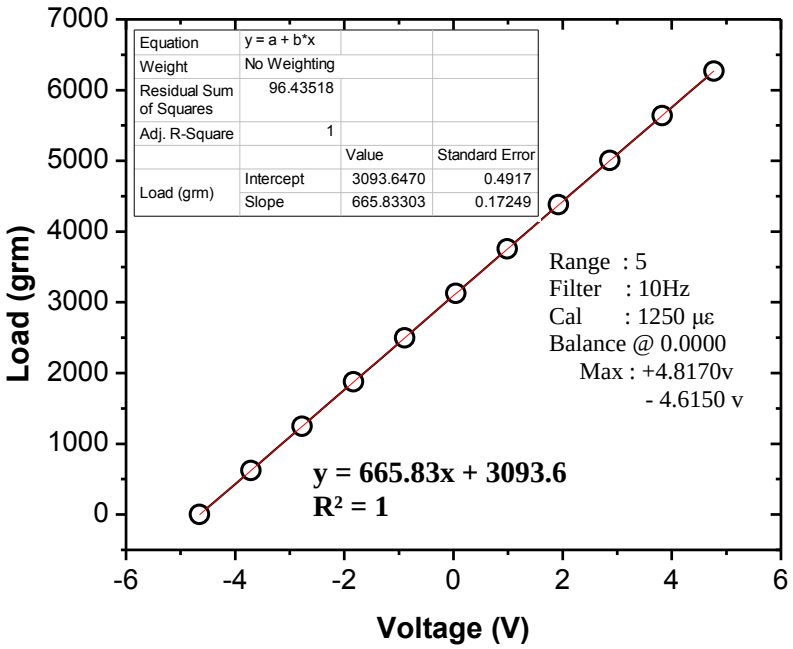

Figure 3.33: Calibration curve for load cell-upper water tank

3.3.5. Preparation of the specimen and testing procedure

3.3.5.1. Preparation of the specimen

1. Prior to test, all the sensors, connections of the apparatus were carefully checked and the availability of required items was checked.

2. Specimen size used in this study is 75mm in diameter and 150mm in height. First the membrane was cut in to required size in height. Since, it is necessary to fix many strain transducers in to specimen membrane, locations of those sensors were marked on the latex membrane before it was fixed to the apparatus (Figure 3.34 (a)).

3. O-ring and fastener were inserted to pedestal and grease was applied around the lower cap as a lubricant. Porous stone with thickness of 8mm was placed on lower plate and membrane was fixed properly (Figure 3.34 (b)).

4. Split-mould was connected in to lower cap carefully without damaging the membrane and with protecting the verticality of the membrane. Then the mould was tightened well to avoid any pressure leakage (Figure 3.34 (c)).

5. Membrane top was folded down in mould and vacuumed gauge was connected to the outlet of the mould and a vacuum of 20kPa was applied between the inside wall of the split-mould and the latex membrane by means of a vacuum line to the split mold, to hold the membrane tightly against the split-mold sides (Figure 3.34 (d)).

6. A manually made sand collector fixed to mould top to collect the sand which are flowing away from the mould mouth during the sand flowing (Figure 3.34 (e)). Then the known mass of dry sand was poured in to the mould by using pluviator with appropriate opening. The pouring height is varied with desired density and the pouring height should found by conducting few trials with different heights. Then the sand was poured maintaining the same pouring height between top surface of the already poured sand and tip of the funnel opening (Figure 3.34 (f)). Pouring direction was continuously changed from clockwise to anti-clock wise after reach rotation of 360^0 to have a uniformly distributed specimen without particle segregation.

When the test case is simulating a cavity, a glucose block explained in Chapter 3.1.3 was inserted to specimen at specific elevation during pouring of sand (Figure 3.34 (g)).

7. After completing the sand pluviation, the top of the specimen was trimmed slightly using a spatula to form a uniform top (Figure 3.34 (h)). Then the specimen was covered by placing the second porous stone on top of sand (Figure 3.35 (a)). After that the weight of the remained sand was measured.

8. The top cap with load cell was placed on position and fixed by screws. The drainage tubes were connected to the loading cap and pedestal and the internal connection of the load cell was made (Figure 3.35 (b)).

9. The counter balance was erected on upper surface of the cell cap and the weight of the top cap was balanced by counter balance and the voltage reading of the load cell at this stage was considered as zero.

10. A thin layer of white grease was applied around loading cap. Then it was gradually moved down till it slightly touches the porous stone. Then the top cap was clamped, the portion of the membrane was pulled off the split-mould and stretched around porous stone and top platen without disturbing the specimen (Figure 3.35 (c)). Then the top plate was unlocked.

11. A vacuum pressure of 25kPa was applied to the top and bottom through drainage tubes to apply some effective confining pressure to the specimen in order to disturb any disturbance that might occur when the mould is removed. At this time, the vacuum which had been applied to mould was removed gradually. After removing the vacuum in the mould, split-mould was carefully (Figure 3.35 (d)).

12. The specimen diameter at three locations and height was measured (Figure3.35 (e)).

13. Next step was to connect all the deformation transducers in specimen. Four LDT s were fixed with the help of small hinges (Figure 3.35 (f)) before fixing the LDT, they were placed as non-deformed position and strain at that point was set as zero. Then it was fixed with allocating a compressive strain. Three clip gauges were supported on small Aluminum blocks which were glued in to specimen (Figure 3.35 (g)). Arrangement and location of sensors are shown in Figure 3.36.

14. During shearing the specimen, the specimen will undergo under large axial and radial strains which could damage the strain transducers. Therefore, there should be a mechanism to detach the sensors from specimen before shearing. So, when fixing the Clip gauges and LDTs, each transducer was connected to a thin strong thread and the connection was taken out side from the triaxial cell through the top cover of the cell chamber. It allows detaching the transducers at any time by pulling the thread from outside.

15. All connections for load cell, LDTs and CGs were checked and top cap was locked. Then the counter balance system was detached and connections given from transducers to amplifiers were disconnected. Cell was inserted carefully without disturbing the transducer's position, after applying grease on outer rubber ring of top cap (Figure 3.35 (h)). Then the counter balanced system was re-erected, clamp was released and load cell was again set at zero.

16. The vacuum pressure was replaced by cell pressure. The cell pressure was applied through regulator by increasing the cell pressure gradually and simultaneously decreasing vaccum pressure. The cell pressure was kept to 25kPa and the load cell value was maintained to zero. The cell was connected to the loading system with motor and loading control was set to manual system. During this process, the load cell was still maintained at zero.

17. The control computer programm "Digit Show Basic" was executed and specimen parameters and calibration factors were fed. Then the cell pressure input was changed to the E/P and pressure was set to be 25kPa.
18. External Displacement Transducer was placed accurately with connecting to the loading piston and the initial physical displacement was set as zero.

19. Loading path was fed to the software and motor and E/P was controlled by computer. After checking all the calibration factors, specimen properties and connections; the loading was executed.

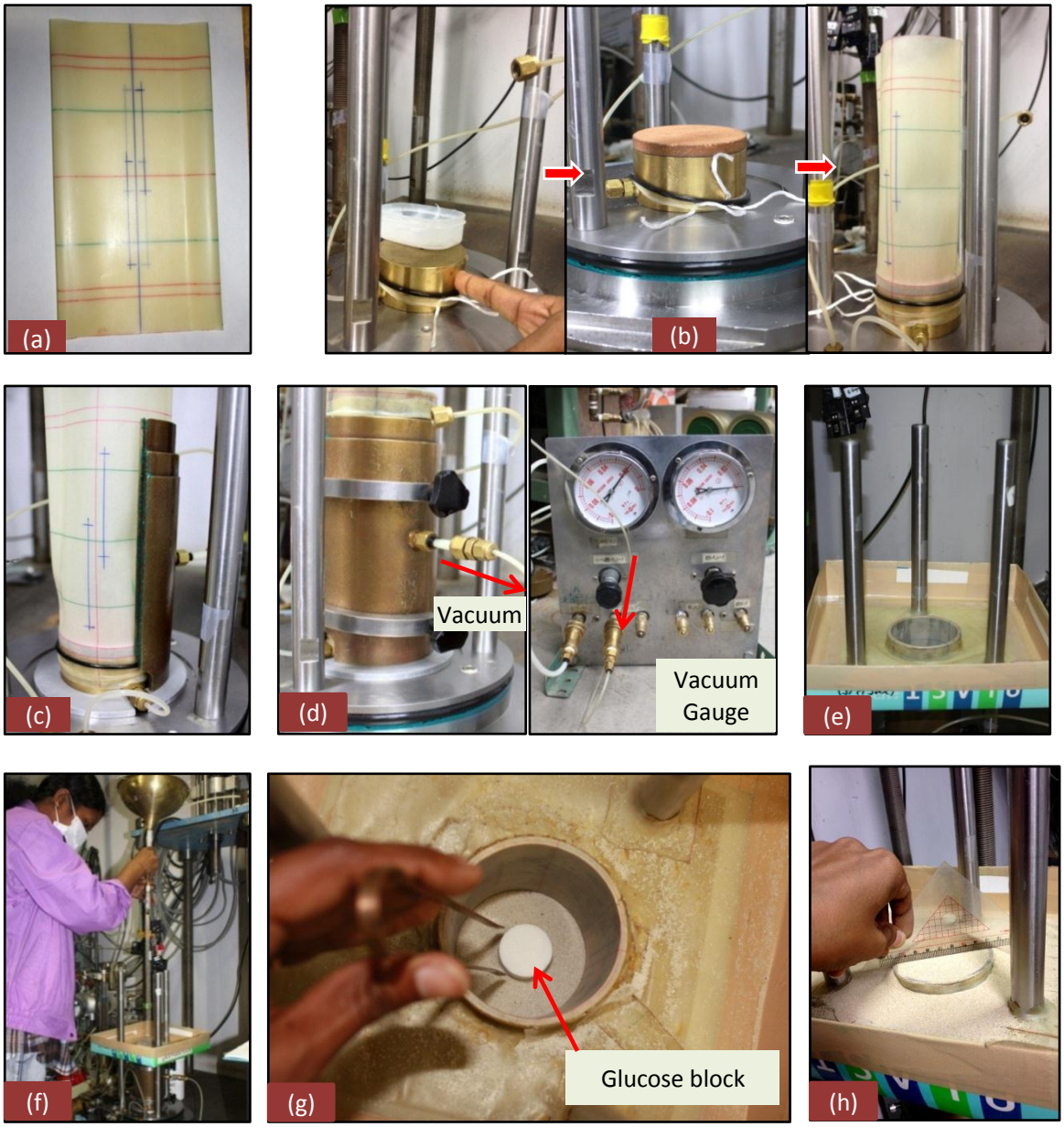

Figure 3.34: Preparation of specimen-I; (a)Membrane, (b)Fixing of membrane, (c) Setting of split-mould, (d)Applying vacuum to mould, (e) Fixing of sand collector, (f)Pouring of sand by funnel, (g) Inserting glucose block in to specimen and (h) Trimming of specimen

Figure 3.35: Preparation of specimen-II; (a) Placing of the porous stone, (b) Fixing of counter balance system, (c) Fixing of specimen in to loading plate, (d) After removing the mould, (e) Measuring the diameter of the specimen, (f) Hinge for fixing LDT, (g) Aluminum block to hold the Clip gauge and (h) Inserting of the cell cover

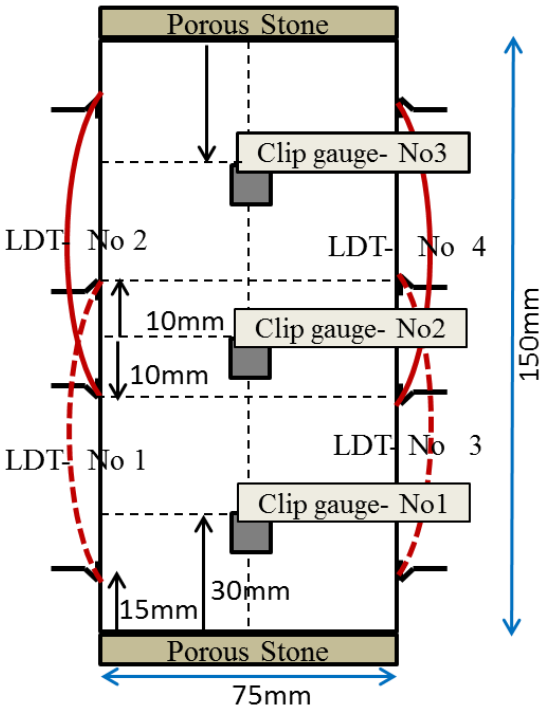

Figure 3.36: Arrangement of LDTs and Clip gauges

3.3.5.2. Testing procedure and loading path

Specimens of 75mm in diameter, 150mm in height with different relative densities were tested. Sand was placed by air pluviation method and the specimen was set at isotropic stress state of 25 kPa. For experiments which represent the ground loosening caused by cavities, a glucose block was inserted in to the specimen while air pluviation. All the tests were conducted under drained condition which means that the total stress and effective stress was equal when, the back pressure was zero.

Stress path contains few special steps and the schematic diagram is shown in Figure 3.37.

Step 01: The stress condition of the erected specimen was increased from 25 to 50kPa under isotropic condition and left it for around 12 hours to dissipate the creep effect.

Step 02: Small cyclic loading was applied axially with 11 cycles which has peak to peak strain amplitude of 0.001% in the dry stage.

Step 03-a: Then 1500ml of water was inserted from bottom cap with rate of 14-20ml/min and drainage was allowed from top cap. The reason for flowing water from bottom was to make the water penetration in a much uniform manner (Figure 3.38).

Step 03-b: Once upper water tank was empty when approximately 1500ml of water was penetrated; water input valve from bottom was closed and the specimen was kept in the same condition for nearly 10 minutes to stabilizing of existing water.

Step 03-c: Drainage was started from bottom cap.

Step 04: Second small cycling loading was applied after 24 hours from Step 03-c. After step 03-a, axial and radial strains were monitored and once the deformations were constant, step 04 was executed.

Step 05-a: Then the second cycle of water (200ml) was inserted from bottom cap with rate of 14-20 ml/min and drainage was allowed from top cap.

Step 05-b: After 200ml of water was penetrated; water input valve from bottom was closed and the specimen was kept in the same condition for nearly 10 minutes to stabilizing of existing water.

Step 05-c: Drainage was initiated from bottom cap.

Step 06: Third small cycling loading was applied after 24 hours from Step 05-c.

Step 07: Then the LDTs and Clip gauges were detached from the specimen and sheared the specimen with strain rate of 0.1% per minute.

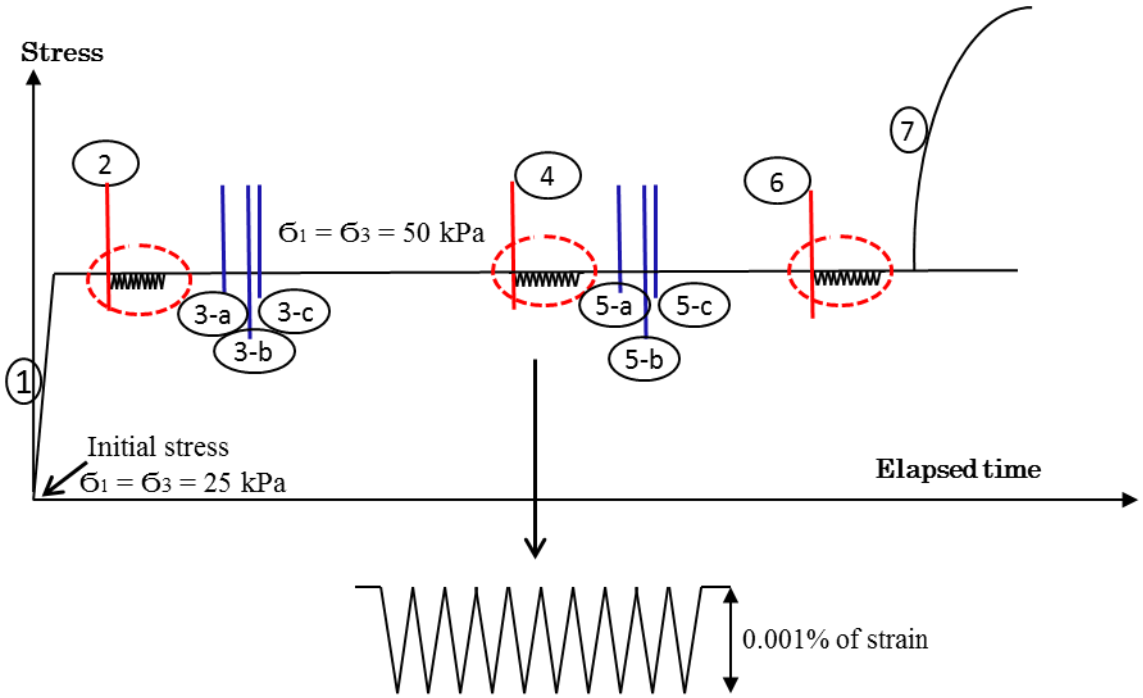

Figure 3.37: Stress path and special steps of the test

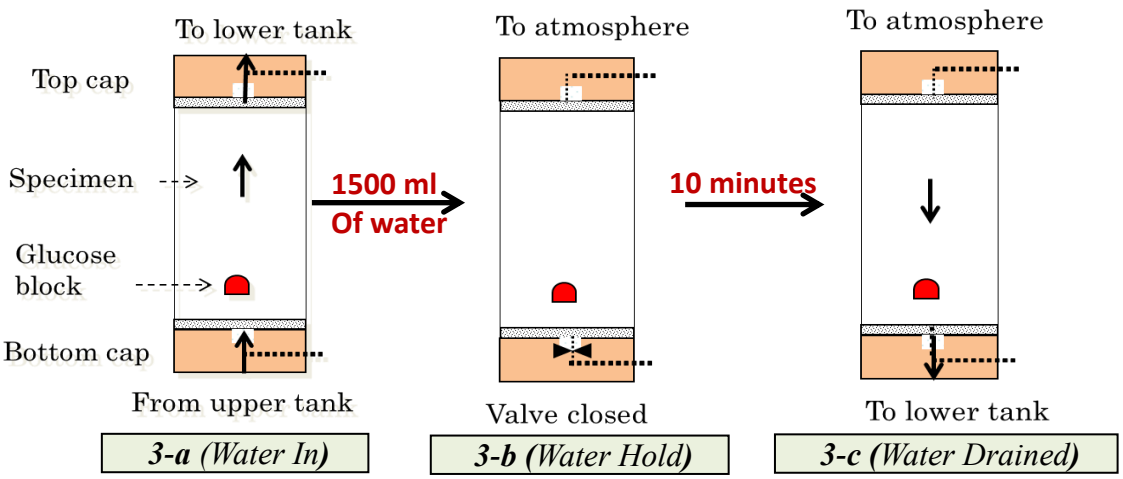

Figure 3. 38: Water infiltration and drainage

3.4. Apparatus and testing procedure – CT X-ray images for Triaxial test

3.4.1. Introduction

As explained in 3.3, triaxial tests were conducted to find the mechanical properties of loosened sand. The mechanism which was done to form the loosening in triaxial test was initially confirmed by performing two-dimensional model tests as in 3.2. However the extend of ground deformation or loosening formed by dissolving glucose in the Triaxial test is not visible or transparent as in model tests. Hence, a decision was made to check the real condition, extend of loosening in triaxial test by CT X-ray scanning images.

Initial imagination about behaviour of ground loosening in three dimensional triaxial specimens was explained in Chapter 3.1 (Figure 3.2).

One accelerated experiment was done to observe the behaviour of loosening by using a specimen with 50mm in diameter and 100mm in height which was smaller than normal tests in university. Because, CT X-ray scanning test was conducted in Port and Airport Research Institute (PARI) in Kurihama, Japan. The facilitated triaxial machine in that research institute for CT X-ray scan was specially manufactured for that particular condition.

Due to the lack of time, it was decided to repeat one specific test (similar to a test which was already conducted in the university) in the same control conditions, but size of the glucose block was scaled down corresponds to the specimen size.

Series of X-ray images were taken before infiltrating water, after infiltrating water, after drainage and at several stages during the shearing.

3.4.2. Material properties

Toyoura sand with similar properties as Table 3.1 was used for this experiment.

3.4.3. Apparatus

3.4.3.1. Traxial apparatus

Triaxial apparatus was a small scaled apparatus which was specially manufactured for that particular CT X-ray scanning machine. The loading system is a small scale, moveable type and can be detached easily whenever required (Figure 3.39).

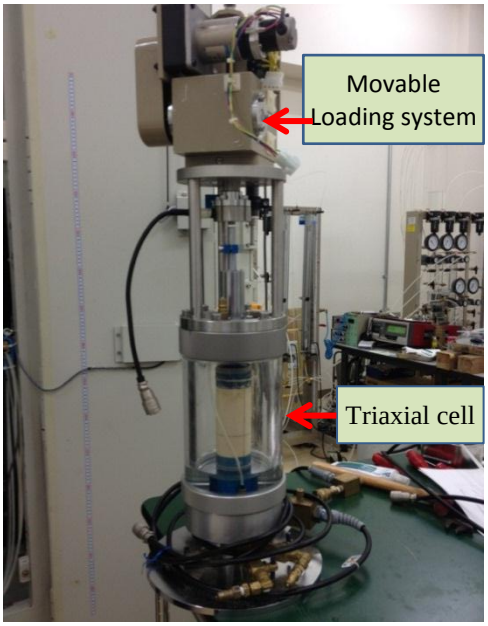

Figure 3.39: Movable Triaxial apparatus

3.4.3.2. CT X-ray scanner

This micro X ray CT scanner was used to observe the density distribution of the cross section of the specimen in non-destructive condition by transmission of the multidirectional irradiation of X rays. In this machine, a particle with about 0.1mm diameter can be identified for specimens with 50mm diameter.in diameter. X-ray room and the components of the system are shown in Figure 3.40 to Figure 3.43.

Figure 3.40: X-ray room

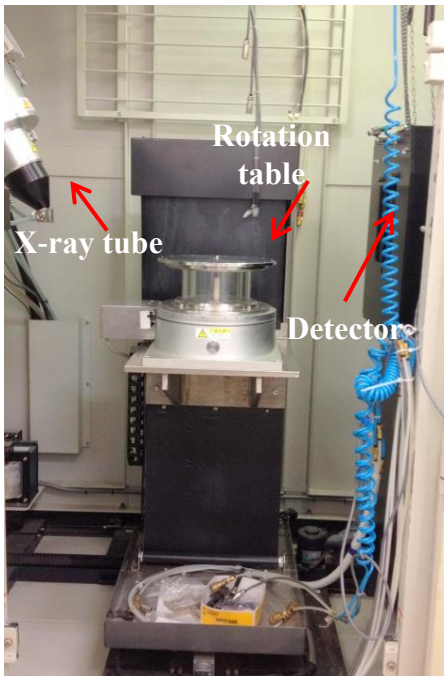

Figure 3.41: Components of X-ray system

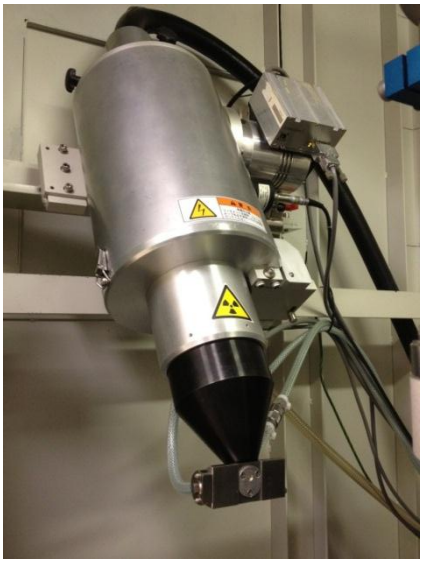

Figure 3.42: X-ray tube

Figure 3.43: Detector

3.4.4. Preparation of the specimen

The specimen was prepared as the same way as explained in Chapter 3.3.5. But the size and the location of the glucose was scaled down according to the specimen (Figure 3. 44 and Figure 3.44).

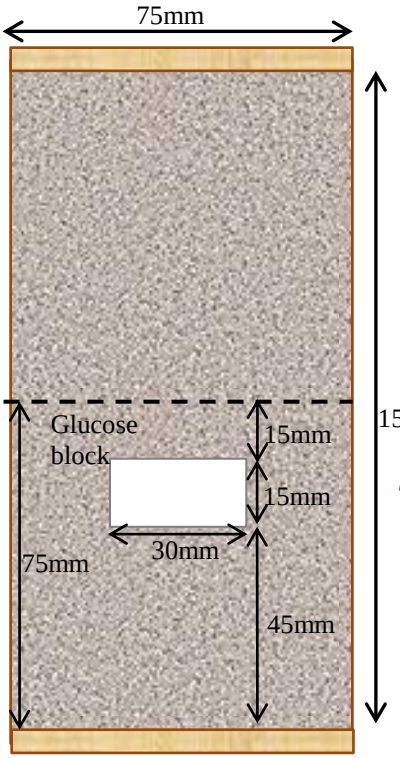

Figure 3. 44: Laboratory Specimen

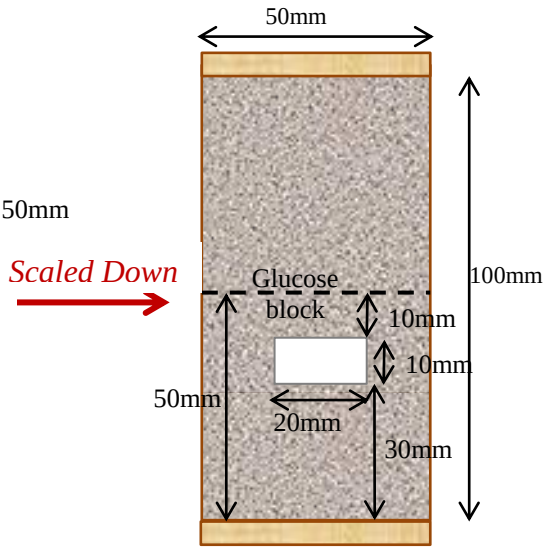

Figure 3. 45: Scaled down Specimen for X-ran scan

In this experiment the specimen with the triaxial cell will place on the rotating table of X-ray room and the specimen shouldn't be disturbed by fixing any other metal devices on specimen. Therefore the displacement transducers (LDTs and Clip gauges) were not possible to attach here. Only the external displacement transducer was attached to the loading piston to measure the axial strain during the shearing. The specimen which was prepared for this test is shown in Figure 3.46.

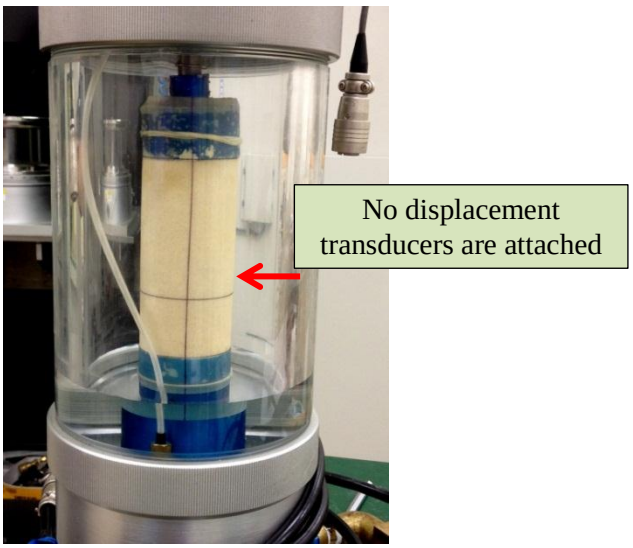

Figure 3. 46: Specimen for X-ray scan.

3.4.5. Testing procedure

The testing procedure was slightly modified in this test. The time consumed for one particular test in the university laboratory was 4 days and this test was accelerated to complete by 2 days. The time allowed to dissipate the creep effect was reduced than normal condition.

The rate of water infiltration and amount of water infiltration was not possible to control as same as in laboratory. However, attempt was given to control the each important parameter approximately similar.

Specially, all the loading, water infiltration and drainage processes had to stop while progressing of scanning. Therefore, continuous shearing process was not possible, due to requirement of observing the pattern of ground deformation during the initial period of shearing. Hence, shearing was stopped and again continued at strain levels of 3%, 6%, 10% and 15 % after taking images at each stage. The methodology flow chart is given below in Figure 3.47.

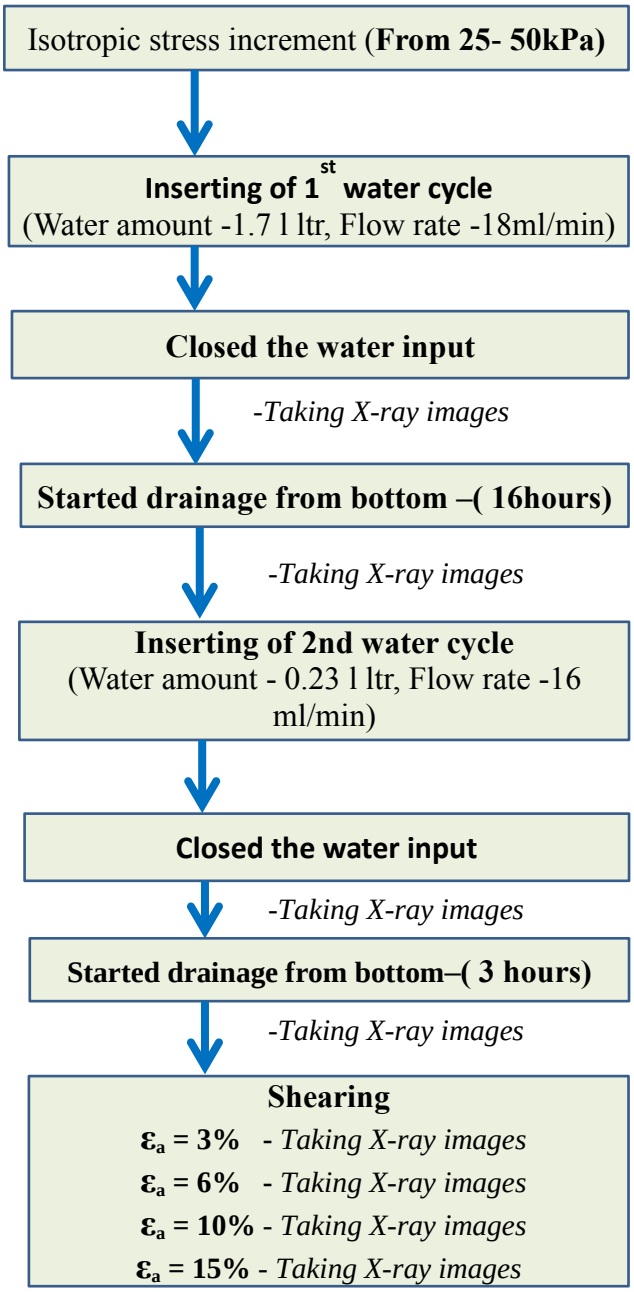

Figure 3. 47: Methodology of taking CT X-ray images of Triaxial specimen with cavity

CHAPTER 4

THEORIES AND DATA ANALYSIS POCEDURE

4.1. General soil mechanics

Soil is an assemblage of solid particles formed by weathering and/or transportation process. In between the solid particles there are voids. These voids are occupied by either water or air or both. Therefore, the soil is a three phase material. Phase diagramme of soil is given in Figure 4. 1.

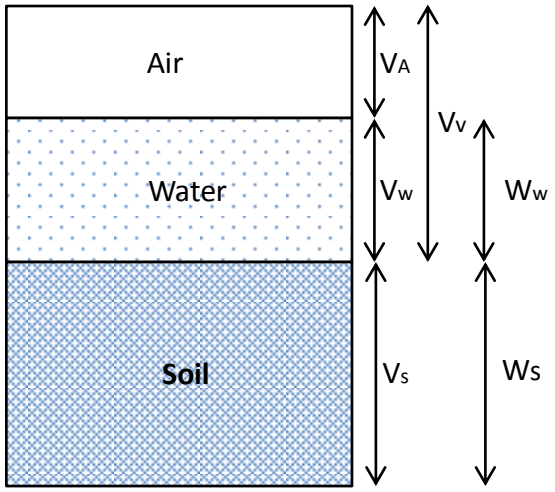

V : Total volume
Vv : Volume of void
Vs : Volume of solid particles
Vw : Volume of water
Va : Volume of air
W : Total mass
Ws : Mass of solid
Ww : Mass of water
W_A : Mass of air =0

Figure 4. 1: Phase diagramme of soil

The relation between volume of soil and void are described by void ratio (e) and porosity (n).
Void ratio (e) is the ratio of the volume of voids (V_v) to the volume of solid (V_s), usually expressed as a decimal.

Void ratio (e)

$$e = \frac{Vv}{Vs} \qquad (4.1)$$

Porosity (e)

$$n = \frac{Vv}{V} \tag{4.2}$$

Both void ratio and porosity indicate the relative percentage of voids volume in the soil. They are related as;

$$e = \frac{Vv}{Vs} = \frac{Vv}{V - Vv} = \frac{Vv/V}{1 - Vv/V} = \frac{n}{1-n} \tag{4.3}$$

Moisture content (w)

Water plays a fundamental part in determining the engineering of any soil. There are some define related to the water present.

$$w = \frac{Ww}{Ws} \tag{4.4}$$

Degree of saturation (Sr)

$$Sr = \frac{Vw}{Vv} * 100\% \tag{4.5}$$

Specific gravity (Gs)

$$Gs = \frac{W_s}{V_s \gamma_w} \tag{4.6}$$

Relationship between densities

Bulk unit weight, $\gamma = \frac{W}{V}$ (4.7)

Dry unit weight, $\gamma_d = \frac{W_s}{V}$ (4.8)

$$\gamma = \frac{W}{V} = \frac{Ws + Ww}{V} = \frac{Ws\left(1 + \frac{Ws}{Ws}\right)}{V} = \frac{Ws}{V}(1+w) = \gamma_d(1+w)$$

$$\gamma_d = \frac{\gamma}{1+w} \tag{4.9}$$

Relationship between Unit weights, Void ratio, Moisture content and Specific gravity

From Eq.4.8 and Eq.4.6

$$\gamma_d = \frac{W_s}{V} = \frac{Gs\gamma_w V_s}{V} = \frac{G_s \gamma_w}{V/V_s} \tag{4.10}$$

From eq. 4.3

$$e = \frac{V - V_s}{V_s}, \quad \text{And} \quad 1 + e = \frac{V}{V_s}, \quad \text{substituting in Eq.4.10}$$

$$\gamma_d = \frac{Gs\gamma_w}{1+e} \quad \text{And} \quad 1 + e = \frac{G_s\gamma_w}{\gamma_d},$$

$$e = \frac{G_s\gamma_w}{\gamma_d} - 1 \tag{4.11}$$

Relative density (Dr)

Relative density is used to indicate the insitue densities and this value gives a chance to compare the overall composition of voids and soil for a specific soil. It is the ratio of the actual density to the maximum possible density of soil.

$$Dr = \frac{e_{\max} - e}{e_{\max} - e_{\min}} * 100 \tag{4.12}$$

Where,

Dr, is the relative density given as percentage and maximum is 100%.

Using the definition of dry unit weight, D_r can be expressed as,

$$Dr = \frac{\left[\frac{1}{\gamma_{d(\min)}}\right] - \left[\frac{1}{\gamma_d}\right]}{\left[\frac{1}{\gamma_{d(\min)}}\right] - \left[\frac{1}{\gamma_{d(\max)}}\right]} * 100 \tag{4.13}$$

e_{max} is the void ratio and $\gamma_{d(min)}$ is the lowest dry unit weight of the soil in loosest condition. e_{min} is the void ratio and $\gamma_{d(max)}$ is the highest dry unit weight of the soil in densest condition. e is the instantaneous void ratio γ_d is insitue dry unit weight of the soil.
e_{max}, e_{min} , $\gamma_{d(max)}$ and $\gamma_{d(min)}$ are determined in laboratory, adopting specified procedures.

Table 4.1. Soil condition based on relative density (Kulathilaka, S.A.S 2007)

Relative density (%)	**Description**
10-15	Very loose
15-50	Loose
50-70	Medium
70-85	Dense
85-100	Very dense

4.2. Data Analysis- Model tests

4.2.1. Effect of ground loosening

As explained in chapter 3.2, artificial ground loosening was formed by dissolving glucose inside the model test. Figure 4.2 shows a typical example of ground loosening caused by one model having initial relative dry density of 73% with inserting a semi cylindrical glucose block with diameter of 57mm and length of 50mm. Figure 4.2(a) shows the initial condition and Figure 4.2(b) shows the loosened ground after water infiltration and drainage.

Extent of loosened region

After dissolution of glucose, some void spaces were formed and soil sited above the glucose block was deformed. General demarcation of height of ground affected by deformation and loosening was done by observing the deformations of colour sand layers. These colour sand were placed horizontally in the model to separate each 2 cm of Toyoura sand during preparation of the model in order to observe the deformation.

This fact itself was not enough to demarcate the height of loosening in an accurate manner. Therefore, the penetration resistance through different vertical profiles was checked (4.2.2) by small cone penetrometer as explained in Chapter 3.2. Then the height affected by loosening was demarcated after conjunction with penetrometer results and color sand's layer deformations. Calculation of length of the affected area and demarcation of the loosened part was done by using the image analyzing software called "Image J".

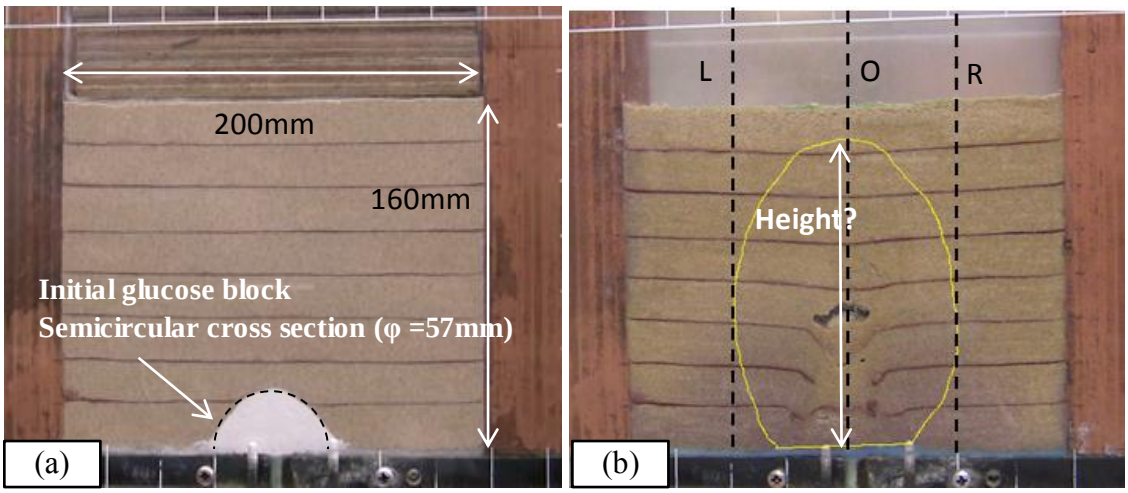

Figure 4. 2: Typical model ground (a) Initial condition (b) After ground deformation

4.2.2. Penetration resistance

One of the best ways to check the strength reduction on loosened ground is by comparing resistance against penetration resistance. Penetration resistance measured by this cone

penetrometer is the summation of skin friction and cone tip resistance (Figure 4.3). Cone tip resistance is the soil resistance to advance the cone tip through soil and skin friction is the resistance developed between the soil and the cylindrical skin of the penetrometer. The resistance force was directly measured though the load cell and interpreted as a load in "N"

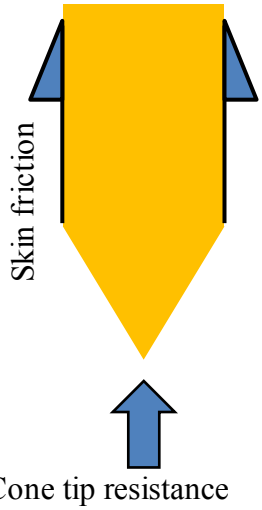

Figure 4.3: Components of the penetration resistance force

The maximum height of loosened area (Figure 3.2(b)) is a very important factor to be found in this test. By plotting the penetration resistance over penetration depth in a vertical profile reflects the maximum effect of loosening on ground. Penetration resistance through all the vertical profiles shows tendency of decreasing after achieving a peak value. Both left and right sides profiles turning back at same elevation which is deeper than central profile. This effect was due to non-uniform stress distribution due to wall friction effect. However, penetration resistance of central profile always starts to decrease at higher elevation than corner profiles in model tests with loosening. Therefore maximum height of loosening was considered as turning point of penetration resistance through central profile. The effective width of the deformed area can't be accurately identified by checking the penetration resistance due to effect of wall friction. Sample plot of penetration depth vs. penetration resistance vs. is shown in Figure 4.4.

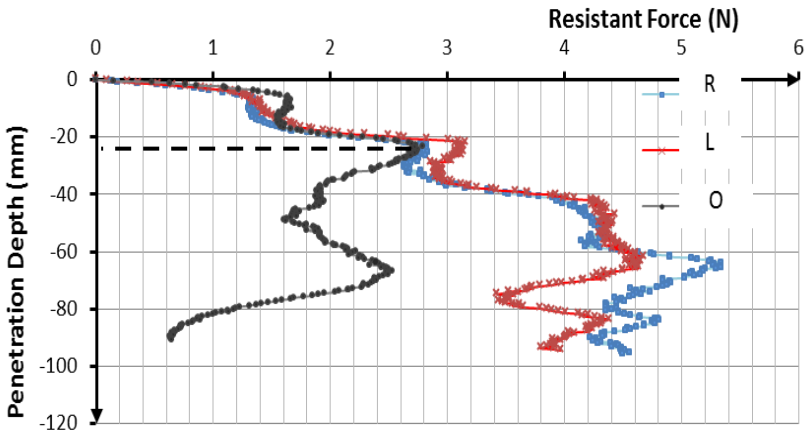

Figure 4.4: Typical plot of Penetration depth Vs. Penetration resistance

4.3. Data Analysis- Triaxial tests

4.3.1. Stress Analysis

As explained in the previous chapter, all the test were conducted under drained condition which means that total stresses and effective stresses were the same while back pressure was zero. In these experiments, minor effective principal stress (σ_3') was directly measured by using HCDPT.

In these experiments the deviator stress or the load applied by loading piston was measured through a load cell and results were automatically recorded in to computer. Therefore, major effective principal stress was calculated as below.

The axial stress was computed by using Eq. 4.14.

$$\text{Deviator stress, } \sigma_d = \frac{\text{Applied vertical load}}{\text{Cross sectional area of specimen}} \qquad \text{Eq. 4.14}$$

$$\text{Axial stress, } \sigma_1 = \sigma_3 + \sigma_d \qquad \text{Eq. 4.15}$$

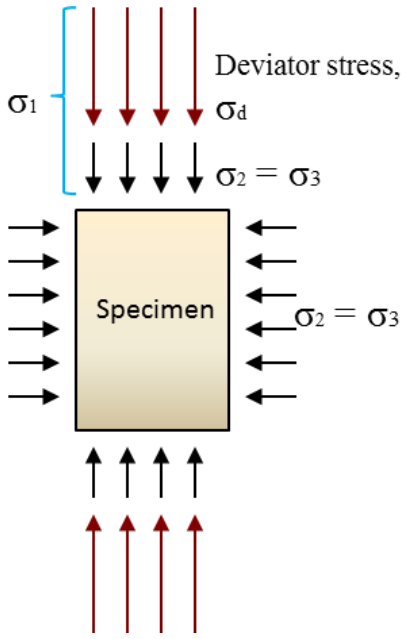

Figure 4. 5: Stresses applying on triaxial specimen

4.3.2.Strain Analysis

Strain is a normalized measure of deformation representing the displacement between particles in the body relative to a reference length. Generally, strain can be calculated by eq. 4.16.

$$\varepsilon_{1\to 2} = \frac{\Delta H_1}{H_0} = \frac{H_0 - H_1}{H_0}$$ Eq.4.16

However, for a small duration of time, the initial reference height of the specimen is changing and H_0 is slightly different at next condition. This effect is not considered in Eq. 4.16. In order to consider this effect, the analysis of deformations were obtained by using true or logarithmic strain because it can give a more direct measure of materials with considering the accumulation of deformation during the process.

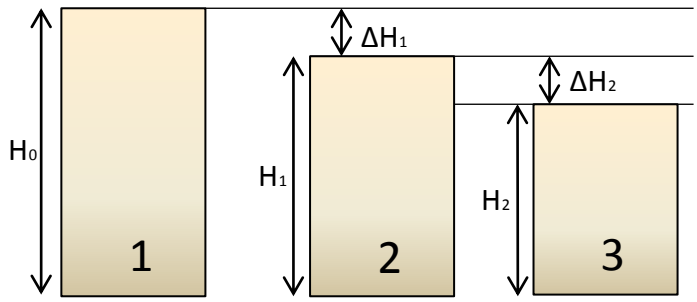

Figure 4.6: Variation of axial strain

As given in Eq. 4.16,

$$\varepsilon_{1\to 2} = \frac{\Delta H_1}{H_0} = \frac{H_0 - H_1}{H_0}$$

$$\varepsilon_{2\to 3} = \frac{\Delta H_2}{H_1} = \frac{H_1 - H_2}{H_1}$$ Eq.4.17

For the general case,

$$\varepsilon_{1\to x} = -\int_{H_1}^{H_x} \frac{\Delta H}{H}$$ Eq. 4.18

$$\varepsilon_{1\to x} = -(\ln H_x - \ln H_1)$$ Eq. 4.19

$$\varepsilon_{1\to x} = -\left(\ln \frac{H_x}{H_1}\right)$$ Eq. 4.20

Therefore, eq.4.21, 4.22, 4.24 was used to calculate the axial strain, radial strain and volumetric strain respectively.

$$\varepsilon_{axial} = -\left(\ln\frac{H_{current}}{H_{initial}}\right) * 100 \quad \text{Eq.4.21}$$

$$\varepsilon_{radial} = -\left(\ln\frac{\emptyset_{current}}{\emptyset_{initial}}\right) * 100 \quad \text{Eq.4.22}$$

$$\varepsilon_{volumetric} = \varepsilon_{axial} + 2 * \varepsilon_{radial} \quad \text{Eq.4.24}$$

In case of axial strain two different strains were calculated based on LDT s and EDT. The strain range calculated by LDT s is very small and it was used to evaluate the Young's modulus and Poisson's ratio. The large axial strain caused during the shearing was evaluated by data received by EDT. For strain calculation of EDT, Initial height of the specimen was considered as $H_{initial}$. But for LDTs, the distance between two hinges of LDT were considered as $H_{initial}$. Since, there are 4 LDTs; average of one pair at the same elevation was taken as one.

One pair of LDT which fixed to bottom half of the specimen will give the axial strain at lower part, while the other pair of LDT will give the strain at top half. However, average of all 4 LDTs was used when comparing the overall behaviour among each test condition.

In case of radial strain, the initial diameter ($\phi_{initial}$) was directly measured at three different heights same as where the Clip gauges were fixed by using a pi gauge tape. Radial strains were computed separately for lower and upper half of the specimen by averaging two relevant Clip gauges.

4.3.3. Young's modulus (E)

Young's modulus, E was calculated by Eq.4.25, evaluating the tangent of stress-strain curve obtained during small cyclic loading. Cyclic loading is consisted of 11 small strain cyclic cycles with 0.001% of strain amplitude. Gradient for each cycle was separately calculated and finally average of 11 values was taken as result. Cycling loading was applied three times for each test as before water infiltration, after 1st water cycle and after 2nd water cycle. The "E "value computed for 10th cycle of, 2nd cyclic loading for one test condition is shown in Figure 4.7.

$$E = \left[\frac{\Delta\sigma_1}{\Delta\varepsilon_{axial}}\right] \quad \text{Eq.4.25}$$

Where, $\Delta\sigma$ = range of axial stress and $\Delta\varepsilon$ = range of axial strain

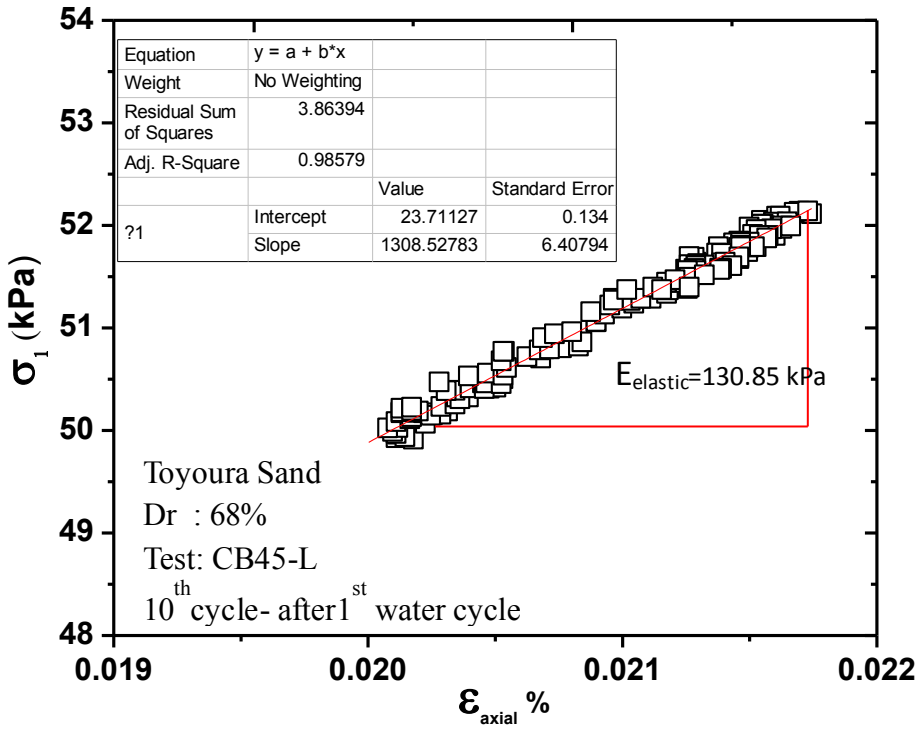

Figure 4.7: Typical stress-strain relation for small strain cyclic loading

4.3.4. Poisson's ratio (ν)

Poisson's ratio is defined as the lateral deformation caused by application of load in longitudinal direction. It was computed by Eq.4.26. Radial strain was measured at lower part, center and top part by 3 clip gauges as explained earlier. Therefore, "ν " value was also computed for lower half and top half of the specimen separately by calculating the axial and radial strains separately for lower and top halves by relevant LDTs and CGs. The "ν "value computed for 10th cycle of, 2nd cyclic loading for one test condition is shown in Figure 4.8.

$$\nu = -\left[\frac{\Delta\varepsilon_{radial}}{\Delta\varepsilon_{axial}}\right] \qquad \text{Eq.4.26}$$

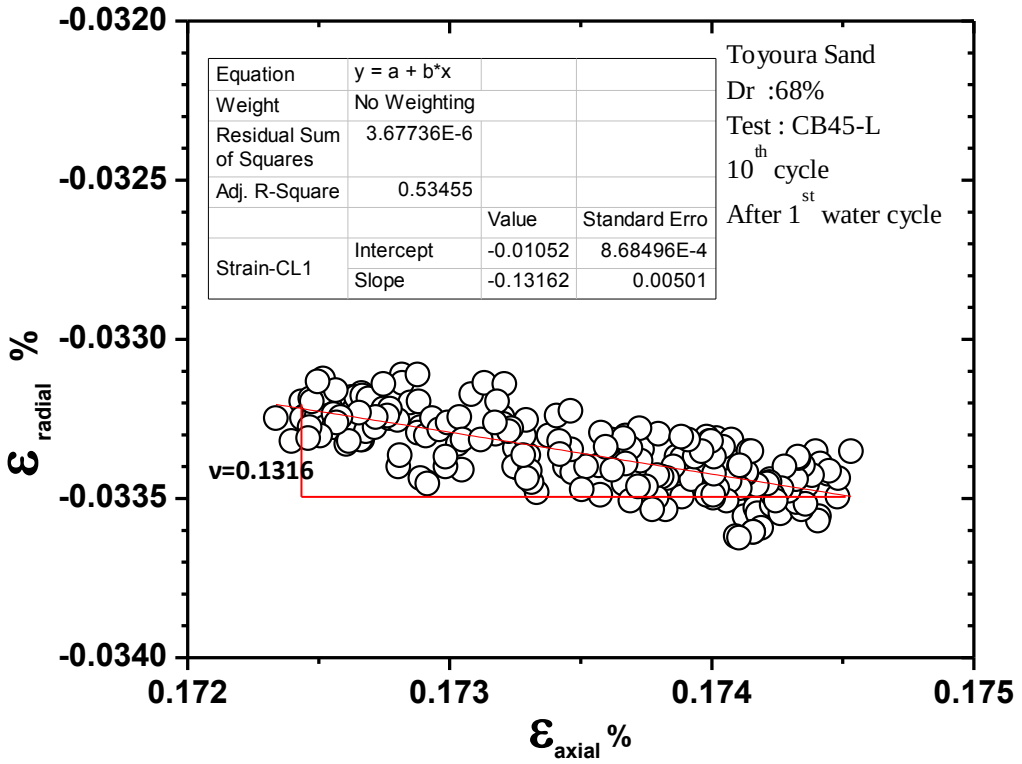

Figure 4.8: Axial - radial strain relation for small strain cyclic loading

4.3.5.Void ratio Function [f (e)]

Stiffness is highly influenced by the density of the specimen. In this study, the specimens having various densities were tested. So the direct comparisons of outcomes from having different densities (void ratios) are not eligible. To compare the quasi-elastic deformation properties among the specimens having various densities (void ratios), void ratio function was used. Many researchers had proposed the normalizing function. Following are some of the widely employed void ratio functions.

$$f(e) = \frac{(2.17 - e)^2}{(1 + e)}$$ (Hardin and Richart, 1963) Eq.4.27

$$f(e) = \frac{(2.97 - e)^2}{(1 + e)}$$ (Hardin and Richart, 1963) Eq.4.28

In this study, Eq 4.28 was used in all cases.

4.3.6. Small strain stiffness (Gs)

Measured Young's modulus "E" can be converted in to the shear modulus, called small strain modulus (Gs). The conversion relationship is derived considering the isotropic, homogeneous and elastic material. The used equation is in Eq. 4.29.

$$\mathrm{Gs} = \frac{E}{2(1+\nu)} \qquad \text{Eq.4.29}$$

Finally, Small strain modulus was normalized by the void ration function, f (e) found by eq.4.28 to avoid the effect of small density or voids in specimen.

CHAPTER -05

RESULTS AND DISCUSSION – MODEL TESTS

5.1. Test Programme

Main objective of conducting this 2-dimentional (2-D) model tests is to determine a way of forming loosened sand artificially in laboratory scale; because, main objective of this research is to measure the mechanical properties of loosened sand using triaxial apparatus. Therefore, there should be a procedure to create loosened sand inside the triaxial specimen. There are two ways either creating internal erosion by allowing soil to displace from triaxial specimen or introduce a potential cavity by a water soluble material and generate loosening by dissolving it with water. Since it is very difficult to implement the first method in traditional triaxial test, attention was directed into second method.

Therefore, 2-D model tests were conducted as explained in Chapter 3.3. Preliminary tests were performed in order to examine the basic facts related to this process such as time taken for dissolving glucose, extend of loosened region compare to potential cavity, required water infiltration rate, drainage conditions, etc. Therefore tests programme was arranged as given in Table 5.1.

Table 5. 1: Test programme of model tests

Test No	**Glucose block**		**Dr %**	**Water inflow rate**	**Remarks**
	Cross section	**Size (mm)**			
1	Semi-circular	5.7ø	70.6%	30 ml/min	Speed water inflow
2	Semi-circular	5ø	71%	30 ml/min	Glucose with lower solubility
3	Rectangular	H =20 W =30	96%	20 ml/min	Dense ground
4	Rectangular	H =20 W =30	98%	20 ml/min	Compacted ground
5	Rectangular	H =20 W =30	37.5%	20 ml/min	Loose ground
6	Rectangular	H =20 W =10	84.3%	20 ml/min	Small cavity
7	No cavity	-	83.1%	20 ml/min	Controlled specimen

5.2. Results

Ground deformations related to each test occurred with dissolving of glucose, is shown in Figure 5.1 to 5.7. Initial condition of the model ground, condition after water drainage is separately shown in Figure (a), (b) of each figure. Further control conditions with test results is summarized in to a table in Figure (c) and penetration resistance details is given in Figure(d) separately in each Figure.

Facts and findings of this series of model tests are discussed in 5.3 under discussion.

Test No-1

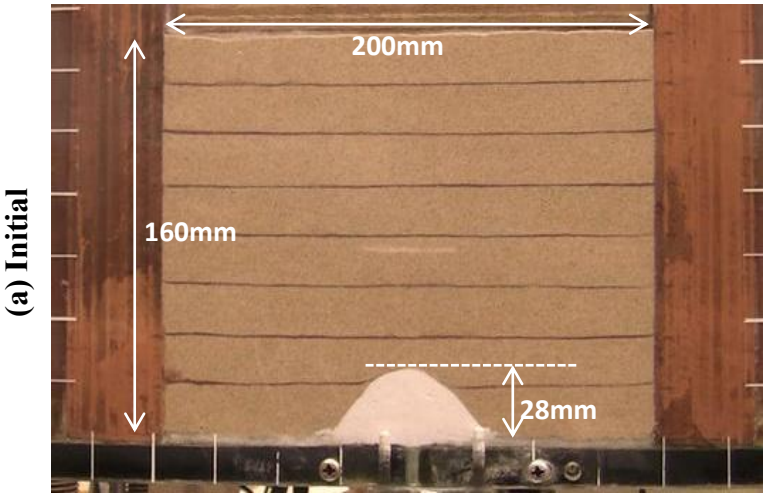

(a) Initial

Toyoura sand	Dr = 73.5%
Glucose Block	Semi circular shape Approximate diameter = 57 mm
Water flow rate	30 ml/minute
Moisture content	Initial = 0% During the penetration test = 23.4%
Maximum height of loosening	H_{max}= 138mm (H_{max} / model height) = 138/160 =86.3%

(c) Conditions and test results

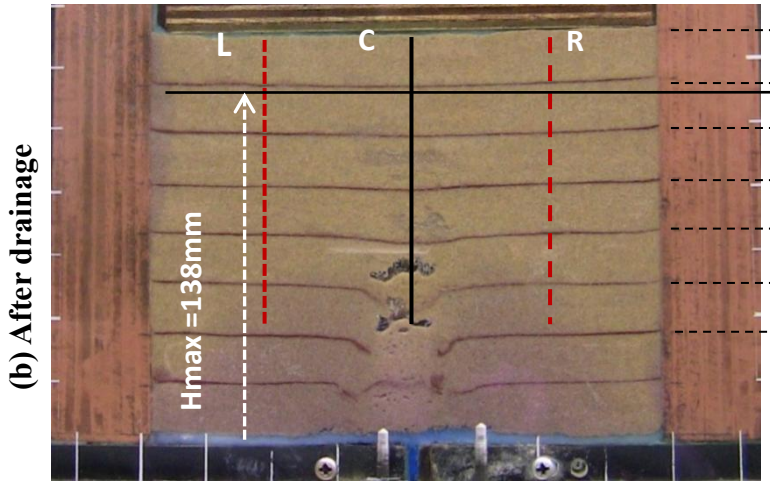

(b) After drainage

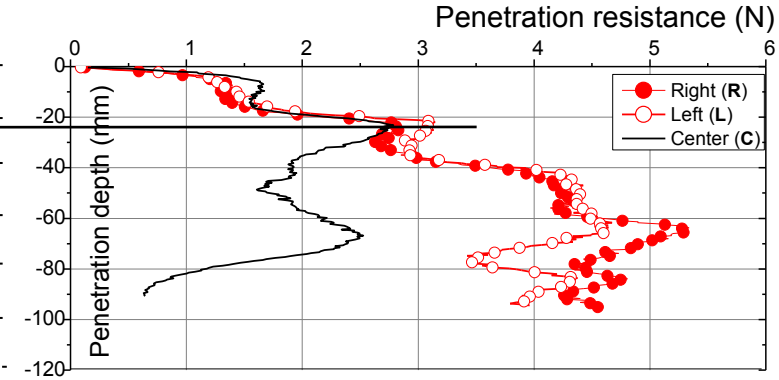

(d) Penetration depth vs. penetration resistance

Figure 5. 1. Test results –Test No1

Test No-2

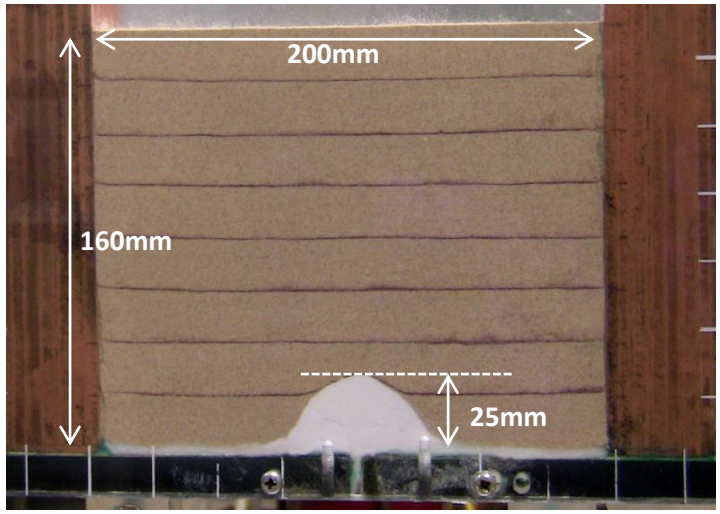

(a) Initial

Toyoura sand	Dr = 70.6%
Glucose Block	Semi circular shape –lower solubility Approximate diameter = 50 mm
Water flow rate	30 ml/minute
Moisture content	Initial = 0% During the penetration test = 23.8%
Maximum height of loosening	H_{max}= 155mm (H_{max} / model height) = 155/160 =96.8%

(c) Conditions and test results

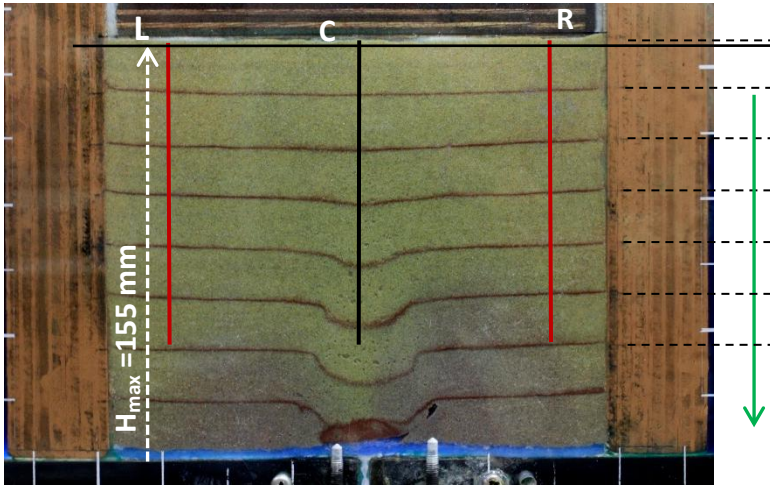

(b) After drainage

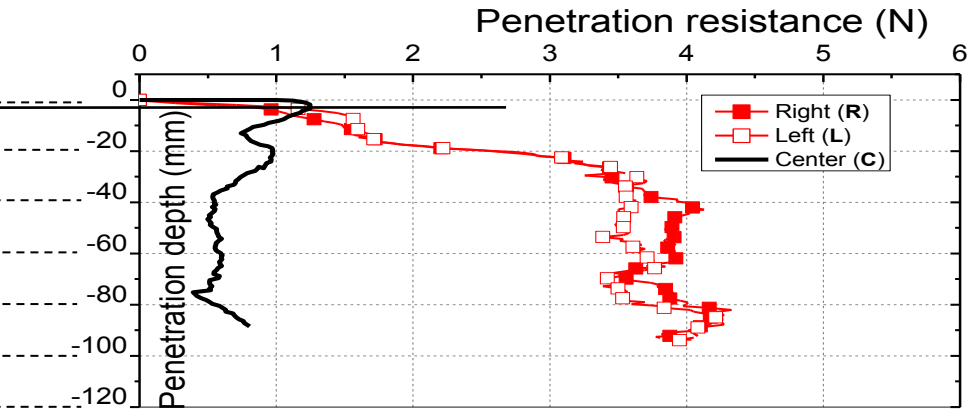

(d) Penetration depth vs. penetration resistance

Figure 5. 2: Test results –Test No2

Test No-3

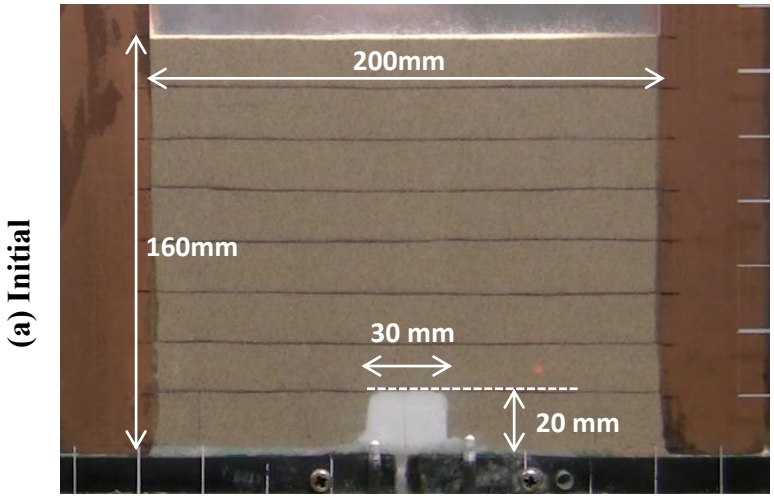

(a) Initial

Toyoura sand	Dr = 96.1%
Glucose Block	Rectangular cross section 2cm height, 3cm Length
Water flow rate	20 ml/minute
Moisture content	Initial = 0% During the penetration test = 22.62%
Maximum height of loosening	H_{max}= 130mm (H_{max} / model height) = 130/160 =81.2%

(c) Conditions and test results

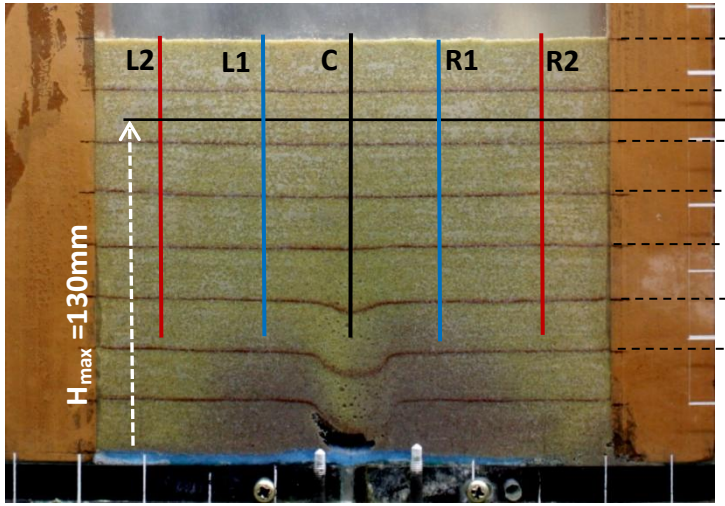

(b) After drainage

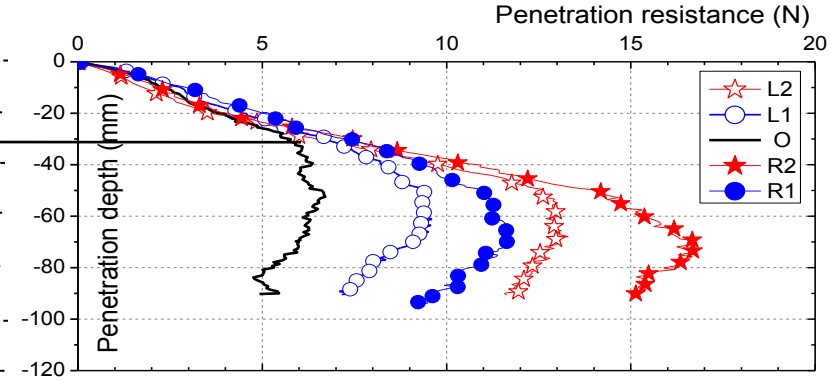

(d) Penetration depth vs. penetration resistance

Figure 5. 3: Test results –Test No3

Test No - 4

(a) Initial

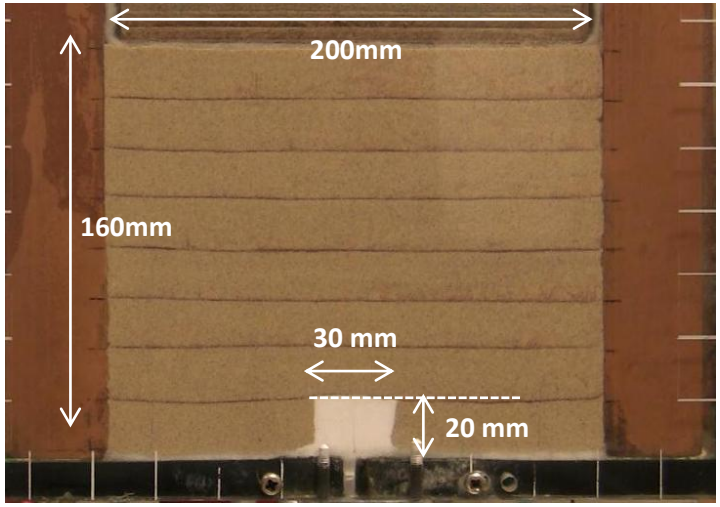

Toyoura sand	Dr = 98.2% (compacted sand)
Glucose Block	Rectangular cross section 2cm height, 3cm Length
Water flow rate	20 ml/minute
Moisture content	Initial = 0% During the penetration test = 24.3%
Maximum height of loosening	H_{max}= 110mm (H_{max} / model height) = 110/160 =68.7%

(c) Conditions and test results

(b) After drainage

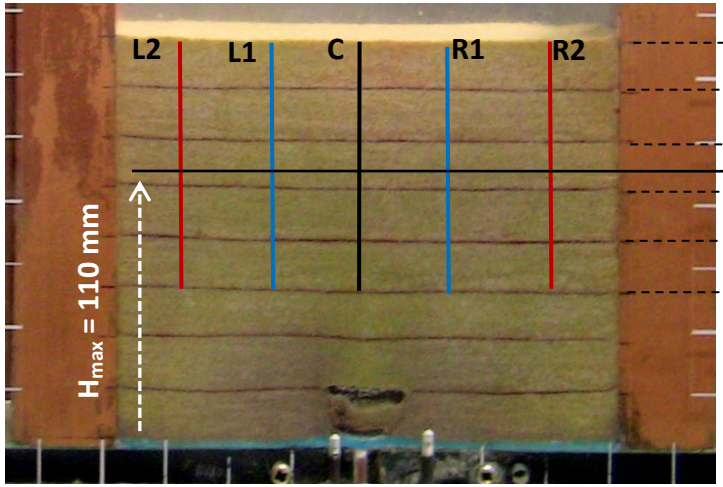

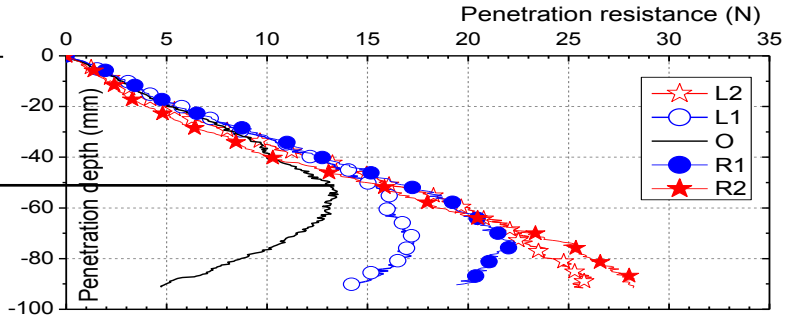

(d) Penetration depth vs. penetration resistance

Figure 5. 4: Test results –Test No4

Test No - 5

(a) Initial

(b) After drainage

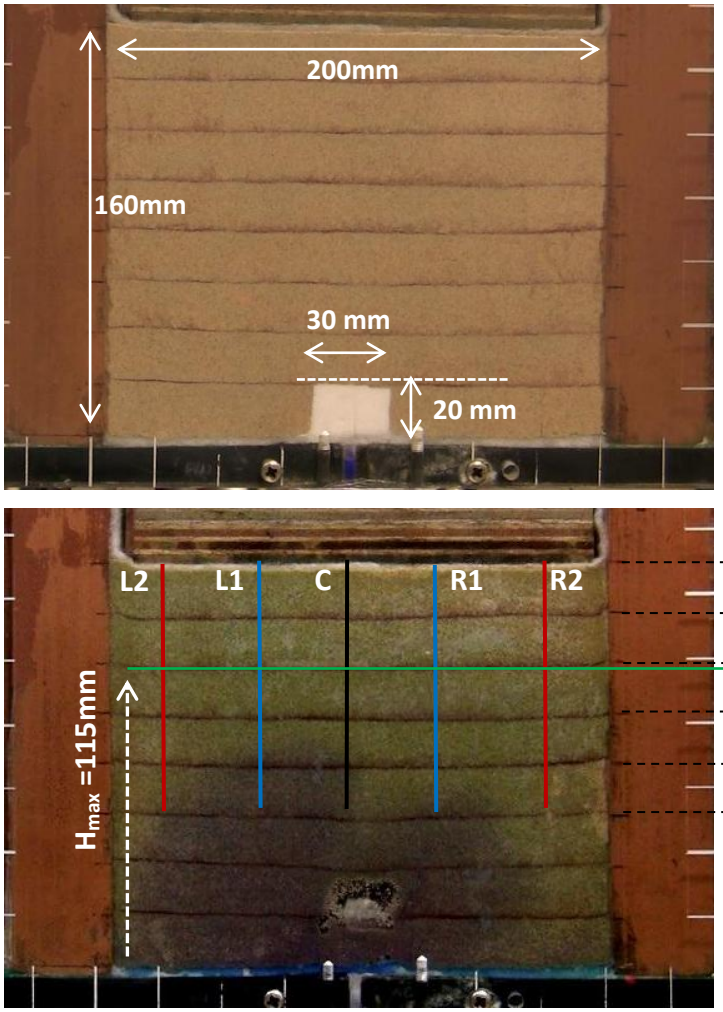

Toyoura sand	Dr = 37.5% (loose sand)
Glucose Block	Rectangular cross section (lower solubility glucose) 2cm height, 3cm Length
Water flow rate	20 ml/minute
Moisture content	Initial = 0% During the penetration test = 26.1%
Maximum height of loosening	H_{max}= 115mm (H_{max} / model height) = 115/160 =72%

(c) Conditions and test results

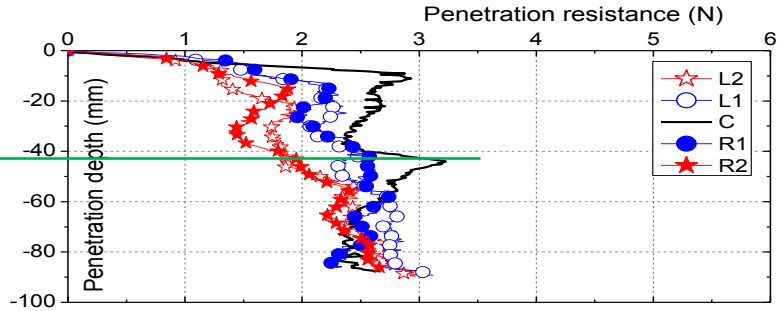

(d) Penetration depth vs. penetration resistance

Figure 5. 5: Test results –Test No5

Test No – 6

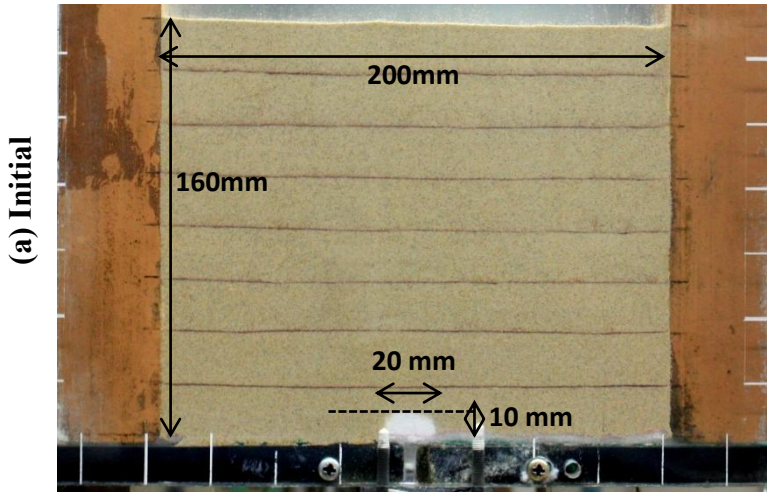

Toyoura sand	Dr = 84.31%
Glucose Block	Rectangular cross section (Rapid solubility glucose) 1cm height, 2cm Length
Water flow rate	40 ml/minute (higher flow rate)
Moisture content	Initial = 0% During the penetration test = 23.4%
Maximum height of loosening	H_{max}= 107mm (H_{max} / model height) = 107/160 =66.9%

(c) Conditions and test results

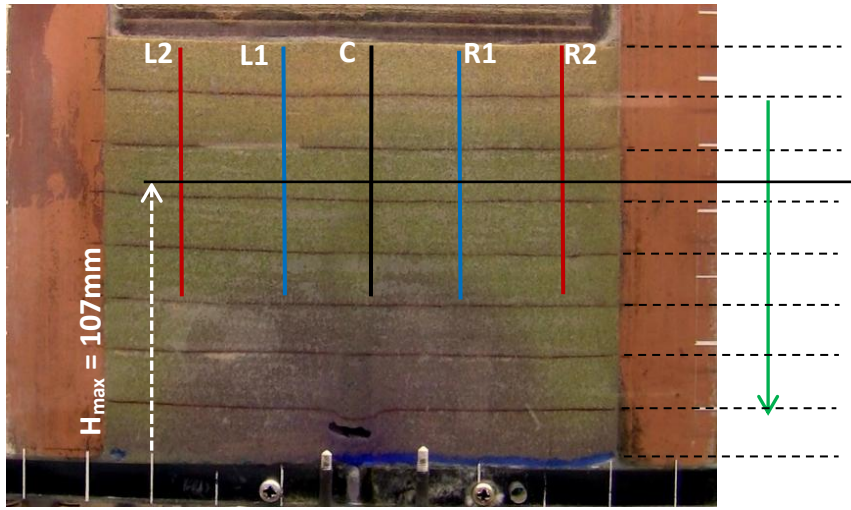

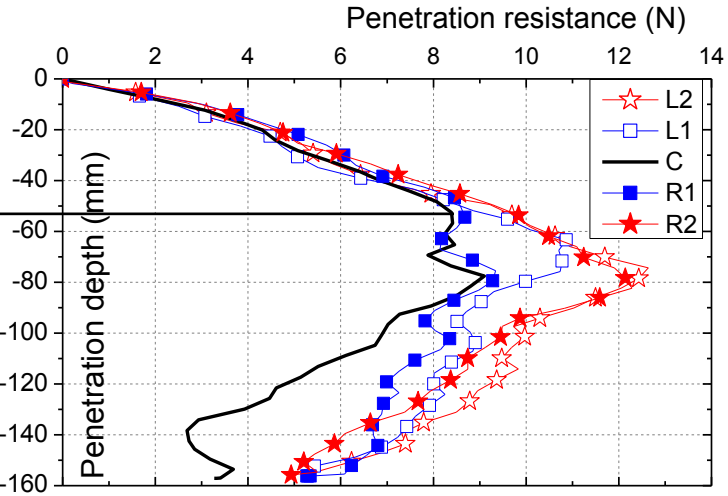

(d) Penetration depth vs. penetration resistance

Figure 5. 6: Test results –Test No6

Test No – 7

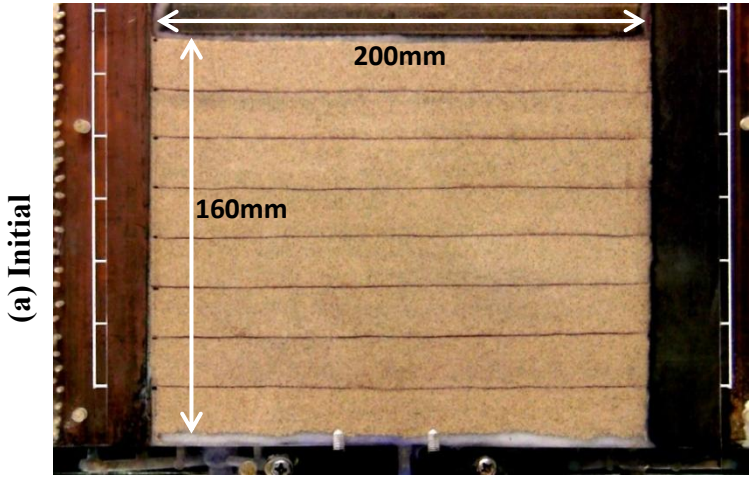

(a) Initial

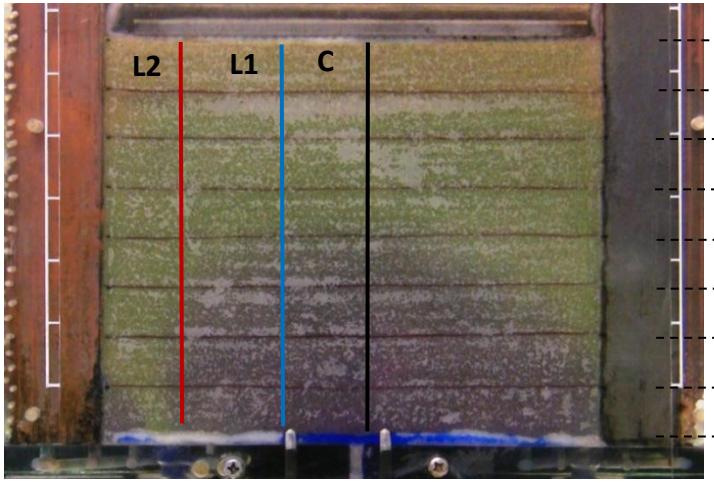

(b) After drainage

Toyoura sand	Dr = 83.1%
Glucose Block	No glucose block Controlled specimen
Water flow rate	20 ml/minute
Moisture content	Initial = 0% During the penetration test = 24.5%
Maximum height of loosening	Penetration resistance through all profiles behaves similar pattern. This is due to wall friction of walls.

(c) Conditions and test results

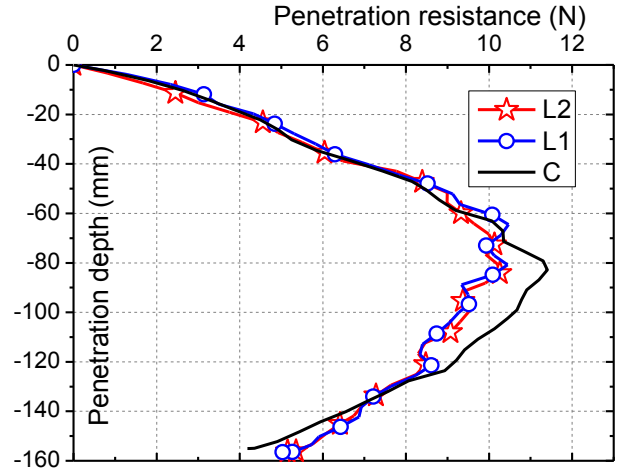

(d) Penetration depth vs. penetration resistance

Figure 5. 7: Test results –Test No7

5.3. Discussion

Main objective of developing artificial ground loosening in uniform grain sand was achieved by above series of model tests. Meanwhile, some important facts related to time required for dissolving of glucose, relationship with extent of loosening to size of glucose block and influence of soil density, compaction effect, and drainage rate on loosening process were observed. In this clause, those findings will be discussed with related experimental records.

5.3.1. Effect of wall friction on penetration resistance in small 2-D models

Special behaviour of penetration test results which was observed through-out the entire test records shown in Figure 5.1 to 5.7. In all most all the tests, penetration resistance has started increasing from ground surface till the 80mm (nearly half of the total model height) and then decreasing even closer to the left and right boundaries where the ground loosening was negligible. Decreasing of resistance at the mid of the way is reasonable for the central profile since, ground loosening can influence on it. However, it is unusual to see the resistance is decreasing even at corners of the model ground. Therefore controlled experiment was done in Test No.7 to observe this effect when the ground was uniform without a cavity. Even in that case, similar behaviour was expected in all the vertical profiles. There are some possible reasons for this behaviour.

- Non-uniform moisture variation in model ground at the moment of penetration test.
- Applied surcharge of $10kN/m^2$ on model ground surface might not uniformly transfer to bottom of the model due to wall friction of acrylic walls of model apparatus.
- Compressible geotextile placed at the bottom surface of model apparatus (to prevent sand particle washing out from opening) might affect the resistance when the penetrometer is closer to the model bottom.

Effect of moisture variation

Therefore one more experiment was conducted in dry model ground to confirm the effect of moisture variation. In this test, surcharged was applied and also the geotextile was placed as previous. Recorded results are shown in Figure (Figure 5.8). It can be clearly observed that even in dry sand, a reduction of resistance for all the profiles has occurred. However, the elevation of this reduction for all 5 profiles seems to be the same. Hence this is either due to effect of wall friction or geotextile.

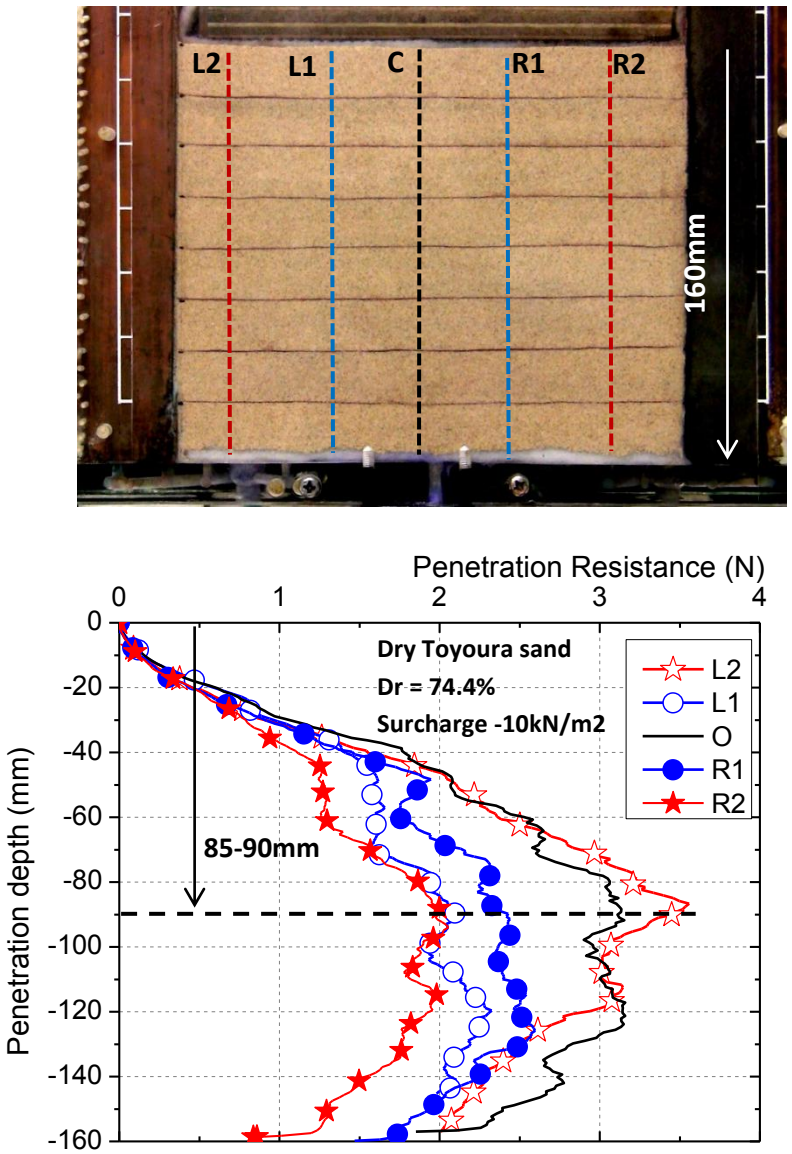

Figure 5. 8: Penetration resistance of dry toyoura sand(surcharge 10kN/m^2)

Effect of non-uniform stress transmission due to wall friction

Sudden reduction of penetration resistance at mid height of the model test has to be due to non-uniform stress transmission from top to bottom. Therefore similar type of model ground was made without glucose and penetration resistance was checked at dry condition without applying any surcharge. Results are shown in Figure 5.9. It was observed that the reduction of resistance is even there but, the elevation of reduction has occurred much closer to the model bottom. When the surcharge was applied, turning point was located at 70mm from bottom surface (Figure 5.8) which is reduced to 30mm when the model was free from surcharge (Figure 5.9). This turning at 30mm from bottom surface must be due to lower resistance caused by compressibility of geotextile placed at bottom surface of model. This fact reveals that the problem is a combination of non-uniform stress transmission due to effect of wall friction and also due to the geotextile.

However, in all three control conditions (no glucose) observed in Figure 5.7, 5.8 and 5.9 shows penetration resistance has decreased at similar elevation for all vertical profiles. This was different from other cases, where central profile shows lower resistance and turning point is always different from other profiles which are away from the center. Therefore, height of the affected loosened region can be identified as the point where the penetration resistance of central stats to decrease. (As analyzed in Figure 5.1(c) to 5.6(c))

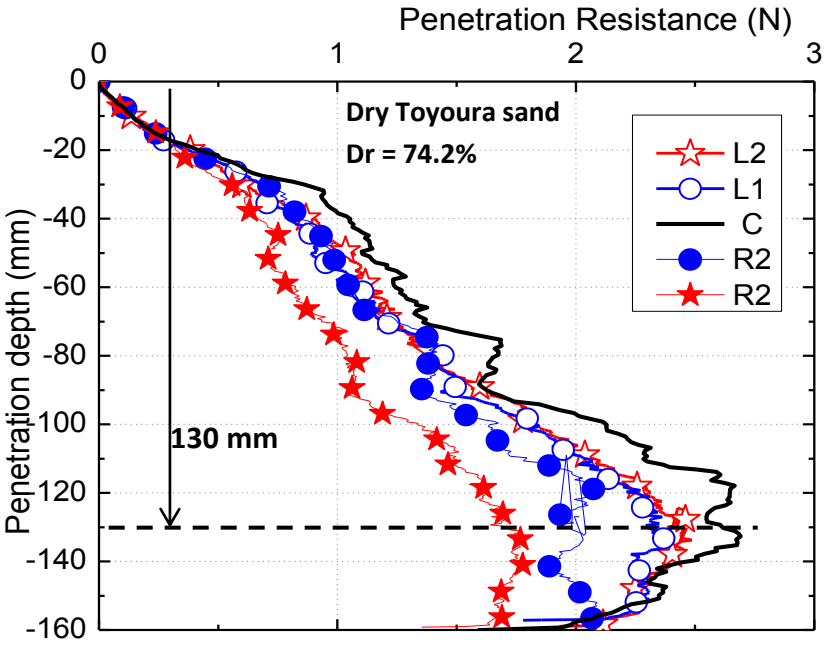

Figure 5. 9: Penetration resistance of dry toyoura sand(no surcharge)

5.3.2. Effect of cavity location refer to exiting ground water table

Conditions of Test No.1 and No.2 are almost similar, only the glucose type was different. In Test No.1, glucose powder imported from Sri Lanka (Brand name –SPC) was used while glucose bought from Japan was used in Test No 2. The difference is water solubility of Sri Lankan type is higher than Japanese type. This affect the condition of the cavity and soil boundary refer to the moisture condition due to time difference taken to dissolve the glucose. Ground deformation variation with time, during the water infiltration and after drainage for both cases is illustrated in Figure 5.10 and 5.11 respectively.

In test1, glucose get dissolved rapidly causing abrupt failure in ground with moving the initial cavity towards the surface. When the ground water level is increasing over a cavity while soil sited on potential cavity ceiling is dry; ground shows rapid failure. Dry soils are forming soil wedges and separating from normal ground along the boundary of dry and wet region. Then these separated soil wedges are collapsing in to initial cavity and replaced it while forming a new type of cavity above the initial one (Figure 5.10 (a, b, c, d)). Cavity has moved up by 3 times of initial cavity height.

Deformation style of Test-2 is different from Test-1. Glucose used in Test – 2 has lower solubility than the other. Until water was infiltrated up to the top level of the model ground, glucose block was not dissolved as shown in Figure 5.11(a). Therefore water input valve was closed for about 45minutes to allow glucose block to get solved. Then the drainage valve was opened slowly, and ground was deformed as shown in Figure 5.11(i). A clear cavity has formed with associated gradual loosening over it. Location of the cavity is not moved as Test-1.

Test-1 represents the condition of ground, when the ground table exists below the cavity and suddenly increasing over cavity. In this stage, dry soil sited above the cavity ceiling shows much collapsible behaviour. Test -2 represents a cavity originated below water table. This shows gradual and steady behaviour than first case. This means cavities located above the ground water table is more dangerous in the rainy season than located in deep ground. However, this effect might applicable for uniform sand under test conditions.

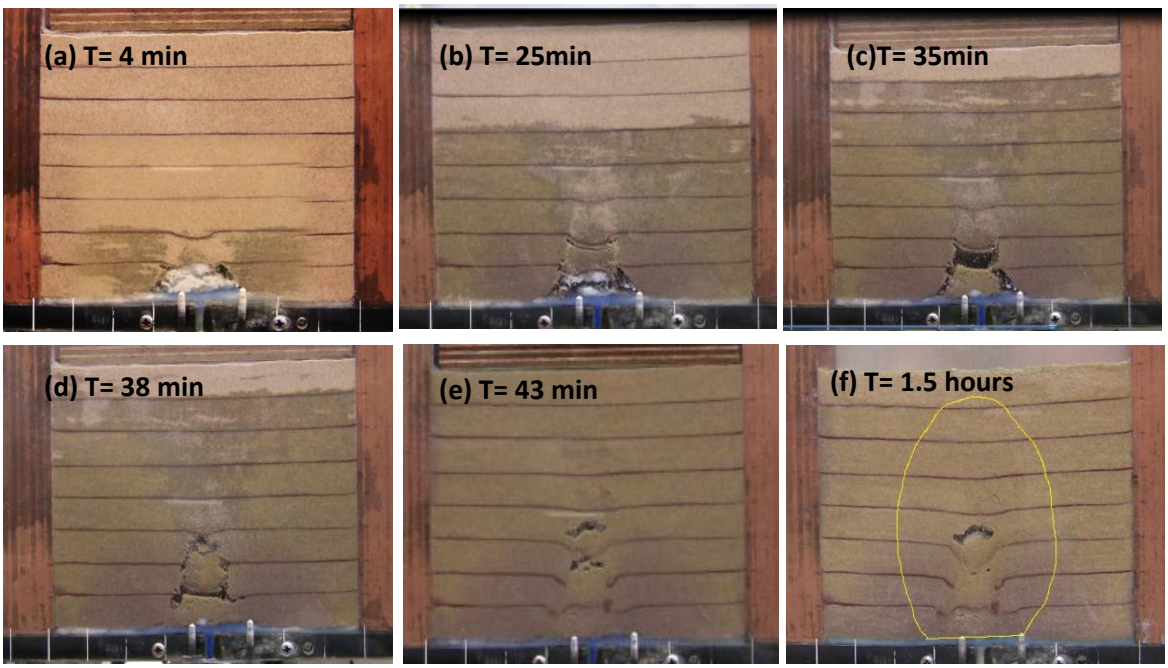

Figure 5. 10: Ground deformations caused during Test-1.

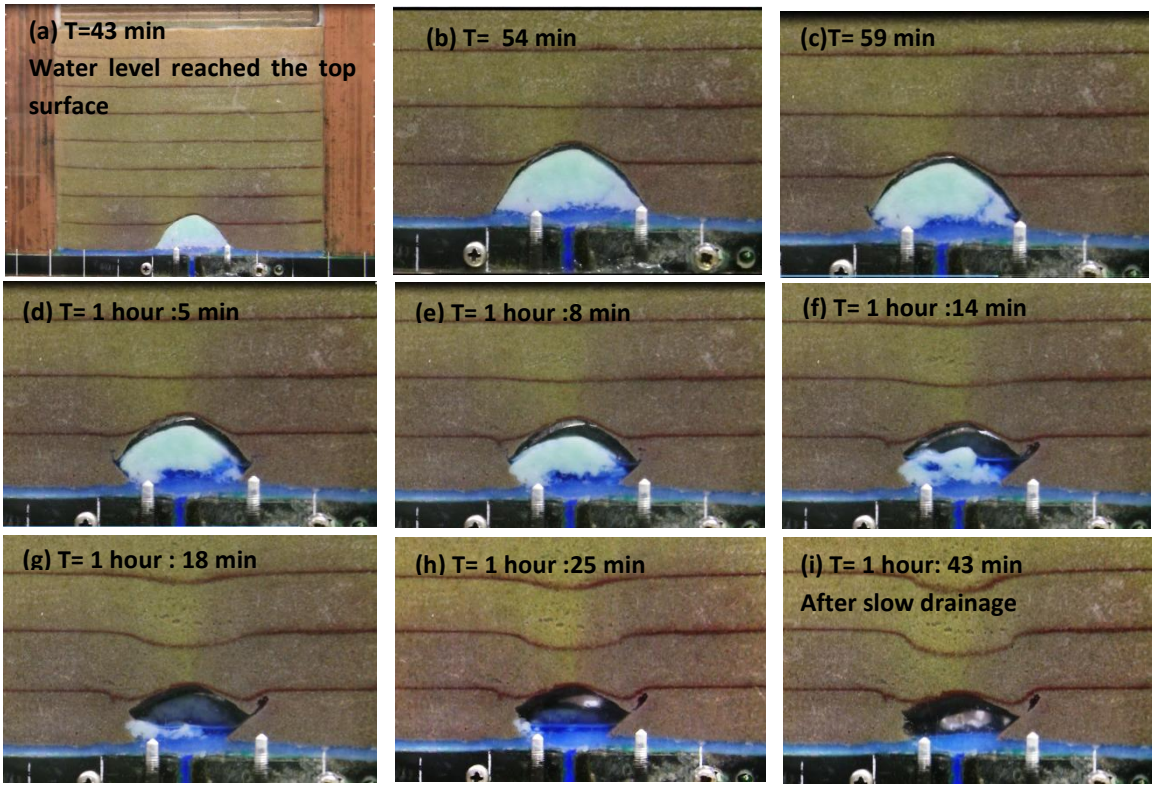

Figure 5. 11: Ground deformations caused during Test-2.

5.3.3. Effect of sudden drainage on cavity collapse

Suction playing a vital role for stability of underground voids. Before starting the drainage originated cavity and surrounding area was much stable. Even for drainage with slower speed, ground deformations were not rapid. However, in Test 2, drainage was started slowly and continued for about 3-4 minutes (Figure 5.12). Soil sited above the originated cavity was slightly displaced down and loosening was improved slightly. Then the drainage valve was fully opened to allow rapid drainage. Cavity was significantly collapsed (Figure 5.12(c)) and loosening effect has spread closer to the ground surface according to the penetration results (Figure 5.2(d)). Therefore even in the real condition, suction supports the cavity stability and prevents the sudden drainage. Whenever the water table is above the cavity and opened a path for sudden drainage, cavity can be collapse suddenly.

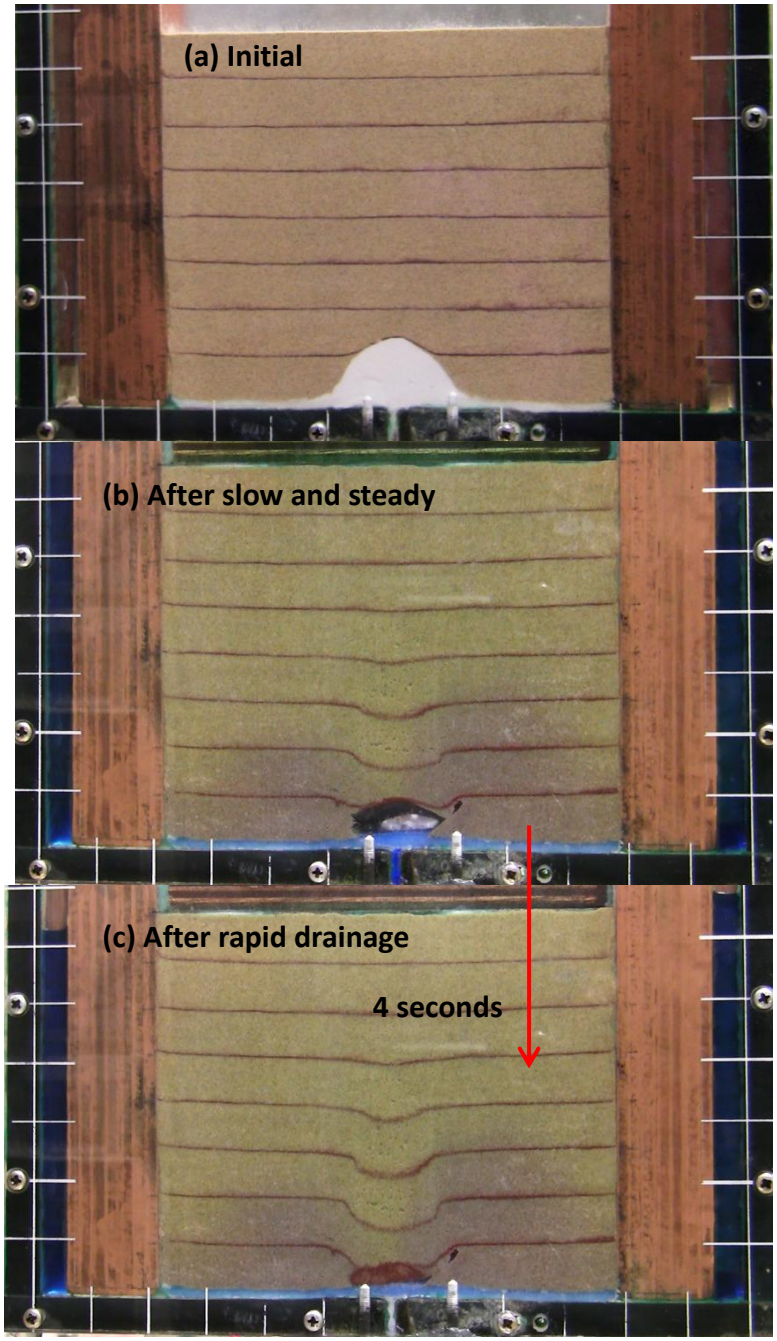

Figure 5. 12: Abrupt cavity failure by sudden drainage

5.3.4. Effect of ground compaction on loosening

Test No.3 and Test No4, were conducted in order to observe the influence of ground compaction effort on loosening phenomenon. Density of Test No.3 is slightly lower (96%) than Test No.4 (98%). But, sand was placed in two different methods as air pluviation technique in Test No.3 and compaction in Test No.4. Results shows higher difference in penetration results (Figure 3.d and 4.d). Compacted ground has nearly two times larger resistance than air pluviated ground though the density was almost similar. Furthermore affected maximum height of loosened region is 81% (4 times of initial cavity height) for air

pluviated sand while it is 68% (3.5 times of initial cavity height) for the compacted ground. This means, soil particle structure of compacted ground is much stable than normally pluviated sand. This effect is clearly observed though the particle size is much uniform in Toyoura sand. Therefore this effect will be observed much more clearly in well graded sand.

5.3.5. Summary

Main objective of initiating a method to form loosened sand in laboratory level was succeeded through dissolving a water soluble material. This method will be useful to form loosened ground in small triaxial specimen.

It was further observed and confirm that cavities exist in above normal ground table are much vulnerable for collapse at rising of ground water table crossing through it. Furthermore, suction seems supportive for the stability of cavities and abrupt cavity collapse was recorded at sudden drainage.

Even though, detail quantitative relation related to cavity propagation was not expected by these model tests, extend of loosening for each test is summarized in Table 5.2 with relative density and volume of glucose block. Since, control conditions of each test are not arranged properly it is difficult to identify a clear relationship between initial cavity height and height of loosened region. However, it is obvious and proved that when the cavity height is larger, loosened region is expanding.

Table 5. 2: Extent of loosening with size of initial glucose block for all 6 tests

Test No	Height of glucose block (mm)	$\frac{(V_{glucose})}{(V_{model})}$ %	Dr%	Affected height of loosening (mm)	(Affected height) /(model height) %	$\frac{H_{loosened\ height}}{H_{glucose\ height}}$	Description
1	28	4%	73.5%	138	86.3%	4.9	
2	25	3%	70.5%	155	96.5%	6.2	Rapid drainage
3	20	1.9%	96.1%	130	81.2%	6.5	
4	20	1.9%	98.2%	110	68.7%	5.5	Compacted soil
5	20	1.9%	37.5%	115	72%	5.7	Lower density
6	10	0.6%	84.3%	107	66.9%	10.7	Smaller cavity

Finally, general knowledge on controlling of water infiltration and drainage, time taken for complete dissolving of different glucose volumes and related area of loosening was observed by this series of model tests. Those facts are very important before implement the technique in triaxial specimen since inside the specimen is not transparent there.

Other than these facts related to the cavity formation and loosening, it was found that wall friction effect of 2-D model tests are very significant in case of small and thin models. This will be very important fact to consider in thin 2-D models.

(Clear images illustrating the process of loosening in each test is given in Appendix-I)

CHAPTER 6

Results and Discussion –triaxial tests

6.1. Test Programme

A number of triaxial tests were performed on Toyoura and Silica sand in order to establish the mechanical properties of loosened soil inside the triaxial specimen. 14 experiments were performed and 12 of those are done with Toyoura sand. Two experiments were performed on Silica sand in order to observe the soil grain size effect on ground loosening. Experiments related to Toyoura sand was categorized in to 5 different types based on the size and location of glucose block inserted as shown in Figure 6.1 to 6.5.

Notifications used for each test condition is illustrated below

- **NC** : **N**o **C**avity (controlled specimen, Figure 6.1)
- **CB45-L** : **C**avity at **45**mm from **B**ottom- **L**arge cavity with ø=30mm, h=15mm
  Cavity volume = 1.5% of specimen (Figure 6.2)
- **CB45-S** : **C**avity at **45**mm from **B**ottom – **S**mall cavity with ø=12mm, h=15mm
  Cavity volume = 0.25% of specimen (Figure 6.3)
- **CB-L** : **C**avity at the **B**ottom – **L**arge cavity with ø=30mm, h=15mm
  Cavity volume = 1.5% of specimen (Figure 6.4)
- **CB-S** : **C**avity at the **B**ottom - **S**mall cavity with ø=12mm, h=15mm (Figure 6.5)
  Cavity volume = 0.25% of specimen

One of each test was performed for two relative densities as approximately Dr = 35% and Dr = 60%. Furthermore two load cases (NC and CB45-L) were conducted to check the effect of confining pressure (Test No. 11 and 12) for increasing the confining pressure up to 100kPa while all other tests were conducted at σ_3 = 50kPa. Test Programme is shown in Table 6.1.

As explained in Chapter 3.3.5.2, water infiltration was carried out two times at step 3(a) and 5(a) drainage was done at step 3(c) and 5(c) corresponds to above. The amount of water penetrated in the 1st water cycle is 1500 ml and the 2nd cycle is only 200ml. the reason is, objectives of above two water cycles are different. Main objective of 1st water cycle is to completely dissolve the glucose block. Therefore 1500ml of water was passed through the

specimen for about 90-100 mints to facilitate enough time for dissolving glucose. The objective of the second cycle was to observe the properties of already loosened soil when it is undergone through another water infiltration. Therefore 2nd water cycle was just enough to completely penetrate the specimen height.

In Test No.3 and Test No.5 given in the Table 6.1, was checked only for one water cycle and the 2nd water cycle was not conducted due to practical problem.

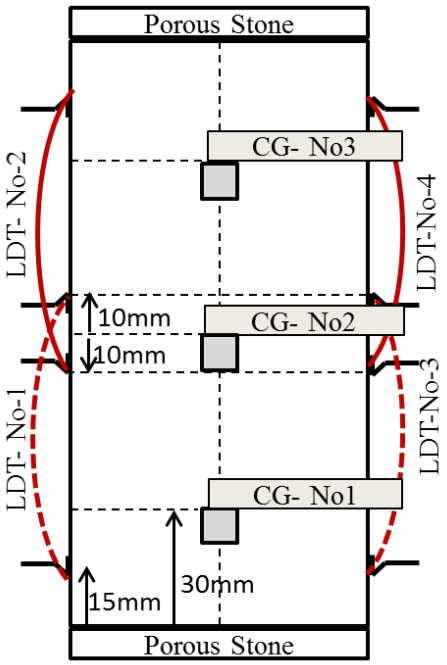

Figure 6. 1: No cavity (NC)

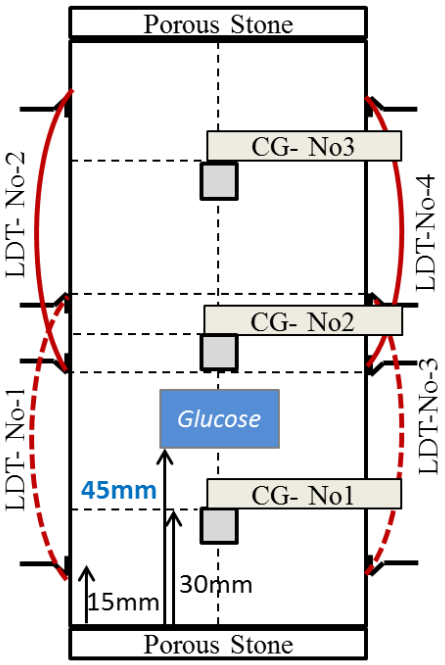

Figure 6. 2: CB45-L

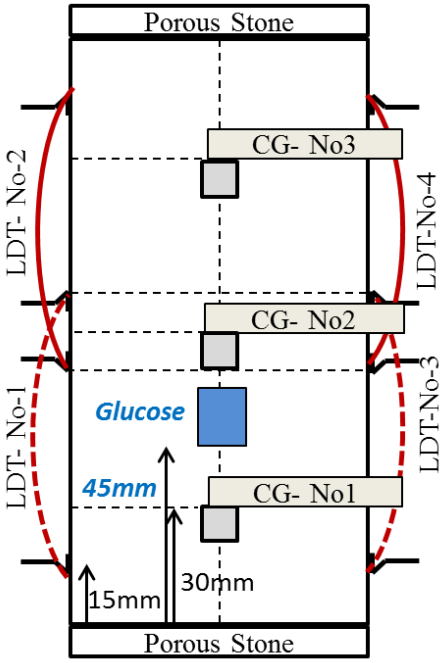

Figure 6. 3: CB45-S

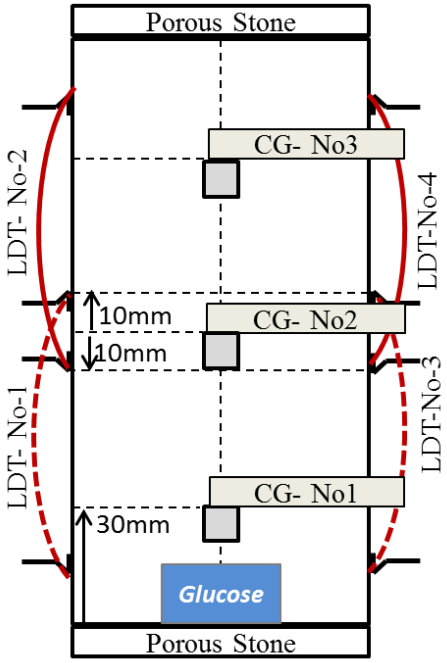

Figure 6. 4: CB-L

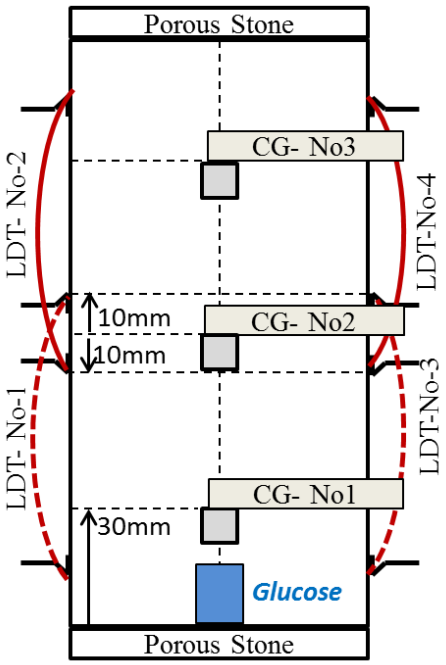

Figure 6. 5: CB-S

Table 6. 1. Schedule of triaxial experiments for both Toyoura and Silica sand

	Initial density (Dr %)	Void ratio (e)	Cavity location	Cavity Size	Confining pressure kPa	Notification	Symbol used in graphs
Toyoura Sand							
N0-1	64.47	0.7077	No cavity (NC)	-	50	NC (Dr,64%)	
N0-2	63	0.7122	CB45	Large(L)		CB45-L(Dr,63%)	
N0-3	59.7	0.7405		Small(S)		CB45-S(Dr,60%)	
N0-4	*		CB	*Large(L)*		*CB -L (Dr,68%)*	Test was failed
N0-5	64%	0.7371		Small(S)		CB -S (Dr,64%)	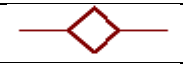
N0-6	35.3	0.8230	No cavity (NC)			NC (Dr,35%)	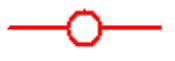
N0-7	36.47	0.8190	CB45	Large(L)		CB45-L (Dr,36%)	
N0-8	36.8	0.8130		Small(S)		CB45-S (Dr,37%)	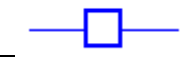
N0-9	36.68	0.8180	CB	Large(L)		CB -L (Dr,37%)	
N0-10	34.99	0.8190		Small(S)		CB -S (Dr,35%)	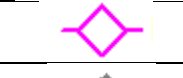
N0-11	37	0.8137	NC		100	NC (Dr,37%) -100kPa	
N0-12	35	0.8243	CB45	Large(L)		CB45-L (Dr,35%) -100kPa	
Silica Sand							
N0-13	58.30	0.6424	NC		50	NC (Dr,58%) -Silica	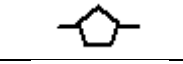
N0-14	61.57	0.6474	CB45	Large(L)		CB45-L(Dr,62%) -Silica	

6.2. Results

As explained in the test programme, 13 experiments were carried out to observe the effect of density, cavity size, cavity location, confining pressure and particle size on soil loosening accompanied with cavities. The variation of axial strain, radial strain, volumetric strain, Young's modulus and Poisson ration were evaluated before water infiltration, after 1st water infiltration and after 2nd water infiltration.

Variation of axial strain, radial strain and volumetric strain with time was plotted for each test condition. The typical behavior for a case with a glucose block is shown in Figure 6.6. Similar tendency is observed while dissolving glucose in all other cases. Variation of axial strain, radial strain , volumetric strain, stress-strain behaviour during shearing, details of water infiltration rate, Young's modulus and Poisson ratio was summarized in to one figure for one experiment and shown in Figure 6.7 to 6.19. Compressive strain of soil was considered as positive throughout this study.

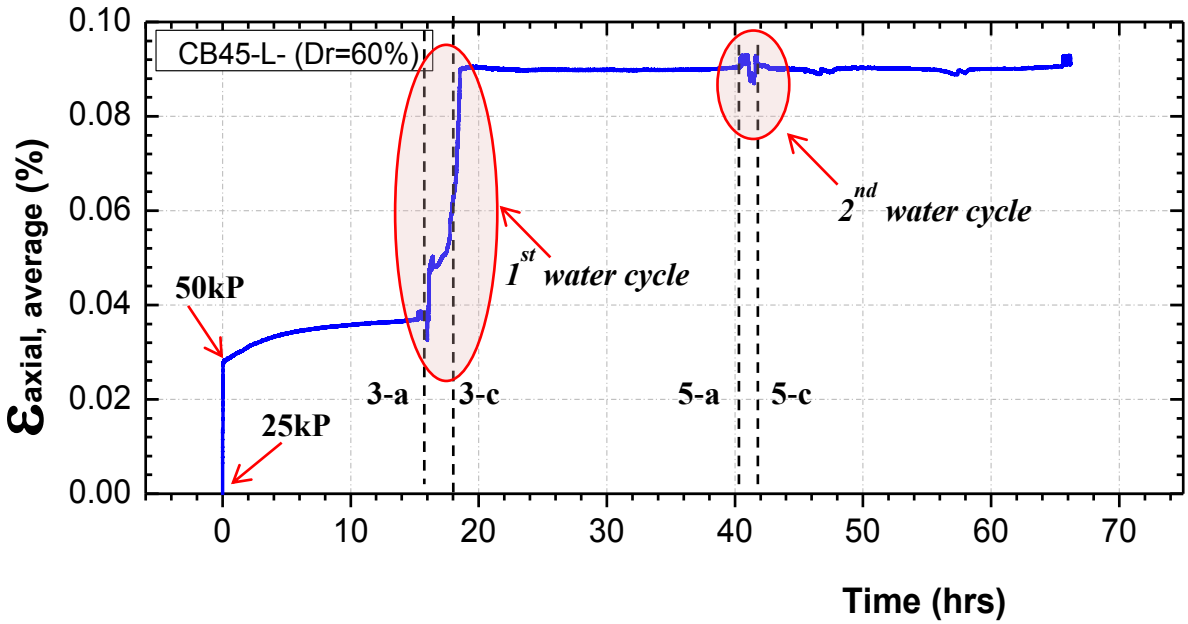

Figure 6. 6. Typical plot for strain vs. time

6.2.1. Test No.1 - NC (Dr, 64%)

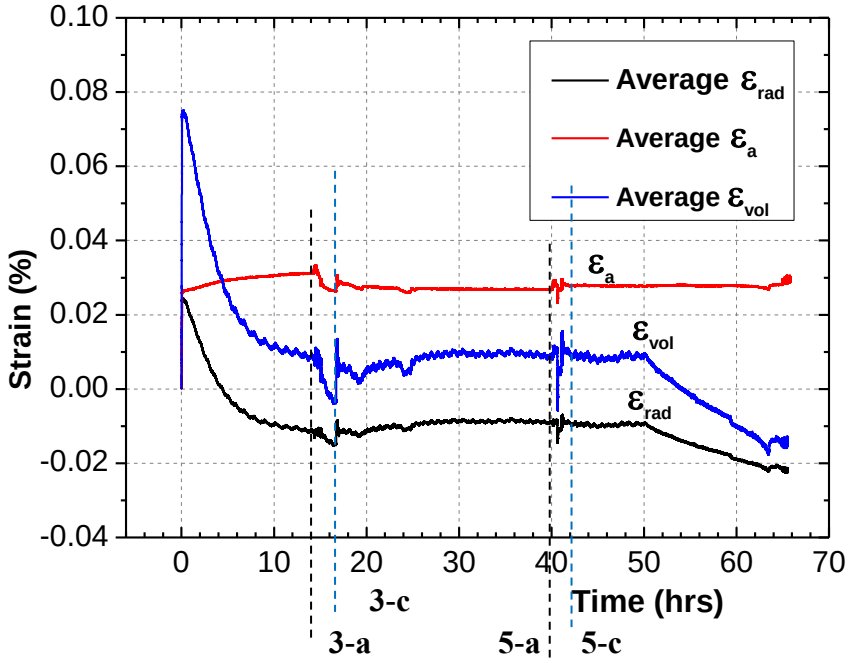

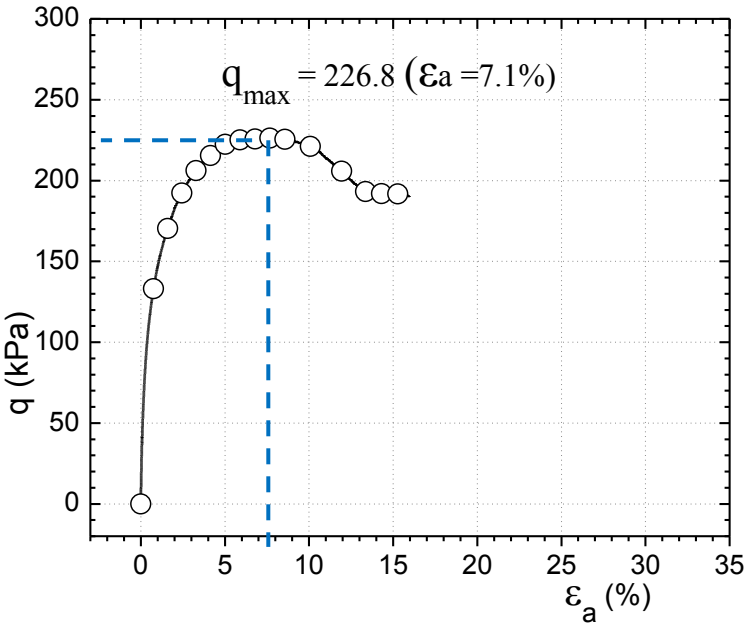

Water inflow rate at 3(a) : 13ml/min
5(a) : 7ml/min
Moisture content at Wet 2 : 21.3%

	Dry		Wet-1		Wet-2	
	Top	Bottom	Top	Bottom	Top	Bottom
E (kPa)	141.2	153.1	136.5	146.5	138.5	148.6
ν	0.13	0.18	0.14	0.18	0.14	0.19

Figure 6. 7. Test results - Test No.1

6.2.2. Test No.2 - CB45-L (Dr, 63%)

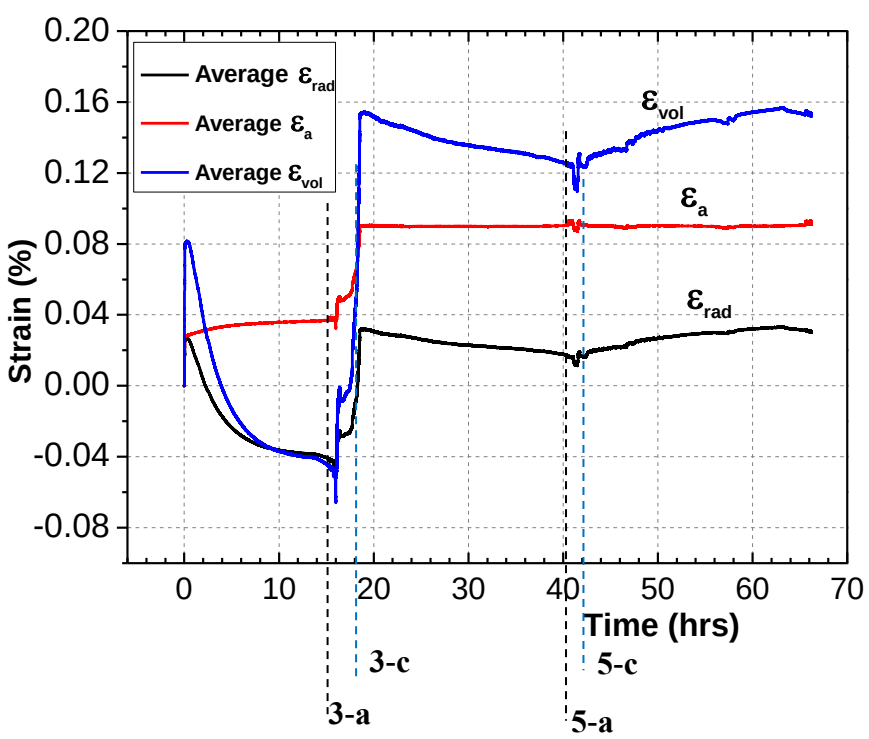

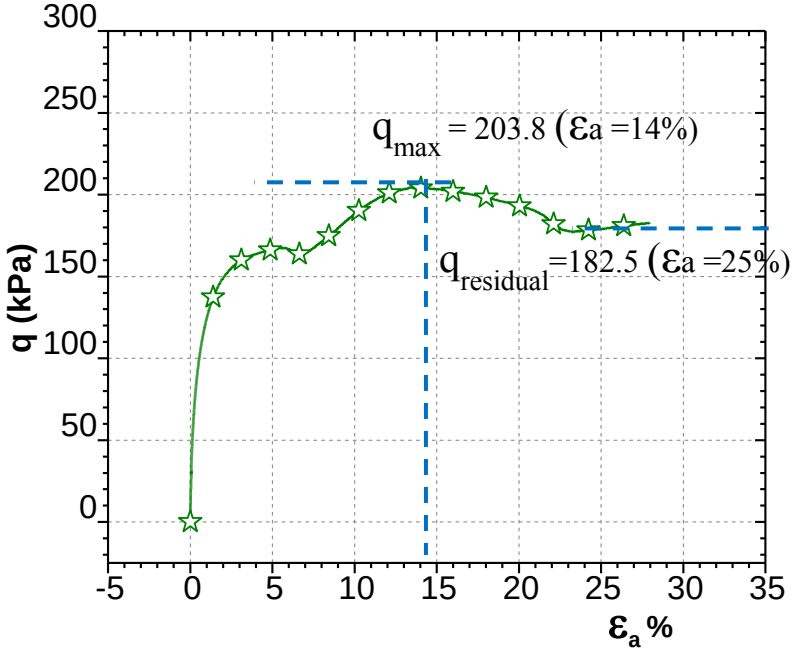

Water inflow rate at 3(a) : 15ml/min
5(a) : 11ml/min

Moisture content at Wet 2 : 20.7 %

	Dry		Wet-1		Wet-2	
	Top	Bottom	Top	Bottom	Top	Bottom
E (MPa)	150.6	155.5	126.8	122.2	123.1	119.9
ν	0.16	0.17	0.15	0.19	0.17	0.20

Figure 6. 8: Test results - Test No.2

6.2.3. Test No.3 - CB45-S (Dr, 60%)

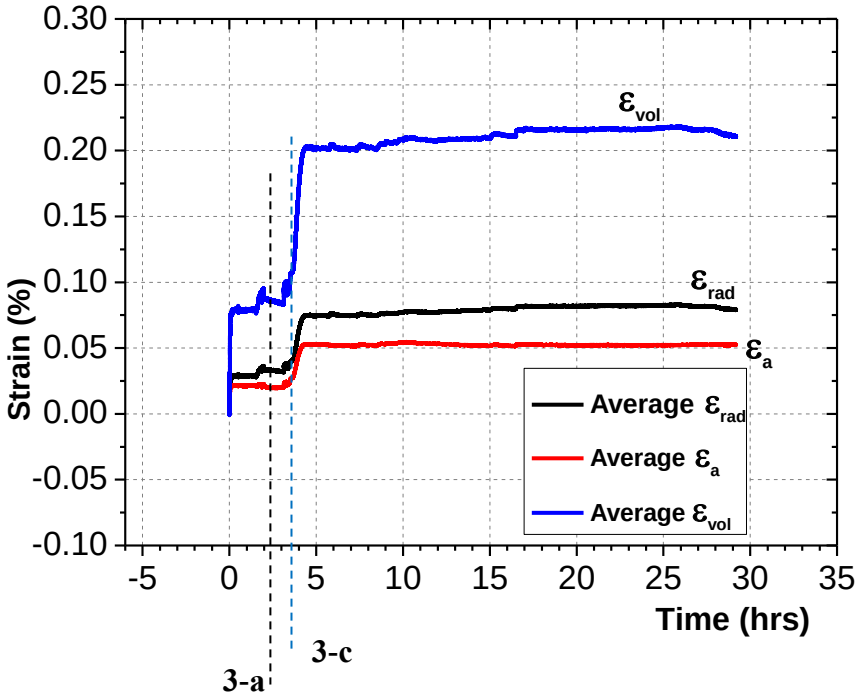

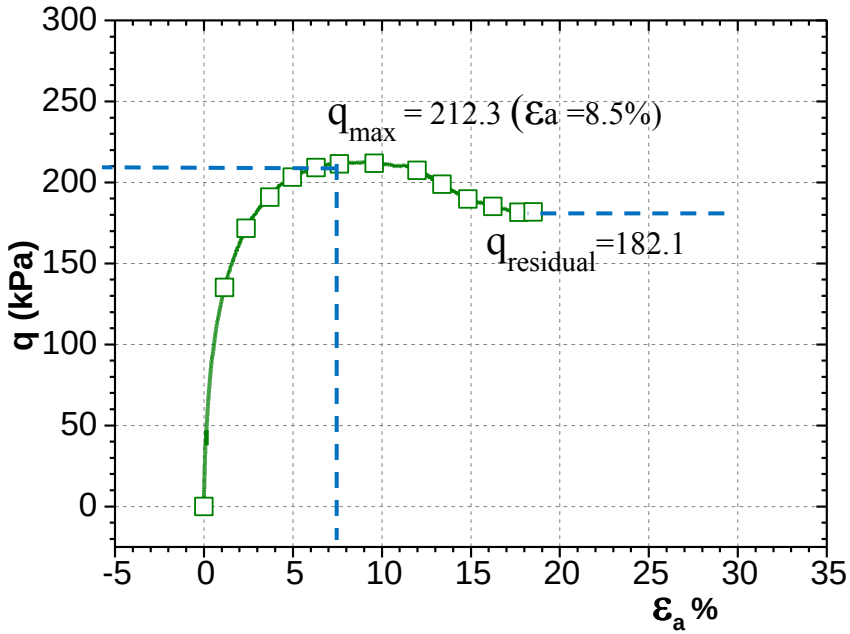

Water inflow rate at 3(a) : 16.3ml/min

Moisture content at Wet 1 : 25.8%

	Dry		Wet-1	
	Top	**Bottom**	**Top**	**Bottom**
E (MPa)	200	139.5	162.6	129.8
ν	NO RECORD			

Figure 6. 9: Test results - Test No.3

6.2.4. Test No.5 - CB -S (Dr, 64%)

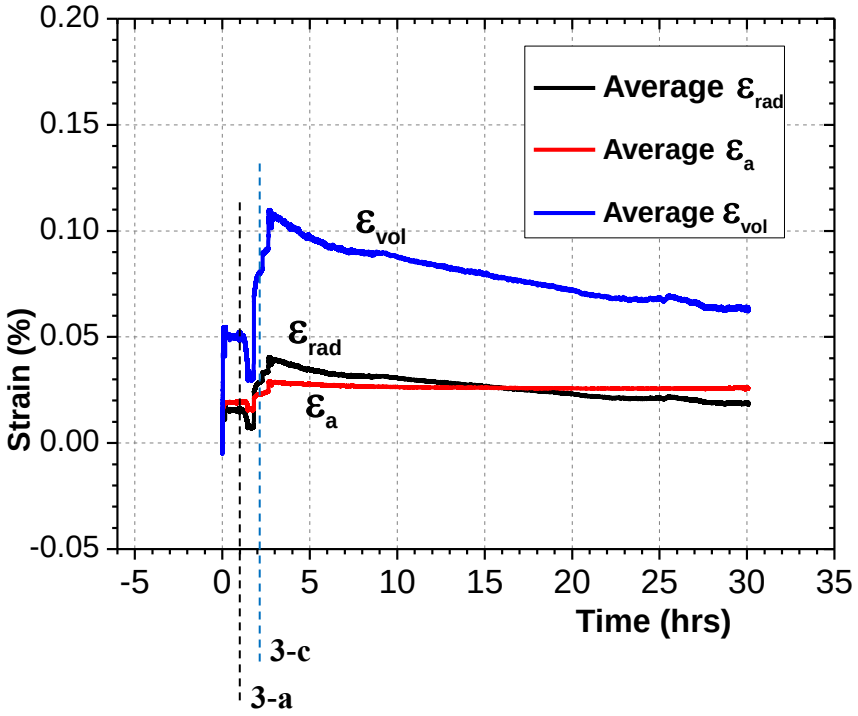

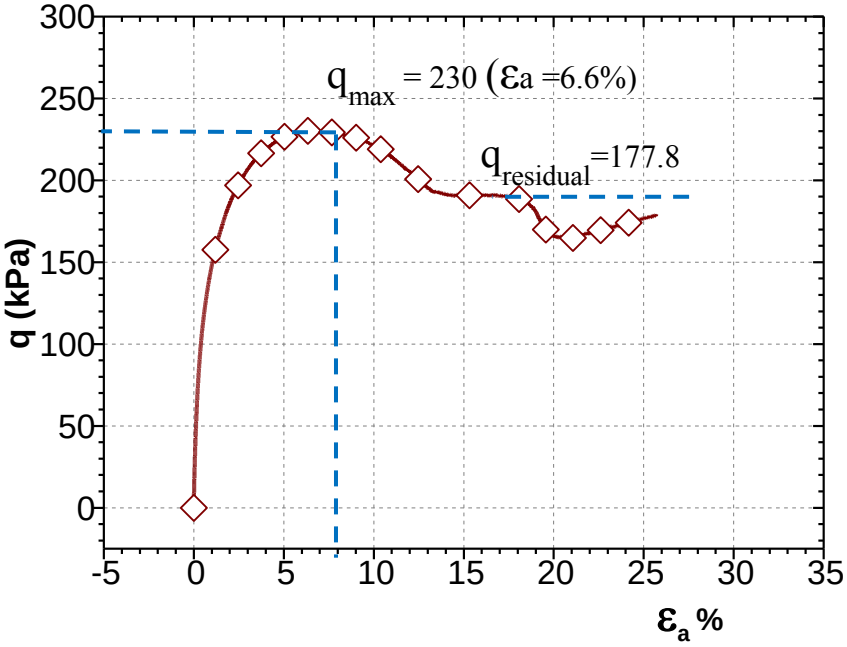

Water inflow rate at 3(a) : 18 ml/min

Moisture content at Wet 1 : 23.55%

	Dry		Wet-1	
	Top	**Bottom**	**Top**	**Bottom**
E (MPa)	177.4	171.5	174.9	148.9
ν	NO RECORD			

Figure 6. 10: Test results - Test No.5

6.2.5. Test No.6 - NC (Dr, 35%)

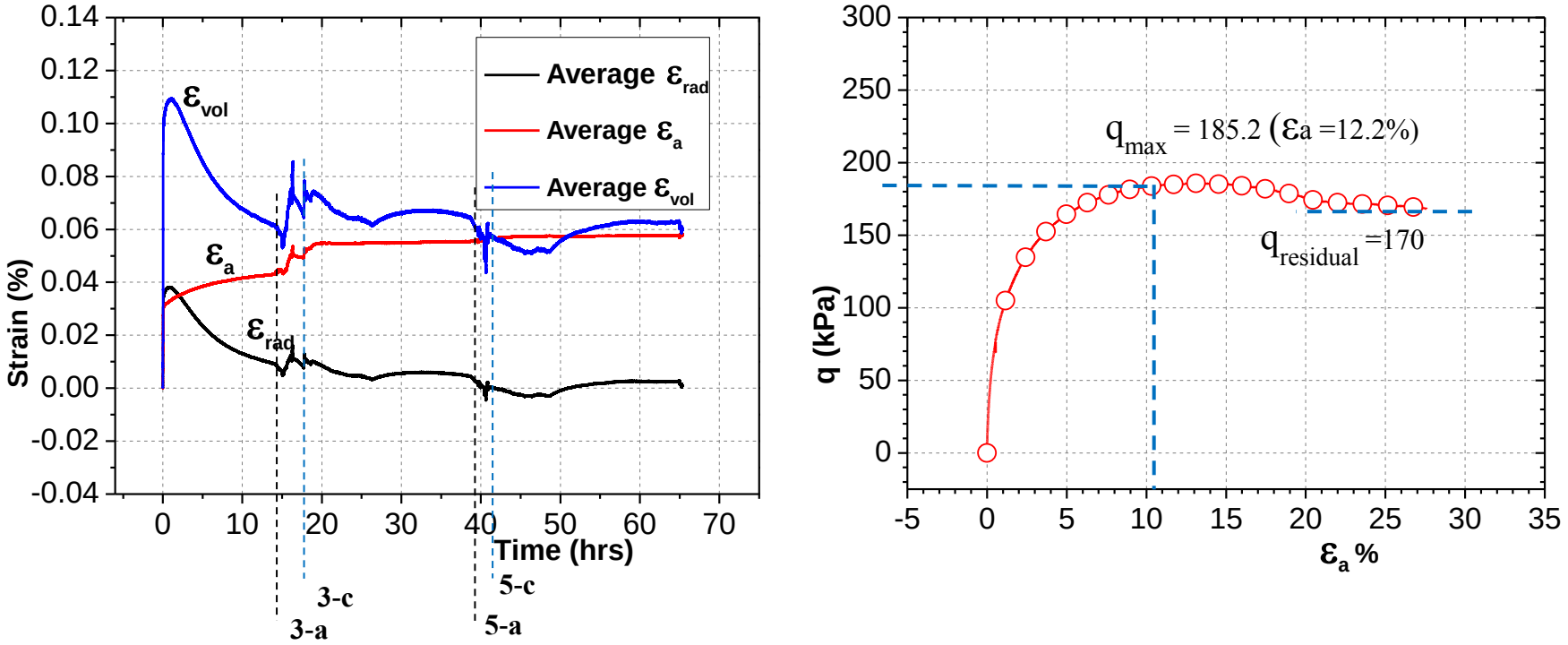

Water inflow rate at	3(a) : 14.7 ml/min
	5(a) : 7.8 ml/min
Moisture content at Wet 2	: 16.2%

	Dry		Wet-1		Wet-2	
	Top	Bottom	Top	Bottom	Top	Bottom
E (MPa)	110.1	117.4	103.5	110.9	107.8	114.8
ν	0.13	0.14	0.15	0.14	0.14	0.17

Figure 6. 11: Test results - Test No.6

6.2.6. Test No.7 - CB45-L (Dr, 36%)

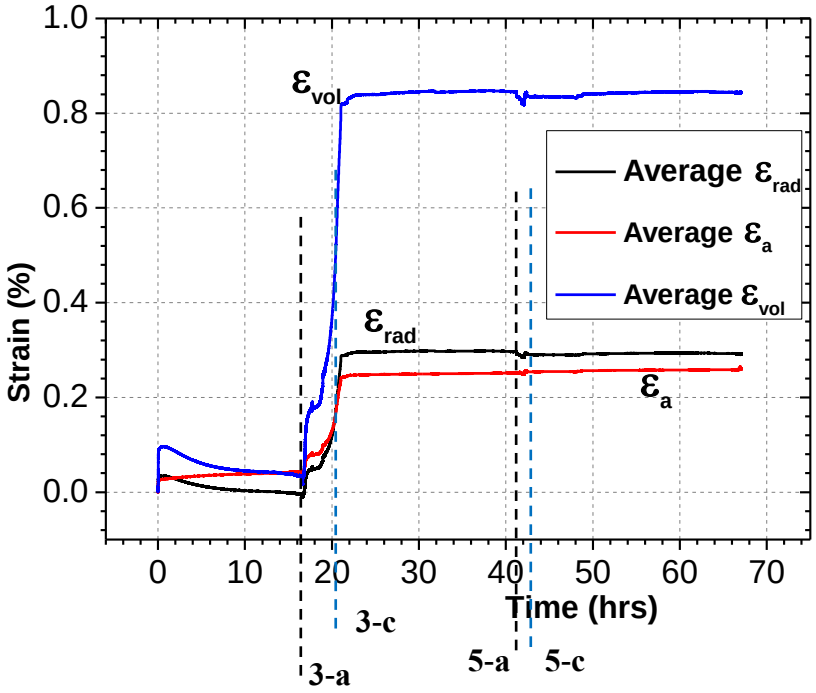

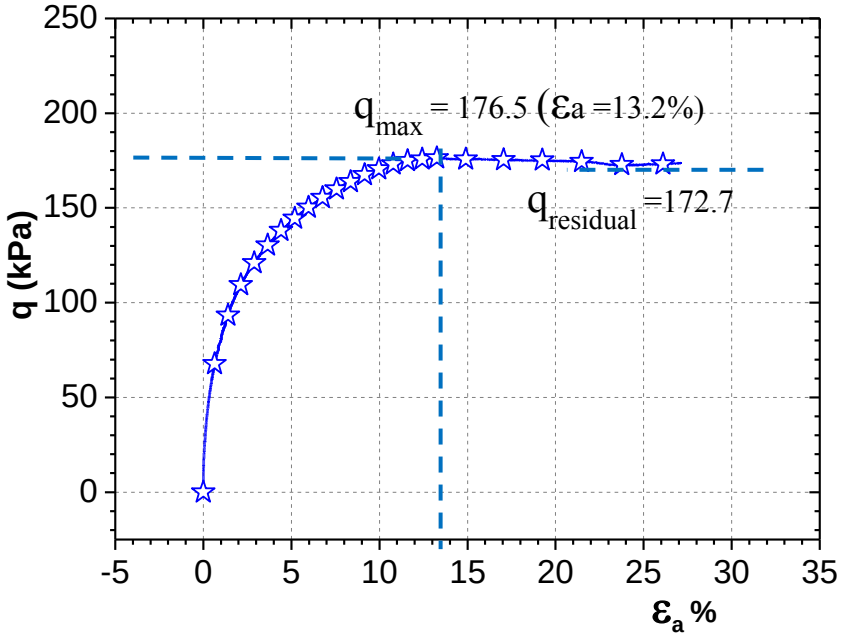

Water inflow rate at	3(a) : 16 ml/min
	5(a) : 7.1 ml/min
Moisture content at Wet 2	: 18.3 %

	Dry		Wet-1		Wet-2	
	Top	Bottom	Top	Bottom	Top	Bottom
E (MPa)	112.2	104.5	92.7	86.4	80.0	72.6
ν	0.17	0.14	0.18	0.18	0.16	0.18

Figure 6. 12: Test results - Test No.7

6.2.7. Test No.8 - CB45-S (Dr, 37%)

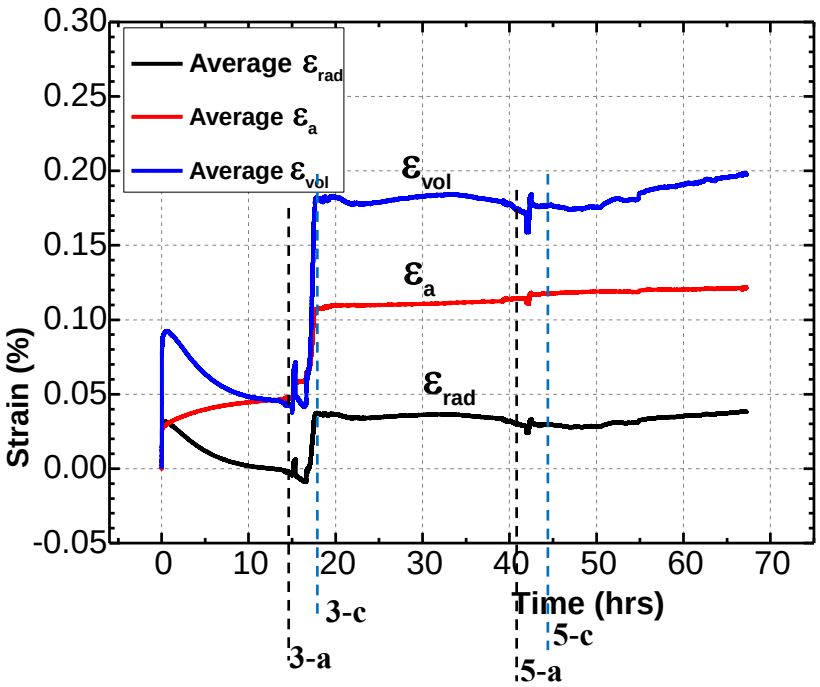

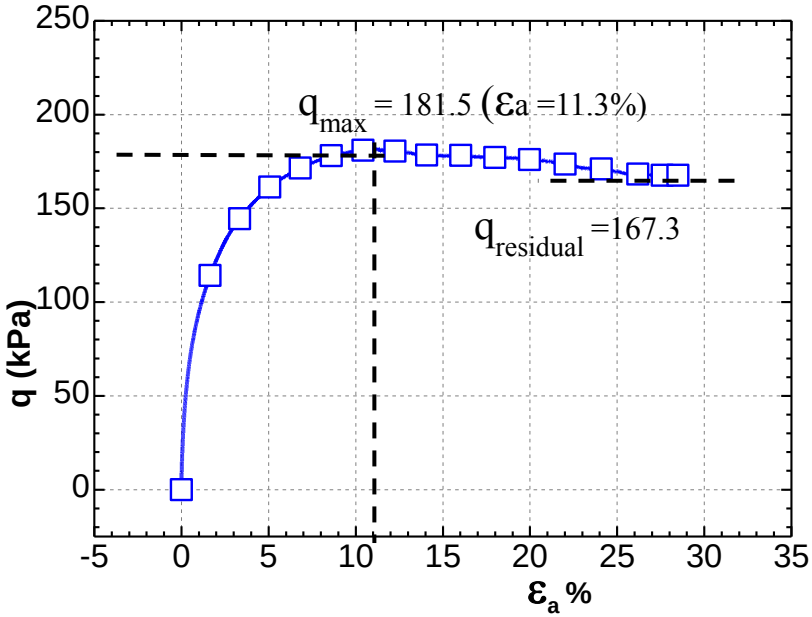

Water inflow rate at 3(a) : 16 ml/min
5(a) : 6 ml/min

Moisture content at Wet 2 : 22%

	Dry		Wet-1		Wet-2	
	Top	Bottom	Top	Bottom	Top	Bottom
E (MPa)	123.8	130.7	103.1	109.8	104.8	110.3
ν	0.16	0.2	0.2	0.21	0.17	0.21

Figure 6. 13: Test results - Test No.8

6.2.8. Test No.9 - CB - L (Dr, 37%)

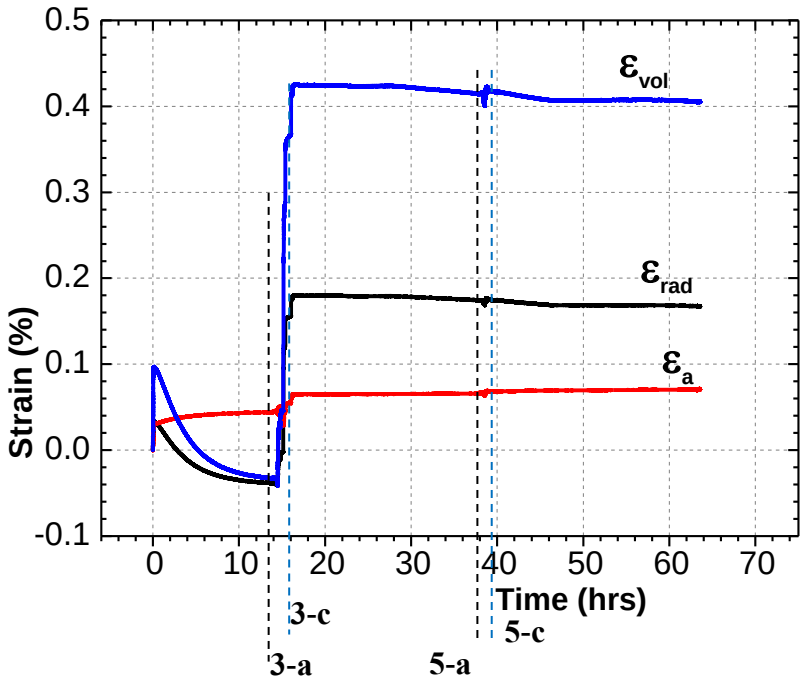

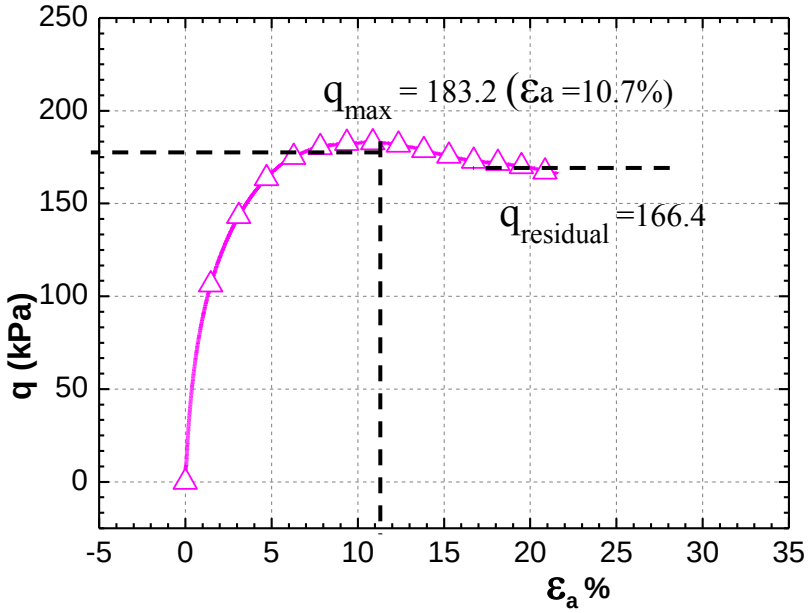

Water inflow rate at 3(a) : 16.2 ml/min
5(a) : 8.1ml/min

Moisture content at Wet 2 : 19.2 %

	Dry		Wet-1		Wet-2	
	Top	Bottom	Top	Bottom	Top	Bottom
E (MPa)	129.1	130.6	121.6	111.8	89.9	93.9
ν	0.17	0.18	0.17	0.35	0.18	0.28

Figure 6. 14: Test results - Test No.9

6.2.9. Test No.10 - CB -S (Dr, 35%)

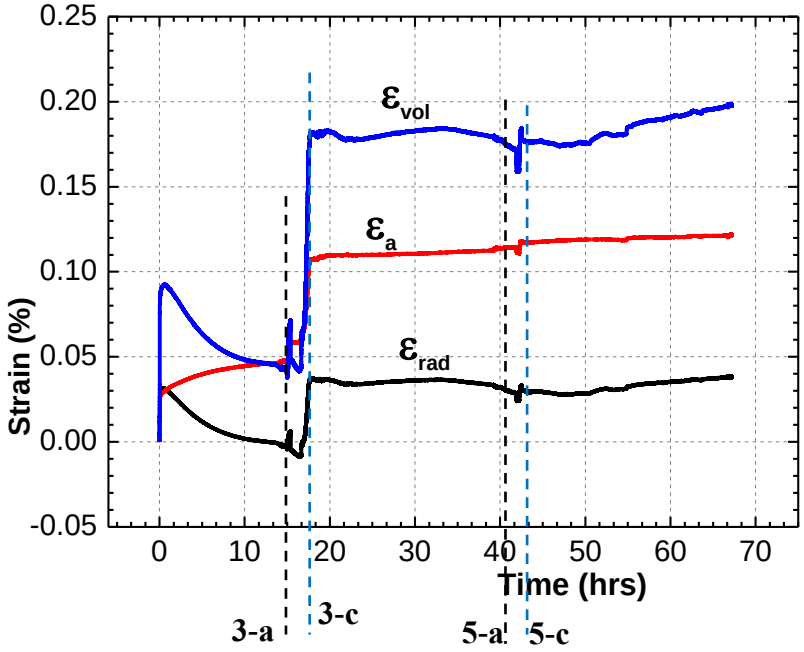

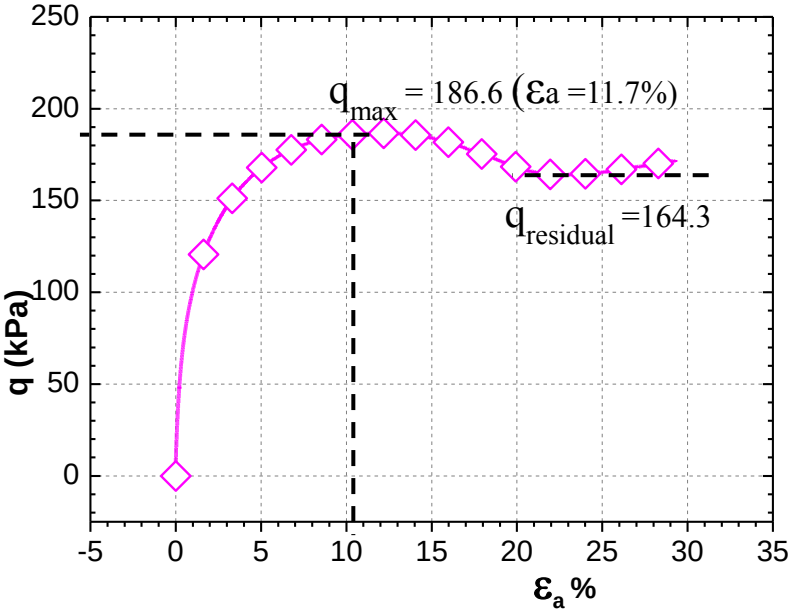

Water inflow rate at 3(a) : 15 ml/min 5(a) : 8 ml/min
Moisture content at Wet 2 : 17.7%

	Dry		Wet-1		Wet-2	
	Top	Bottom	Top	Bottom	Top	Bottom
E (MPa)	102.9	106.4	104.7	96.6	106.3	99.2
ν	0.16	0.16	0.16	0.15	0.17	0.17

Figure 6. 15: Test results - Test No.10

6.2.10. Test No.11 - NC (Dr, 37%) -100kPa

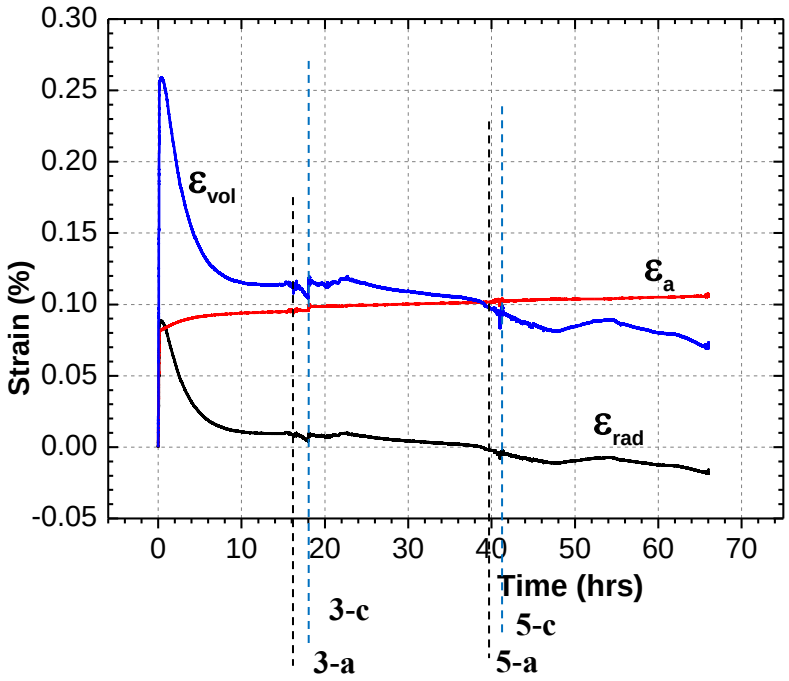

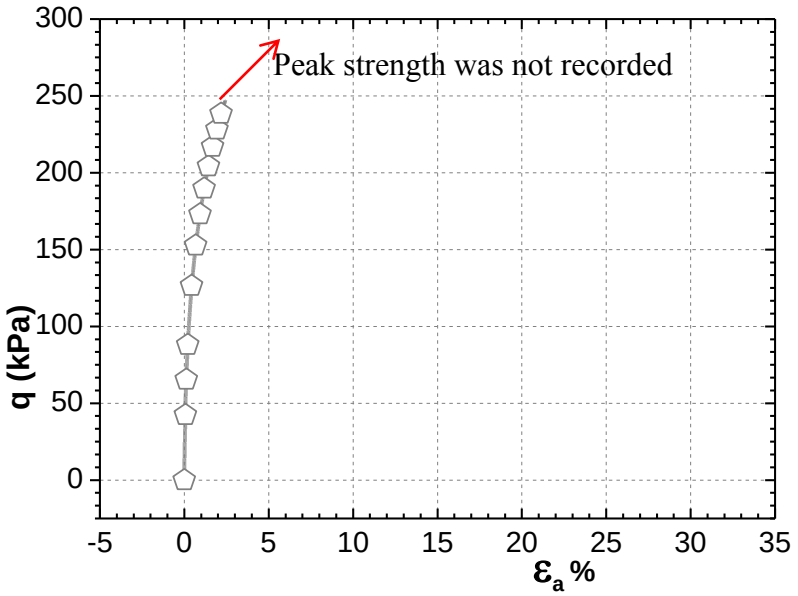

Water inflow rate at	3(a) : 14 ml/min
	5(a) : 7 ml/min
Moisture content at Wet 2 : 25.1%	

	Dry		Wet-1		Wet-2	
	Top	Bottom	Top	Bottom	Top	Bottom
E (MPa)	177.9	191.3	163.7	178.7	163.5	179.2
ν	0.13	0.08	0.14	0.11	0.15	0.12

Figure 6. 16: Test results - Test No.11

6.2.11. Test No.12 - CB45-L (Dr, 35%) -100kPa

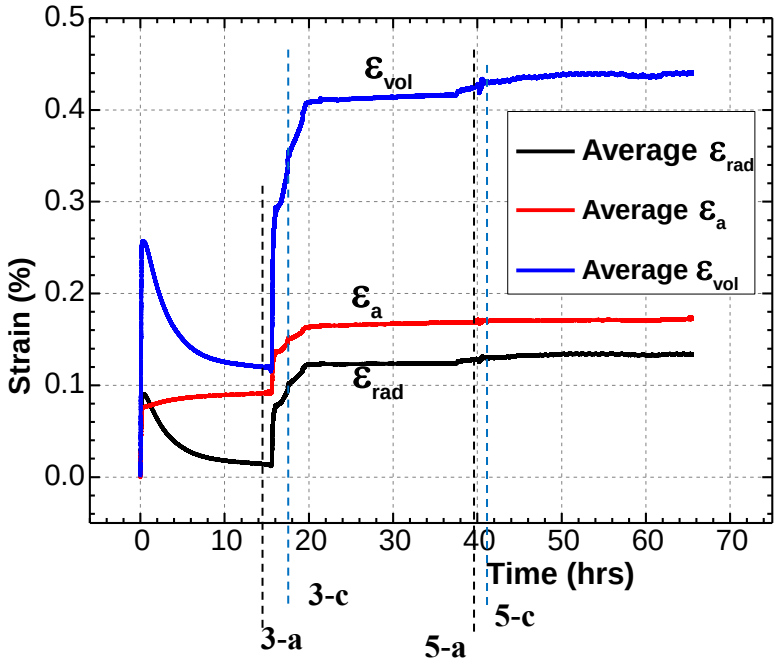

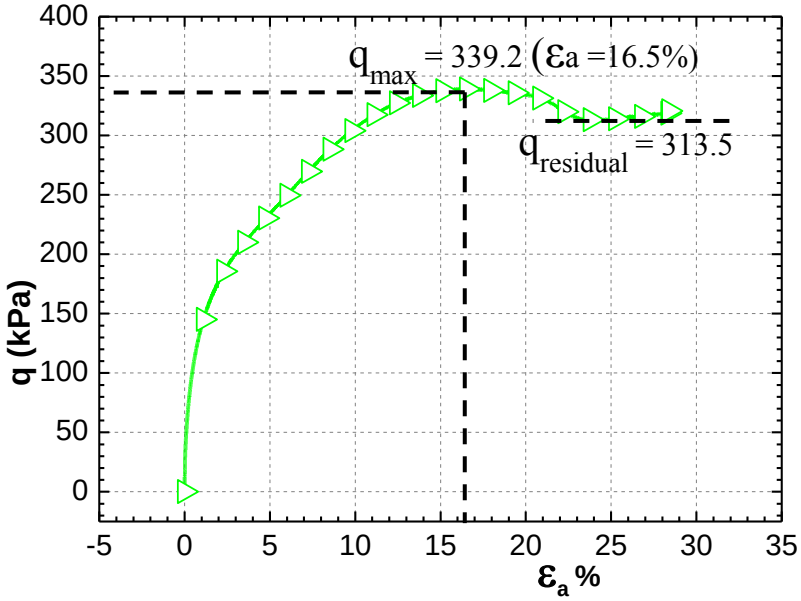

Water inflow rate at 3(a) : 13.9 ml/min
5(a) : 9.1 ml/min

Moisture content at Wet 2 : 25.5%

	Dry		Wet-1		Wet-2	
	Top	Bottom	Top	Bottom	Top	Bottom
E (MPa)	178.8	173.8	148.0	138.3	149.9	142.0
ν	0.17	0.17	0.14	0.19	0.14	0.18

Figure 6. 17: Test results - Test No.12

6.2.12. Test No.13 – NC (Dr, 58%) –Silica

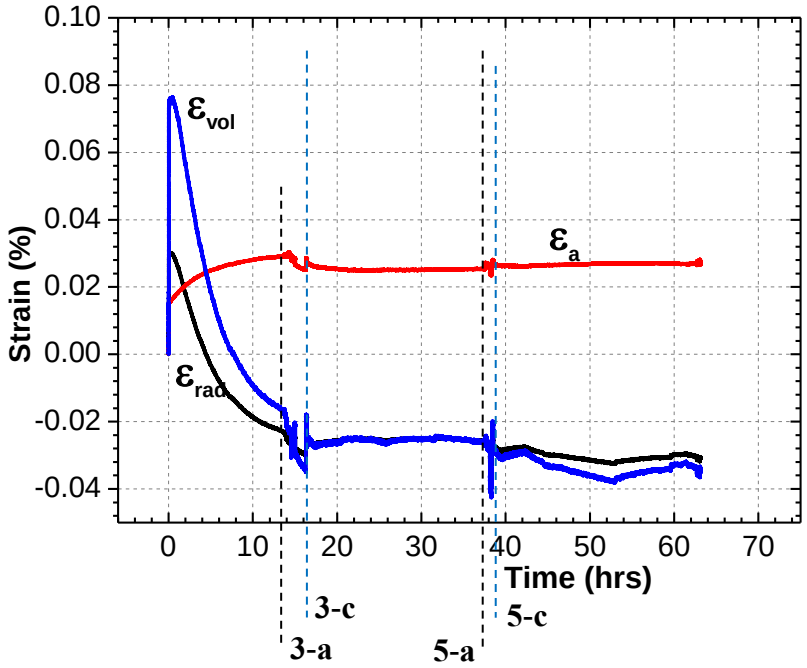

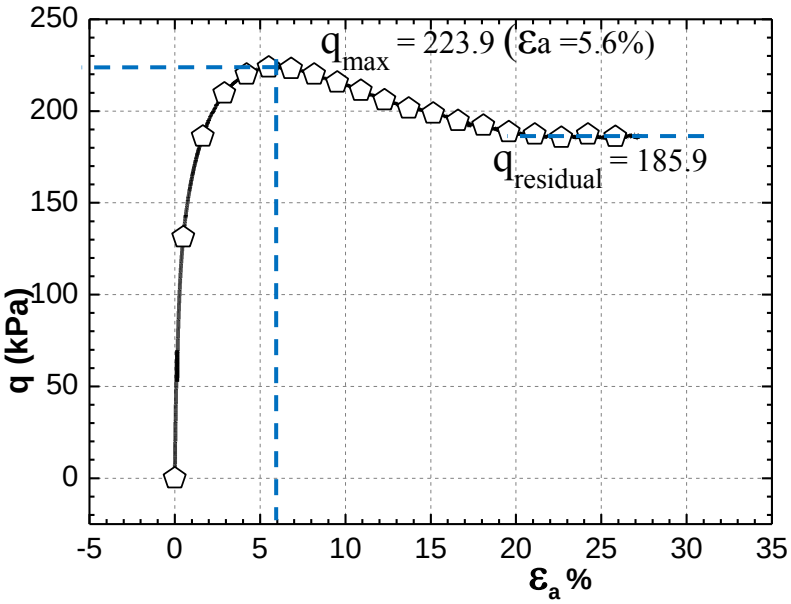

Water inflow rate at	3(a) : 15.6 ml/min
	5(a) : 9.8 ml/min
Moisture content at Wet 2	: 9.6 %

	Dry		Wet-1		Wet-2	
	Top	Bottom	Top	Bottom	Top	Bottom
E (MPa)	166.7	189.6	164.6	182.7	163	181.9
ν	0.14	0.09	0.15	0.09	0.15	0.09

Figure 6. 18: Test results - Test No.13

6.2.13. Test No.14 - CB45-L (Dr, 62%) - Silica

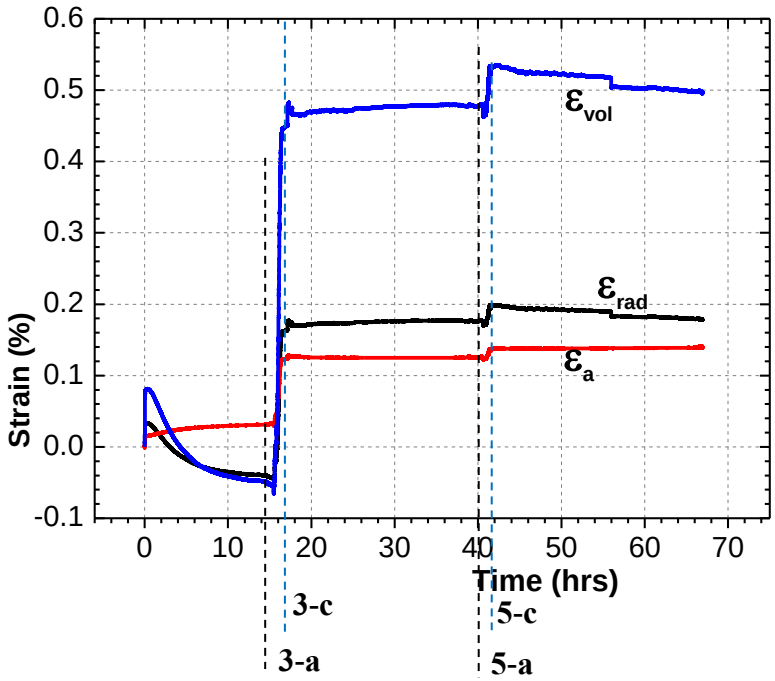

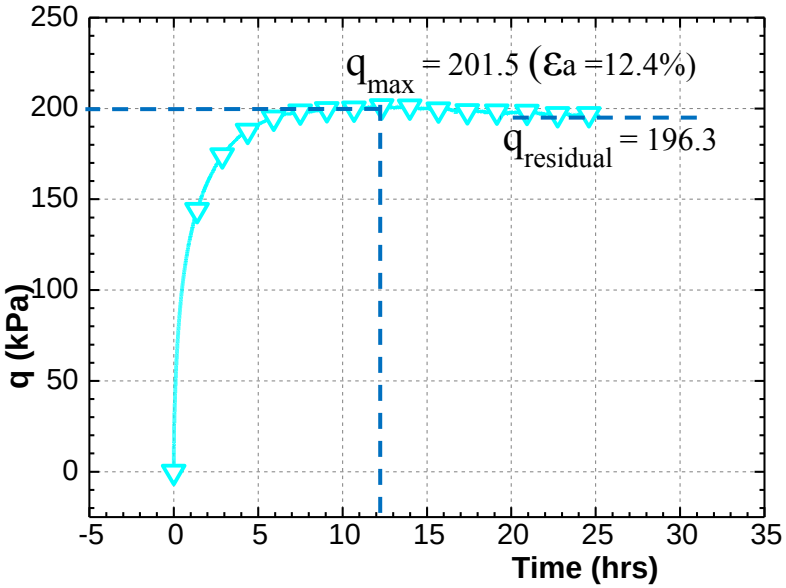

Water inflow rate at 3(a) : 15.9 ml/min
5(a) : 6.4 ml/min

Moisture content at Wet 2 : 8.84 %

	Dry		Wet-1		Wet-2	
	Top	Bottom	Top	Bottom	Top	Bottom
E (MPa)	175.9	203.2	118.9	127.4	118.8	130.3
ν	0.12	0.15	0.19	0.22	0.19	0.25

Figure 6. 19: Test results - Test No.14

6.3. Discussion

In this section, the effect of density, cavity size, cavity location, confining pressure and particle size on properties of loosened Toyoura and Silica sand will be discussed. Basically the variation of axial strain, radial strain, volumetric strain, small strain stiffness, Poisson's ratio and stress-strain behaviour during shearing will be monitored in above each test condition.

So far, the effect of density, cavity size, cavity location or confining pressure on ground loosening associated with underground cavities are not quantitatively evaluated in detail. Loosening process is associated with many local parameters and it is really complex to investigate those properties since the loosening occurs in a non-uniform manner most in partially saturated condition.

In following results step 3(a), 5(a) in each plot represents the water infiltration into specimen and 3(c), 5(c) is the drainage. The dotted lines are drawn just for easily focus the moment of water infiltration in graph and the time related to those vertical lines are not exact. Furthermore, colors and symbols used for plotting of axial strain, radial strain and volumetric strain is different from which was defined for each test in Table 6.1.

6.3.1. Toyoura sand

6.3.1.1. Effect of density

Two relative densities were chosen to observe the effect of density on loosening effect. Relative density with 37% was considered as loosed and 60% was considered as medium dense. Two experiments were conducted for each density, as one is with simulating a cavity (CB45-L) and the other is controlled specimen. Conditions of those four tests are shown below.

Test 1 - NC (Dr = 64%)	-50kPa	-Dense
Test 2 - CB45-L (Dr = 63%)	-50kPa	-Dense
Test 6 - NC (Dr = 35%)	-50kPa	-Loose
Test 7 - CB45-L (Dr = 36%)	-50kPa	-Loose

Variation of axial strain, radial strain, volumetric strain, Poisson's ration and small strain modulus with different densities with loosening effect will be discussed in detail.

6.3.1.1.1. Axial and radial deformations

Axial strain, radial strain and volumetric strains are shown in Figure 6.20, 6.21 and 6.22 respectively. All four tests show similar strain increment during isotropic stress increment from 25kPa to 50kPa. Then the specimen was kept nearly 16 hours at 50kPa of isotropic stress in order to dissipate the creep effect. However, radial strain shows different to each

other, during this period due to creep effect. Creep is the tendency of soil particle to move slowly or deform permanently under the influence of stresses. It happens when the specimen is exposed to sudden stress increment which is less than the maximum compressive strength of soil. However, dense specimens show larger radial expansion than loose specimen in Figure 6.21.

Larger axial and radial deformations were observed in loose specimen after dissolving similar volume of glucose at similar location. $\delta\varepsilon_a$ caused by $_{1st}$ water cycle is 0.21% of the dry condition for loosed specimen and 0.05% for dense specimen. Similarly $\delta\varepsilon_{rad}$ and $\delta\varepsilon_{vol}$ are also increased nearly four times larger in loose specimen than dense.

Table 6. 2: Strain increment by 1st water cycle – effect of density

Strain	**1st water cycle**	
	37%	**63%**
$\delta\varepsilon_a$	0.21	0.05
$\delta\varepsilon_{rad}$	0.23	0.07
$\delta\varepsilon_{vol}$	0.80	0.19

Result shown in Figure 6.20 to 6.22 and Table 6.2 was computed by using the average ε_{rad} from three Clip gauges and average ε_a by four LDTs. However local deformations closer to initial glucose block shows much larger deformations than above. In order to show the tendency and the variation of strain along the specimen, variation of ε_{rad} in three clip gauges of Dr = 37% case are shown in Figure 6.23. Similarly variation of ε_a in four LDTs is shown in Figure 6.24. Figure 6.23 depicts that larger radial compression has occurred just above and below the glucose block. The region can be identified as 1.5 cm above the glucose top surface and 1.5cm below the glucose bottom. That is almost similar to the height of the glucose block. LDT results in Figure 6.24 shows soil sited above the glucose block has collapsed in to void by casing larger compression in lower set of LDTs and extension in Upper LDTs. These results shows significant loosening effect will cause around initial glucose block and the stiffness properties related to this sort of loosened soil will be reflected by deformation transducers.

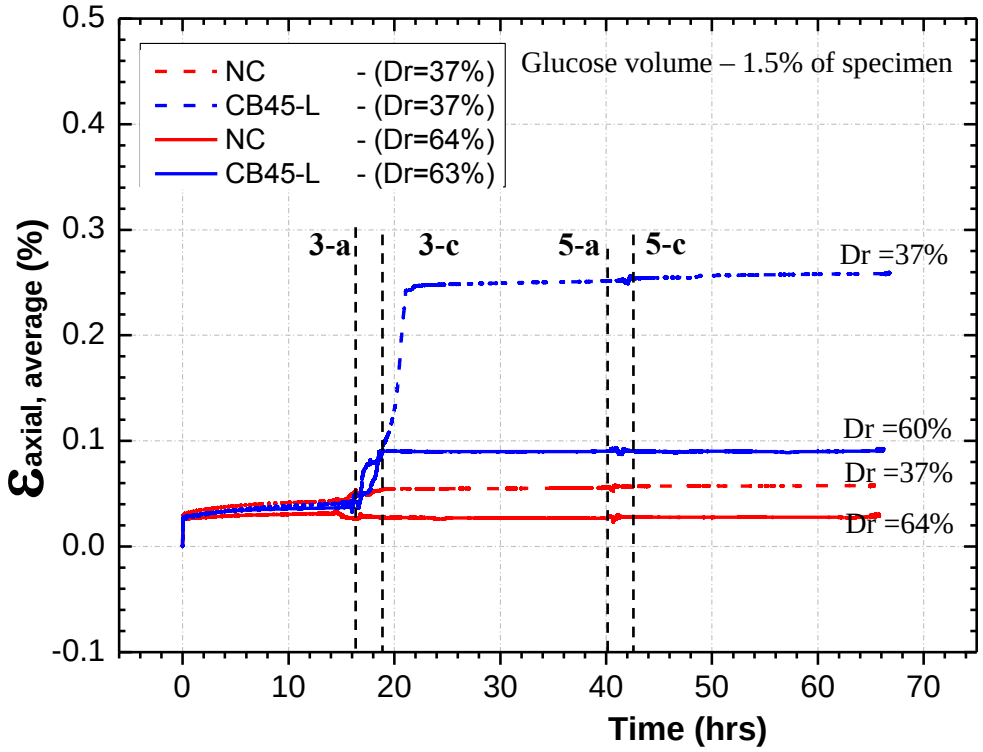

Figure 6. 20: Axial strain variation- effect of density

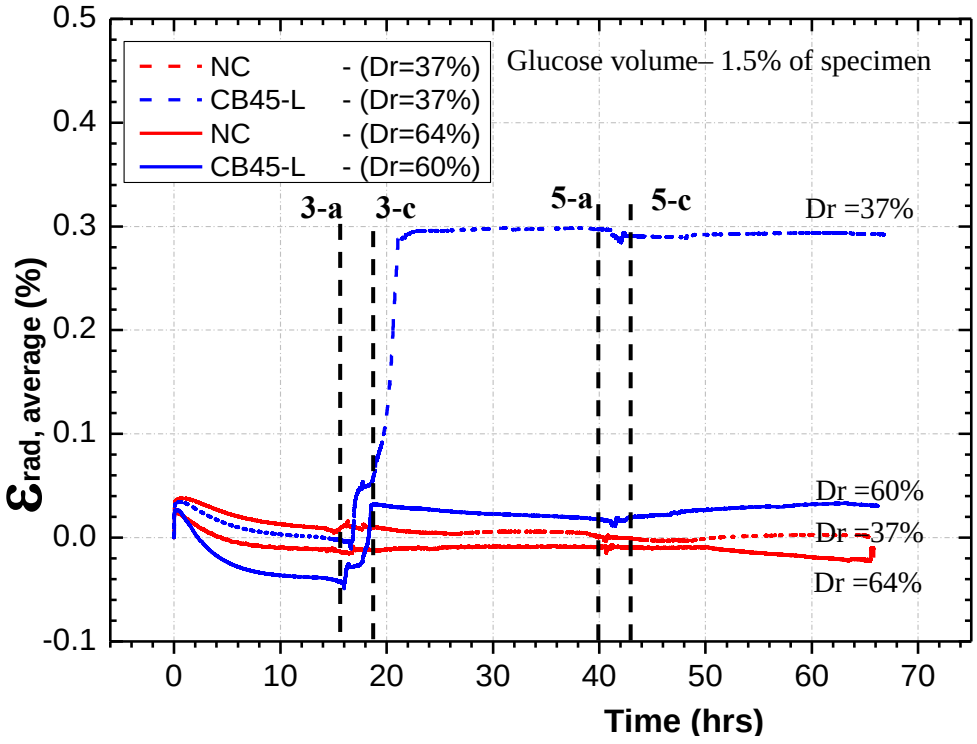

Figure 6. 21: Radial strain variation- effect of density

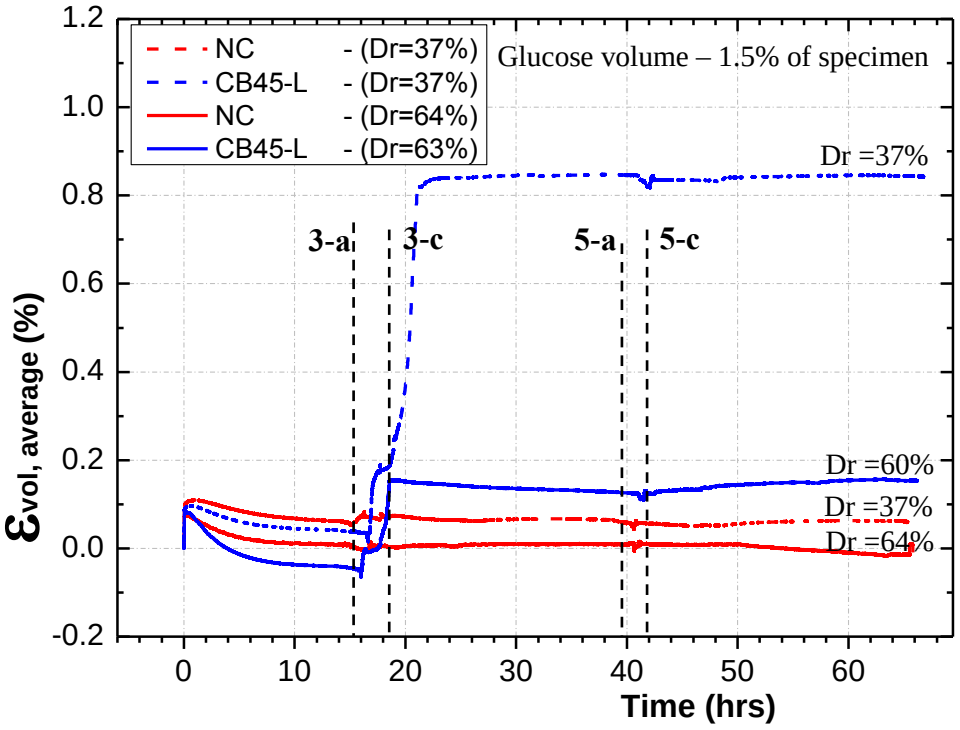

Figure 6. 22: Volumetric strain variation- effect of density

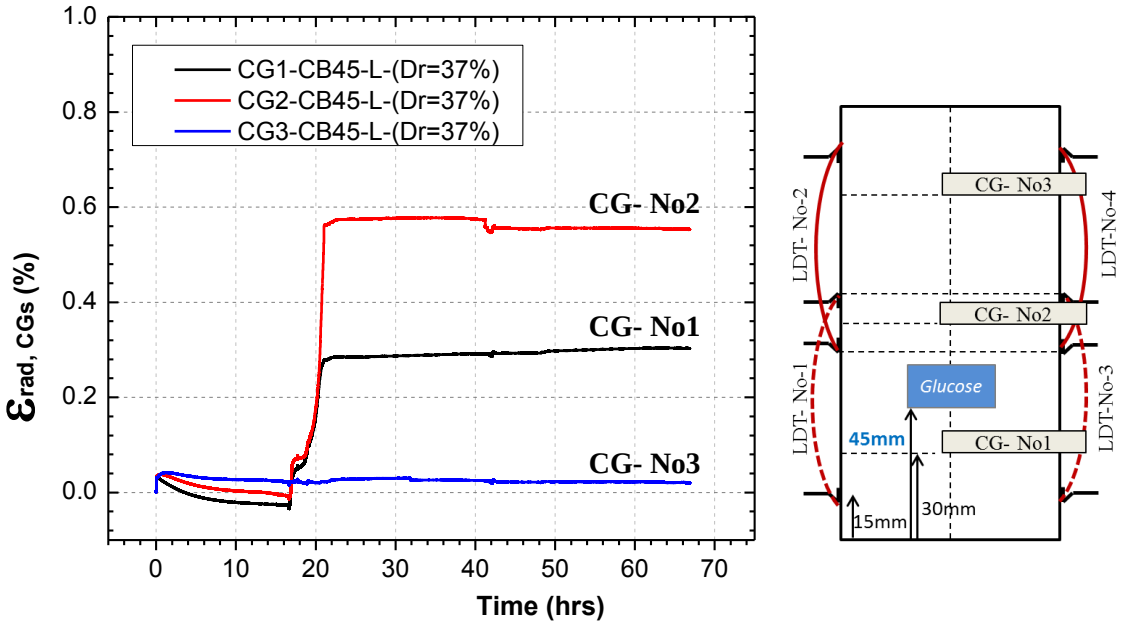

Figure 6. 23: Variation of radial strain in 3 CGs – (CB45-L, Dr=37%)

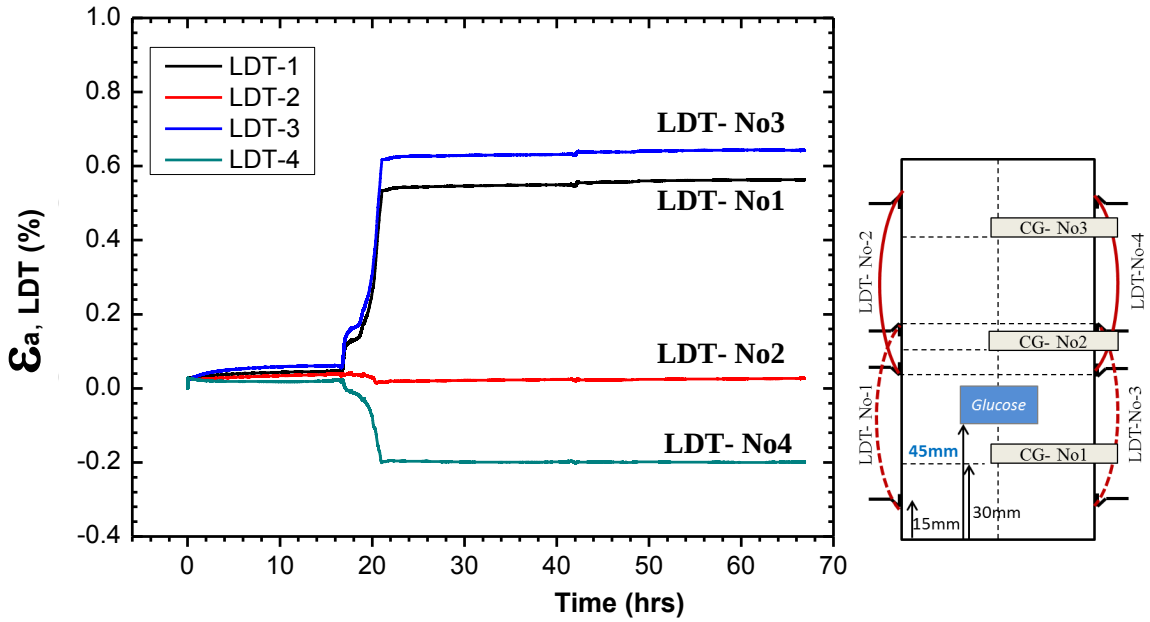

Figure 6. 24: Variation of axial strain in 4 LDTs – (CB45-L, Dr=37%)

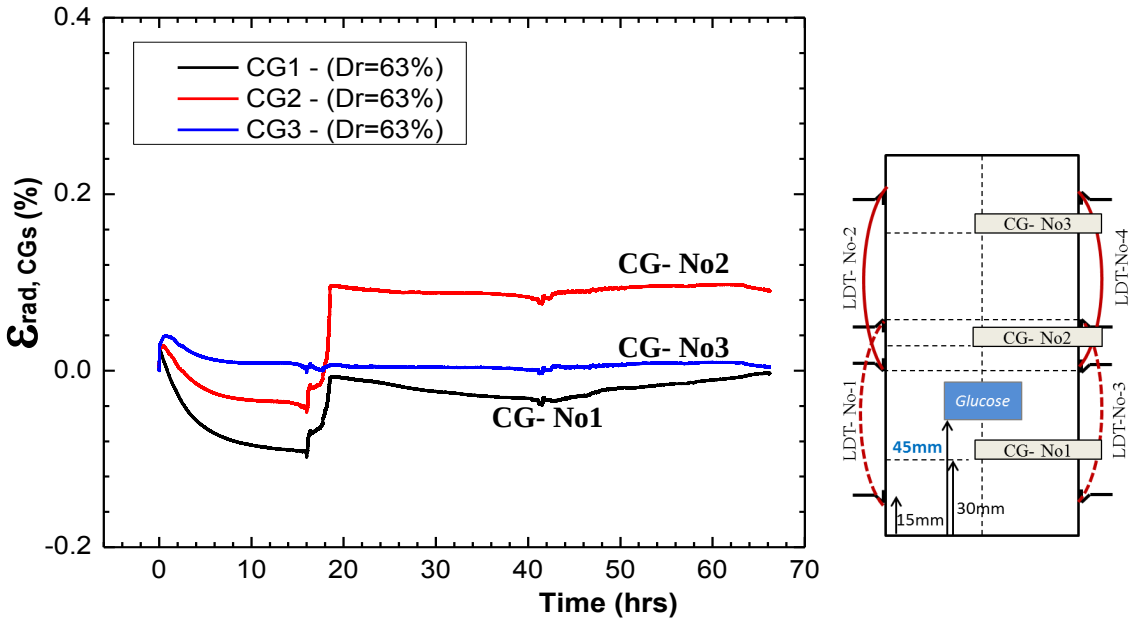

Figure 6. 25. Variation of radial strain in 3 CGs – (CB45-L, Dr =63%)

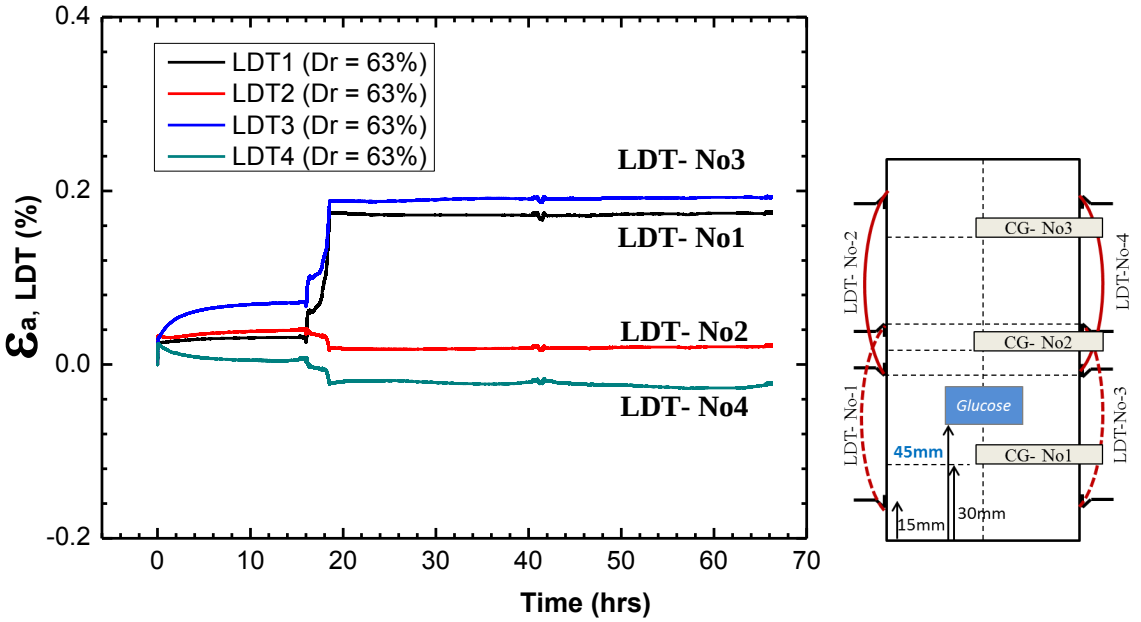

Figure 6. 26: Variation of axial strain in 4 LDTs – (CB45-L, Dr=63%)

6.3.1.1.2. Variation of Poisson's ratio (ν)

When the soil is compressed in vertical direction, it usually tends to expand in the lateral directions perpendicular to the direction of compression. This phenomenon is called as the Poisson's effect and Poisson's ratio (ν) is the ratio of lateral deformation in to vertical deformation. Most soils have Poisson's ratio changing in between 0 to 0.5. This parameter is a very important indicator which reflects the lateral deformation characteristics of a soil. Soil is an elasto plastic material and several researchers have concluded that the stress-strain relationship of soil is almost linear and elastic at very small strain level up to 0.001%.

Therefore Poisson's ratio can be computed by measuring the small radial and axial deformations caused by applying of small cyclic loadings with axial strain range of 0.001%. Two sets of LDTs were fixed at lower and upper halves of specimen to monitor the axial strains separately at each. Similarly radial deformations at lower and upper half of the specimen were measured by using three Clip gauges. Small cyclic loadings having axial stress of 1kPa-2kPa was used to apply a small strain around 0.001%. Exact axial strains applied to lower and upper half of the specimen was measured by LDTs and corresponding radial strains were measured by Clip gauges. This is a modern technique use in the laboratory to compute to Poisson's ratio in uniform specimen.

However, once water is infiltrated and glucose is dissolved, the sand undergoes non-uniform behaviour in this condition. Ground loosening around the cavity will reform the initial soil structure into a new pattern which is unpredictable and non-uniform. Therefore the lateral deformation of soil will be different than the normal soil structure. So far, this property of such non uniform loosened soil is unknown and attempt will be given to

observe the variation of Poisson's ratio in such loosened sand by using Toyoura and Silica sand.

The values of Poisson's ratio which was obtained from this study was plotted separately to observe how the degree of ground loosening will reflect on Poisson's ratio. Variation of "ν" when changing the initial density of sand is shown below in Figure 6.28 and Table 6.7. The increment or decrement of "ν "during 1st water cycle is evaluated as a percentage of the initial "ν" value at dry stage and during 2nd water cycle was evaluated as refer to the "ν" value calculated at after the 1st water infiltration.

When the mentioned graph and table is clearly observed, following facts were revealed.

1. It is very difficult to identify a clear tendency of variation of "ν" when the degree of loosening was changed by soil density.

2. Somehow, a tendency of larger Poisson's ratio was mostly observed in loosened soil than the controlled specimen. The expectation of this testing method was to observe the difference of "ν" value between the loosened soil at the lower half and normal soil at upper half. However, it seems "ν" values at both halves are affected. Therefore clear variation in two parts is not observed. Still, the Poisson's ratio of loosened soil can be considered as the average of those two values.
   The reason for this effect can be the some limitations of arrangement of LDTs. In case CB45, even the top set of LDT is feeling the properties of loosened soil (Figure 6.27). Therefore it is difficult to compare the results by comparing two sets of LDTs.

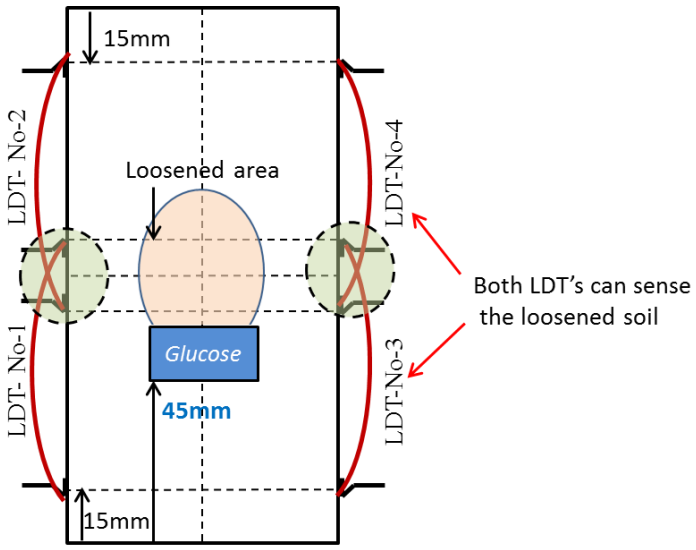

Figure 6. 27: limitation with used LDT arrangement

3. Furthermore the variation of Poisson's ratio of loosened sand has to be theoretically different from uniform sand, because loosening is mostly non uniform in the ground and which can have an unpredictable soil structure arrangement with different scale of voids. Therefore, the relation of transverse and vertical deformations become complex and unpredictable, since the orientation of weaker plan of loosened soil is governed by many local factors around the cavity and loosened area. Hence, this kind of complex behaviour of Poisson's ratio can be expected as in this study.
4. In many test cases which simulate the ground loosening some special feature was observed. After the first water cycle, Poisson's ratio increment in lower part of the specimen is higher than the upper part (Figure 6.40 and Figure 6.42). However, these results are not enough to strongly conclude as Poisson's ratio of loosened soil with a cavity is always larger than uniform soil with similar density. Because, soil particle settlement can be expected in two ways closer to the cavity.
    (a) Soil which is sited on cavity ceiling can be collapsed into existing void during small cyclic loading with minor radial deformations in that particular soil structure. In this case, soil deformation is much localized and Poisson ratio increment of the whole soil specimen may not be larger.
    (b) Second way is, when the cavity ceiling is strong enough to resist the applied cyclic loading, and then the loosened soil which sited on it can affect the global radial displacement of that region causing significant increment in Poisson's effect.

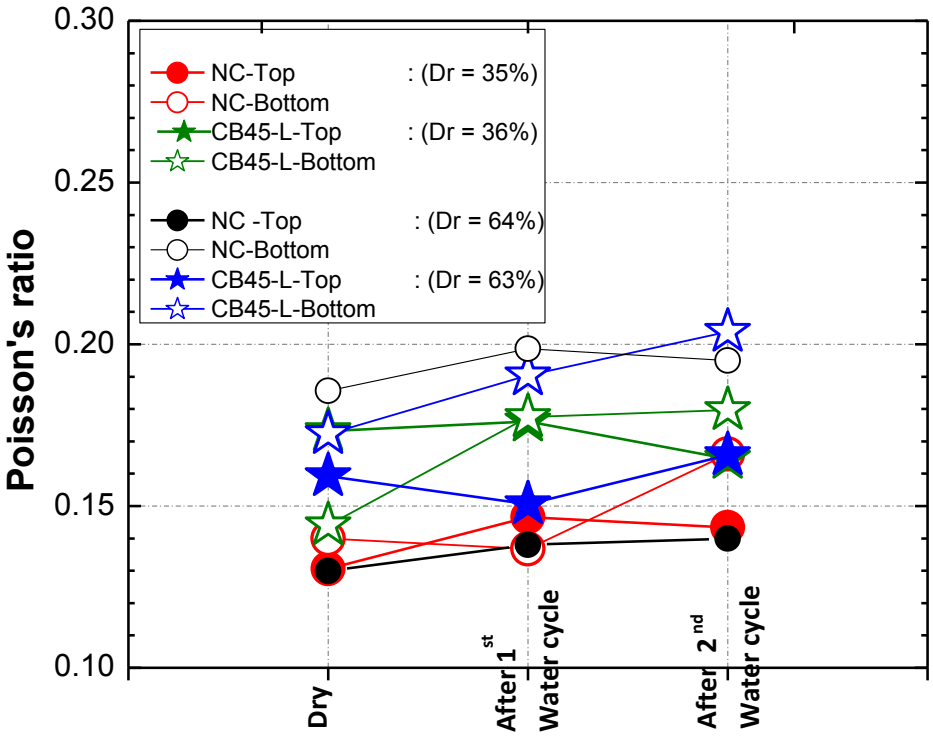

Figure 6. 28: Variation of Poisson's ratio- Effect of density

Table 6. 3: Variation of ν of loosened soil- effect of density

Dr%	Water cycle	NC		CB45-L	
		Top	Bottom	Top	Bottom
35-36%	Increment of ν during 1st water cycle (%)	+12.2	-2.2	+1.7	+23.2
	Increment of ν during 2nd water cycle (%)	-2.1	+2.9	-6.5	+0.2
63-64%	Increment of ν during 1st water cycle (%)	+6.2	-0.05	-5.5	+10.6
	Increment of ν during 2nd water cycle (%)	+1.45	+0.9	+10.1	+1.3

6.3.1.1.3. Variation of stiffness (Young's modulus and Small strain Modulus)

In order to observe the effect of ground loosening on stiffness properties of sand, Young's modulus(E) was evaluated by measuring the vertical stresses, related axial and radial strains at very small amplitude cyclic tests at strain levels less than about 0.001% .

Young's modulus was evaluated at three stages in each test as dry, after the 1st water cycle and 2nd water infiltration. Void ratio and volumetric strain at each stage was measured related to each computed Young's modulus in order to omit the effect of void ratio on stiffness properties. Therefore, Poisson's ratio and void ratio were measured for each Young's modulus value independently and Small strain modulus (G) was evaluated by Eq.

4.29. Then the computed G value was normalized with the void ratio function mentioned in Eq. 4.27. These equations are repeated below.

Void ratio function,

$$f(e) = \frac{(2.17 - e)^2}{(1 + e)}$$ (Given in Eq.4.27)

Small strain modulus or shear modulus,

$$\mathrm{Gs} = \frac{E}{2(1+\nu)}$$ (Given in Eq.4.29)

Density is directly related to the stiffness properties and it can be clearly observed from controlled tests (NC) in Figure 6.29and Figure 6.30. NC (Dr = 64%) shows larger E and G/f(e) value than NC test having Dr = 35%. However, stiffness variation with water infiltration and drainage is not significant in controlled specimens. Minor stiffness reduction was recorded with 1st water cycle. Nevertheless, in case of CB45-L-Dr = 35%, stiffness has been reduced by 16% of the dry value after 1st water infiltration, while similar reduction was observed in case of Dr = 63%. However during the 2nd water infiltration, further strength reduction by similar percentage (15%) was observed in the CB45-L-Dr = 35%, while this reduction is very minor in the loosed specimen. But, radial and axial strains observed in these cases (Table 6.2) show four times larger deformations in loose specimen than dense. Somehow, this is contradicted with the stiffness variation observed here and variation of stiffness during the first water cycle seems to be independent from the density though overall stiffness is larger in dense sand.

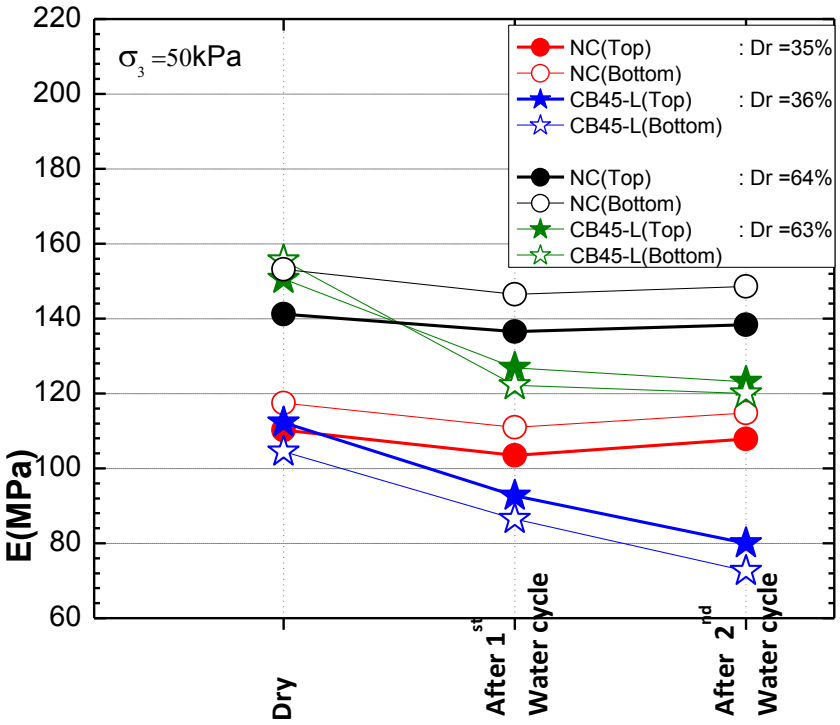

Figure 6. 29: Variation of Young's modulus - Effect of density

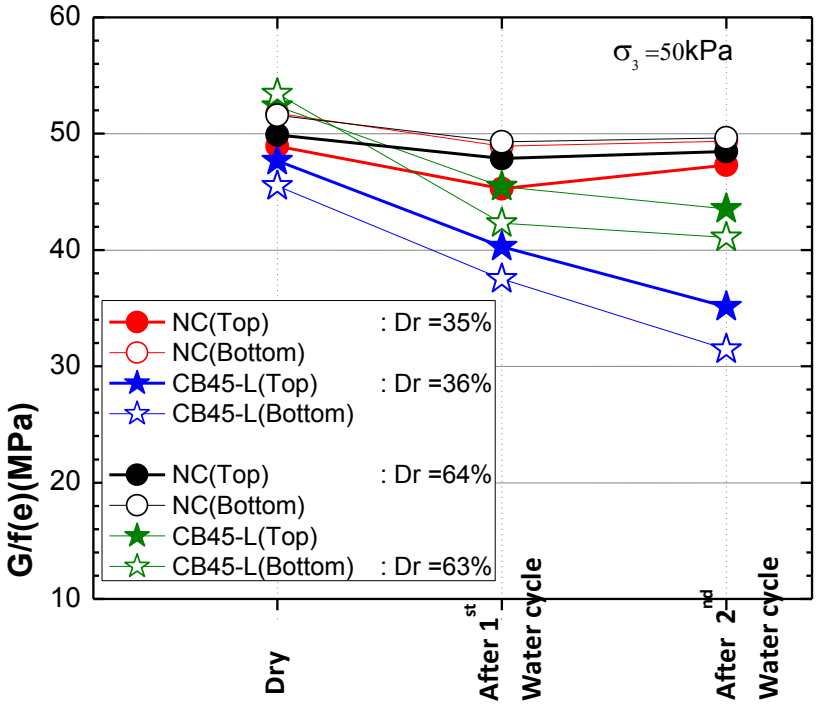

Figure 6. 30: Variation of normalized shear modulus - Effect of density

Table 6. 4: Variation of G/f (e) of loosened soil- Effect of density

Dr%	Water cycle	NC		CB45-L	
		Top	Bottom	Top	Bottom
35-36%	Increment of G/f(e) during 1st water cycle (%)	-7.48	-5.41	-15.51	-17.56
	Increment of G/f(e) during 2nd water cycle (%)	4.45	0.87	-12.82	-16.16
63-64%	Increment of G/f(e) during 1st water cycle (%)	-4.04	-4.40	-13.20	-20.82
	Increment of G/f(e) during 2nd water cycle (%)	1.22	0.67	-4.19	-2.92

6.3.1.1.4. Variation of Shear strength

Deviator stress, q vs. axial strain, ε_a relationship during triaxial shearing of all above mentioned four experiments are shown in Figure 6.31. It is obvious that the peak shear strength is larger in dense specimen than loose as seen in the same figure. However, each loose specimen shows lower stiffness than in the controlled specimen. q_{max} of CB-45 case is always lower than the NC case for both densities. Simply, comparison of strength at similar strain level was done at ε_a related to the q_{max} of controlled specimen (NC) and results are shown in Table 6.5.

- CB45-L cases in two relative densities shows different behaviour in shear strength and this depicts two types of ground loosening are possible. In dense ground, the loosening is not progressive and cavity might be stable even after two cycles of water infiltration and drainage. Because, sudden failure or collapse of ground was observed at closer to ε_a = 6% and this can be due to the sudden collapse of the cavity ceiling. Stiffness of the CB45-L (64%) is not severely affected by loosening until the sudden collapse is caused at 6%. Which confirms the loosening is much localized and propagation is smaller in dense sand.
- Different collapsing type is observed in loose specimen as the specimen shows consistent lower stiffness behaviour until the peak strength. This states the loosening is progressive and there might be no void with significant volume is remained after the water infiltration. This means, loose ground is much vulnerable for propagation of loosening.
- Strength reduction at the strain level refer to the maximum shear strength of control specimen is 74% for the dense specimen and 94% for loose specimen. The reduction is larger in the dense specimen due sudden reduction of shear strength at ε_a = 6%.

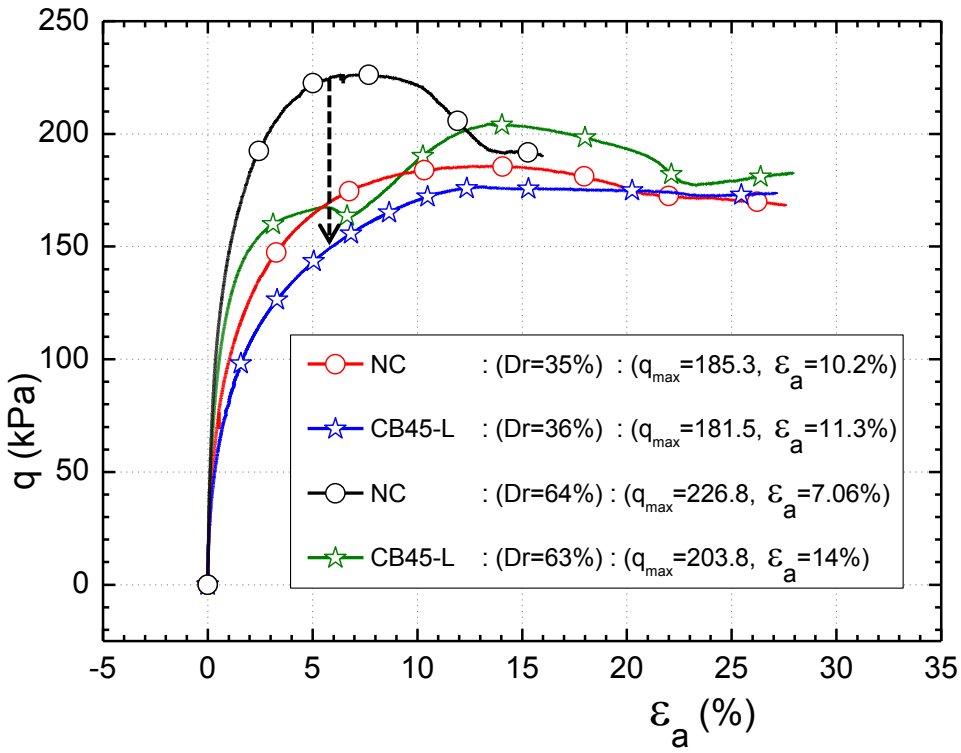

Figure 6. 31: q vs. ε_a of loosened sand – Effect of density

Table 6. 5: Shear strength reduction of loosened sand - Effect of density

Dr%	Referred ε (ε_a at q, max of NC)	q (kPa)		Reduction of q in loosened sand
		NC	CB45-L	$(q_{CB45-L})/(q_{max,NC})$
35-36%	ε = 10.2%	q_{max} = 185.6	175.6	94.6%
63-64%	ε = 7.1%	q_{max} = 226.8	167.8	73.9%

6.3.1.1.5. Summary

- Loose sand shows nearly four times larger axial, radial and volumetric strain than dense soil during formation of loosening and after repetitive infiltration on already formed loosened soil. Radial strains are slightly larger than axial strain in both loose and dense sand.
- Variation of Poisson's ratio of loosened soil becomes very complex due to non-uniform formation of soil structure which is having various sizes of voids in different combinations. Effect of density on degree of transverse deformation

characteristics of loosened soil was not possible since many localized facts are affecting the transverse deformation characteristics of soil.

- Reduction of stiffness characteristics (Young's modulus and normalized shear modulus) in both loose and dense specimens by 1st water cycle is almost similar. However, significant stiffness reduction was further recorded by 2nd infiltration in loose specimen which depicts that loosened soil in loose ground is vulnerable for repetitive infiltration.
- When discussing about the shear strength of loosened sand in loose and dense ground, two mechanisms of failures were found. In the dense sand, initial cavity was much stable and part of the cavity was remained after two water cycles. Therefore, during shearing, ground was capable to withstand 1/3 of maximum strength similar to the normal ground and then the stiffness was gradually reduced with following a sudden collapse after achieving ¾ of peak strength. In the loose ground, loosening might spread and the cavity was completely refilled with sand, thus sudden collapse was not recorded. Stiffness of the soil was decreased even starting at small axial strain during shearing.

6.3.1.2. Effect of cavity size

Effect of cavity size on soil deformation around the cavity was observed by controlling the density and confining pressure is same while changing the diameter of the glucose block. Height of both glucose blocks were 15mm and diameter was 30mm for large glucose block and 12mm for smaller one.

Test 6 - NC (Dr = 35%) -50kPa - No cavity

Test 8 - CB45-S (Dr = 37%) -50kPa - Small cavity (h=15mm, ø = 12mm)

Test 7 - CB45-L (Dr = 36%) -50kPa - Large cavity (h=15mm, ø = 30mm)

6.3.1.2.1. Variation of Axial, radial and volumetric strain

Variation of $\varepsilon_{a,}$ $\varepsilon_{rad,}$ and ε_{vol} is shown in Figure 6.32, 6.33 and 6.34 respectively. It seems that, both ε_a and ε_{rad} are significantly larger in loosed sand than the control specimen. Though the height of the cavity was similar, $\delta\varepsilon_{a,}$ caused after 1st water infiltration is not similar in Test 8 and 9. The reason could be progressive soil collapse which sited on cavity ceiling gets larger when the area of the cavity ceiling is larger. Furthermore, the sensitivity of deformation transducers is getting higher when the ground collapse spreads in radial direction because the distance between the loosened part and the sensor become smaller. However, the volumetric strain caused in the controlled specimen is negligible and $\delta\varepsilon_{vol}$ in large cavity is nearly six times of the smaller cavity which is proportional to the volume ratio of two cavities.

Figure 6.34 shows total volumetric strain observed in small cavity is 0.2% and large cavity case is 0.8%. Volume of glucose block used for each test is 0.25% and 1.5% of specimen. When the ratio between volumetric strain and volume of potential cavity was taken, ratio of larger cavity becomes 6 times of the smaller cavity, which is almost similar to the volume ratio between two potential cavities.

Table 6. 6: Strain increment by 1st water cycle – effect of cavity size

Strain	1st water cycle	
	Small cavity (0.25%)	Large cavity (1.5%)
$\boldsymbol{\delta\varepsilon_a}$	0.06	0.21
$\boldsymbol{\delta\varepsilon_{rad}}$	0.04	0.30
$\boldsymbol{\delta\varepsilon_{vol}}$	0.14	0.80

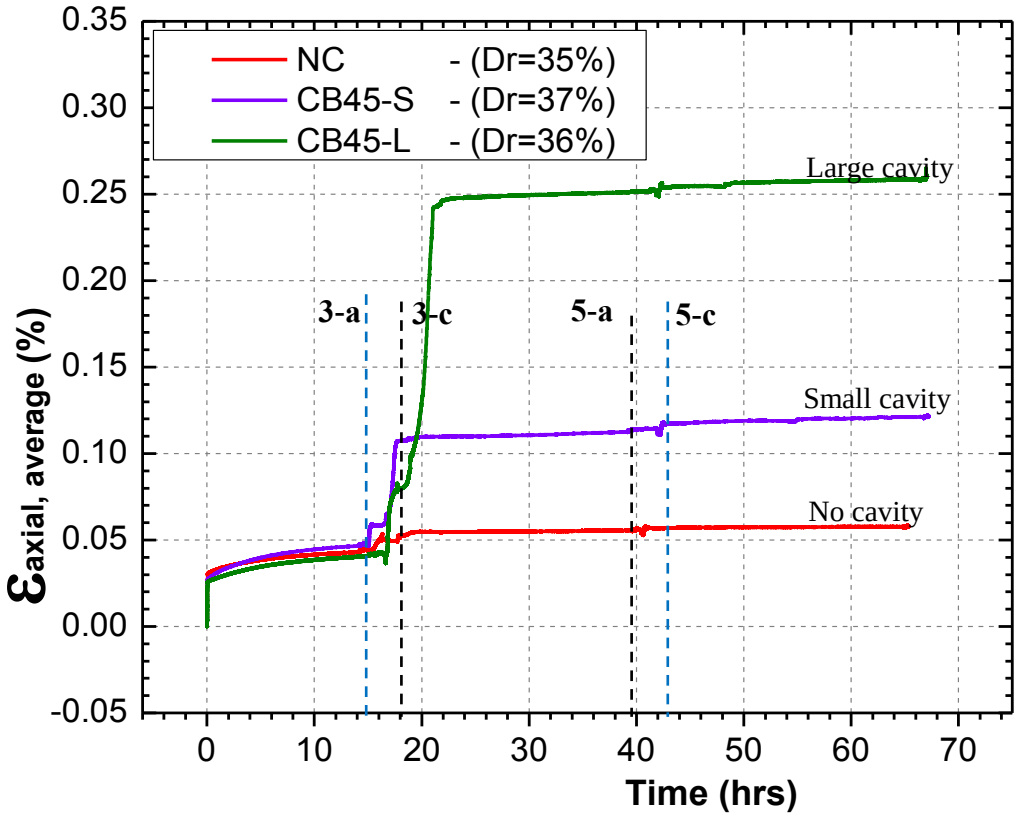

Figure 6. 32: Axial strain variation- effect of cavity size

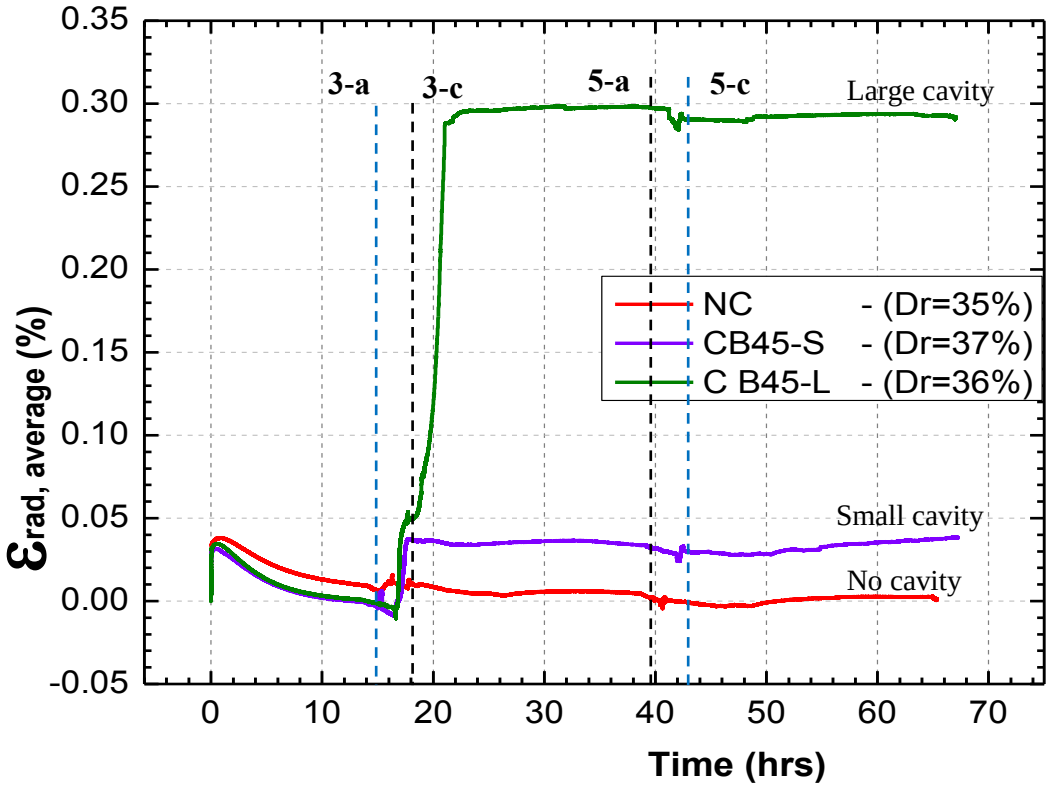

Figure 6. 33: Radial strain variation- effect of cavity size

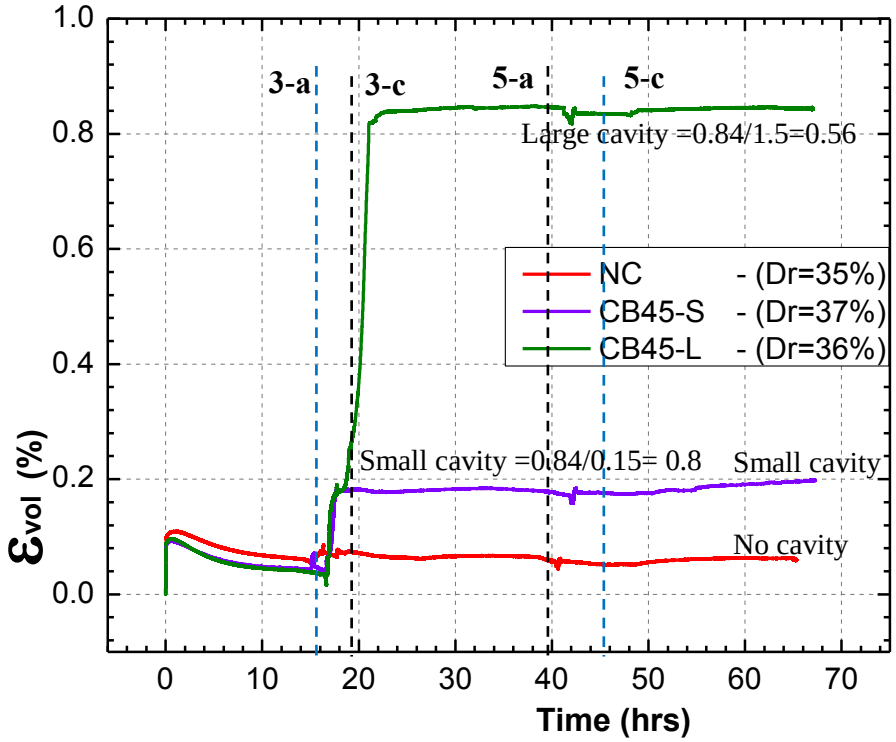

Figure 6. 34: Volumetric strain variation- effect of cavity size

6.3.1.2.2. Variation of Poisson's ratio (ν)

Special features can be observed in the variation of ν in Figure 6.35 and Table 6.7. In case of NC and CB45-S initially top part of the specimen shows lower ν value than bottom while it is opposite in CB45-L. Lower half of the normal specimen shows decrement in ν value after 1st water cycle with increasing the stiffness in transverse direction. However, in other two tests, Poisson's ratio is increased in similar percentage after loosening. As explained in chapter 6.3.1.1.2, it is really difficult to conclude the effect of cavity size on Poisson's ratio of loosened soil, since soil structure is reformed in an unpredictable and non-uniform manner in loosened sand.

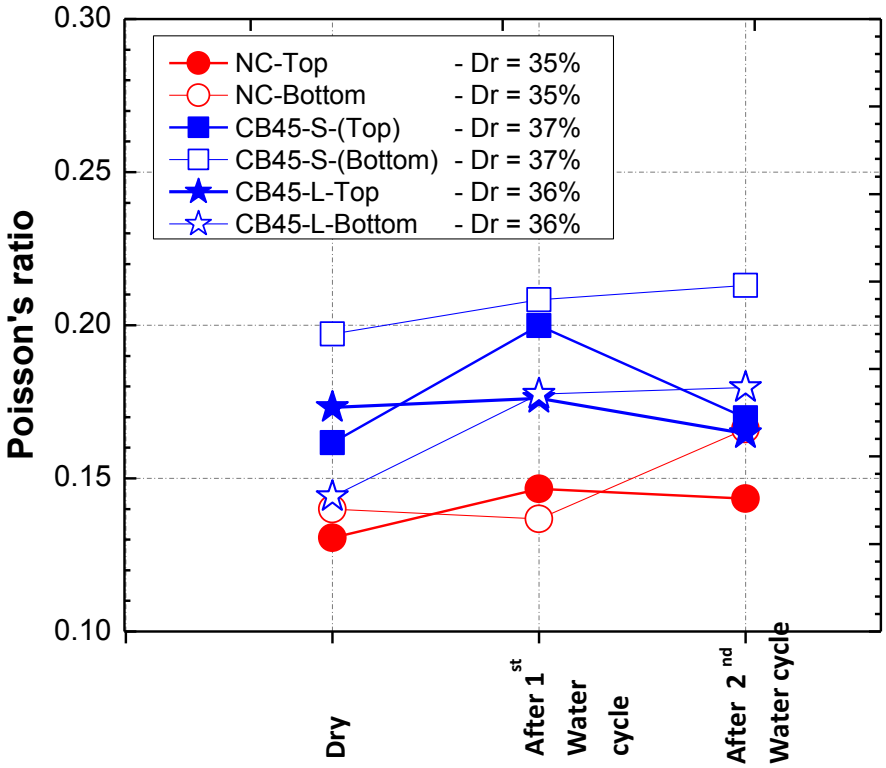

Figure 6. 35: Variation of Poisson's ratio- Effect of cavity size

Table 6. 7: Variation of ν of loosened soil- effect of cavity size

Water cycle	NC (Dr=35%)		CB45-S (Dr=37%)		CB45-L (Dr=36%)	
	Top	Bottom	Top	Bottom	Top	Bottom
Increment of ν during 1st water cycle (%)	+12.2	-2.22	+23.6	+5.7	+1.72	+23.2
Increment of ν during 2nd water cycle (%)	-2.1	+2.93	-15.0	+0.47	-6.55	+0.22

6.3.1.2.3. Variation of stiffness (Young's modulus and Small strain Modulus)

Effect of cavity size on degree of loosening and stiffness properties are shown in Figure 6.36, Figure 6.37 and Table 6.8. Significant variation on E or G/f (e) values is not observed in the controlled specimen. Both small and large size cavities have affected the stiffness of soil and normalized shear modulus has been reduced by similar percentage (around 16%) after 1st water cycle. Specially, soil with large cavity shows further reduction of G/f(e) by nearly15% even by 2nd infiltration while no significant stiffness reduction is observed in CB45-S . Which can be generalized since, the loosening is predominant when the cavity is bigger.

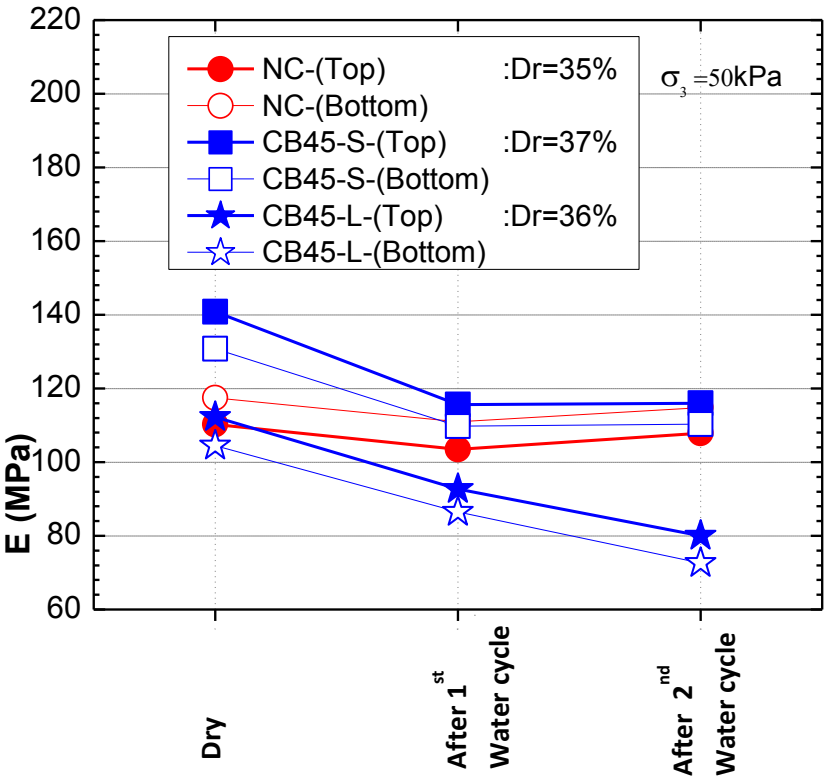

Figure 6. 36: Variation of Young's modulus - Effect of cavity size

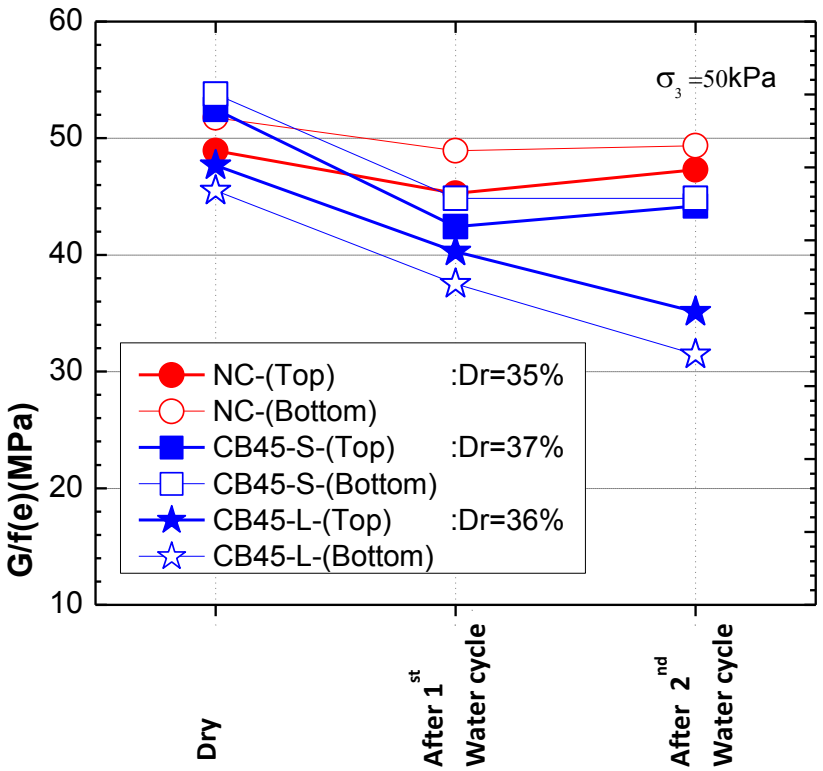

Figure 6. 37: Variation of normalized shear modulus - Effect of cavity size

Table 6. 8: Variation of G/f(e) of loosened soil- Effect of cavity size

Water cycle	NC (Dr=35%)		CB45-S (Dr=37%)		CB45-L (Dr=36%)	
	Top	Bottom	Top	Bottom	Top	Bottom
Increment of G/f(e) during 1st water cycle (%)	-7.48	-5.41	-19.14	16.57	-15.51	-17.56
Increment of G/f(e) during 2nd water cycle (%)	4.45	0.87	4.18	0.011	-12.82	-16.16

6.3.1.2.4. Variation of Shear strength

Effect of cavity size on degree of loosening was evaluated by evaluating the Young's modulus and normalized shear modulus for two densities.

Test 6 - NC (Dr = 35%) -50kPa - No cavity

Test 8 - CB45-S (Dr = 37%) -50kPa - Small cavity (h=15mm, ø = 12mm)

Test 7 - CB45-L (Dr = 36%) -50kPa - Large cavity (h=15mm, ø = 30mm)

Test 1 - NC (Dr = 64%) -50kPa - No cavity

Test 3 - CB45-S (Dr = 60%) -50kPa - Small cavity (h=15mm, ø = 12mm)

Test 2 - CB45-L (Dr = 63%) -50kPa - Large cavity (h=15mm, ø = 30mm)

E and G/f(e) variation with water infiltration process is shown in Figure 6.38 for loose soil and Figure 6.39 for dense. Reduction of strength compare to the control specimen was computed for the ε_a related to the peak shear strength of NC case and given in Table 6.9.

In both loose and dense conditions, loosened soil shows lower stiffness than controlled specimen. In loose sand (Dr =35%), both NC and CB45-S shows similar behaviour in the Figure 6.38 only minor strength reduction is recorded in CB45-S. However, CB45-L where the large cavity was placed, stiffness has been decreasing from beginning of the shearing till it reaches the maximum. However, in loose sand, q_{max} is not significantly affected by loosening effect though the stiffness is reduced slightly. Sudden collapse of loosened soil was not recorded which means loosened part has been gradually settled during shearing.

Even in the dense soil, NC and CB45-S shows similar behaviour in the initial stage of the shearing. However, after 1-2% of applied shearing strain (εa), loosened soil starts to behave softer than the control specimen where a cavity wall failure occurs around 7% strain only in large cavity sample, whereas small cavity sample follows the same pattern of loose soil. At the time of cavity wall failure in dense sample with large cavity, strength has been reduced at least by 1/3 of control specimen. Which can be quite significant in real life loosened ground failures.

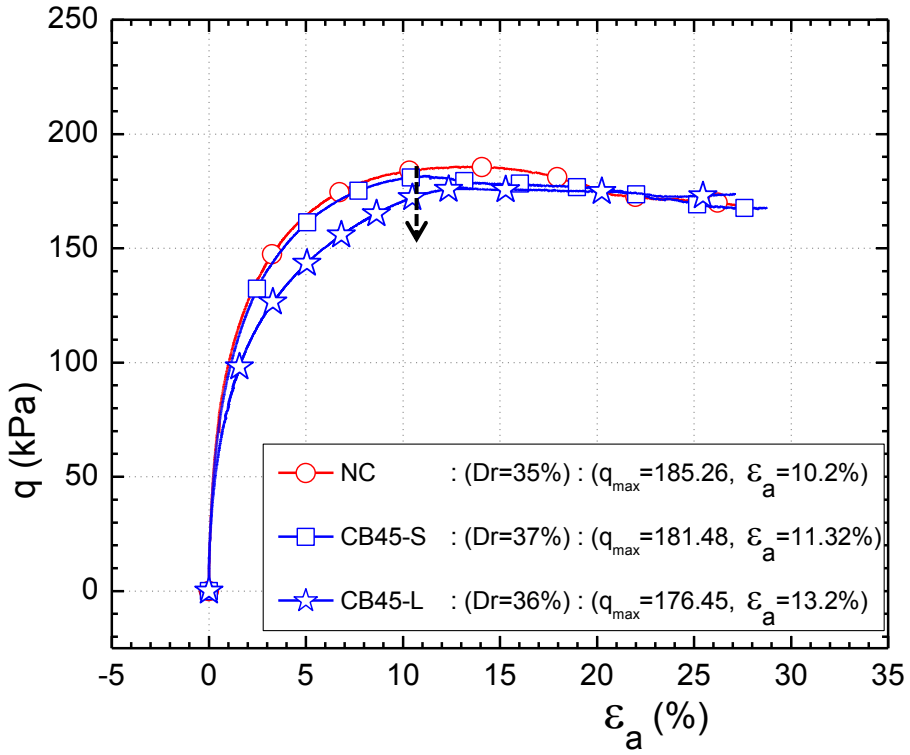

Figure 6. 38: q vs. ε_a of loosened sand – Effect of cavity size (Dr= 36%)

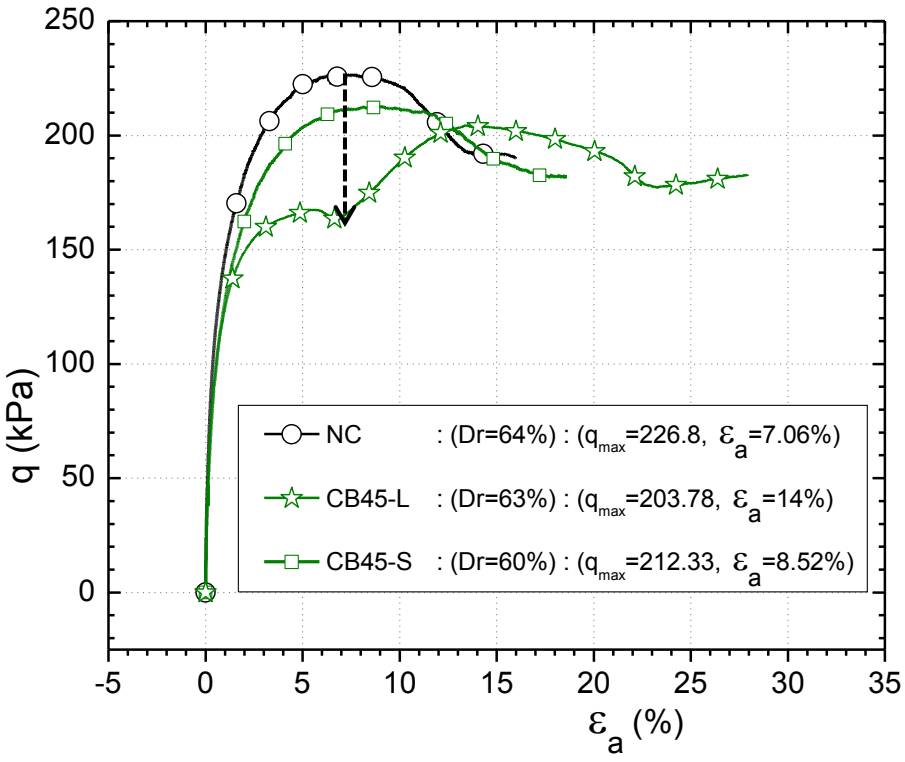

Figure 6. 39: q vs. ε_a of loosened sand – Effect of cavity size (Dr= 63%)

Table 6. 9: Shear strength reduction of loosened sand - Effect of cavity size

Dr%	Referred ε (ε_a at q_{max} of NC)	q (kPa)			Reduction of q in loosened sand (q_{CB45})/($q_{max,NC}$)	
		NC	CB45-S	CB45-L	CB45-S	CB45-L
35%	ε_a = 10.2%	q_{max} = 185.6	181.2	175.6	97.6%	94.6%
63%	ε_a = 7.1%	q_{max} = 226.8	210.8	167.8	92.9%	73.9%

6.3.1.2.5. Summary

- As expected, small void which has 0.25% volume of specimen shows smaller axial, radial and volumetric strains than large void with 1.5% volume of specimen. Loosening caused by small cavity shows larger axial strain than radial while large cavity caused the opposite deformation behaviour. Simultaneously, in the smaller cavity diameter is 12mm and height is 15mm whereas in large cavity diameter is 30mm and height is the same. So, larger deformation has already caused in the direction of larger dimension of cavity. Therefore ground deformations are also influenced by the dimensions of the initial cavity.

- Variation of Poisson's ratio of loosened soil becomes very complex due to non-uniform formation of soil structure which is having various sizes of voids in different combinations. Effect of cavity size on degree of transverse deformation characteristics of loosened soil was not possible since many localized facts are affecting the transverse deformation characteristics of soil.

- Reduction of stiffness characteristics (Young's modulus and normalized shear modulus) of loosened sand in both small and large cavity specimens by 1st water cycle is almost similar. However, significant stiffness reduction was further recorded by 2nd infiltration in specimen with large cavity which depicts that when the initial cavity volume is larger ground is vulnerable for repetitive infiltration.

- When discussing about the shear strength of loosened sand caused by small and large size of cavity, no significant influence was observed in the loosened sand with small void (0.25% of initial volume). The behaviour and the peak strength were almost similar to the normal ground. However, ground loosening created by 0.15% of volume cavity, has affected the stiffness and after aching 1/3 of peak strength the stiffness was reduced causing peak strength to be decreased slightly.

6.3.1.3. Effect of cavity location

In order to observe the variation of soil deformation with cavity location, similar size of glucose block was dissolved in two specimens with similar density and confining pressure. In CB45-L, the height from specimen top to glucose top surface is six times the height of the glucose block while it is 9 times in CB-L. Height of both glucose blocks were 15mm and diameter was 30mm.

Test 6 - NC (Dr = 35%) -50kPa - No cavity

Test 8 - CB-L (Dr = 37%) -50kPa - Large cavity (h=15mm, ø = 30mm)

Test 7 - CB45-L (Dr = 36%) -50kPa - Large cavity (h=15mm, ø = 30mm)

6.3.1.3.1. Axial and radial deformations

Although the cavity size, density and confining pressure were similar, near ground deformation seems to be different with location of the cavity (Figure 6.40- 6.42). In CB45-L, the height from specimen top to glucose top surface is six times the height of the glucose block while it is 9 times in CB-L. This depth difference has affected ε_a, to be increased nearly six times in Case CB45-L., while the radial deformations are almost in the same range. However, this depth difference has caused two times larger $\varepsilon_{vol,}$ case CB45-L.

However the arrangement of Clip gauges in two cases might affect this variation of ε_{rad}. In CB45, both CG1 and CG2 are affecting and average ε_{rad} will be increased while only CG1 is affected in CB. (Appendix-II)

In order to confirm this effect in detail, decision was made to perform few more tests with changing the confining pressure to simulate the deferent depth conditions. σ_3, 50 kPa was used to simulate the cavity condition at shallower depth (3-4m) and σ_3, 100 kPa for deeper cavities. This will be discussing in the clause 6.3.1.4.

Table 6. 10: Strain increment by 1st water cycle – effect of cavity location

Strain	1st water cycle	
	Cavity located at bottom	Cavity located at 45mm from bottom
$\boldsymbol{\delta\varepsilon_a}$	0.034	0.206
$\boldsymbol{\delta\varepsilon_{rad}}$	0.217	0.301
$\boldsymbol{\delta\varepsilon_{vol}}$	0.456	0.803

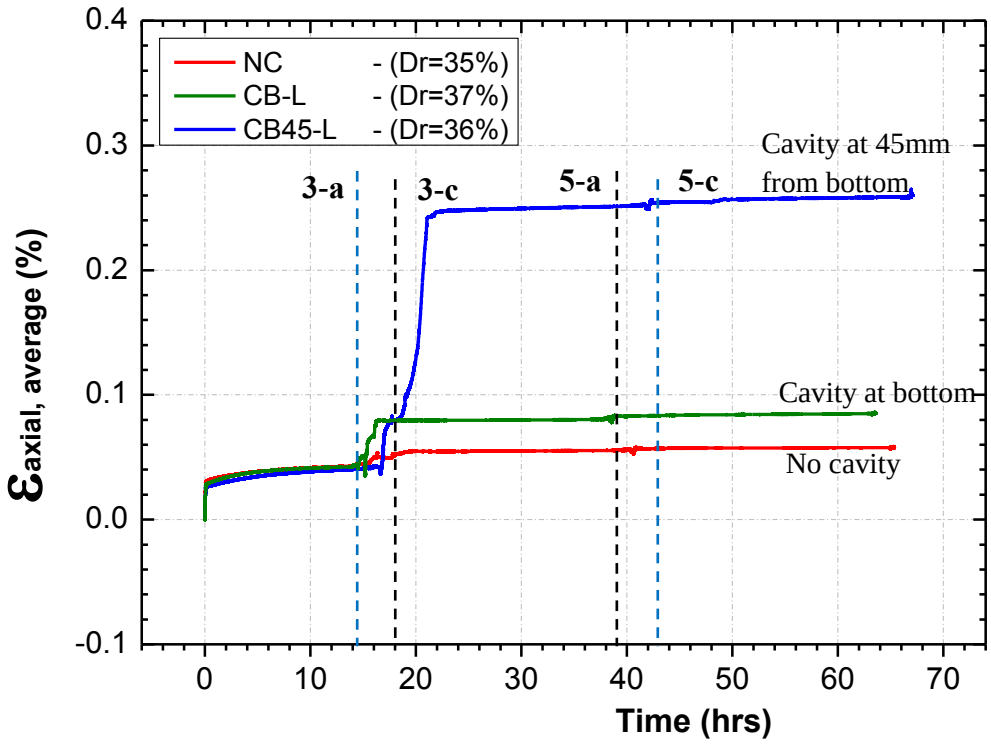

Figure 6. 40: Axial strain variation- effect of cavity location

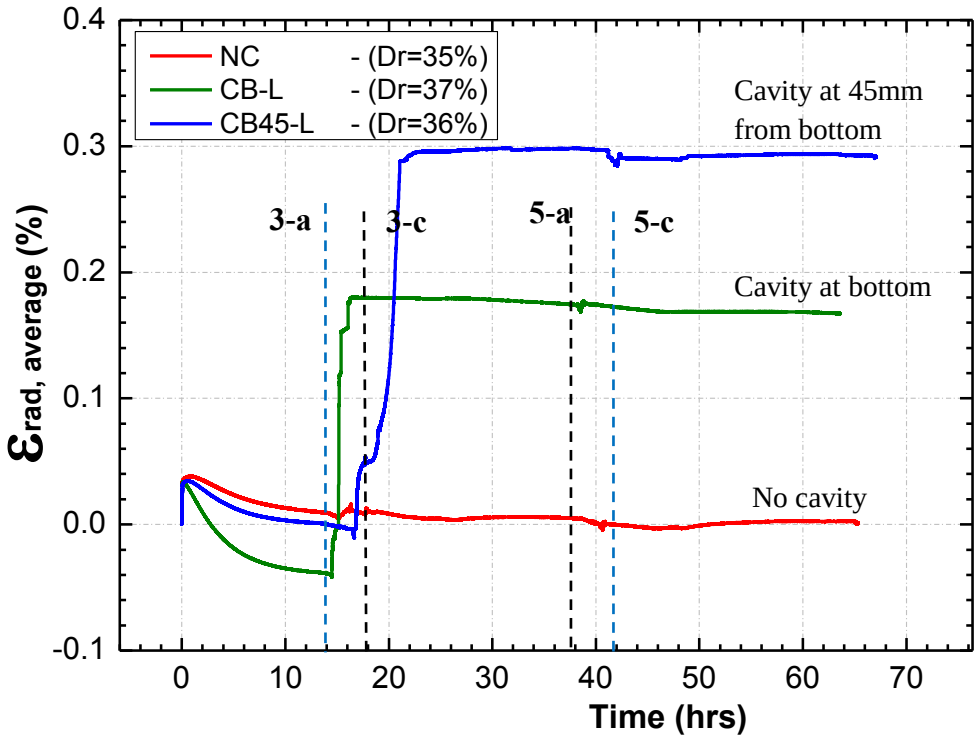

Figure 6. 41: Radial strain variation- effect of cavity location

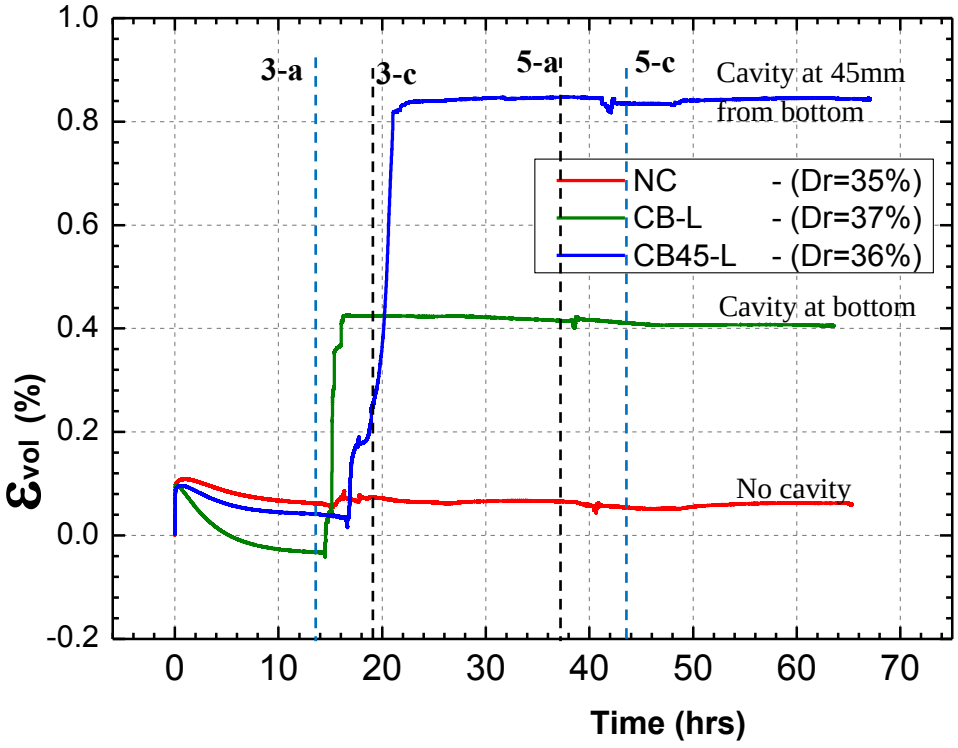

Figure 6. 42: Volumetric strain variation- effect of cavity location

6.3.1.3.2. Variation of Poisson's ratio

Variation of degree of loosening with cavity location was evaluated by measuring the Poisson's ratio in the same experiments and results are shown in Figure 6.43 and Table 6.11. In both loosened specimens, Poisson's ratio of specimens has been increasing with 1st water infiltration while it is almost constant in the controlled specimen. Larger increment of ν is recorded at lower part of the specimen in CB-L than CB45-L. As explained in clause 6.3.1.1.2, the abrupt behavior is expected to be due the arrangement of deformation transducers or non-uniform pattern of loosening. Measurements taken after the second water cycle shows reduction of Poisson ratio, only for the CB-L, which can only be due to healing of the cavitation by washed in of neighboring materials. None of the other samples, including control specimen have shown any variation in the parameter.

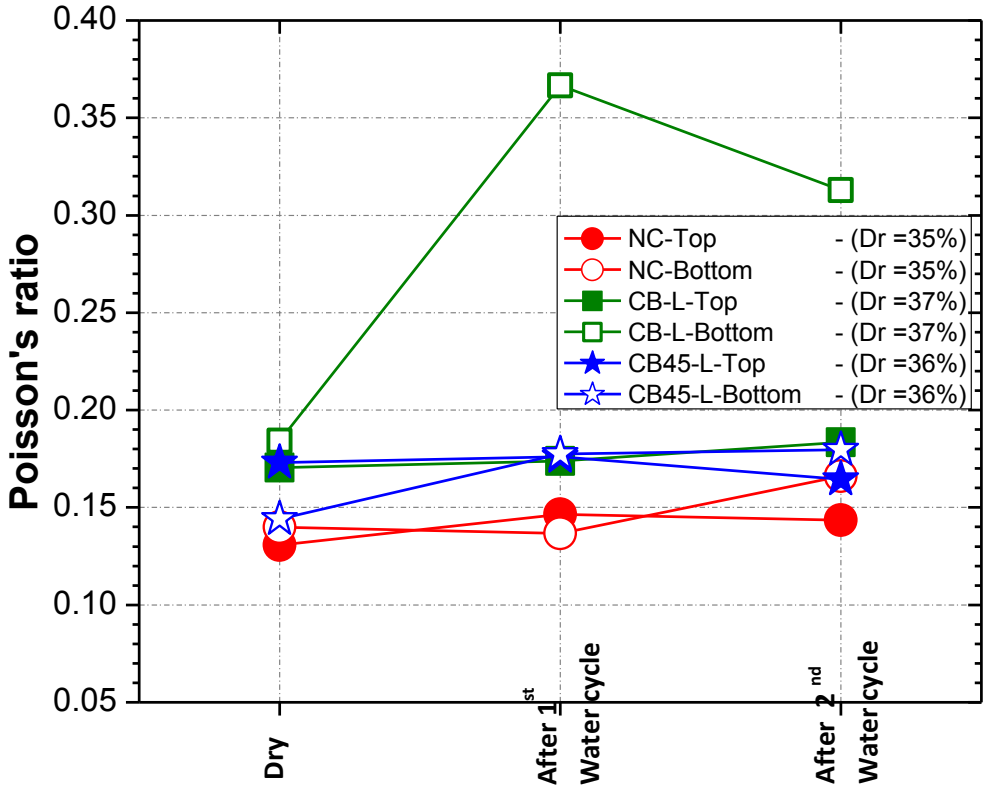

Figure 6. 43: Variation of Poisson's ratio- Effect of cavity location

Table 6. 11: Variation of ν of loosened soil- effect of cavity location

Water cycle	NC (Dr=35%)		CB-L (Dr=37%)		CB45-L (Dr=36%)	
	Top	Bottom	Top	Bottom	Top	Bottom
Increment of ν during 1st water cycle (%)	+12.2	-2.22	+1.97	+90	+1.72	+23.2
Increment of ν during 2nd water cycle (%)	-2.1	+2.93	+5.5	-7.22	-6.55	+0.22

6.3.1.3.3. Variation of stiffness (Young's modulus and Small strain Modulus)

Young's modulus and normalized shear modulus haven't shown significant variation with respect to cavity location, however same pattern has been observed. Comparatively higher values for both parameters were observed with cavity at the bottom of the sample, which can be seen in figure 6.44, 6.45 and Table 6.12. Slightly higher Young's modulus and normalized shear modulus at initial stage in cavity at bottom situation is not the desired result, which can be probably due to higher relative density. Two graphs further illustrate that second water cycle has affected these two parameters than the first water cycle in CB-L whereas a uniform reduction was observed with CB45-L. Generally it can be seen that cavity close to the free surface has lower strength characteristics in comparison with deep cavities.

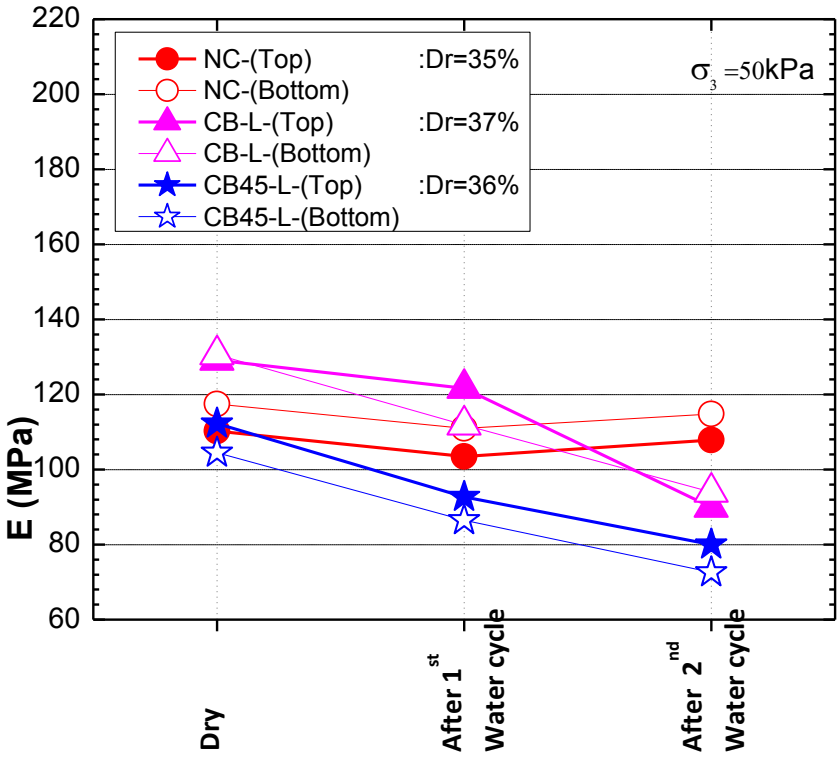

Figure 6. 44: Variation of Young's modulus- Effect of cavity location

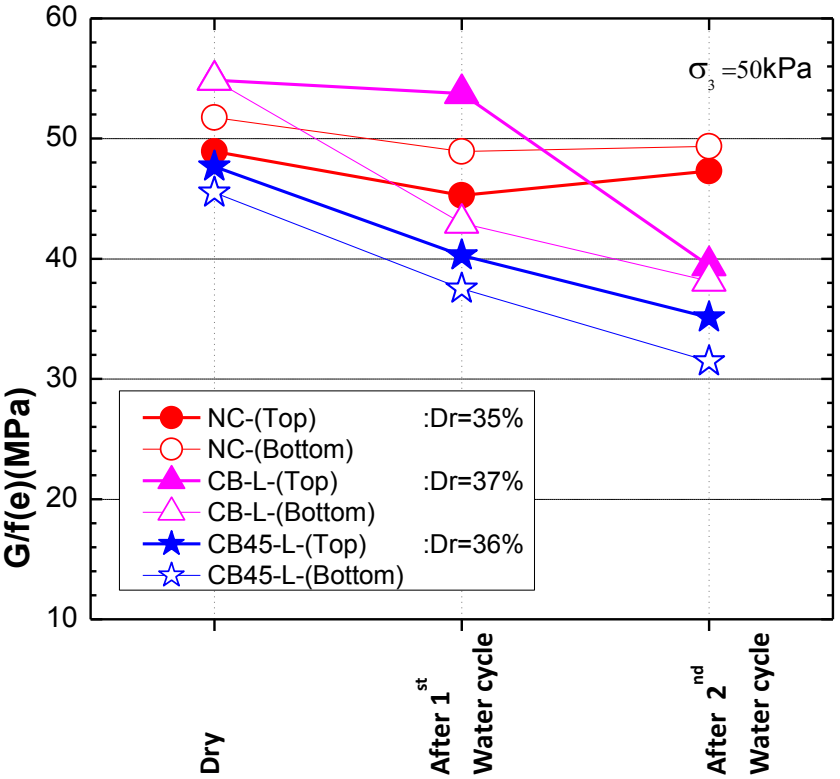

Figure 6. 45: Variation of normalized shear modulus - Effect of cavity location

Table 6. 12: Variation of G/f(e) of loosened soil- Effect of cavity location

Water cycle	NC (Dr=35%)		CB-L (Dr=37%)		CB45-L (Dr=36%)	
	Top	Bottom	Top	Bottom	Top	Bottom
Increment of G/f(e) during 1st water cycle (%)	-7.48	-5.41	-2.04	-21.65	-15.51	-17.56
Increment of G/f(e) during 2nd water cycle (%)	4.45	0.87	-26.64	-11.24	-12.82	-16.16

6.3.1.3.4. Variation of Shear strength

Shear strength variation with applied strain is shown in figure 6.46. Although cavity location was altered (vertical position), no significant variation in shear strength was observed. The control specimen and the CB-L specimen both have shown exact same response curves suggest that placing the cavity in the bottom of the sample will not affect the strength at all. However, when the location of the loosening is altered, (CB45-L) slight reduction in peak strength was observed. In all three cases, no strength variation was observed until the applied strain reached 1%, at which 1/3 of maximum shear strength has been attained by the material.

The reason observed for the similar behaviour of controlled specimen and cavity at bottom is, the location of loosened soil was sited at the very bottom than where the formalized shear band was. Therefore effect of loosening on shear strength was not observed in Case-CB. However, when the loosened soil was located at the neighborhood of the shear band (in case CB-45), the effect of loosening has affected the stiffness properties of soil. Therefore As observed in real life examples, location of the cavity (vertical) is a major factor that determines the strength, although which is not reflected here due to lack of experiments with different vertical locations for the cavitation. Therefore the same effect (effect of depth of cavity) was analyzed again by changing the confining pressure and results are shown in clause 6.1.3.4.

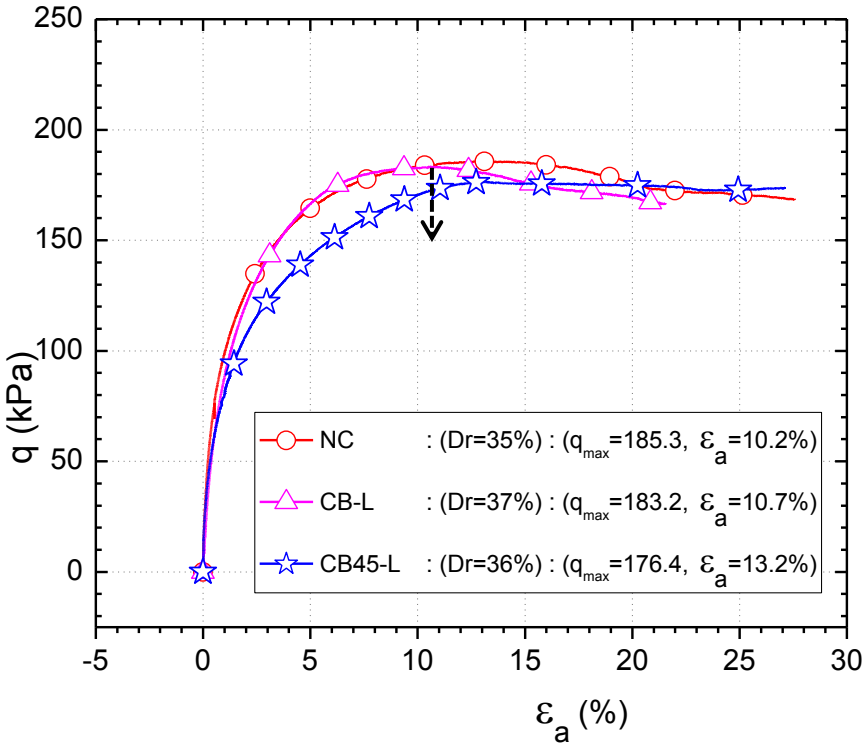

Figure 6. 46: q vs. ε_a of loosened sand – Effect of cavity location (Dr= 37%)

Table 6. 13: Shear strength reduction of loosened sand - Effect of cavity location

Referred ε (ε_a at q_{max} of NC)	q (kPa)			Reduction of q in loosened sand (q_{CB45})/($q_{max,NC}$)	
	NC	CB-L	CB45-L	CB-L	CB45-L
ε_a = 10.2%	q_{max} = 185.6	181.8	175.6	98%	94.6%

6.3.1.3.5. Summary

- By changing cavity location only for the same confining pressure has not affect the deformations characteristics significantly. Deformation characteristics measured by deformation transducers placed closer to the cavity show almost similar range of strain, though the average value was slightly larger in CB45.
- Variation of Poisson's ratio of loosened soil becomes very complex due to non-uniform formation of soil structure which is having various sizes of voids in different combinations. Effect of cavity location on degree of transverse deformation characteristics of loosened soil was not possible since many localized factors are affecting the transverse deformation characteristics of soil.

- Reduction of stiffness characteristics (Young's modulus and normalized shear modulus) of loosened sand in both CB and CB45 cases shows similar reduction in the stiffness parameters for both water cycles.
- When discussing about the shear strength of loosened sand caused by CB and CB45, no significant influence was observed in the loosened sand with CB. Cavity placed at the very bottom of the specimen creates the loosening area which is sited below the formed shear band. Therefore, effect on shear strength by such loosened soil in deeper ground has no significant influence on shear strength of soil. However when the cavity elevation was moved by 45mm up (CB45), where the loosened soil was located at the neighborhood of the shear band, the effect of loosening has affected the stiffness properties of soil. Stiffness has been decreasing with causing slightly lower peak strength at last.
- By changing only the cavity location without changing the confining stress has not influenced on loosening phenomena. Therefore the same effect (effect of location of cavity) was analyzed again by changing the confining pressure and results are shown in clause 6.1.3.4.

6.3.1.4. Effect of confining pressure

When the cavity location was slightly changed in Test No.7 and Test No.09, it was observed that the ground deformations around the cavity were larger when the cavity was closer to ground surface ground. In order to confirm his fact, different confining pressures was applied in two experiments while controlling the density, cavity size and location is same. In both cases large glucose block was used with height of 15mm and diameter of 30mm. initial volume of the void was 0.15% of specimen volume. Confining pressure, σ_3 = 50 kPa was used to simulate the cavity condition at shallower depth (3-4m) and σ_3, 100 kPa for deeper cavities.

Test 6 - NC (Dr = 35%) -50kPa - Shallow ground (3-4m)

Test 7 - CB45-L (Dr = 36%) -50kPa - Shallow ground (3-4m)

Test 11- NC (Dr = 37%) -100kPa - deeper ground (6-8m)

Test 12- CB45-L (Dr = 35%) -100kPa - Deeper ground (6-8m)

6.3.1.4.1. Axial, radial and volumetric strain

Variation of all three types of strains is shown in Figure 6.47to Figure 3.49 and the stress increments occurred during the 1st water cycle is given in Table 6.14. It is clearly visible that both ε_a and ε_{rad} has been increased under lower confining pressure. That fact depicts, cavities at shallower depth are much vulnerable to form larger ground deformations. And growth or the propagation of ground loosening in deeper ground seems to be slower and smaller. Behaviour of each LDT and CG is shown in Appendix II.

Table 6. 14: Strain increment by 1st water cycle – effect of confining pressure

Strain increment	1st water cycle	
	50kPa CB45-L (Dr =36%)	100kPa CB45-L (Dr =36%)
$\boldsymbol{\delta\varepsilon_a}$	0.25	0.08
$\boldsymbol{\delta\varepsilon_{rad}}$	0.29	0.11
$\boldsymbol{\delta\varepsilon_{vol}}$	0.81	0.29

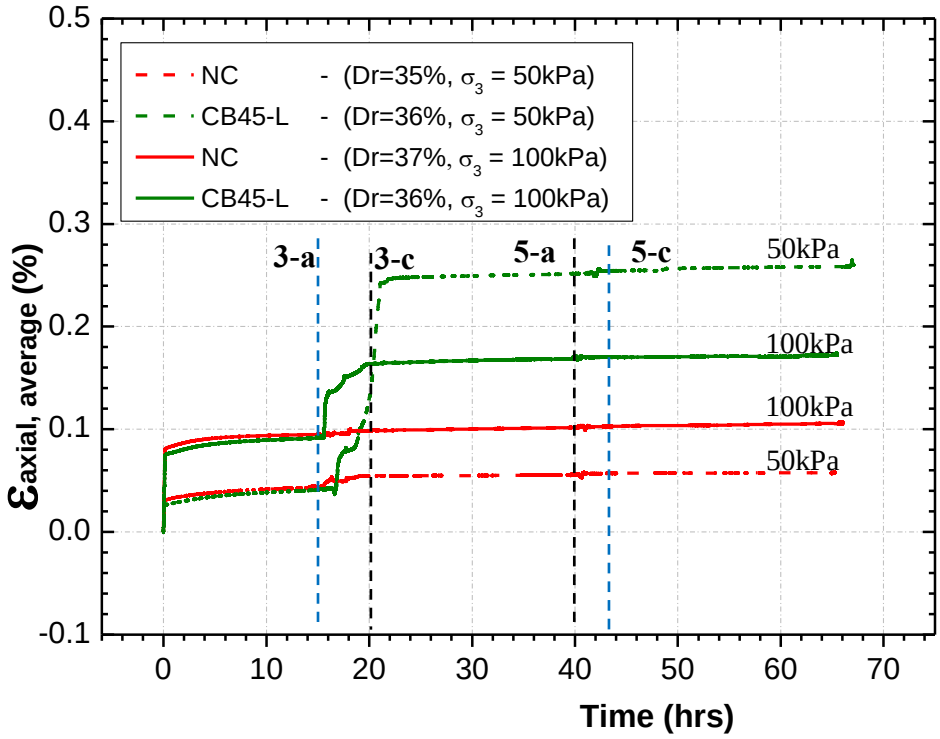

Figure 6. 47: Axial strain variation- effect of confining pressure

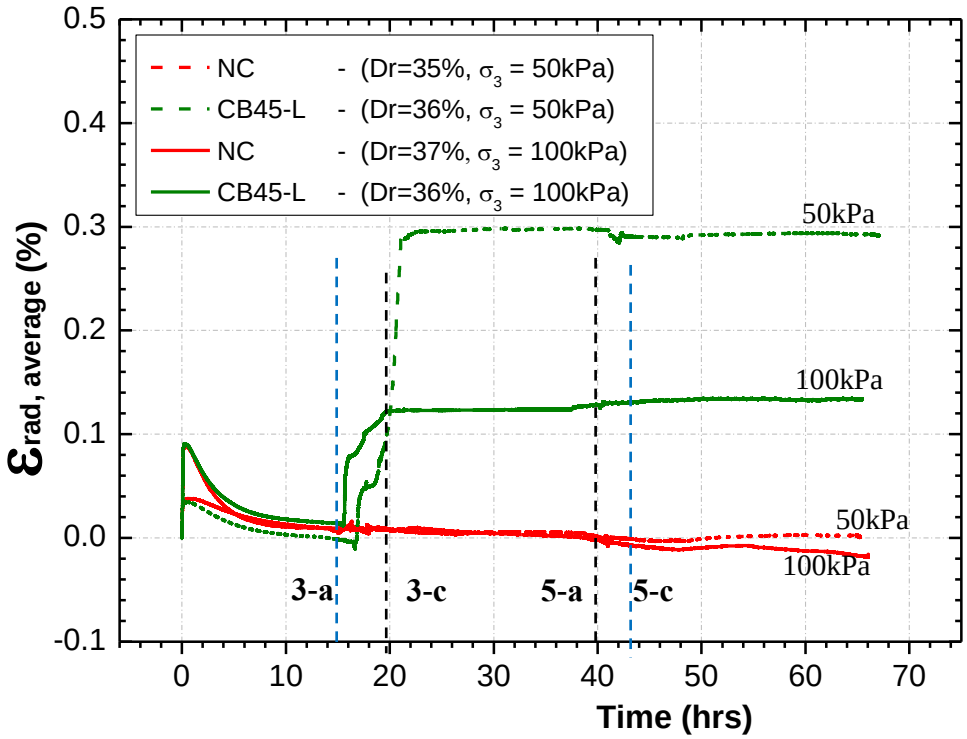

Figure 6. 48: Radial strain variation- effect of confining pressure

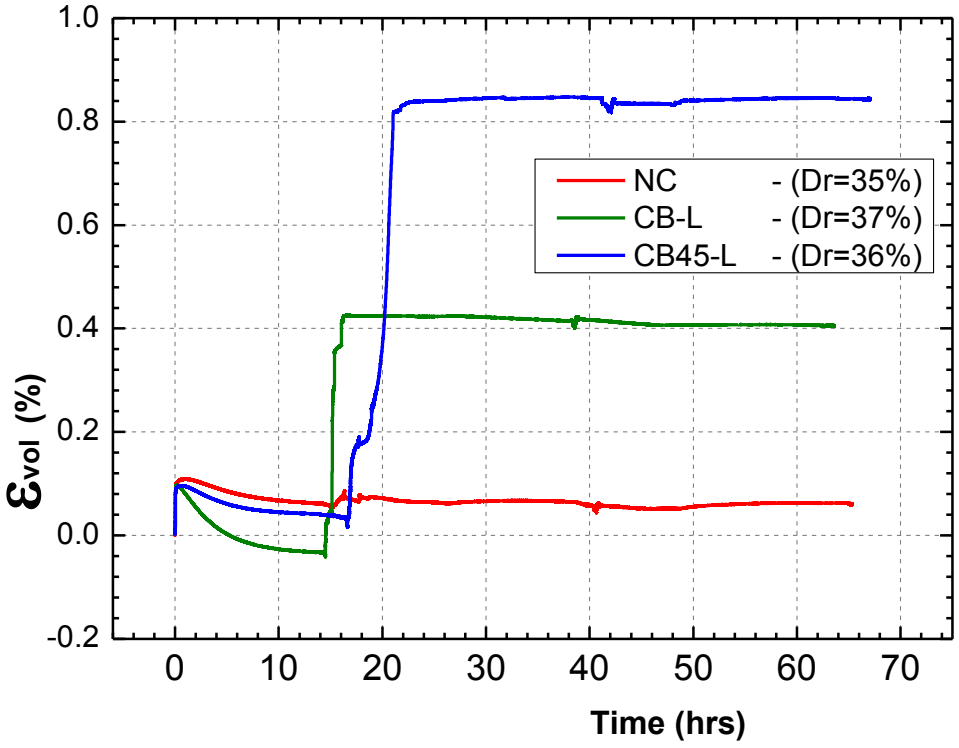

Figure 6. 49: Volumetric strain variation- effect of confining pressure

6.3.1.4.2. Variation of Poisson's ratio

No conclusive variation has been observed with respect to different confining pressures. Contrasting results were observed with CB45-L with 100 kPa of confining pressure, where Poisson's ratio is lesser than the CB45-L with 50 kPa confining pressure. None of the tests have shown consistent results; even the control specimens were not consistent. The only explanation which may be applicable to explain these contrasting results is the local deformations which may cause initial loosening and becoming dense at the second stage of water cycle. As observed in 6.3.1.1.2, 6.3.1.2.2 and 6.3.1.3.2, it is evident that evaluation of Poisson's ratio of loosened soil is not accurate in this study and the reasons were explained in 6.3.1.1.2.

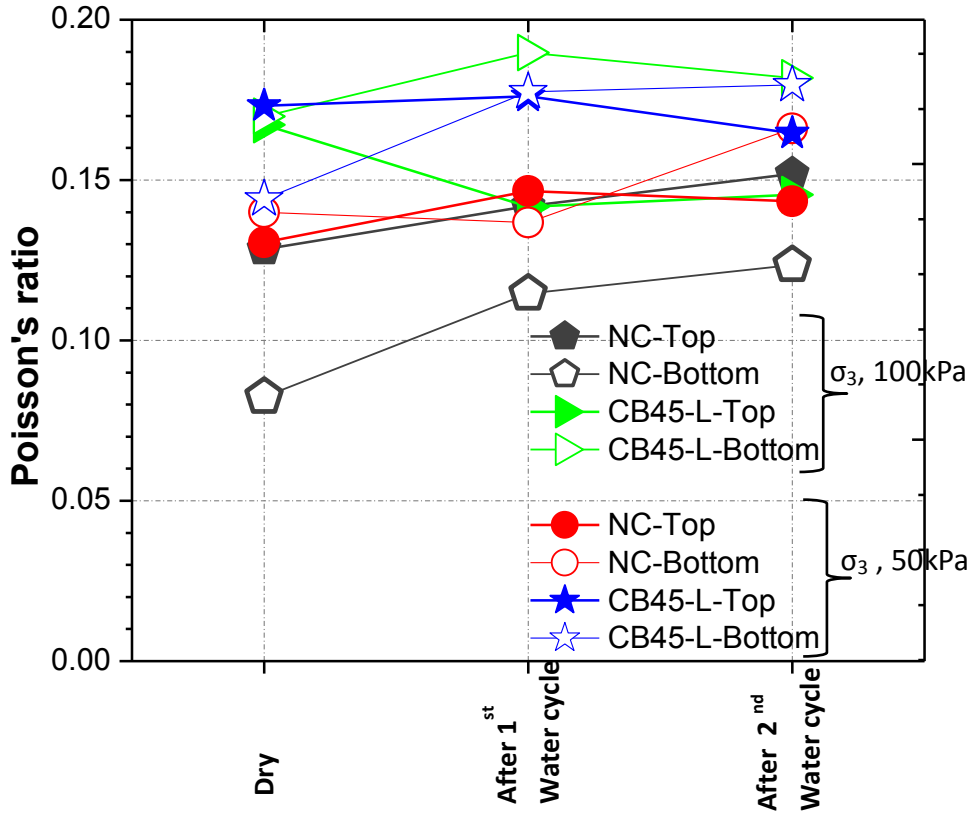

Figure 6. 50: Variation of Poisson's ratio- Effect of confining pressure

Table 6. 15: Variation of ν of loosened soil- effect of confining pressure

σ_3	Water cycle	NC (37%)		CB45-L (36%)	
		Top	Bottom	Top	Bottom
50kPa	Increment of ν during 1st water cycle (%)	+12.2	-2.22	+1.72	+23.2
	Increment of ν during 2nd water cycle (%)	-2.1	+2.93	-6.55	+0.22
100kPa	Increment of ν during 1st water cycle (%)	+10.5	+39.0	-15.3	+11.7
	Increment of ν during 2nd water cycle (%)	+7.12	+0.88	+2.65	-0.79

6.3.1.4.3. Variation of stiffness (Young's modulus and Small strain Modulus)

It is quite obvious that with higher confining pressure, higher stiffness's can be observed even with cavities and Figure 6.50, 6.51 and Table 6.16 confirms the observations. However, it has been observed that after the second water cycle, stiffness parameters have either improved or remain in the same value in case of higher confining pressure (100kPa). In case of low confining pressure (50 kPa), both Young's modulus and normalized shear

modulus have reduced in both water cycles. This situation can be seen as a self-healing mechanism (filling up the artificially created void or loosening) in case of higher confining pressures which simulates higher depths. These results depict that, cavities at shallower depths are more vulnerable for repetitive infiltration processes. However, these results can be used only to predict the probable trend only for the selected material.

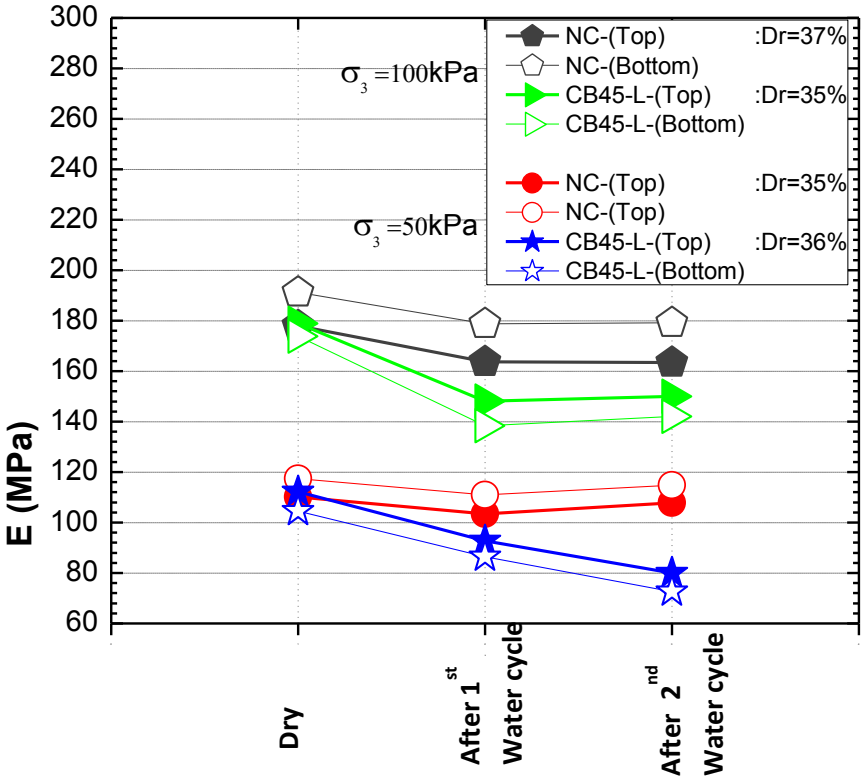

Figure 6. 51: Variation of Young's modulus - Effect of confining pressure

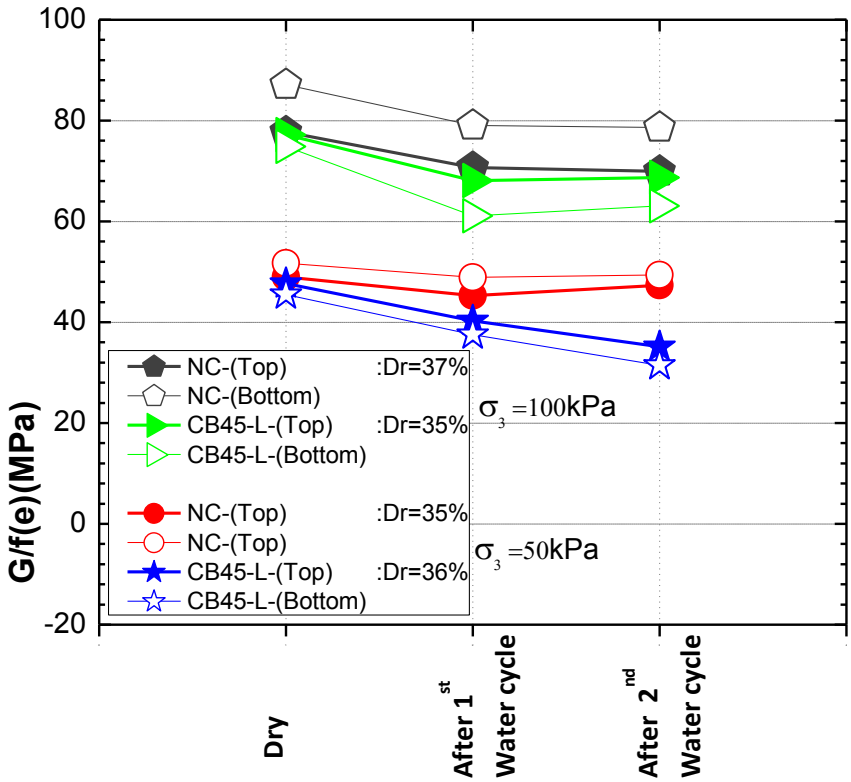

Figure 6. 52: Variation of normalized shear modulus - Effect of confining pressure

Table 6. 16: Variation of G/f(e) of loosened soil- Effect of confining pressure

σ_3	Water cycle	NC (37%)		CB45-L (36%)	
		Top	Bottom	Top	Bottom
50kPa	Increment of G/f(e) during 1st water cycle (%)	-7.48	-5.41	-15.51	-17.56
	Increment of G/f(e) during 2nd water cycle (%)	4.45	0.87	-12.82	-16.16
100kPa	Increment of G/f(e) during 1st water cycle (%)	-9.06	-9.24	-11.75	-18.4
	Increment of G/f(e) during 2nd water cycle (%)	-1.02	-0.56	0.87	3.29

6.3.1.4.4. Variation of Shear strength

It is obvious that the shear strength of soil increased with the confining pressure as observed in results in Figure 6.53 and Table 6.17. Unfortunately complete stress- strain relationship was not observed in controlled specimen of 100kPa due to a technical error. However, existing part of that curve shows significantly large stiffness than the loosened sand even at very small axial strain levels. Furthermore, percentage of shear strength reduction is larger at high confining pressure. However, steady conclusion cannot be made due to lack of experiments.

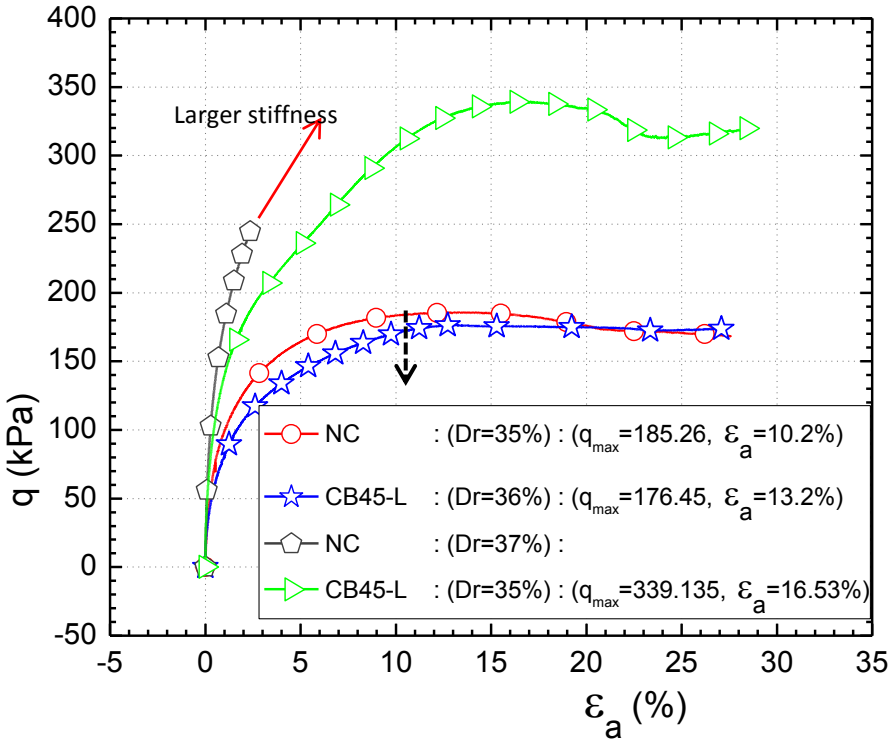

Figure 6. 53: q vs. ε_a of loosened sand – Effect of confining pressure (Dr= 37%)

Table 6. 17: Shear strength reduction of loosened sand - Effect of confining pressure

σ_3 (kPa)	Referred ε (ε_a at q_{max} of NC)	q (kPa)		Reduction of q in loosened sand $(q_{CB45})/(q_{max,NC})$
		NC	CB45-L	CB45-L
50	ε_a = 10.2%	q_{max} = 185.6	175.6	94.6%
100	ε_a = not recorded%	not recorded%	335.4	-

6.3.1.4.5. Summary

- Obviously there is a significant effect on deformation characteristics of soil from confining stress of ground. In case of 50kPa, the axial, radial and volumetric strains caused by 0.15% volume of cavity is three times larger than the σ_3 = 100kPa. Therefore cavities at shallower depth show significant ground deformations than in deeper ground.
- Variation of Poisson's ratio of loosened soil becomes very complex due to non-uniform formation of soil structure which is having various sizes of voids in

different combinations. Effect of cavity location on degree of transverse deformation characteristics of loosened soil was not possible since many localized factors are affecting the transverse deformation characteristics of soil.

- In case of stiffness parameters, similar stiffness reduction was recorded in both closer and higher confining pressures during the 1st water cycle. However, in case of lower confining pressure (50 kPa), both Young's modulus and normalized shear modulus have reduced even in the 2nd water cycle which was not observed in 100kPa. This situation can be seen as a self-healing mechanism (filling up the artificially created void or loosening) in case of higher confining pressures which simulates higher depths. Furthermore, it can be revealed that, cavities at shallower depths are vulnerable for repetitive infiltrations.

- When discussing about the shear strength of loosened sand caused by different confining pressures, significant influence was observed. Higher peak strength was recorded even for loosened sand under σ_3 = 100kPa, though the stiffness was reduced even at lower strain level. Under lower confining pressure, peak strength of loosened sand is almost similar to the normal specimen and the value is nearly half of the peak strength of 100kPa.

6.3.2. Silica Sand

Effect of particle size on ground loosening behaviour in sand soil was observed by using two types of sand. Mean diameter (D_{50}) of Toyoura sand is 0.196mm and it is less than half of the D_{50} of Silica sand which is 0.45mm.

Test 1 - NC (Dr = 64%) -50kPa - Toyoura sand

Test 2 - CB45-L (Dr = 63%) -50kPa - Toyoura sand

Test 13- NC (Dr = 58%) -50kPa - Silica sand

Test 14- CB45-L (Dr = 61%) -50kPa - Silica sand

6.3.2.3.1. Axial and radial deformations

Variation of ε_a, ε_{rad} and ε_{vol} for Silica sand is shown in Figure 6.54 to Figure 6.56 respectively. The comparison of strain increment during 1st water cycle for Silica sand and Toyoura sand for similar conditions are shown in Table 6.6.

Results depicts that the particle size has a significant effect on ground loosening in these test conditions. When the particle size is 0.45mm, the soil structure has become week in radial direction than axial. Volumetric strain is also increase more than twice of Toyoura sand.

Specially, ground has further deformed in the second infiltration in Silica sand, which was very smaller in Toyoura sand (Between Step 5-a and 5-c in Figure 6.54 to 3.56). The effect of porosity and soil grain structure seems to be very important for this phenomenon.

Table 6. 18: Strain increment by 1st water cycle – Effect of loosening in Silica sand

Strain increment	1st water cycle	
	Silica sand (D_{50} =0.45mm) CB45-L(Dr =62%)	Toyoura sand(D_{50} =0.196mm) CB45-L(Dr =63%)
$\delta\varepsilon_a$ %	0.093	0.050
$\delta\varepsilon_{rad}$ %	0.219	0.067
$\delta\varepsilon_{vol}$ %	0.523	0.188

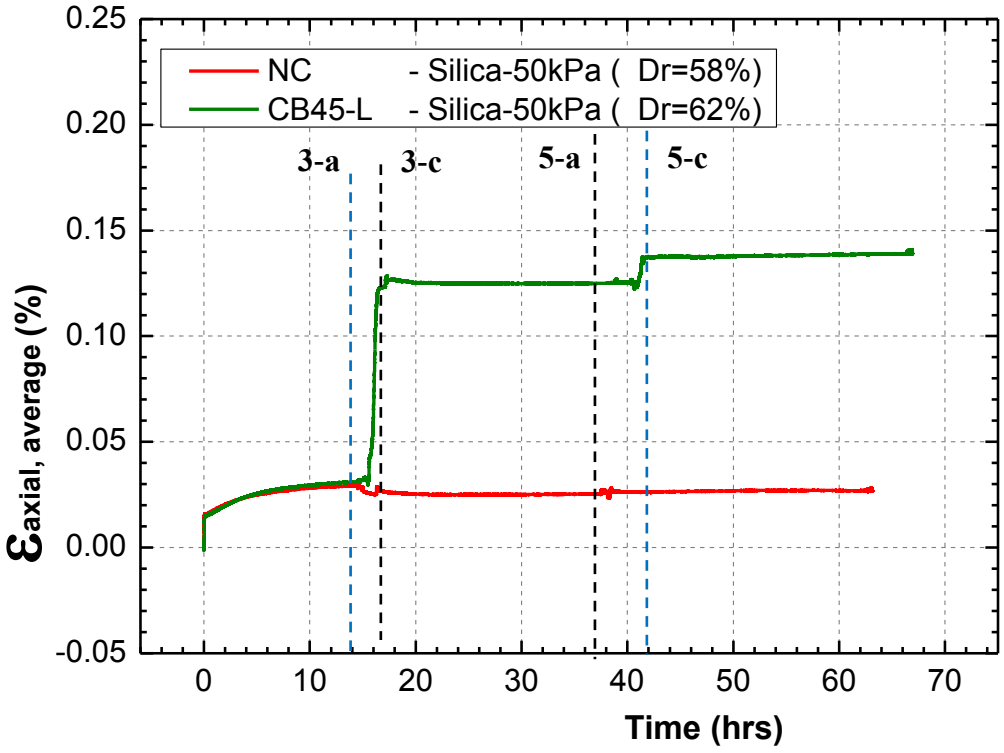

Figure 6. 54: Axial strain variation- Silica sand

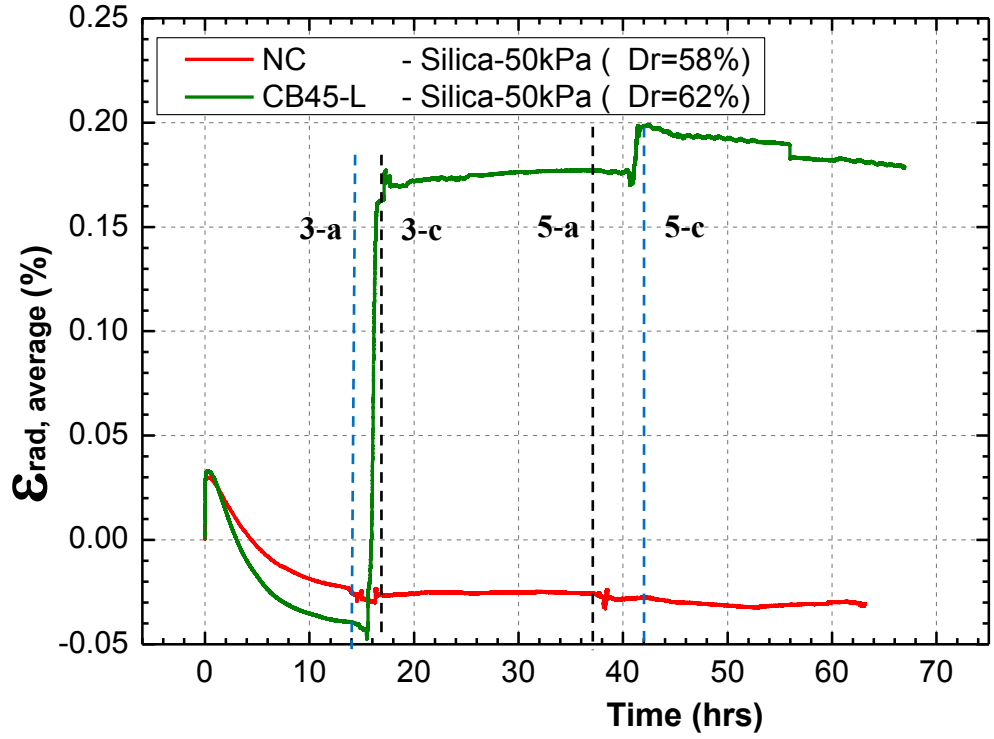

Figure 6. 55: Radial strain variation- Silica sand

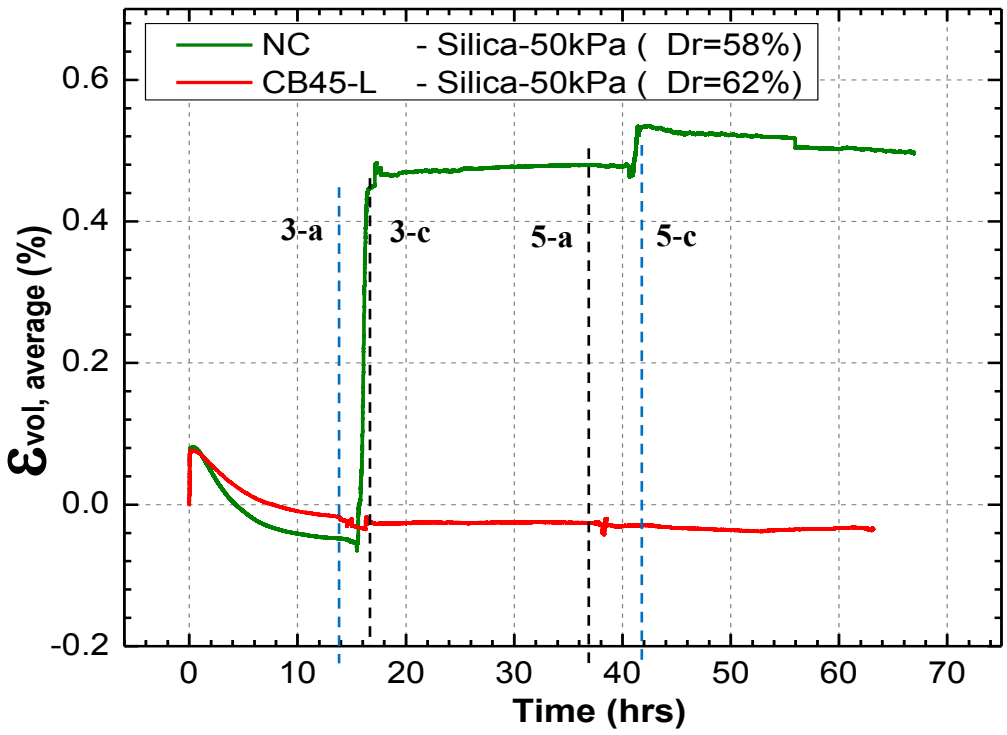

Figure 6. 56: Volumetric strain variation- Silica sand

6.3.2.3.2. Variation of Poisson's ratio

Results are shown in Figure 6.57 and Table 6.19 clearly shows that in the controlled specimen, top part is having lower "ν" value than the lower part which is opposite in the case. When the cavity is introduced, lower part shows larger "ν" value than the top part. Somehow, after the 1st water infiltration, increment of "ν" value is significantly increase in loosened sad. Furthermore, 2nd infiltration also has cased further increment in "ν". This behaviour is different from Toyoura sand. That means, the particle size is also an important factor since, the porosity and the particle structure is playing an important role with Poisson's effect.

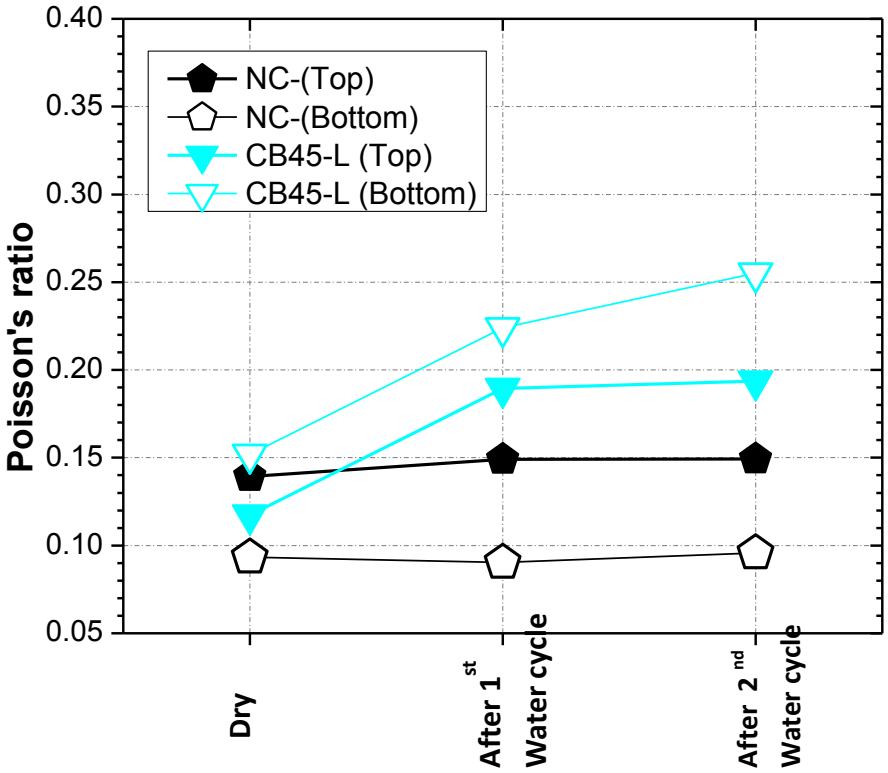

Figure 6. 57: Effect of soil loosening on Poisson's ratio – Silica sand

Table 6. 19: Variation of ν of loosened soil- Silica sand

Water cycle	NC (Dr=58%)		CB45-L (Dr=62%)	
	Top	Bottom	Top	Bottom
Increment of ν during 1st water cycle (%)	+7.12	-3.2	+61.6	+47.4
Increment of ν during 2nd water cycle (%)	+0.1	+0.53	+2.23	+3.1

6.3.2.3.3. Variation of stiffness (Young's modulus and Small strain Modulus)

Variation of young's modulus and normalized shear modulus of Silica sand with formation of loosening is shown in Figure 6.58 and 6.59. Related stiffness increment and decrement during water infiltration and drainage for Silica and Toyoura sand is summarized in Table 6.20 and Table 6.21 respectively.

While control specimen stands in a steady manner even after two water cycles, loosened sand shows progressive failure. Specially, percentage of strength reduction in 1st water cycle in Silica sand is twice than Toyoura sand. Second infiltration shows much steady behaviour than Toyoura sand which is confirmed with ε_a, ε_{rad} and ε_{vol} behaviour in Figure 6.54 to 6.56. Contraction behaviour was observed with second infiltration in Silica sand which can heal the degree of loosening. This effect might be the reason for steady stiffness at 2nd infiltration.

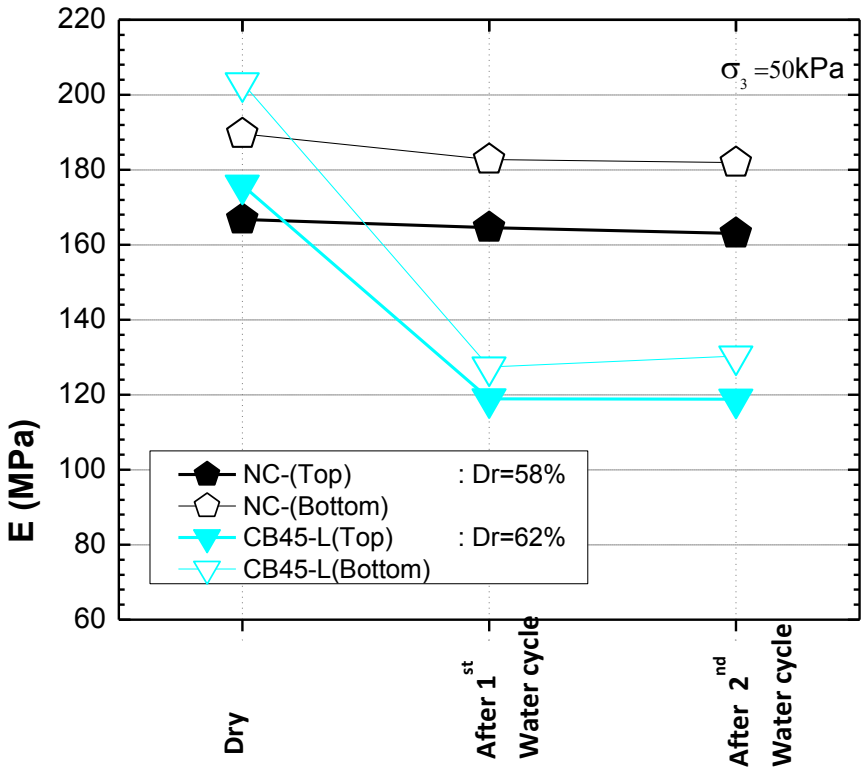

Figure 6. 58: Effect of soil loosening on Young's modulus – Silica sand

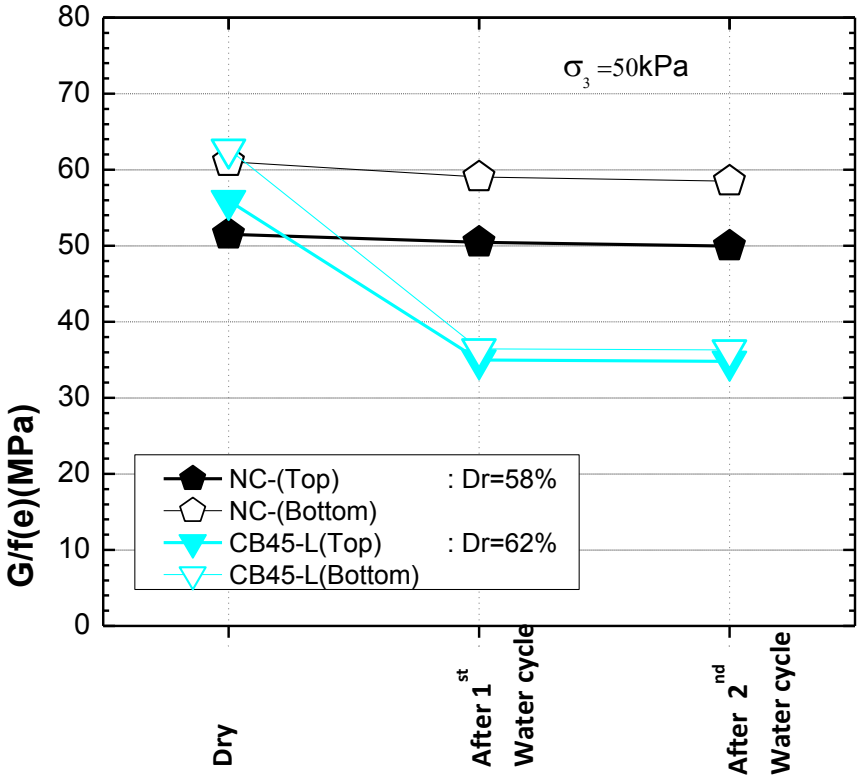

Figure 6. 59: Effect of soil loosening on normalized shear modulus – Silica sand

Table 6. 20: Variation of G/f(e) of loosened soil- Silica sand

Water cycle	NC (Dr =58%)		CB45-L (Dr =62%)	
	Top	Bottom	Top	Bottom
Increment of G/f(e) during 1st water cycle (%)	-2.07	-3.26	-37.47	-41.90
Increment of G/f(e) during 2nd water cycle (%)	-0.97	-0.93	-0.54	-0.37

Table 6. 21: Variation of G/f(e) of loosened soil- Toyoura sand

Water cycle	NC (Dr =64%)		CB45-L (Dr =63%)	
	Top	Bottom	Top	Bottom
Increment of G/f(e) during 1st water cycle (%)	-4.036	-4.40	-13.20	-20.82
Increment of G/f(e) during 2nd water cycle (%)	1.22	0.67	-4.19	-2.92

6.3.2.3.4. Shear strength

Shear strength variation was observed by deviator stress-strain relationship as shown in Figure 6.60 and 6.61. In loosened specimen of silica sand shows consistent behaviour after achieving the peak strength. Stiffness has been decreasing after achieving the 1/3 of peak strength of loosened sand.

When compare this behaviour with Toyoura sand (Figure 6.61), both controlled specimens are following the similar stress-strain relation while loosened specimens are different to each other. Failure of Toyoura sand is sudden and it can be assumed that, small cavity might be remained and cavity ceiling was collapsed at this stage. Silica sand is behaving gradual softening with lower peak strength.

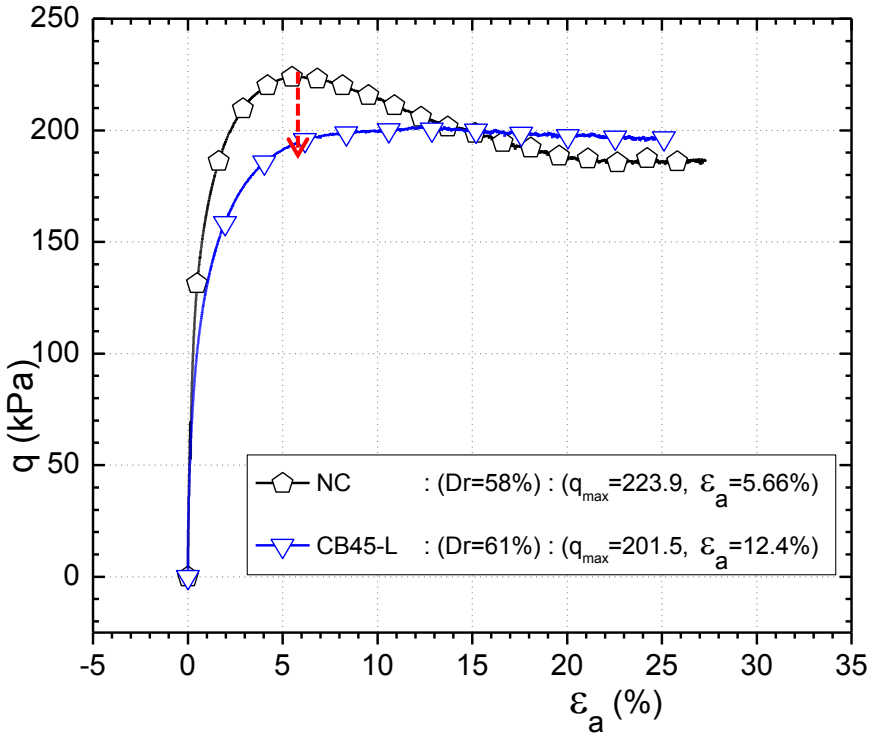

Figure 6. 60: q vs. ε_a of loosened Silica sand – Effect of particle size

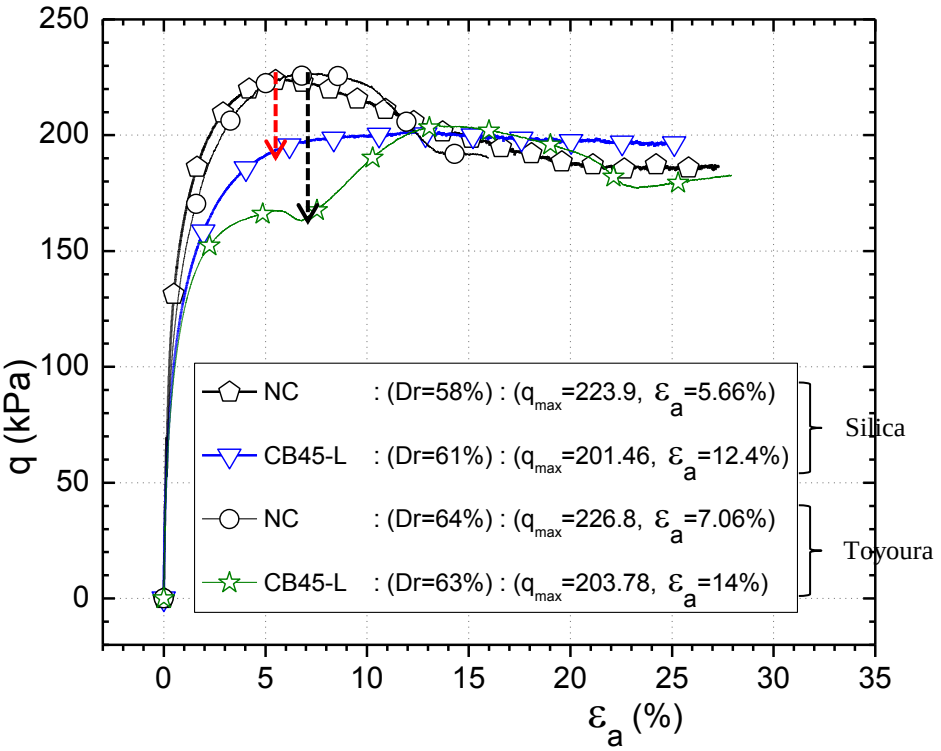

Figure 6. 61: q vs. ε_a of loosened Silica and Toyoura sand – Effect of particle size

Table 6. 22: Shear strength reduction of loosened Silica sand - Effect of confining pressure

Sand	Referred ε (ε_a at q_{max} of NC)	q (kPa)		Reduction of q in loosened sand (q_{CB45})/($q_{max,NC}$)
		NC	CB45-L	CB45-L
Silica	ε_a = 5.66%	q_{max} = 223.9	192.43	85.9%
Toyo ura	ε_a = 7.06%	q_{max} = 226.8	167.8	74%

6.3.2.3.5. Summary

- Particle size of Silica sand is nearly equal to twice of Toyoura sand. During the 1st water infiltration, Silica sand shows larger axial, radial and volumetric strain than Toyoura sand. During the second infiltration Silica sand shows further contractive deformations when deformation level is negligible in Toyoura sand. Which means in Silica sand loosening was further affected the surrounding area and might be the degree of loosening was reduced when the area of loosening was increased.

- Poisson's ratio of control specimen of Silica sand shows consistent values throughout the test. However, in loosened Silica sand Poisson's ratio has significantly increased by 1st water cycle and it was unchanged by 2nd infiltration. It confirms that, as explained in previous fact, deformations were further increased by 2nd infiltration causing degree of loosening to be decreased with self-healing effect.

- In case of stiffness parameters, stiffness was reduced to almost half of the initial value with 1st water infiltration. However, 2nd infiltration has not been affected further reduction in stiffness.

- Shear strength was also significantly affected by decreasing 15% of the peak strength. Loosened Silica sand shows softer behaviour after achieving 1/3 of peak strength.

6.3.3. Evaluation of Young's modulus of loosened sand by parametric analysis

Young's modulus and shear modulus evaluated using the displacement measured by LDTs doesn't exactly represent the characteristics of loosened sand. Still, Young's modulus of specimen shows lower value (75-85%) than control specimen. The reason is LDTs are not directly attached to loosened region, which is located at central part. Actual Young's modulus related to loosened sand should be much lower than what was evaluated.

Therefore parametric analysis was conducted to get more reasonable "E" value. Height of loosened region was decided with respect to initial potential cavity by X-ray CT images (Figure 7.6). More details about X-ray CT images taken for visualization of loosening are explained in Chapter 7. As observed in loose Toyoura sand (Dr -41%), extend of loosened region is twice of the height of potential cavity. Width of loosened region is almost similar to the initial width of potential cavity. Therefore assumption was made as loosened region is twice of the height of cavity for lower density (Around Dr = 35-40%). Furthermore, Young's modulus of soil not affected by loosening (E_1 and E_3 in Figure 6.62-b), was assumed to be similar as Young's modulus of control specimen (E_0 in Figure 6.62-a). Different Young's modulus was allocated for loosened sand (E_2) and evaluated as explained below.

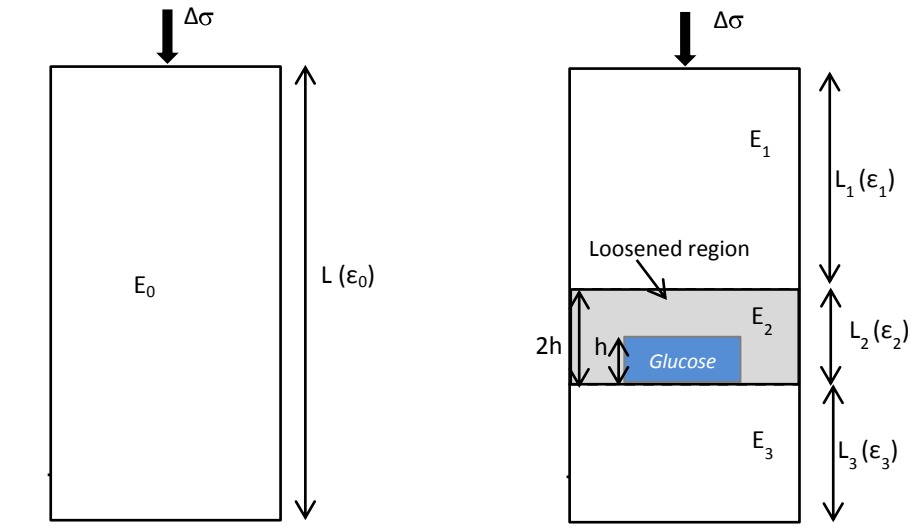

(a) Controlled specimen (b) Specimen with loosening

Figure 6. 62: Schematic for evaluation of Young's modulus by parametric study

E_0, E_1, E_3- Young's modulus of non-loosened soil
E_2 - Young's modulus of loosened soil
L_2 - Height of loosened region
L_1 - Height from specimen top to loosened region
L_3 - Height from specimen bottom to base of glucose block

$E_0 = E_1 = E_3$ Eq.6.1

$$E_0 = \frac{\Delta\sigma}{\varepsilon_0}$$ Eq.6.2

$$\varepsilon_0 = \varepsilon_1 = \varepsilon_3 = \frac{\Delta\sigma}{E_0}$$ Eq.6.3

If the total displacement in Figure6.62 (b) is d, and displacement of each section is d_1, d_2 and d_3,

$d = d_1 + d_2 + d_3$ Eq.6.4

$$d_1 = \varepsilon_0 L_1$$

$$d_3 = \varepsilon_0 L_3$$

Therefore d_2 can be evaluated. Thereby ε_2 is known and E_2 can be evaluated by Eq.6.5.

$$E_2 = \frac{\Delta\sigma}{\varepsilon_2}$$ Eq.6.5

Table 6. 23: Young's modulus of loosened Toyoura sand

Test	L_1,L_2,L_3 mm	E_0 MPa	E_2 MPa	E_2/E_0
NC (Dr=35%)	150, 0, 0	107		
CB45-L (Dr=36%)	75, 30, 45	107	49	46%
CB-L (Dr=37%)	120, 30, 0	107	51	48%
CB45-S (Dr=37%)	75, 30, 45	107	65	61%
CB-S (Dr=36%)	120, 30, 0	107	56	52%

Table 6.23 shows the Young's modulus of loosened sand evaluated (after 1st water drainage) by parametric analysis. Reduction of average Young's modulus evaluated by measured displacement of LDT was 75-90% of non-loosened region. However, values evaluated by new approach shows that Young's modulus of loosened sand is much lower and varies 45-60% of the non-loosened value.